NOVEMBER 1991

GROUNDWATER QUALITY IN PUMPING WELLS LOCATED NEAR SURFACE WATER BODIES

Technical Completion Report No. 261

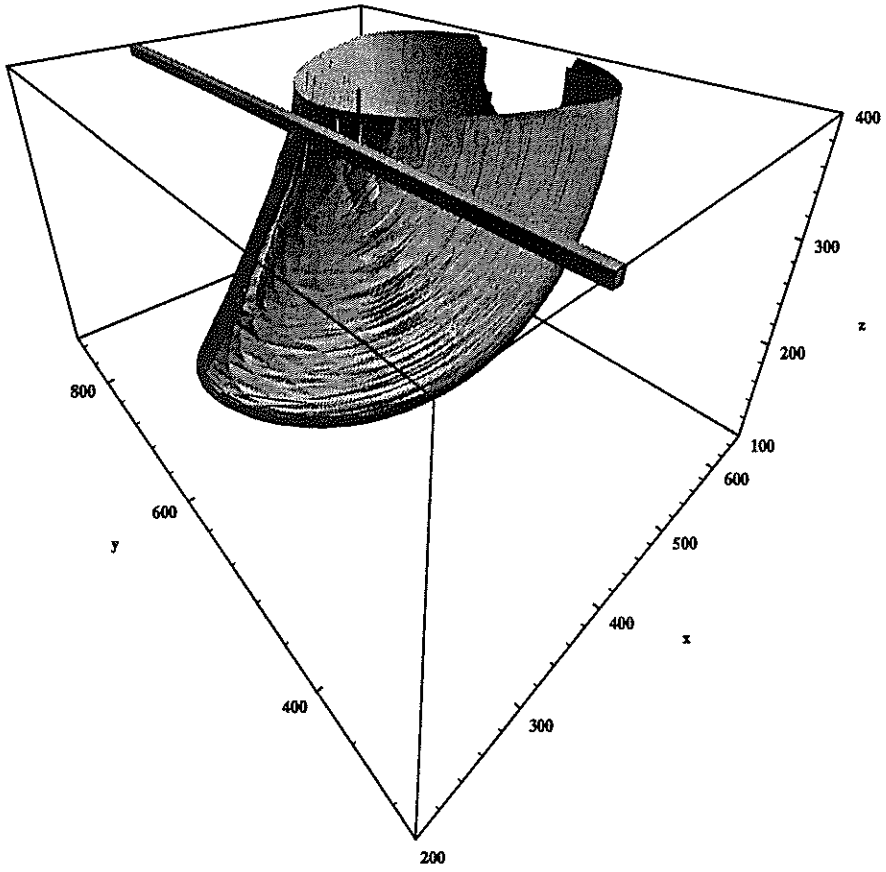

The 7000-day capture zone for a partially penetrating well near a shallow, gaining stream

NEW MEXICO WATER RESOURCES RESEARCH INSTITUTE
New Mexico State University
Box 30001, Dept. 3167
Las Cruces, New Mexico 88003-0001
Telephone (505) 646-4337 FAX (505) 646-6418

GROUNDWATER QUALITY IN PUMPING WELLS LOCATED NEAR SURFACE WATER BODIES

John L. Wilson and William R. Linderfelt
Department of Geoscience
New Mexico Institute of Mining and Technology

TECHNICAL COMPLETION REPORT

Account Number 1423620

November 1991

New Mexico Water Resources Research Institute

in cooperation with

Department of Geoscience
New Mexico Institute of Mining and Technology

The research on which this report is based was financed in part by the U.S. Department of the Interior, Geological Survey, through the New Mexico Water Resources Research Institute.

DISCLAIMER

The purpose of Water Resources Research Institute technical reports is to provide a timely outlet for research results obtained on projects supported in whole or in part by the institute. Through these reports, we are promoting the free exchange of information and ideas, and hope to stimulate thoughtful discussion and actions that may lead to resolution of water problems. The WRRI, through peer review of draft reports, attempts to substantiate the accuracy of information contained in its reports, but the views expressed are those of the author(s) and do not necessarily reflect those of the WRRI or its reviewers. Contents of this publication do not necessarily reflect the views and policies of the U.S. Department of the Interior, nor does mention of trade names or commercial products constitute their endorsement by the United States government.

ACKNOWLEDGEMENTS

Several individuals contributed to this report directly or indirectly. Some of these are acknowledged by their authorship of individual sections. In one way or another Peter Riordan (Section 2), John Chow, Ken Lee (Section 3), Joan Newsom (Section 3), Shawn Leppert (Section 3 & 4), Robert Terberg (graphics), Annette Schafer–Perini (algorithms and the Appendix), and Allan Gutjahr (geostatistics and probability) contributed to the technical aspects of this work. Edith Montoya helped with the administrative problems. To all we are grateful.

This project was funded by the U.S. Geological Survey, through grant number 14–08–0001–G1632 and the New Mexico Water Resources Research Institute, through project numbers 1345682 and 1423620. Some of the computer codes used and improved by the project were initially supported by the Department of Energy under contract DE–AC03–85BC–10850.

ABSTRACT

Well-water quality depends on the relative amounts of water drawn from different hydrologic units (aquifers, streams, etc.), and the particular capture zones within those units. A contaminant spilled within an aquifer capture zone will eventually enter the well. A spill outside the capture zone may eventually discharge elsewhere, perhaps to a nearby stream. If under normal circumstances the stream is gaining, pumping can locally reverse gradients, causing it to become losing. Stream water can then enter the well by induced infiltration. For wells located near surface water bodies, a variety of two and three-dimensional analytical and numerical models of induced infiltration and capture zones are presented. The capture zone models use particle tracking. The propensity for and rate of induced infiltration is enhanced by higher pumping rates, closer streams, less well penetration, increased stream penetration, less ambient aquifer discharge to the stream, nearby aquifer pinch outs, and a variety of other factors. Induced infiltration does not seem to be very sensitive to the ambient flow's source, whether it is local vertical recharge or lateral inflow. Two types of capture zones are defined: ultimate capture zones that include that portion of the aquifer that will eventually discharge to the well, and time-dependent capture zones that include only that portion of the aquifer that discharges to the well within a prescribed time. Capture zones are strongly influenced by the source and direction of ambient aquifer flow, nearby aquifer boundaries, and three-dimensional flows caused by partial penetration of the well or the stream. For example, when local vertical recharge is the principle source of ambient flow,the capture zone tends to 'cusp' (elongate) along groundwater divides and barrier (pinchout) boundaries. This allows the well to capture contamination from long distances away, albeit at great travel times. Partial penetration of the stream allows the well to capture by underflow ambient groundwater from the opposite stream bank, even though the well may not induce infiltration from the stream itself. Capture zone models involve uncertain parameters that lead to 'fuzzy' capture zone boundaries. These boundaries are represented by contour lines of equal capture probability.The concept of 'fuzzy' capture zones is illustrated for a simple model. Hydrodynamic and macro dispersion are other sources of uncertainty. They allow a particle to wander across the capture zone boundary. Thus a source of contamination outside of the capture zone has a finite probability of being incorporated into the well water. Another interpretation of these probabilities, at least for long-term continuous sources of contamination, is that they define the proportion of the contaminant that will eventually find its way to the well.

TABLE OF CONTENTS

LIST OF FIGURES

LIST OF TABLES

SECTION 1

INTRODUCTION

INTRODUCTION

In many areas of the United States groundwater wells are drilled into the sedimentary deposits that are found in low–lying areas located near gaining surface water bodies, such as streams, rivers and lakes. For brevity, these surface water bodies will be refered to as 'streams'. Pumping from nearby wells often induces water to be drawn through the bottom of the stream, to infiltrate through the aquifer, and to flow into the well. This diversion of water from the stream into the well is called induced infiltration. The well also collects ambient aquifer flow, which would otherwise discharge as base flow to the gaining stream. Traditionally water resource managers have been concerned with the depletion of streamflow caused by induced infiltration. This is particularly true in New Mexico. Recently attention has begun to focus on new issues involving well–water quality. Well water is a mixture of water from the stream and the aquifer, and its quality reflects these diverse origins. Streamflow depletion is a short–term, time–dependent process for a gaining stream, since over the long–term the net steady–state depletion of the stream is given by the well pumping rate. The opposite is true of the water quality issue, where the major concern is usually the long–term use of water under various pumping schedules.

Well–water quality depends on the relative amounts of water drawn from different hydrologic units (aquifers, streams, etc), and the particular capture zones within those units. A contaminant spilled within an aquifer capture zone will eventually enter the well. A spill outside the capture zone may eventually discharge elsewhere, perhaps to the nearby stream. If the spill is upstream of the well, some of the contaminant may still enter the well by induced infiltration from the stream, which also may carry its own contaminant load.

Four years ago Congress passed the Safe Drinking Water Act of 1986. It contains a wellhead protection provision, in an attempt to protect public water supply wells and well fields from contamination from man-made sources. A wellhead protection area is defined as the "surface and subsurface area surrounding a water well or well field, supplying a public water system, through which contaminants are reasonably likely to move toward and reach such water well or well field." That is, a wellhead protection area is defined by a capture zone. Once a wellhead protection area is defined, contaminant sources within it are to be assessed and appropriate control measures implemented. Having raised the issue, the Congress turned to the states to establish wellhead protection programs, but failed to provide significant funding for program implementation (less than one–tenth of one percent of the funding for Superfund), and little funding for research. The Environmental Protection Agency's (EPA) Office of Ground-Water Protection (OGWP) was formed to provide administrative and technical guidance to the states. One of the most important technical questions facing OGWP and the states has been how to delineate a wellhead protection area (WHPA). The OGWP responded to this question with a set of guidelines that were published shortly after the legislation became law (EPA, 1987). Then they sponsored the development of more sophisticated mathematical models that presumably improved delineation capabilities (EPA, 1990). Some preliminary results from the work presented in this report were incorporated into these EPA models.

OBJECTIVES

The goal of this report is to present several simple models of well water quality for pumping wells that are located near streams and other gaining surface water bodies, such as rivers and lakes.

The models address the following specific questions:

- Under what conditions does induced infiltration take place?
- What are the contributions of the stream and other sources to the well? How much water is drawn from each source?
- What are the capture zones and related travel times? Where is the water coming from and how long does it take to reach the well?
- How do the answers to these questions depend on the assumed stream–aquifer conceptual model and related parameters? For example, what are the effects of well location and pumping rate, aquifer properties, hydrodynamic or macro–dispersion, time varying pumping rate, parameter uncertainty, etc?

PURPOSE

The models' primary purpose is to help engineers, scientists, and other water resources professionals better understand the mechanics of stream–aquifer interaction and related capture zones, when well–water quality is of concern. The models' secondary purpose is to assist with the preliminary screening of policy decisions, or for a 'first cut' evaluation of site specific design or operation decisions. It may also be tempting to use them in the assessment of liability for past contamination activities, but that is not the intent since the models are generic and somewhat idealized. Finally the models can be used also for numerical model validation, as in EPA (1990).

One of the models' principle applications is for wellhead protection, where they can be employed in a variety of the roles outlined above, and for many other potential applications. Consider the following situations. Each requires a well–water quality estimate that depends on understanding induced infiltration and related capture zones.

- Water quality in a perennial stream is impaired by mine tailings. A regulatory agency wishes to decide on permissible limits of pumping from a downstream well located along the banks of the stream, such that concentrations of certain constituents in the well water do not exceed recommended limits. In this case the rate of induced infiltration as a function of pumping rate must be estimated.
- There has been a large oil spill into a river. The spill is moving down the river, contaminating municipal water intakes one by one. Some downstream communities use induced infiltration through wells instead of intakes. Should the wells be shut down? If so, when and for how long?
- An aquifer's water quality has been degraded by septic tanks. Nitrate levels exceed recommended levels for drinking water. A downgradient pumping well draws water from the aquifer and an adjacent river. At what rate must

the well pump to ensure that the aquifer nitrate levels are sufficiently diluted by low nitrate river water?

- The discharge pipe from an industrial treatment plant empties into a stream along the shoreline opposite to a municipal well field. Should there be an upper limit to the well field withdrawal rates, to ensure that the groundwater pumping is not intercepting some industrial discharge? Is there a preferred location for the pipe discharge, to minimize or eliminate this possibility?

- Organic solvents have spilled into the soil has occurred near a water supply well field located near a stream. What is the propensity for dissolved organics from the spill to find their way through the aquifer to the well? That is, is the spill within the well's capture zone? How long before dissolved components reach the well? How much dilution will occur in the well? Will the solvent also migrate to the stream? If so, how much of that will be subsequently recaptured by the well's induced infiltration?

- A hazardous waste site is located on the banks of a small river in New England. On the opposite bank, and somewhat upstream, lies a municipal well field. The site owners argue that it is not a threat to the well field because it is not only on the other side of the river, it is also downstream. "There is no conceivable pathway for contamination to move from our facility to the well field," they argue. However, there is a possibility of underflow beneath the river. The municipality asks "What is the well field capture zone, and how much, if any, of the opposite shore does it include?"

- A highway interchange expansion is planned in the vicinity of a water supply well located on the banks of a lake. Two issues have arisen related to wellhead protection. First, should road deicing salt applications on the interchange be controlled to minimize potential sodium contamination of the well? Secondly, what land use restrictions should be placed on future businesses to control potential contamination from leaking storage tanks and other potential sources of contamination? Both issues concern the delineation of capture zones. The regulatory agency prohibits underground storage tanks within the '5–year capture zone of the well,' an area defined such that there is a 90% probability that the travel time from the tank location to the well exceeds five years.

- Engineers desire to capture a pollutant plume before it reaches a nearby lake. They plan to place one or more extraction wells along a line between the lake and the plume, and to remove the plume as it passes by. They need to determine how many wells to use, their location, and their pumping rates. In particular, they want to minimize the amount of induced infiltration so that they pump the plume and not the lake.

This last example is a reminder that the models presented here have applications in aquifer remediation, as well as wellhead protection and the other uses illustrated.

Finally, it is important to realize that the simple models presented in this report do not replace detailed site–specific investigations.

SCOPE

Most of this report invokes a two–dimensional conceptualization of aquifer flow. Flow to a well is intrinsically areal in nature because the flow approaches the well bore radially. Areal, or vertically integrated, models assume that the flow is essentially horizontal and that hydraulic equipotentials are essentially vertical (Bear, 1979). This conceptualization is commonly employed in groundwater hydrology, and is the origin of such concepts as transmissivity and aquifer storativity, and of many models including the Theis drawdown equation. Using this essentially horizontal flow conceptualization, the issue of induced infiltration is introduced in Section 2 for fully penetrating streams and wells. Several different aquifer geometries are examined, and induced infiltration is calculated as a function of well location and pumping rate, aquifer size and geometry, and the various recharge sources. Section 3 extends these results to look at spatial capture zones, with special emphasis on the influence of the source of aquifer recharge, the effects of large stream gradients, variable aquifer thickness, and spatially variable aquifer properties. The effects of parameter uncertainty on capture zones is discussed in Section 4, and the concept of 'fuzzy capture zones' is introduced. Three–dimensional aquifers and capture zones are introduced in Section 5. Section 6 presents the summary and conclusions. Appendix A describes some of the mathematical methodology employed.

SECTION 2

INDUCED INFILTRATION IN AQUIFERS WITH AMBIENT FLOW

INTRODUCTION

Throughout the northeastern United States it is common to find high capacity shallow wells pumping from phreatic aquifers in alluvial or glacial valleys. These wells are commonly located in low–lying areas near streams, wetlands or ponds. One can only guess at the rationale which led early well designers to examine and eventually select a particular well site, but such factors as the small depth to groundwater, the large thickness of saturated pervious deposits near the center and/or lowest portion of the valley, and the proximity to a nearby surface water bodies seem to have played a dominant role. A simple groundwater balance shows that there is insufficient natural rainfall recharge to supply the wells at their historic pumping rates, and that a portion of the pumpage is induced artificially into the aquifer from nearby surface water bodies (Rorabaugh, 1956). Well drawdowns in groundwater levels adjacent to or beneath surface water bodies create gradients and thus induce flow out of the surface water body. The potential for induced infiltration is clearly documented in the theory of well hydraulics (Theis, 1941; Kazman, 1946, 1948; Ferris et al., 1962; Hantush, 1965; Walton, 1970; Bear, 1979), although there have been few related field studies.

The amount of induced infiltration is a function of many factors, including aquifer transmissivity, aquifer geometry, pumping rates, the strength of the hydraulic connection between the aquifer and surface water body, and the presence of other water sources for the well. Quantifying the amount of induced infiltration in terms of these parameters is an important factor in conjunctive water use as water demand increases and the reliability of surface supplies is threatened by streamflow depletion. This problem has been well studied, particularly in the western states (Theis, 1941; Kazman, 1948; Glover and Balmer, 1954; Rorabaugh, 1956; Hantush, 1959, 1965; Walton, 1970; and many others). In the east, streamflow depletion is usually not the issue, but water quality is. Because of the potential for ground and surface water pollution from varied sources and by varied pollutant species, quantifying the amount of induced infiltration becomes important in evaluating the reliability of well–water quality.

The two induced infiltration problems, streamflow depletion and water quality, are different. The depletion problem is inherently time dependent. When pumping starts, the well initially obtains its supply of water from aquifer storage. Eventually the well's cone of depression intercepts the surface water body and begins to induce infiltration, depleting the streamflow. As time passes, the drawdown comes to an equilibrium, with the stream losing as much water as the well is pumping. If under ambient conditions the stream is gaining, it is not necessary for the well to actually reverse gradients and induce infiltration. It depletes streamflow simply by capturing some of the ambient aquifer discharge before it reaches the stream. In fact, as long as the stream and aquifer

are in hydraulic connection, the rate of streamflow depletion is relatively independent of whether or not the stream is actually gaining or losing, and the actual sources of the water being pumped. However, in a water quality analysis these two conditions are paramount. A polluted stream that is gaining even under pumping conditions cannot generally pollute an aquifer. If the pumping rate is increased and the polluted gaining stream becomes a losing stream over a short distance, due to induced infiltration toward the well, it pollutes only the aquifer between the well and the stream. As the pollution enters the well, it is diluted by the other sources of well water, such as the ambient aquifer flow. If, on the other hand, it is the aquifer that is polluted, then the well pumping rate can be increased until it induces infiltration of a enough good quality stream water to dilute the pollution. Over the long–term, these water quality issues can often be viewed from a steady–state perspective, for wells which pump more or less continuously in order to supply water for industrial or domestic use. Pumping for irrigation is usually too intermittent to be amenable to steady–state analysis.

Although the streamflow depletion problem has been studied for many years, the water quality induced infiltration problem has not. We have encountered this problem in numerous practical situations in the northeast, and developed the simple models presented here to aid in its study. The models help us understand induced infiltration phenomena, and provide a 'first cut' analysis of alternative well field designs and pumping rates from a water quality perspective, or assist in the delineation of well–head protection zones. They may also help in characterizing past pollution events involving wells, aquifers, and streams or other surface water bodies. The models are presented in the form of dimensionless curves, describing the conditions under which induced infiltration occurs and giving the amount of induced infiltration as a percentage of well discharge. Under ambient conditions the surface water body is assumed to be gaining, supplied by ambient aquifer flow. Under pumping conditions the well captures a combination of induced infiltration stream water, and ambient aquifer flow from both natural vertical recharge and lateral inflows. The aquifer is assumed to be homogeneous and isotropic. The surface water body and the well are assumed to fully penetrate the aquifer; the flow is essentially horizontal. In a phreatic aquifer, the drawdown is assumed to be small compared to the ambient saturated thickness, leading to the Dupuit approximation. The surface water body is assumed to be hydraulically connected to the aquifer, and a 'skin effect' caused by a possible clogging layer of low conductivity lining the surface water body is ignored. Temperature variation and its effect on aquifer hydraulic conductivity is also ignored. Equilibrium (steady–state) conditions are assumed; the approach is most applicable to average long–term conditions at continuously used water supply wells. Well tests, such as those described by Rorabaugh (1956), are usually too short in duration for equilibrium to occur.

The equations for induced infiltration in a semi–infinite aquifer with ambient aquifer flow are developed first. This review serves a pedagogic purpose by introducing the approach, concepts, and notation for a simple case. More sophisticated cases are then concisely presented, with combinations of barrier and steam boundaries, and sources of recharge, Although the term 'stream' is used consistently in the text, the approach also applies to ponds, lakes, and wetlands.

WELL IN A SEMI−INFINITE AQUIFER

Consider a homogeneous semi−infinite aquifer bounded on one side by a fully penetrating stream. The aquifer can be confined or phreatic; Figure 2−1 illustrates the phreatic case. A uniform ambient flow, q_a [L^2/T], discharges toward the stream, which acts as a constant head boundary. The well, located distance d from the stream, pumps at rate Q_w [L^3/T]. Under steady−state conditions this situation is described by the Laplace equation, $\nabla^2\Phi = 0$, where there is a sink strength of Q_w at x=0 and y=d. The state varible Φ[L^3/T] takes on different definitions in confined and phreatic aquifers

$$\Phi = \begin{cases} Th & , \text{ confined or linearized phreatic aquifer,} \\ \frac{Kh^2}{2} & , \text{ Dupuit type phreatic aquifer,} \end{cases} \qquad (2-1)$$

where h [L] is depth averaged head (water table elevation in the phreatic aquifer case), K [L/T] is horizontal hydraulic conductivity, and T= [L^2/T] is transmissivity. As the note indicates, the upper definition in (2−1) applies when the concept of transmissivity is employed in a confined or phreatic aquifer. As shown later, both forms of the model provide identical results for induced infiltration (although it can be shown that results for the interior of the aquifer are different, and thus influence capture zones and other interior features). The solution for Φ is easily found by superpositon of the ambient flow and the drawdown due to the well. The drawdown is in turn found via image well theory. The result is

$$\Phi(x,y) = \Phi_o + q_a y - \frac{Q_w}{4\pi} \ln\left[\frac{(y+d)^2 + x^2}{(y-d)^2 + x^2}\right], \qquad (2-2)$$

in which $\Phi_o = \Phi(h = h_o)$ is evaluated at the stream boundary, where $h=h_o$. The first term in (2−2) represents the stream surface elevation, the second term is the rising head away from the stream caused by ambient flow, and the third term is the well drawdown. Darcy's law can then be employed to yield the specific discharge integrated over the depth, here called the 'discharge per unit width', $q = -\nabla\Phi$[L^2/T]. To compute infiltration we need only examine this discharge along the stream boundary, y=0, or

$$q_o(x) = q(x,0) = -\left.\frac{\partial\Phi}{\partial y}\right|_{y=0} = -q_a + \frac{Q_w}{\pi}\left[\frac{d}{(d^2 + x^2)}\right]. \qquad (2-3)$$

In the absense of pumping, the stream is gaining and the discharge to the stream is in equilibrium with the ambient flow: $q_o=-q_a$ if $Q_w=0$.

For small pumping rates the stream continues to gain, as shown in Figure 2−2a, and the well continues to collect all its water from the ambient flow field. A critical situation is reached at a higher pumping rate, pictured in Figure 2−2b, for which the well just begins to draw water from the stream. This pumping rate is called the critical pumping rate, Q_c. Mathematically, the critical pumping rate occurs when the stagnation point down−gradient of the well (point A in Figure 2−2a) moves onto the stream (Figure 2−2b), so that $q_o=0$ at the origin (x=y=0). Setting (2−3)

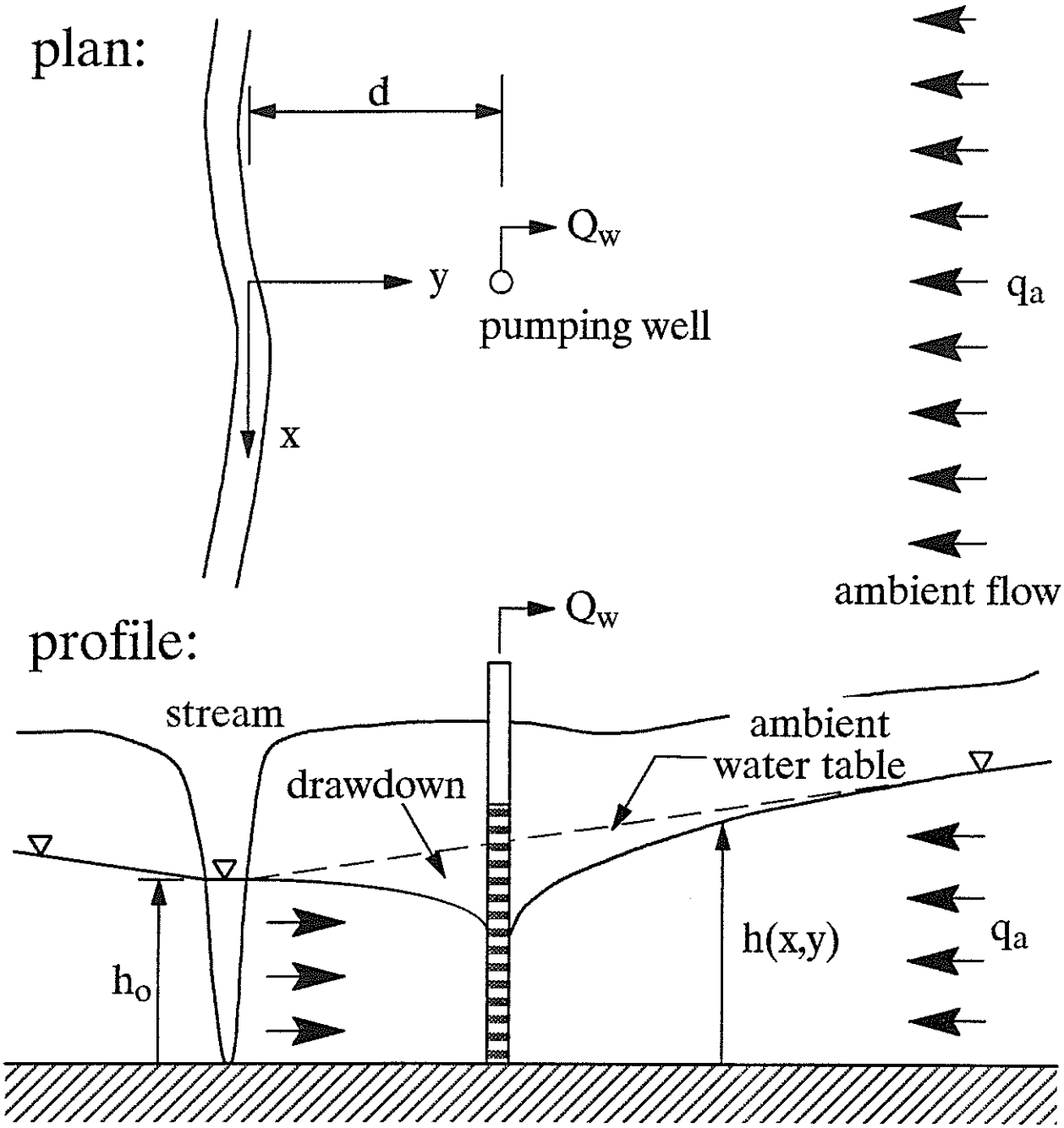

Figure 2–1 Schematic of a pumping well in the vicinity of a stream in the presence of an ambient aquifer flow in a semi–infinite aquifer.

to zero at x=0 gives the critical pumping rate $Q_c = \pi d q_a$, which is directly proportional to the ambient flow rate and the distance between the well and the stream. Pumping at rates above this critical value induce infiltration from the stream, and the stream begins to lose water to the well. The stagnation point 'splits' and moves equidistance up and down the stream to points A and A' in Figure 2–2c. Actually, the stagnation point does not really split; this is just the appearance of a second image stagnation point not visible in our view when $Q_w < Q_c$(see, e.g., Bear, 1979). The induced infiltration takes place between points A and A' and is calculated by integration.

Let the x–coordinates of the stagnation points A and A' be given by $\pm x'$. The coordinates are found using equation (2–3) and the property that $q_o=0$ at a stagnation point,

$$\frac{x'}{d} = \left[\frac{Q_w}{\pi d q_a} - 1\right]^{1/2} = (\beta - 1)^{1/2}, \qquad (2-4)$$

where β is the dimensionless pumping rate,

$$\beta = \frac{Q_w}{\pi d q_a}. \qquad (2-5)$$

Then equation (2–3) is integrated between $\pm x'$ to yield the induced infiltration rate, Q_s [L^3/T],

$$Q_s = \int_{-x'}^{+x'} q_o \, dx = -2q_a x' + \frac{2Q_w}{\pi}\tan^{-1}\left(\frac{x'}{d}\right). \qquad (2-6)$$

Substituting the stagnation point location from (2–4) into this equation yields the final expression for induced infiltration, Q_s, here expressed as a proportion of the total pumping rate, Q_w:

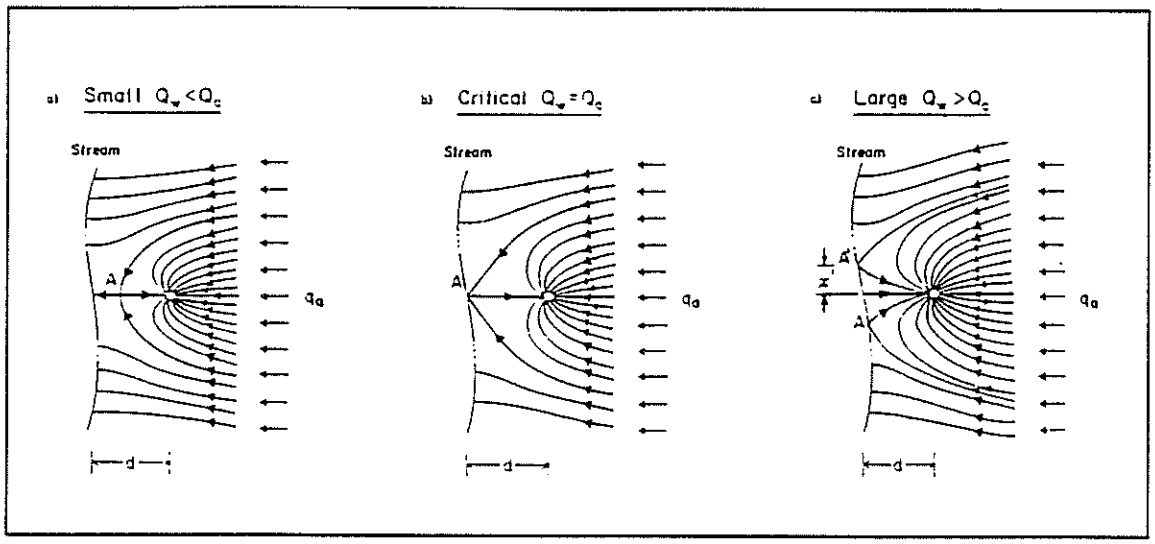

Figure 2–2 Flow patterns for a semi–infinite aquifer in the vicinity of a well and a stream for a) a subcritical pumping rate, b) critical pumping rate, and c) for pumping above the critical rate. For the latter case the zone of induced infiltration is located along the stream between the stagnation points A and A'.

$$\frac{Q_s}{Q_w} = \frac{2}{\pi}\left[\frac{-(\beta-1)^{1/2}}{\beta} + \tan^{-1}\{(\beta-1)^{1/2}\}\right]. \qquad (2-7)$$

This dimensionless relationship is plotted in Figure 2−3. The critical dimensionless pumping rate is $\beta = \beta_c = 1$, and equations (2−4) and (2−7) apply only when pumping exceeds this value, that is, when $\beta \geq 1$. The graph shows that the amount of induced infiltration increases with higher pumping rates and for wells closer to the stream, and decreases with higher ambient flow rates. The remaining water in the well, here labled Q_a, comes from the ambient flow and is given by $Q_a = Q_w$ when $\beta \leq 1$, and $Q_a = Q_w - Q_s$ when $\beta \geq 1$. Although the proportion of pumped water coming from the ambient flow decreases at higher pumping rates, the actual amount of ambient water increases, as illustrated in Figure 2−4. Note that the solution is indifferent to whether the aquifer is confined or phreatic.

This example is a special case of the more general models examined below and has been studied before, usually in a different context. In potential flow theory, the typical application concerns an injection−production well pair in a confined aquifer (Jacob, 1950; DaCosta and Bennett, 1960, which is discussed in Bear, 1979; Edelman, 1972; and others). The author first

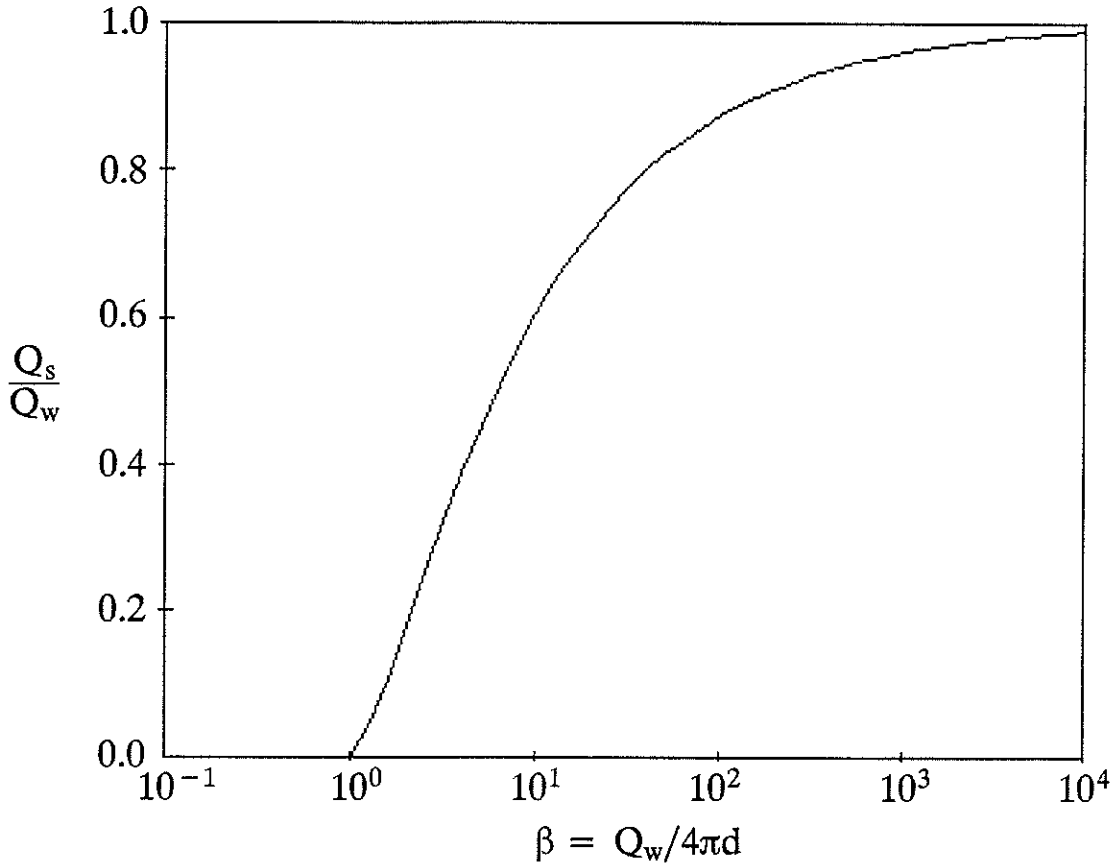

Figure 2−3 Induced infiltration as a function of dimensionless pumping rate.

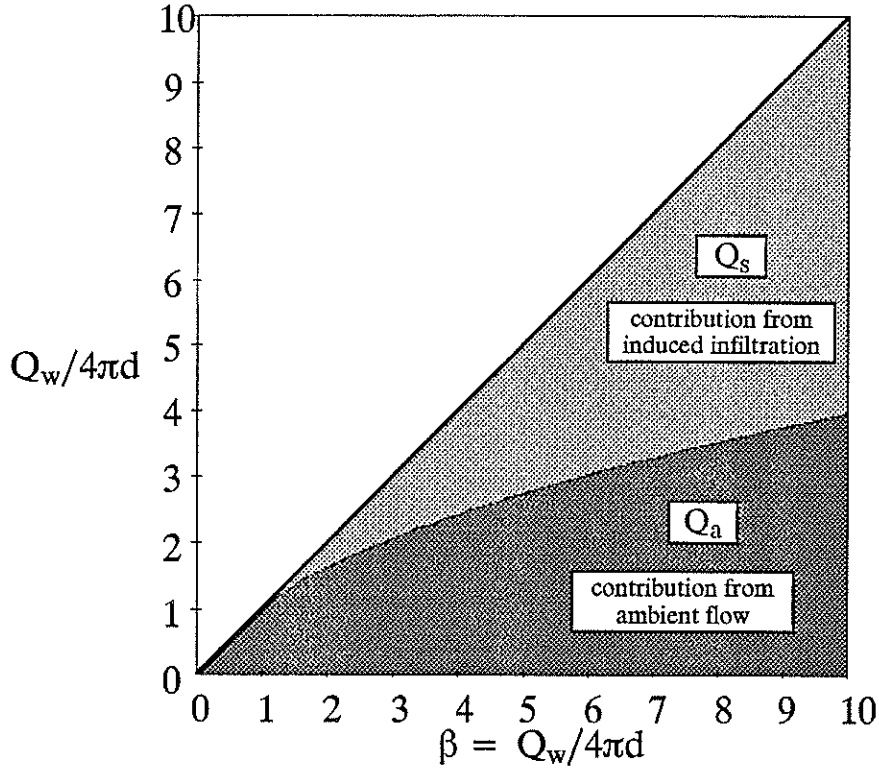

Figure 2–4 Contributions of ambient flow and induced infiltration to pumpage.

encountered it twenty years ago as a graduate student; it is posed in Milne–Thomson's 1949 text on Theoretical Hydrodynamics (Prob. 5, p. 234 of 1968 edition). Finally it has also been presented in the present context (Wilson, 1981; Newsom and Wilson, 1988b).

WELL BETWEEN A STREAM AND A BARRIER

Suppose that beyond the well the aquifer pinches out or is interrupted by a non–conformity. As depicted in Figure 2–5, we represent this as a barrier, across which some flow may be possible. In the northeastern United States, this barrier typically represents bedrock or glacial till; in the west it could be a fault block. The lateral inflow across the barrier, q_L, is assumed to be independent of any drawdown in the aquifer. A uniform local vertical recharge, N [L/T], is applied at the top of the aquifer. The well draws water from the local recharge and lateral inflow, and for sufficiently strong pumping it induces infiltration from the stream. We hypothesize that the rate of induced infiltration should be greater in this case, because of the enhanced drawdown caused by the barrier. We use the same procedure employed to analyze the simple semi–infinite aquifer. First the head field is determined and used to construct the discharge to or from the stream. Second, the critical pumping rate is determined by setting the discharge to zero at the origin (x=y=0). Third, for higher pumping rates the discharge is examined for stagnation points, and the induced infiltration rate is computed by integrating the discharge to the stream between these points.

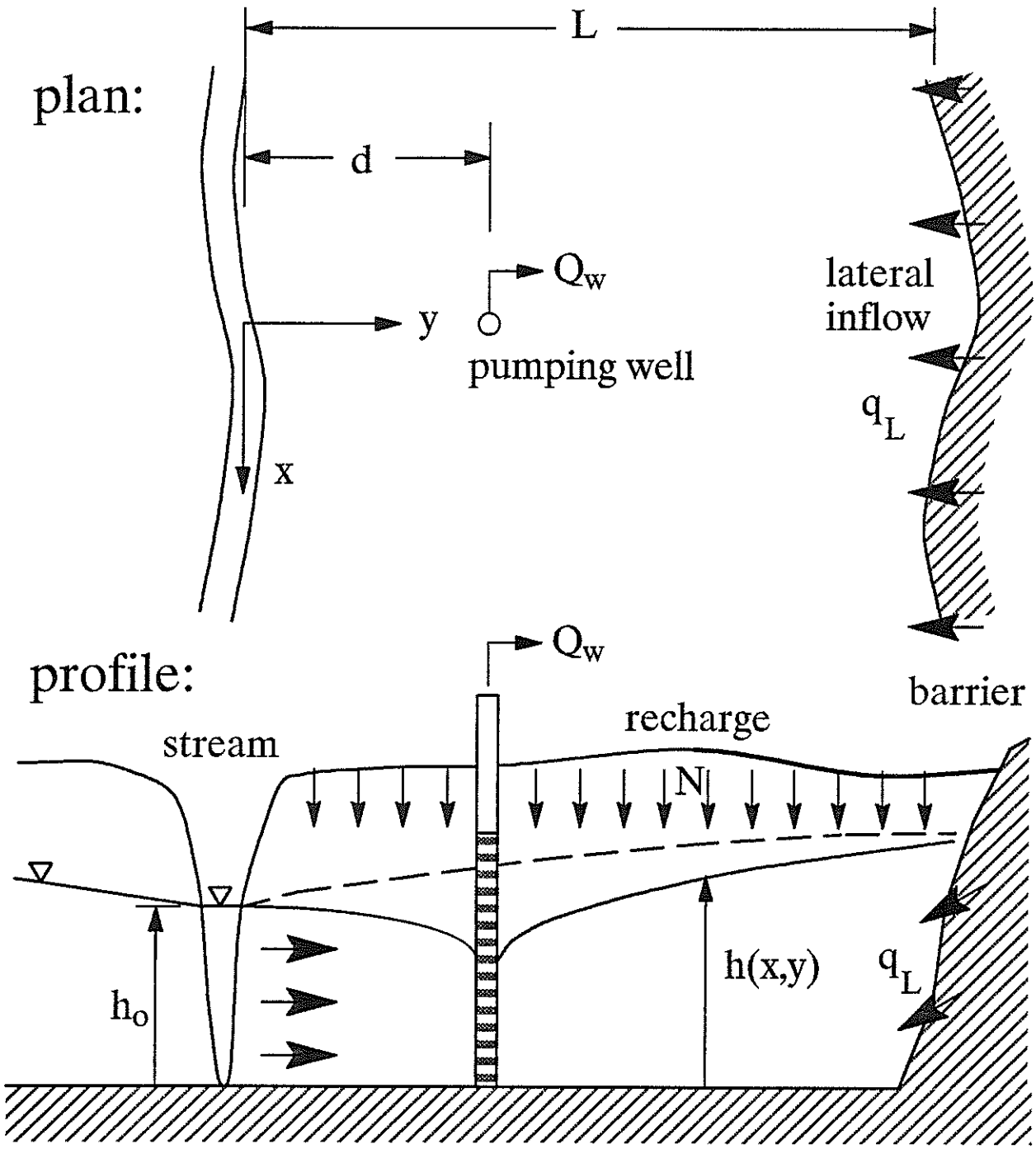

Figure 2–5 Schematic of a pumping well located between a stream and a barrier.

The aquifer of Figure 2−5 is sometimes refered to as an infinite strip aquifer. The flow field is described by the Poisson equation, $\nabla^2\Phi = -N$, where the same definitions apply. The aquifer can be confined or phreatic. The stream is assumed to be a constant head boundary and the barrier is a prescribed flux boundary. This linear flow problem is decomposed into two parts. In the first part we find the ambient head Φ_a before pumping by solving the one dimensional Poisson equation across the aquifer along axis y, for any x. The result is $\Phi_a(x,y) = \Phi_o + q_L y + Ny(2L-y)/2$. The first two terms are analogous to the first two terms in (2−2) for the semi−infinite aquifer. The third term represents the effect of local recharge. The second part of the solution addresses the drawdown due to the well. Here the Laplace equation applies and we take the barrier boundary as a no−flow boundary. A series solution for this case can be found by image well analysis, but it converges slowly. Conformal mapping provides an exact approach. The Schwarz−Christoffel transform (see, eg, Milne−Tompson, 1968) is appropriate, where the transformed space for an infinite strip is the semi−infinite quarter space shown in Figure 2−6. Representing the strip by the complex coordinate $z = x + iy$, and the transformed space by $\zeta = \xi + i\,\eta$, the transformation is $\zeta = \exp(\pi z/2L)$, where $i=\sqrt{-1}$. In the transformed domain we can simulate both the stream and the barrier with only three image wells, as illustrated in Figure 2−6b. The real well is located at $\zeta_w = \exp(i\pi d/2L)$. When we subtract this drawdown from the ambient head Φ_a, we get an expression for head and flow anywhere in the aquifer, as influenced by both ambient flow and pumping:

$$\Omega(x,y) = \Phi + i\Psi = \Phi_o + \left\{ \left[\frac{Ny(2L-y)}{2} + q_L y \right] + i \left[-Nx(L-y) - q_L x \right] \right\} + \frac{Q_w}{2\pi} \left[\ln\left(\frac{\zeta - \zeta_w}{\zeta - \zeta_w^*} \right) + \ln\left(\frac{\zeta + \zeta_w^*}{\zeta + \zeta_w} \right) \right]. \qquad (2-8)$$

The symbol Ω represents the complex potential, and the * indicates a complex conjugate. The real part of this equation represents the head, via Φ, while the imaginary part represents the stream function, Ψ. The first term is the constant head boundary at the stream. The second term is due to the ambient flow caused by local recharge N and lateral inflow q_L. The last term is due to the pumping. We have included the stream function caused by the ambient flow as the imaginary part of the second term. It changes with distance from the stream because of the local recharge.

The discharge to or from the stream q_o is found by differentiating the complex potential (2−8), and evaluating the resulting expression for $-\partial\Phi/\partial y$ along the x−axis, y=0. The differentiation is based on the condition (eg, Milne−Thomson, 1968):

$$\frac{d\Omega}{dz} = \frac{\partial\Phi}{\partial x} + i\,\frac{\partial\Psi}{\partial x} = \frac{\partial\Psi}{\partial y} - i\frac{\partial\Phi}{\partial y} = -q_x + iq_y \qquad (2-9)$$

which yields the velocity (discharge per width) field for the model ($q_x = -\partial\Phi/\partial x, q_y = -\partial\Phi/\partial y$). We seek the imaginary part of the second expression. In this case it is given by

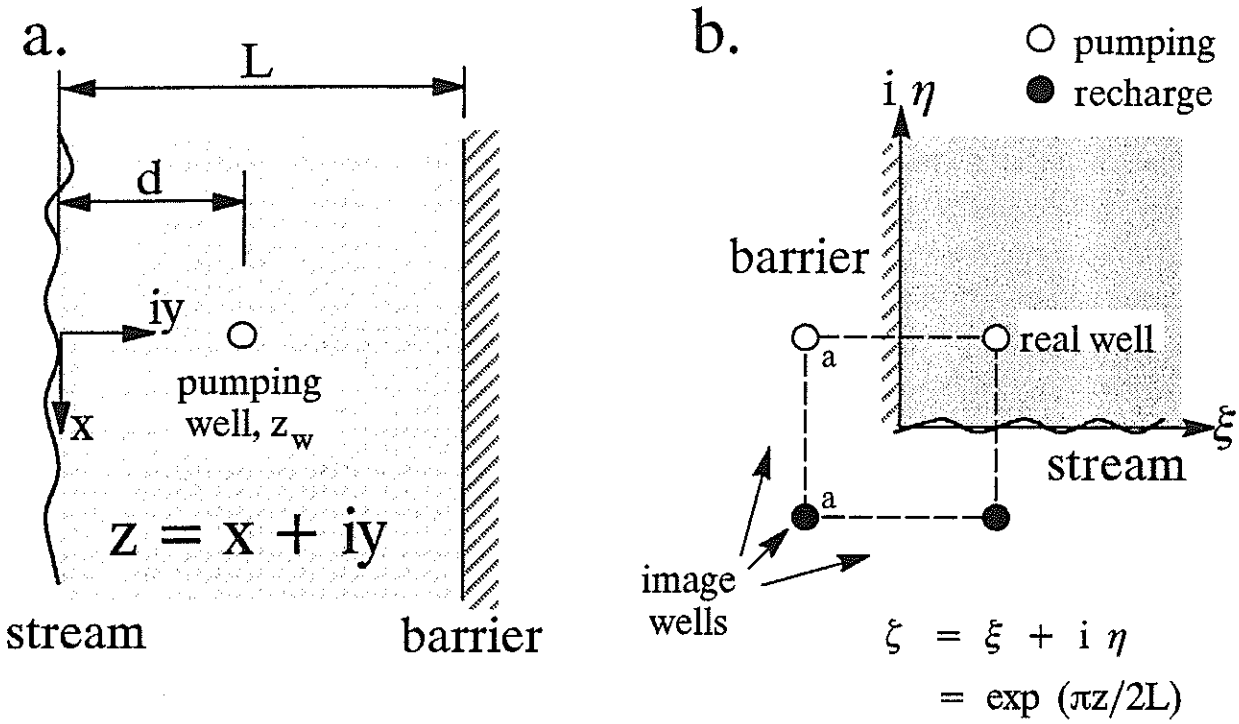

Figure 2–6 Transformation of a) the infinite strip aquifer into b) a semi–infinite quarter space aquifer where the boundary conditions are preserved with three image wells.

$$\frac{d\Omega}{dz} = i\,[\,-N(L-y)-q_L\,] + \frac{Q_w}{2L}\left[\frac{1}{\frac{\zeta}{\zeta_w}-\frac{\zeta_w}{\zeta}} - \frac{1}{\frac{\zeta}{\zeta_w^*}-\frac{\zeta_w^*}{\zeta}}\right] \qquad (2-10)$$

where $\partial/\partial z = (\pi\zeta/2L)\partial/\partial\zeta$ has been used. To evaluate this expression we substitute in the transform $\zeta = \exp(\pi z/2L) = \exp(\pi x/2L)[\cos(\pi y/2L) + i\sin(\pi y/2L)]$ and expand, using the definitions of $\sinh x = 1/2\,[e^x - e^{-x}]$ and $\cosh = 1/2\,[e^x + e^{-x}]$. The result is

$$\frac{d\Omega}{dz} = i\,[\,-N(L-y)-q_L\,] + \left[\frac{1}{2\sinh(X-X_w)\cos(Y-Y_w) + i\,2\cosh(X-X_w)\sin(Y-Y_w)}\right] - \left[\frac{1}{2\sinh(X-X_w)\cos(Y+Y_w) + i\,2\cosh(X-X_w)\sin(Y+Y_w)}\right], \qquad (2-11)$$

where dimensionless coordinates $X = \pi x/2L$ and $Y = \pi y/2L$ have been introduced. The subscript w represents the well location. This expression can be resolved into real and imaginary parts to yield the velocity field with x and y components

$$q_x = -\,Real\,[\frac{d\Omega}{dz}] = -\frac{\partial\Phi}{\partial x} =$$

$$\frac{Q_w}{4L\cosh(X - X_w)}\Big[\frac{\cos(Y - Y_w)\tanh(X - X_w)}{\cos^2(Y - Y_w)\tanh^2(X - X_w) + \sin^2(Y - Y_w)}$$

$$- \frac{\cos(Y + Y_w)\tanh(X - X_w)}{\cos^2(Y + Y_w)\tanh^2(X - X_w) + \sin^2(Y + Y_w)}\Big], \quad (2-12a)$$

$$q_y = Img\,[\frac{d\Omega}{dz}] = -\frac{\partial\Phi}{\partial y} =$$

$$-[\,N(L - y) + q_L\,]$$

$$+ \frac{Q_w}{4L\cosh(X - X_w)}\Big[\frac{\sin(Y - Y_w)}{\cos^2(Y - Y_w)\tanh^2(X - X_w) + \sin^2(Y - Y_w)}$$

$$- \frac{\sin(Y + Y_w)}{\cos^2(Y + Y_w)\tanh^2(X - X_w) + \sin^2(Y + Y_w)}\Big]. \quad (2-12b)$$

For the well location as defined in Figure 2−5 we have $X_w = 0$ and $Y_w = \delta$, and along the stream $Y=0$. With these substitutions Equation (2−12b) yields the flow to or from the stream:

$$q_o(x) = q(x,0) = -\frac{\partial\Phi}{\partial y}\Big|_{y=0} = -q_a + \frac{Q_w}{2L\cosh(X)}\left[\frac{\sin\delta}{(\cos^2\delta\,\tanh^2 X + \sin^2\delta\,)}\right] \quad (2-13)$$

where

$$q_a = (q_L + NL), \quad (2-14a)$$
$$\delta = \pi d/2L, \text{ and} \quad (2-14b)$$
$$X = \pi x/2L. \quad (2-14c)$$

The symbol q_a represents the ambient discharge to the stream, and it equals the lateral inflow and local recharge. The other two factors are scaled dimensionless distance to well and x−coordinate, respectively. The critical pumping rate is found by setting the discharge in (2−13) to zero, and can be expressed either as a dimensionless function of well location d,

$$\beta_c = \frac{Q_c}{\pi d q_a} = \frac{\sin\delta}{\delta}, \quad (2-15a)$$

or as a function of aquifer size L,

$$\alpha_c = \frac{Q_c}{2Lq_a} = \sin\delta\,. \quad (2-15b)$$

These two functions are plotted in Figure 2−7. Incidentally, the velocities in equations (2−12a) and (2−12b) can also be used to define capture zones for the well, as described in Section 3.

For pumping greater than the critical value the stagnation points $\pm x'$ are found by setting (2−13) to zero and solving for $x'=x$. We express the results in terms of the dimensionless pumping rate, $\alpha = \beta\delta = Q_w/2Lq_a$, as a function of the dimensionless distance $X' = \pi x'/2L$:

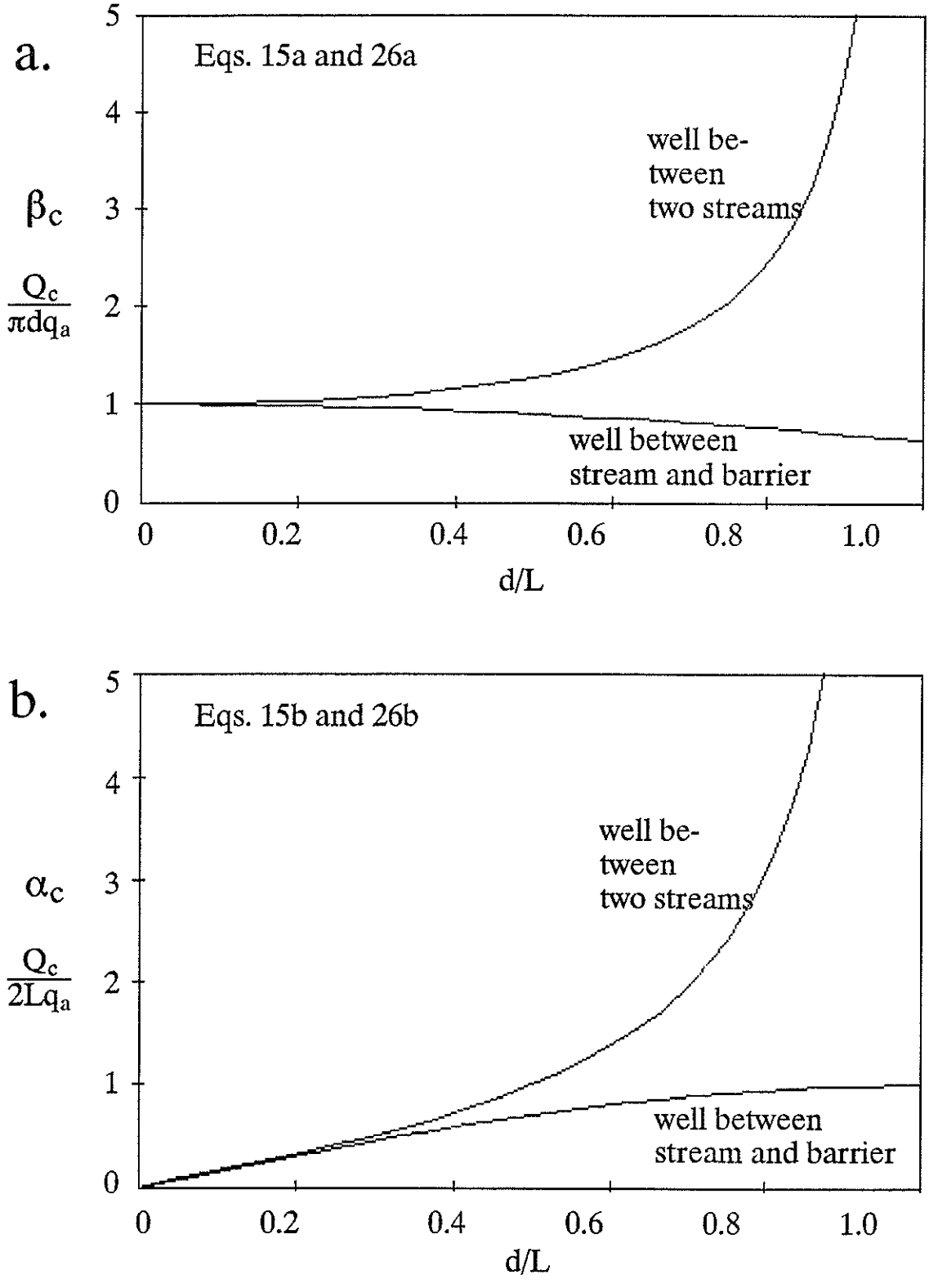

Figure 2–7 Critical dimensionless pumping rate necessary to induce infiltration as a function of well location (d/L) scaled by a) distance from the stream (d), and b) distance between barrier and stream (L).

$$\alpha = \frac{Q_w}{2Lq_a} = \beta\delta = \frac{\cosh X'}{\sin\delta}\ (\sin^2\delta\ +\ \cos^2\delta\ \tanh^2 X'\ ). \qquad (2-16)$$

Induced infiltration is found by integrating the discharge (2−13) between these limits,

$$Q_s\ =\ -\ 2q_a x' + \frac{2Q_w}{\pi}\sin\delta \int_0^{X'} \frac{dX}{(\sin^2\delta\ +\ \cos^2\delta\ \tanh^2 X)\ \cosh X}\ , \qquad (2-17)$$

where we have used the symmetry about the y axis. The integral in the last term, represented below by the symbol I, is evaluated by a change of variables, $w = \sin^{-1}(\tanh X)$, so that it becomes

$$I = \int_0^{w'} \frac{dw}{(\sin^2\delta + \cos^2\delta\ \sin^2 w)} = \frac{1}{\sin\delta}\tan^{-1}\left(\frac{\tan w'}{\sin\delta}\right)\ , \qquad (2-18)$$

where w′ is evaluated at X′. By definition $\tan w' = \sinh X'$. The final dimensionless form of the induced infiltration equation for a well between a stream and a barrier is:

$$\frac{Q_s}{Q_w} = \frac{2}{\pi}\left[\frac{-X'}{\alpha} + \tan^{-1}\left(\frac{\sinh X'}{\sin\delta}\right)\right]$$

$$= \frac{-2x'q_a}{Q_w} + \frac{2}{\pi}\tan^{-1}\left(\frac{\sinh \pi x'/2L}{\sin \pi d/2L}\right). \qquad (2-19)$$

The rate of infiltration for a given pumping rate is found by substituting in the stagnation point solution from (2−16). The results are plotted in Figure 2−8. The results depend only on the magnitude of the ambient discharge, q_a, and not its composition, and are indifferent to the type of aquifer, whether it is confined or phreatic.

Figures 2−7b and 2−8b describe what happens for an aquifer of a fixed width, L, as a well is moved to different positions, d. If instead the well is located a fixed distance from the stream, but in aquifers of different widths, the description is contained in Figures 2−7a and 2−8a.

In finite width aquifers, a well located on the barrier boundary can be pumped hard enough to induce infiltration, after it has used up the available water from local recharge and ambient flow ($\alpha_c \rightarrow 1$ as $d/L \rightarrow 1$; Figure 2−7b). As the well is moved closer to the stream it takes less pumping to induce infiltration ($\alpha_c \rightarrow 0$ as $d/L \rightarrow 0$). For pumping above the critical value, the rate of infiltration increases with higher pumping rates, less local recharge and lateral inflow, and decreasing distance to the stream (Figure 2−8b). When local recharge and lateral inflow are negligible ($\alpha > 100$), or when wells are located very near the stream ($d/L < 10^{-4}$ for $\alpha > 0.1$), almost all of the pumped water is induced infiltration.

For a well located at a fixed distance, d, from a stream, the pumping rate necessary to induce infiltration increases in larger aquifers (Figure 2−7a). The well simply has more aquifer from which to draw its recharge, and depends less on induced infiltration. When the aquifer is five or more times wider than the distance from well to stream, the critical pumping rate approaches the asymptotic value found for semi−infinite aquifers ($\beta_c \rightarrow 1$, Figure 2−7a). For pumping rates sig-

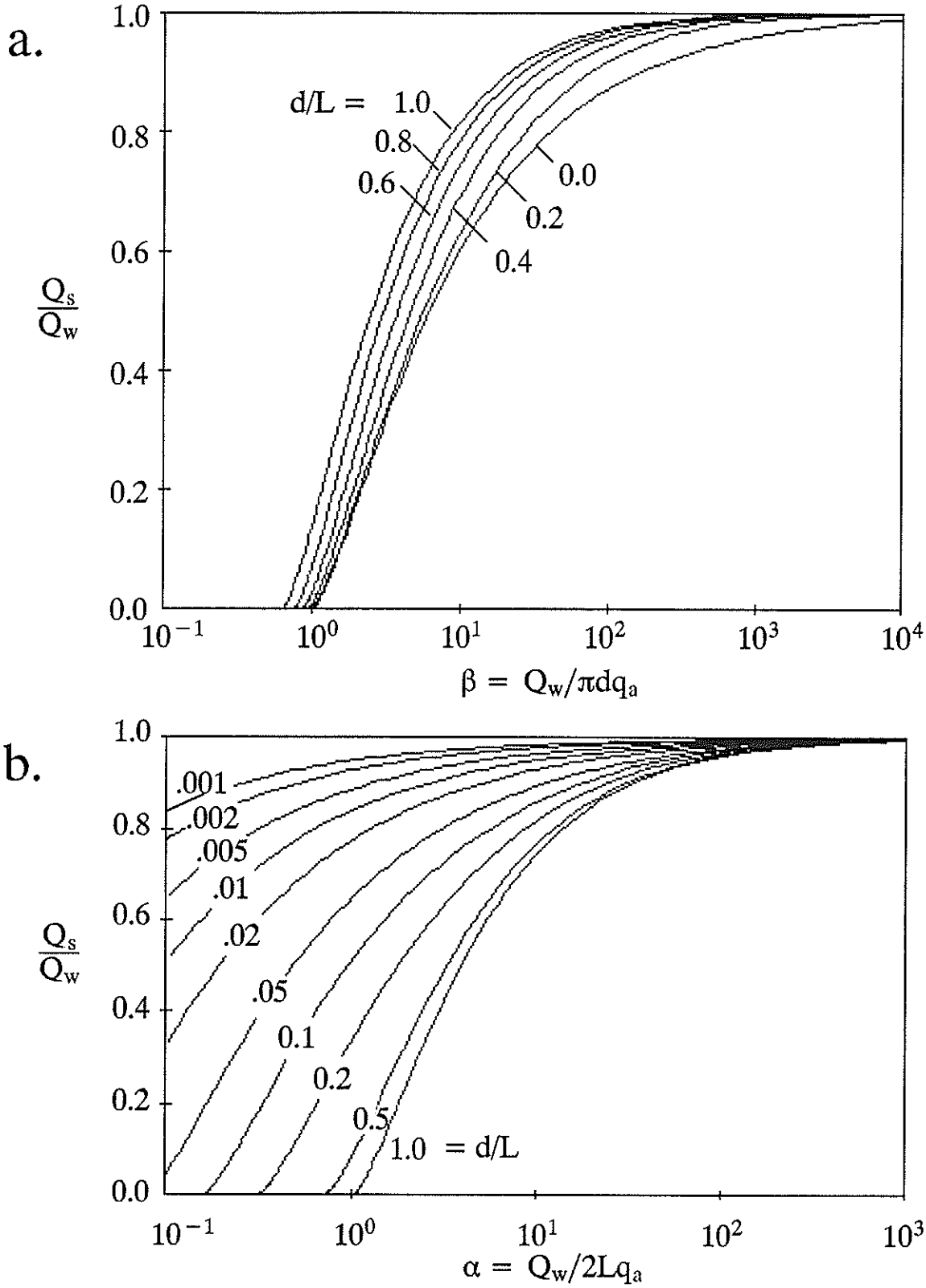

Figure 2–8 Induced infiltration from a well located between a stream and a parallel barrier, as a function of dimensionless pumping rate, and ambient discharge to the stream, $q_a=NL+q_L$, scaled by a) distance from the stream (d), and b) distance between the stream and the barrier (L).

nificantly above the critical value, the rate of induced infiltration is substantially higher in finite width aquifers, as described by the fairly compact envelop of curves in Figure 2−8a. The lower curve in the figure represents the semi−infinite case, d/L =0. Comparing this case to d/L = 0.2, we see that the critical pumping rate is the same, but when pumping at $\beta = 100$, the finite aquifer has almost 5% more induced infiltration. As pumping increases, the well has a greater propensity to 'feel' the presence of the barrier boundary, and thus a greater potential to induce infiltration. For fixed d in small aquifers (d/L→ 1), the barrier is closer to the well than is the stream,. When the barrier is adjacent to the well, the amount of pumping necessary to induce infiltration is only slightly less than that required in a semi−infinite aquifer ($\beta_c = 2/\pi \approx 0.64$compared to 1.0; Figure 2−7a). The results in both Figures 2−7a and 2−8a are somewhat surprising in that aquifer size seems to count for so little. This misleading conclusion ignores the role of ambient discharge to the stream, a normalizing factor in the curves, which would typically be smaller in smaller aquifers.

In summary, the presence of the barrier boundary increases the propensity for, and rate of, induced infiltration. Induced infiltration is independent of the mix of lateral inflow and local recharge, and does not depend on whether the aquifer is confined or phreatic.

WELL BETWEEN TWO STREAMS

Let us now look at the case of a well located between two streams as depicted in Figure 2−9. This situation is typical for many watersheds. It could also be used to conceptualize a well pumping between irrigation and drainage canals. The streams can have the same or different elevations, h_1 and h_2, and there is local recharge N between them. The well draws water from the local recharge, and, for sufficiently strong pumping, induces infiltration from one or both streams. As we will see, the well always draws some water from the higher stream when that stream is high enough to be losing under ambient conditions.

This is another confined or phreatic strip aquifer with the flow described by the Poisson equation, $\nabla^2\Phi = -N$. Each stream is treated as a constant head boundary. The ambient head, Φ_a, is found by solving the one−dimensional Poisson equation across the aquifer, and is described by $\Phi_a(x,y) = \Phi_1 + (\Phi_2 - \Phi_1)y/L + Ny(L-y)/2$. The first two terms represent the effects of stream elevation. The third term represents the mounding caused by local recharge. The well drawdown is again calculated using a Schwarz−Christoffel transform. The transformed space for an infinite strip aquifer bounded by two streams is a semi−infinite half space with a constant head boundary on the side. In this decomposed problem, both streams are assigned the same prescribed head, $\Phi = 0$, and are represented through a single image recharge well. The new transformation is $\zeta = \exp(\pi z/L)$. Alternatively, one could use the previous transform, by exchanging the sign of the two image wells that are labled 'a' in Figure 2−6. Either way we determine the drawdown and subtract it from the ambient head Φ_a, yielding the following expression for head and flow as represented by the complex potential:

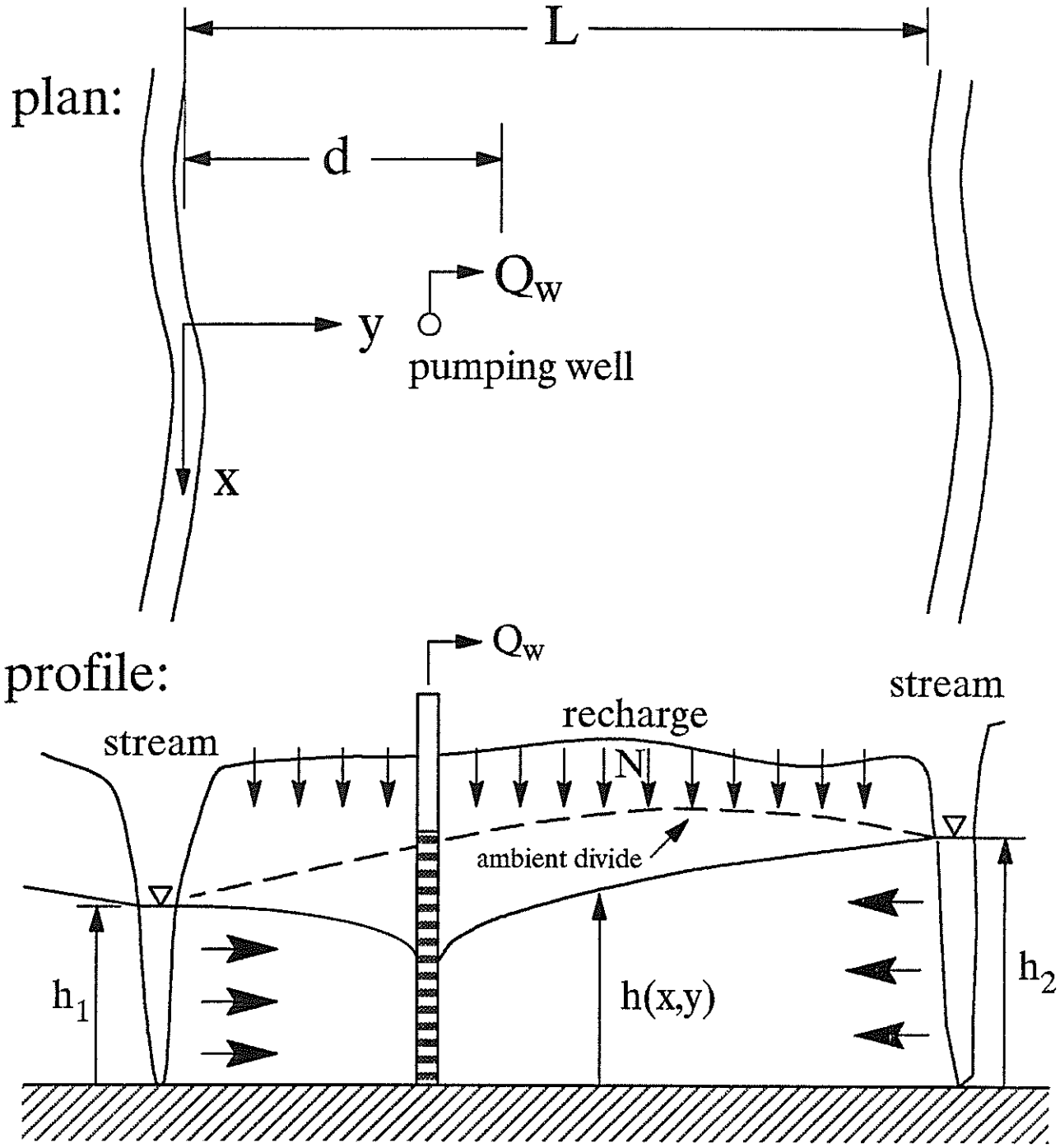

Figure 2–9 Schematic of a pumping well located between two parallel streams.

$$\Omega(x,y) = \Phi + i\Psi$$

$$= \left[\frac{Ny(L-y)}{2} + \frac{(\Phi_2 - \Phi_1)}{L}\, y + \Phi_1 \right] + i \left[\frac{-Nx(L-2y)}{2} - \frac{(\Phi_2 - \Phi_1)}{L}\, x \right]$$
$$+ \frac{Q_w}{2\pi}\left[\ln\left(\frac{\zeta - \zeta_w}{\zeta - \zeta_w^*} \right) \right] \qquad (2-20)$$

The discharge to or from the streams is easily found by differentiation,

$$\frac{d\Omega}{dz} = i \left[\frac{-N(L-2y)}{2} - \frac{\Phi_2 - \Phi_1}{L} \right] + \frac{Q_w}{2L}\left[\frac{1}{1 - \frac{\zeta_w}{\zeta}} - \frac{1}{1 - \frac{\zeta_w^*}{\zeta}} \right], \qquad (2-21)$$

where $\partial/\partial z = (\pi\zeta/L)\partial/\partial\zeta$ has been used. Again we substitute in the transform $\zeta = \exp(\pi z/L)$ and expand, leading to the x and y components of the velocity field,

$$q_x = -\,Real\,[\frac{d\Omega}{dz}] = -\frac{\partial\Phi}{\partial x} =$$

$$+ \frac{Q_w}{4L}\left[\frac{\exp - (2X_w - 2X) - \cos(2Y_w - 2Y)}{\cosh(2X_w - 2X) - \cos(2Y_w - 2Y)} + \frac{\exp - (2X_w - 2X) - \cos(2Y_w + 2Y)}{\cosh(2X_w - 2X) - \cos(2Y_w + 2Y)} \right] \qquad (2-22a)$$

$$q_y = Img\,[\frac{d\Omega}{dz}] = -\frac{\partial\Phi}{\partial y} =$$

$$- \frac{N(L-2y)}{2} - \frac{\Phi_2 - \Phi_1}{L}$$

$$+ \frac{Q_w}{4L}\left[\frac{\sin(2Y_w - 2Y)}{\cosh(2X_w - 2X) - \cos(2Y_w - 2Y)} + \frac{\sin(2Y_w + 2Y)}{\cosh(2X_w - 2X) - \cos(2Y_w + 2Y)} \right] \qquad (2-22b)$$

where the same dimensionless parameters X and Y are used. Finally, for the well location in Figure 2−9, the flow to or from the stream is found by setting $X_w = 0$, $Y_w = \delta$ and $Y=0$ in (2−22b):

$$q_o(x) = q(x,0) = -\left.\frac{\partial\Phi}{\partial y}\right|_{y=0}$$
$$= -q_a + \frac{Q_w}{2L}\left[\frac{\sin(2\delta)}{\cosh(2X) - \cos(2\delta)} \right]. \qquad (2-23)$$

The ambient discharge to the stream is

$$q_a = \frac{NL}{2} + \frac{\Phi_2 - \Phi_1}{L}, \qquad (2-24)$$

while $\delta = \pi d/2L$ and $X = \pi x/2L$ are the same dimensionless parameters used for the stream−barrier case. The discharge to or from the stream at x=L is given by a similar expression. In fact,

we can assume that (2−23) applies to either stream by reorienting the coordinate system so that y and d are measured from the stream of interest. Please note that we have not yet made assumptions about the relative magnitude of Φ_1 and Φ_2. Finally, these equations are again independent of the aquifer type, whether it is confined or phreatic.

The rate of local recharge, N, plays a significant role in determining sources of pumped water. If the rate is sufficiently large, a groundwater divide forms between the streams, as illustrated in Figure 2−9, and both streams receive ambient discharge from the aquifer. Induced infiltration for this case is given below. If the rate is sufficiently small, and the streams are of unequal elevation, then there is no divide. Under ambient conditions, the critical recharge rate below which no divide occurs is given by

$$N_c = 2\frac{|\Phi_2 - \Phi_1|}{L^2}, \qquad (2-25)$$

which is found by equating (2−24) equal to zero. The higher, or upper stream loses water to the aquifer while the lower stream gains the discharge. In this case, there is no need for pumping in order to induce infiltration from the upper stream, it loses water naturally ($q_a < 0$). A well pumping from this aquifer will always sample both the local vertical recharge and this natural throughflow from losing stream to gaining stream, whatever the pumping rate. In this case, it is necessary to actually model capture zones in order to determine how much of the pumped water comes from the upper stream, and how much comes from local recharge.

The critical pumping rate necessary to induce infiltration is found by setting the discharge in (2−23) to zero, yielding

$$\beta_c = \frac{Q_c}{\pi d q_a} = \frac{\tan\delta}{\delta} \text{ and } \alpha_c = \frac{Q_c}{2Lq_a} = \tan\delta \qquad (2-26a,b)$$

where $\alpha = \beta\delta$. These two functions are plotted in Figure 2−7 for positive values of ambient discharge to the stream. For pumping greater than the critical value, the stagnation points $\pm x'$ are found by setting (2−23) equal to zero and solving for

$$\alpha = \frac{Q_w}{2Lq_a} = \beta\delta = \frac{\cosh(2X') - \cos(2\delta)}{\sin(2\delta)}. \qquad (2-27)$$

as a function of the dimensionless distance $X' = \pi x'/2L$. Induced infiltration is found by integrating the discharge (2−23) between these limits,

$$Q_s = -2q_a x' + \frac{2Q_w}{\pi}\sin 2\delta \int_0^{X'} \frac{dX}{\cosh 2X - \cos 2\delta} \; . \qquad (2-28)$$

The integral in the last term is evaluated by using formula 2.443.3 in Gradshteyn and Ryzhik (1980), leading to the final dimensionless form of the induced infiltration equation for a well between a two parallel streams:

$$\frac{Q_s}{Q_w} = \frac{2}{\pi}\left[\frac{-X'}{\alpha} + \frac{1}{2}\cos^{-1}\left\{\frac{1-\cosh(2X')\cos(2\delta)}{\cosh(2X')-\cos(2\delta)}\right\}\right]$$

$$= \frac{-2x'q_a}{Q_w} + \frac{1}{\pi}\cos^{-1}\left[\frac{1-\cosh(\pi x'/L)\cos(\pi d/L)}{\cosh(\pi x'/L)-\cos(\pi d/L)}\right] \qquad (2-29)$$

The rate of infiltration for a given pumping rate is found by substituting in the stagnation point solution from (2−27). The results are plotted in Figure 2− 10.

Figures 2−7b and 2−10b describe what happens for an aquifer of a fixed width, L, as a well is moved to different locations between the streams. If instead the well is located a fixed distance from one of the streams, but in aquifers of different widths, the description is contained in Figures 2−7a and 2−10a.

In finite width aquifers, the amount of pumping necessary to induce infiltration from a stream depends on the proximity of the well to the stream (Figure 2−7b). By symmetry arguments a well located midway between the two streams will induce infiltration from both streams at the same pumping rate ($\alpha_c = 1$). A well located farther from one stream than the other, preferentially induces infiltration from the nearer stream. For example, a well three times farther from one than another will induce infiltration from the closer stream at a rate far smaller than one third of the rate it takes to induce infiltration from the other ($\alpha_c = 0.41$ at d/L= 0.25 vs. $\alpha_c = 2.41$ at d/L= 0.75 in Figure 2−7b). When a well is located very close to one stream, and far from the other, then it is difficult to induce infiltration from the far stream unless it is significantly higher in elevation. In this case, the critical pumping rate for induced infiltration from the near stream approaches that for the semi−infinite aquifer ($\beta_c \rightarrow 0$ as d/L$\rightarrow$ 0; Figure 2−7a).

Once the critical pumping rate is exceeded, the rate of induced infiltration from a stream increases with higher pumping rates, less ambient discharge to the stream, and decreasing distance between the stream and the well (Figure 2−10b). For a sufficiently high pumping rate ($\alpha \gtrsim 200$), the amount of induced infiltration from a stream is inversely proportional to its position within the aquifer. Thus the well that is located three times farther from one stream tha the other, ultimately draws three times more water from the nearer stream than the farther. Wells located much nearer one stream than another behave as if they were in a semi−infinite aquifer (compare Figures 2−8 and 2−10 for d/L=0.1 and 0.2).

Figure 2−11 illustrates what happens for a well located 1/5th of the distance across the aquifer (d/L=0.2 from the near stream and d/L=0.8 from the far stream). At a low pumping rate, all water comes from local recharge. The well's capture zone does not extend as far as either stream (see Section 3). At a slightly higher pumping rate ($\alpha_c = 0.32$), the well begins to induce infiltration from the near stream. Increased pumping induces infiltration from this stream and increases the size of the well's capture zone within the aquifer. But its not until the pumping rate reaches a substantially higher rate ($\alpha_c = 3.08$) that the capture zone actually extends far enough to induce infiltration from the far stream. When the pumping rate increases an additional order of magni-

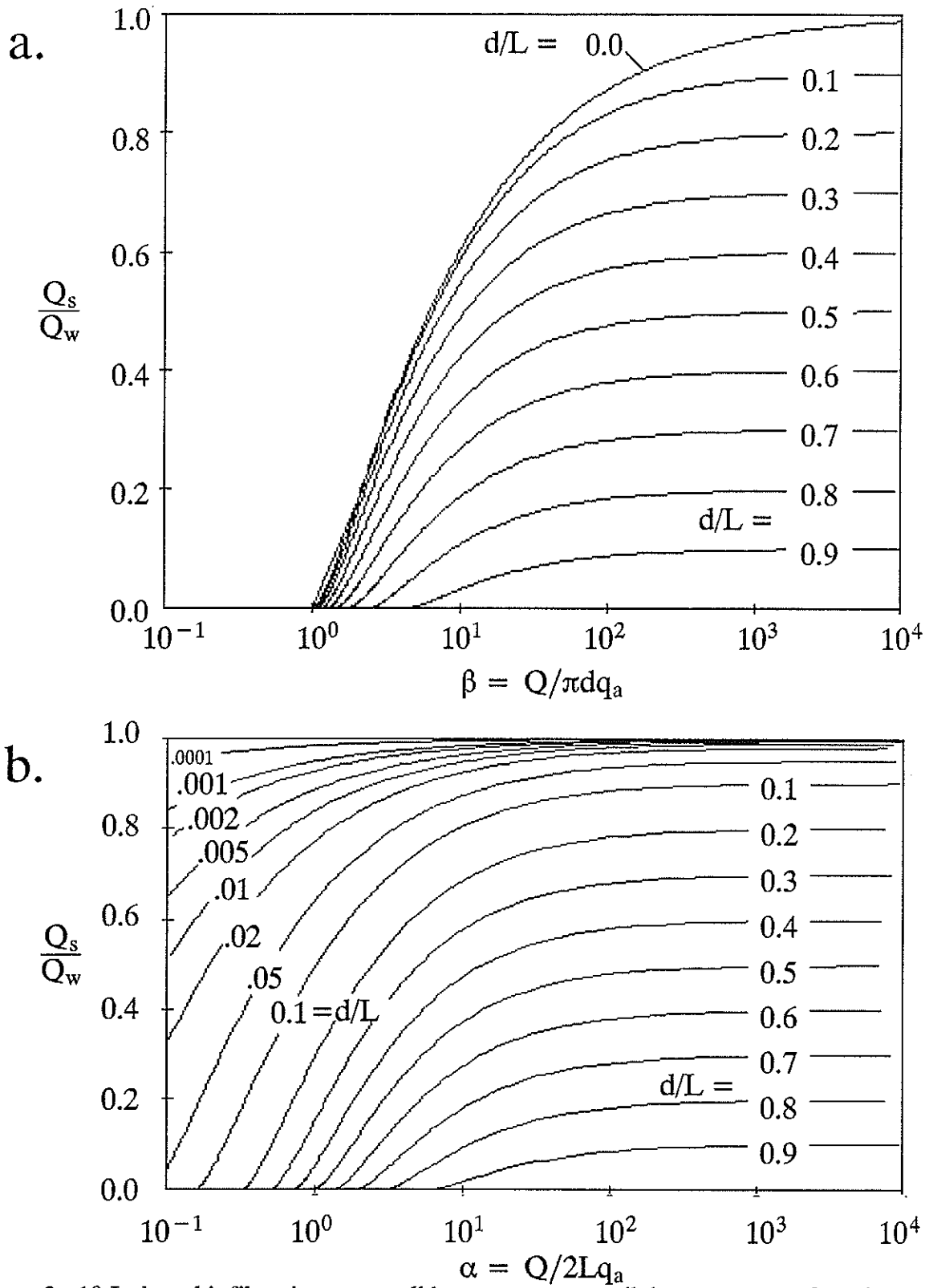

Figure 2–10 Induced infiltration to a well between two parallel streams, as a function of dimensionless pumping rate, and ambient discharge to the stream of interest (q_a). scaled by a) distance from the stream of interest (d), and b) distance between the two streams (L).

tude ($\alpha \geq 200$), almost all pumped water comes from induced infiltration. The amount from each stream is inversely proportional to the distance between the well and the stream. The size of the capture zone, and the amount of local recharge withdrawn, grows with each increase of pumping rate, even as the local recharge becomes less important compared to the induced infiltration.

In summary, the presence of the second stream boundary decreases the propensity for and the rate of induced infiltration from the first stream. The second stream offfers an additional source of recharge. Once again, the induced infiltration rate does not depend on whether the aquifer is confined or phreatic, or on the source of the ambient flow, as long as the considered stream is a gaining stream. They do not apply to a losing stream.

SUMMARY AND CONCLUSIONS

Induced infiltration causes a gaining stream to become, at least locally, a losing stream. There are two induced infiltration problems. Where water rights are at issue, the problem is one of streamflow depletion. Where water quality is the issue, the problem is identifying the actual water sources, each with their own chemical fingerprint. The streamflow depletion problem has been studied for years; the water quality problem has not. Because of the potential for pollution of both ground and surface waters from varied sources and by varied pollutant species, quantification of the amount of induced infiltration is an important factor in evaluating the reliability of well–water quality.

In this Section we have presented several simple models that address this problem. The models help with our understanding of induced infiltration phenomena, and can provide a 'first cut' analysis of alternative well field designs and pumping rates from a water quality perspective, or assist in the delineation of well–head protection zones. They may also be of some help in characterizing past pollution events involving wells, aquifers, and streams or other surface water bodies.

The models are presented in the form of dimensionless curves, describing the conditions under which induced infiltration occurs and giving the amount of induced infiltration as a percentage of well discharge. Under ambient conditions, the surface water body is assumed to be gaining, supplied by ambient aquifer flow. Under pumping conditions, the well captures a combination of induced infiltration stream water, and ambient aquifer flow from both local vertical recharge and lateral inflows. The aquifer is assumed to be homogeneous and isotropic. The surface water body and the well are assumed to fully penetrate the aquifer; the flow is essentially horizontal. In a phreatic aquifer, the drawdown is assumed to be small compared to saturated thickness, leading to the Dupuit approximation. The surface water body is assumed to be hydraulically connected to the aquifer, and the 'skin effect' caused by a possible clogging layer of low conductivity lining the surface water body is ignored. Temperature variation and its effect on aquifer hydraulic conductivity is also ignored. Equilibrium (steady–state) conditions are assumed; the approach is most applicable to average long–term conditions at 'continuously' used water supply wells. Although we have used the term 'stream' consistently in the text, the approach also applies to ponds, lakes, and wetlands.

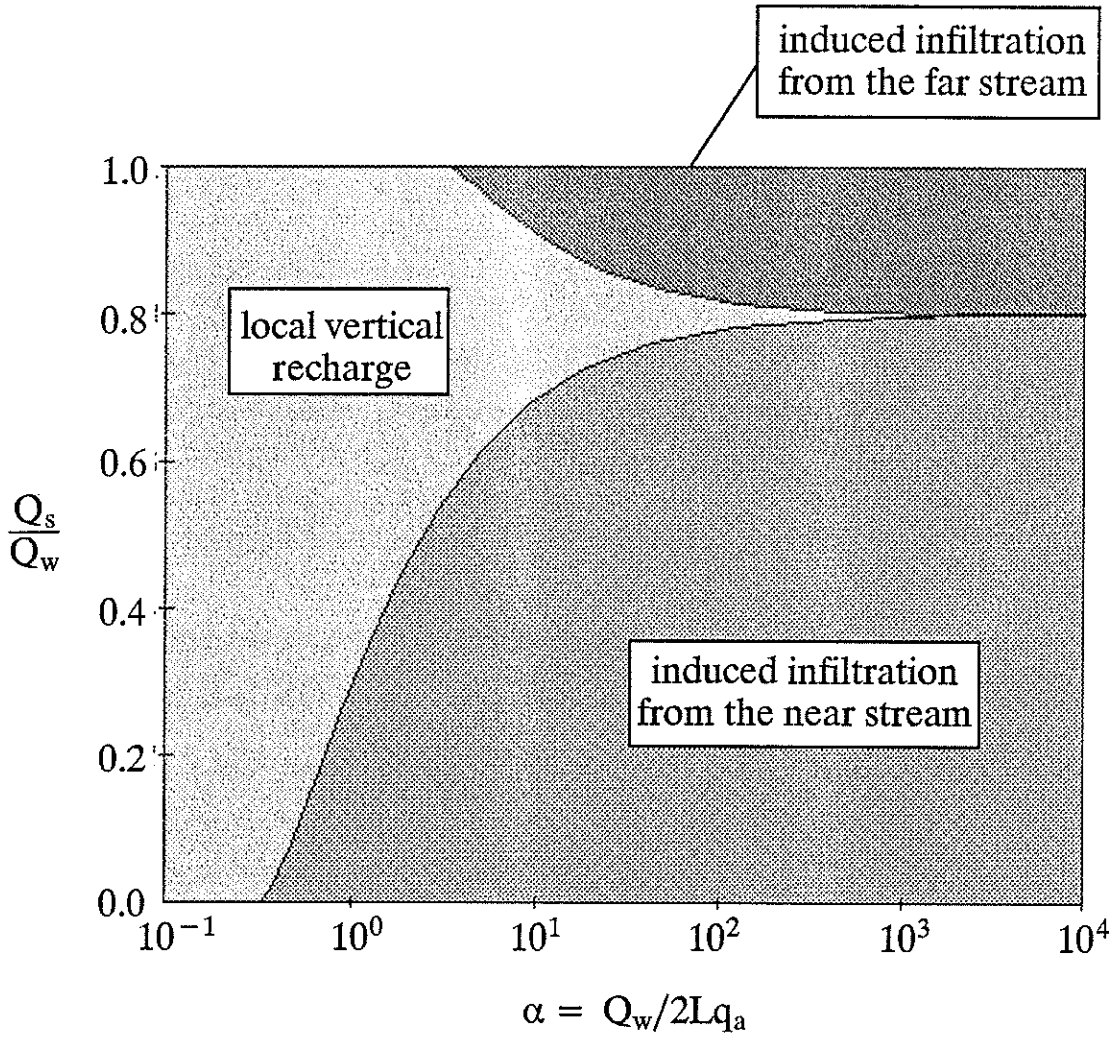

Figure 2–11 Induced infiltration to a well from each of the two parallel streams (darker greys), as a function of the dimensionless pumping rate scaled by the distance between the two streams (L). The well is located at a distance of 0.2L from the near stream and 0.8L from the far stream.

Induced infiltration to wells located near streams is essentially independent of the source of ambient discharge to the stream, whether it's local recharge or some lateral inflow. Infiltration also appears to be indifferent to the form of the essentially horizontal flow model used to examine it (eg, confined or phreatic).

For a gaining stream it takes a critical pumping rate to induce water to leave the stream, enter the aquifer, and travel to the well. Pumping at rates greater than this critical value induces infiltration and leads to a mixture of water of different origins and quality in the well bore. The propensity for and rate of induced infiltration increases with pumping rate, decreasing distance between the well and the stream, and lower ambient discharge to the stream. If the aquifer is finite, and there is a nearby parallel barrier boundary, induced infiltration is enhanced. The well's cone of depression is reflected off the boundary, increasing the hydraulic gradient from the stream to the aquifer. The closer the well is to the barrier boundary, the greater the amount of induced infiltration. If the finite aquifer is bounded by two parallel streams, the induced infiltration from either one is reduced by the presence of the other, which acts as an additional source of recharge.

SECTION 3

TWO–DIMENSIONAL CAPTURE ZONES

INTRODUCTION

Well-water quality depends on the relative amounts of water drawn from different hydrologic units (aquifers, streams, etc), and the particular capture zones within those units. A contaminant spilled within an aquifer capture zone will enter the well eventually. A spill outside the capture zone may eventually discharge elsewhere, perhaps to the nearby stream. We define two types of capture zones. Steady-state or time-dependent capture zones are defined by the area that will contribute water to the well at any time in the future or within a prescribed time limit, respectively.

Examples of capture zone analyses are given in Wilson (1981), Keeley and Tsang (1983). Javendel and Tsang (1984), Javendel et al. (1984), EPA (1987, 1990), Larson et al. (1987), Shafer (1987a,b), Morrisey (1987), and Bair et al. (1991). With the exception of Wilson (1981) and EPA(1990), most of this work is site specific or looks at the generic situation of a well or wells in an infinite uniform flow field. As described in this section, capture zone geometry is altered by presence of a surface water body, such as a stream or lake. Work related to this issue, and described in this section, has been presented or published by Lee (1986), Lee and Wilson (1986), Newsom and Wilson (1988b), Linderfelt et al. (1989), Wilson and Linderfelt (1989), Leppert (1990), Schafer–Perini (1990), and Schafer–Perini and Wilson (1991a).

In this section we first develop some simple two-dimensional capture zone delineation models for a well located near a stream boundary (Lee, 1986), following the conceptualizations presented in Section 2. These analytical solutions examined capture zones as a function of well location and pumping rate for various hydrogeologic parameters and boundaries. The aquifer is assumed infinite in the direction parallel to the stream with the remaining boundary specified as one of three types: 1) an infinite boundary, 2) a barrier boundary, or 3) a stream boundary. The ambient flow is perpendicular to the stream boundary, for the purpose of examining capture zone delineation with respect to varying pumping rate, Q_w, ambient flow rate, q_a, and distance d of the well from the stream.

Using the above three basic models as templates, we extend the conceptualizations by slight modification of the entire models. This includes adding additional terms such as another well, or varying the representation of existing terms. The variations we will examine here include:

- Ambient Flow at Angle to the Stream Boundary
- Time-Dependent Capture Zones: Fronts
- Multiple Wells
- Aquifer Heterogeneity
- Aquifer Anisotropy

The groundwater flow is considered to be steady and essentially horizontal. In all cases both the surface water body and the well are assumed to fully penetrate the aquifer. In a phreatic aquifer the drawdown is assumed to be small compared to saturated thickness, leading to the Dupuit approximation. The surface water body is assumed to be hydraulically connected to the aquifer, and the 'skin effect' caused by a possible clogging layer of low conductivity lining the surface water body is ignored. Temperature variation and its effect on aquifer hydraulic conductivity is also ignored. As in Section 2 the steady flow approach is most applicable to average long-term conditions at continuously used water supply wells. With the exception of the analyses presented at the end of this section the aquifer is homogeneous and isotropic. Finally, transverse dispersion across capture zone boundary streamlines, and dispersion of time-dependent capture zones is ignored.

We utilize both analytical and numerical flow field solutions in deriving the results presented in this section. Numerical solutions are used as noted in place of analytic derivations because they are sometimes easier to implement; nevertheless, the derivation of the analytic counterpart for all solutions is straightforward. The numerical flow field results are based on a two–dimensional five point finite difference flow code (see Appendix A; Aziz and Settari, 1979; Russel and Wheeler, 1983;) with a multigrid solver (e.g., McCormick, 1987). Side–of–grid block velocities are bilinearly interpolated (see Appendix A; Farmer, 1987; Goode, 1987; Schafer–Perini and Wilson, 1991a). The ultimate capture zone is determined by finding a critical point, usually a stagnation point, and numerically tracking particles backward from it along the dividing streamline that defines the capture zone (Lee, 1986: Lee and Wilson, 1986). These backward paths are almost always convergent, further reducing numerical tracking error. Particles are tracked with an adaptive Euler method using adjustable distance steps (Zheng, 1988; Leppert, 1990). In some of the simpler cases presented, usually those with no local recharge, streamfunction solutions could be directly derived for the dividing streamlines (see equation 2–8). Time-dependent capture zones are defined by adaptively tracking a front of particles moving backwards from the pumping well. This numerical technique is described in Appendix A (Schafer–Perini, 1990; Schafer–Perini and Wilson, 1991a).

THREE BASIC FLOW SCENARIOS

Semi–Infinite System

This system consists of a fully penetrating well in an aquifer with a fully penetrating gaining stream. The aquifer extends to infinity on the right, and to the top and bottom, as shown schematically in Figure 2–1. To compare the numerous scenarios presented in this section, the equation of state and/or boundary conditions are presented where appropriate. The equation of state for the semi–infinite system is given by

$$\frac{\partial^2\Phi}{\partial x^2} + \frac{\partial^2\Phi}{\partial y^2} + Q_w[\delta(x - x_w), \delta(y - y_w)] = 0, \qquad (3-1)$$

subject to the boundary conditions

$$y = 0, \Phi = \Phi_0$$
$$y = \infty, q_L = q_y \qquad (3-2)$$

with the aquifer extending to $\pm\infty$ in the x direction parallel to the stream. The pumping rate is given by Q_w [L^3/T], $(x_w,y_w)= (0,d)$ are the coordinates of the well, $q_a=q_L$ is lateral recharge [L^2/T] = ambient discharge to the stream, and Φ_o is the reference potential or stream stage. The flow potential, Φ, is defined by

$$\Phi = \begin{cases} Th & , \text{ confined or linearized phreatic aquifer,} \\ \frac{Kh^2}{2} & , \text{ Dupuit type phreatic aquifer.} \end{cases} \qquad (3-3)$$

The solution can be found using superposition and is given by (see equation 2−2)

$$\Phi(x,y) = \Phi_o + q_a y - \frac{Q_w}{4\pi} \ln\left[\frac{(y+d)^2 + x^2}{(y-d)^2 + x^2}\right]. \qquad (3-4)$$

Differentiation of Φ with respect to x and y coordinates leads to definition of the velocity field in a Cartesian coordinate system:

$$V_x = \frac{1}{nb}\frac{d\Phi}{dx} \quad ; \qquad V_y = \frac{1}{nb}\frac{d\Phi}{dy} \qquad (3-5)$$

where n is the porosity and b is the aquifer thickness (perhaps approximated by h_o in a phreatic aquifer, where $\Phi_o = Th_o$; see Figure 2−1). For convenience we assume that b is constant, and thus our model is one of a confined or linearized phreatic aquifer. The stagnation point for a given Q_w, q_a, and d is found by setting $V_x=V_y=0$ and solving for the roots, expressed as (x,y) coordinates. The dimensionless pumping rate, β, is defined by $\beta=Q_w/\pi d q_a$. For ambient flow perpendicular to the stream, the stagnation point for pumping less than the critical rate, $\beta < \beta_c$, is located (see Figure 2−2a) at

$$Y' = \frac{y'}{d} = (1-\beta)^{\frac{1}{2}} \ , \qquad X' = \frac{x'}{d} = 0,$$

where β_c is defined as the value of β when the capture zone just reaches the stream boundary (see Section 2; Figure 2−2b). For pumping greater than the critical rate, $\beta > \beta_c$, there are two stagnation points in the domain at (see equation 2−4, and Figure 2−2c)

$$Y' = 0; \qquad X' = \pm\,(\beta - 1)^{\frac{1}{2}}. \qquad (3-6)$$

Between these two points the stream locally becomes a losing stream and induced infiltration occurs. DaCosta and Bennett (1960), Bear and Jacobs (1965), Edelman (1972), Bear (1979), Wilson (1981), Lee (1986), EPA (1990) and others have previously examined capture zones for this situation, or the equivalent geometry consisting of an injection−production well pair in an infinite flow field (simplest model of pump-and-treat schemes).

Delineation of the ultimate capture zone relies on the stagnation point locations. Hypothetical 'particles' are then placed into the negative velocity field, slightly offset from the stagnation point. These particles are then tracked backwards using a numerical adaptive distance−increment tracking scheme to define the dividing streamline that delineates the ultimate capture zone. Examples of three capture zones found using particle tracking are shown in Figure 3−1 where the stream is on the left and the aquifer continues to infinity in the other three directions. These three capture zones correspond to the depiction of subcritical, critical, and supercritical pumprates shown in Figure 2−1.

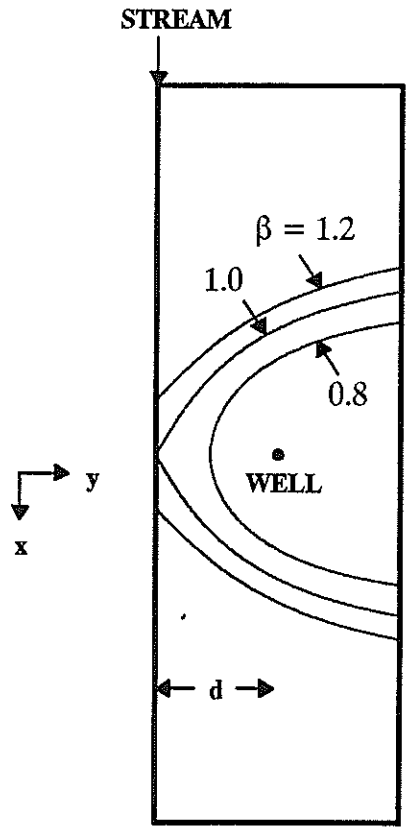

Figure 3–1. Capture zones for a well pumping at three different rates (dimensionless) in a semi-infinite aquifer.

As the pumping rate increases, the capture zone becomes larger. At a low pumping rate, the well depends on the ambient lateral inflow for its pumpage. Upgradient of the well, the capture zone widens until it captures just enough of this ambient flow to satisfy the well. This width is given by $w=Q_w/q_a$. At the critical pumping rate, the capture zone just begins to touch the stream. Induced infiltration occurs at higher pumping rates (see Section 2), as the capture zone intersects the stream. As pumping increases, the rate of growth of the capture zone slows, because there are now two sources that supply water to the well. The capture zone width is given by $w=(Q_w-Q_s)/q_{a,}$, where Q_s is given by (2–6) and Figure 2–3.

Stream–Barrier System

The stream–barrier strip aquifer case is shown in Figure 2–5. The equation of state is:

$$\frac{\partial^2\Phi}{\partial x^2} + \frac{\partial^2\Phi}{\partial y^2} + N + Q_w[\delta(x - x_w), \delta(y - y_w)] = 0 \qquad (3-7)$$

subject to the boundary conditions

$$\begin{aligned} y = 0, \Phi &= \Phi_0 \\ y = L, q_L &= q_y \end{aligned} \qquad (3-8)$$

with the aquifer extending to $\pm\infty$ in the x direction parallel to the stream and barrier boundaries. The term N [L/T] represents spatially uniform vertical recharge to the system.

The solution was derived in Section 2 using conformal mapping techniques. The flow potential is the real part of the complex function Ω, *Real*(Ω), where Ω is given by (2–8):

$$\Omega(x,y) = \Phi + i\Psi = \Phi_o + \left\{ \left[\frac{Ny(2L - y)}{2} + q_L y \right] + i \left[-Nx(L - y) - q_L x \right] \right\} + \frac{Q}{2\pi}\left[\ln\left(\frac{\zeta - \zeta_w}{\zeta - \zeta_w^*}\right) + \ln\left(\frac{\zeta + \zeta_w^*}{\zeta + \zeta_w}\right) \right]. \qquad (3-9)$$

ζ and ζ_w are given by $\zeta = \exp(\pi z/2L)$ and $\zeta_w = \exp(i\pi d/2L)$, respectively, and $i = \sqrt{-1}$. Total recharge to the system and ambient discharge to the stream is given by $q_a = q_L + NL$. The dimensionless pumping rate is defined by $\beta = Q_w/\pi d q_a$. Critical β is given by (2–15), $\beta_c = \sin(\delta)/\delta$ where $\delta = \pi d/2L$. The stagnation point, y′, for $\beta < \beta_c$ is found for x=0 by setting the q_y component (2–12b) to zero:

$$\beta = \frac{-2\delta\,(1 - 2Y'NL/\pi Q_0)\sin(Y' - \delta)\sin(Y' + \delta)}{\sin(Y' + \delta) - \sin(Y' - \delta)} \qquad (3-10)$$

where $Y' = y'\pi/2L$. For $\beta > \beta_c$ the stagnation point at x′ are given by (2–16):

$$\beta = \frac{\cosh X'\left[\cos^2\delta\,\tanh^2 X' + \sin^2\delta\right]}{\delta \sin\delta} \qquad (3-11)$$

where $X' = x'\pi/2L$.

Figure 3–2 shows capture zones for a well pumping at a low rate in the stream–barrier system. Three different ambient flow cases are illustrated: 1) the ambient discharge to the stream, q_a, is due only to lateral inflow across the barrier, 2) q_a is due only to local vertical recharge, and 3) q_a is composed of 50% lateral inflow and 50% vertical recharge. Although the components vary, the total amount of ambient discharge to the stream is the same in all three cases. Since the vertical recharge is spread out, while the lateral inflow is concentrated on the barrier boundary, the capture zone is larger when vertical recharge is the major source of water to the well. When it is the only source, the capture zone 'cusps out' along the barrier. This cusping shape is typical near a no-flow boundary. The capture zone extends out along the barrier 'searching' for water to meet the pumping demand (Lee, 1986). As a consequence, there is a possibility that wells will pull in contamination from distant sources along the barrier.

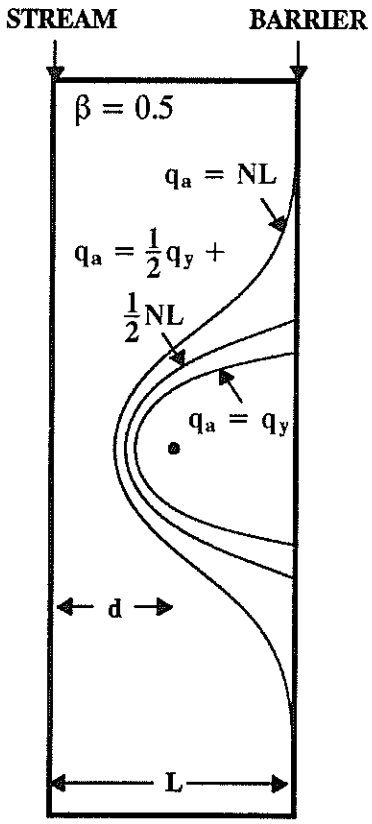

Figure 3–2. Capture zones for a well in a stream-barrier bounded aquifer for three combinations of recharge: 1) lateral ($q_a = q_y$); 2) 50% lateral and 50% vertical; 3) vertical (q_a = NL)

Stream–Stream System

The stream–stream strip aquifer system is bounded by a fully penetrating stream on the left and on the right as depicted in Figure 2–9. The governing equation is the same as (3–7) subject to the following boundary conditions:

$$\begin{aligned} y = 0, \Phi &= \Phi_1 \\ y = L, \Phi &= \Phi_2 \end{aligned} \qquad (3-12)$$

with the aquifer extending to $\pm \infty$ in the x direction parallel to the stream boundaries.

The solution to the flow field was derived in Section 2. From (2–20), the potential Φ is given by the real part of the complex function Ω,

$$\begin{aligned} \Omega(x,y) &= \Phi + i\Psi \\ &= \left[\frac{Ny(L-y)}{2} + \frac{(\Phi_2 - \Phi_1)}{L} y + \Phi_1 \right] + i \left[\frac{-Nx(L-2y)}{2} - \frac{(\Phi_2 - \Phi_1)}{L} x \right] \\ &\quad + \frac{Q}{2\pi} \left[\ln\left(\frac{\zeta - \zeta_w}{\zeta - \zeta_w^*} \right) \right] \end{aligned} \qquad (3-13)$$

where terms are defined as in the stream barrier system except that now $q_a = NL/2 + (\Phi_2 - \Phi_1)/L$. With two streams and the possibility of a groundwater divide within the flow domain, two sets of stagnation points must be considered, one for $y<d$ and one for $y>d$. For $y<d$, critical β is defined by $\beta_c=\tan(\delta)/\delta$. For $y>d$, the critical β is $\beta_c=2(1-\sin^2\delta)/\delta\sin 2\delta$. The stagnation point, y', for $\beta<\beta_c$, $0<y<L$, and $x'=0$ is found using

$$\beta = \frac{q_a + NL(1 - 2Y'/\pi)}{q_0} \frac{2}{\delta} \left[\frac{\sin(2(\delta - Y'))}{1 - \cos(2(\delta - Y'))} + \frac{\sin(2(\delta + Y'))}{1 - \cos(2(\delta + Y'))} \right]. \qquad (3-14)$$

For $\beta>\beta_c$ and $y'=0$ the stagnation point, x' is found using (2–27)

$$\beta = \frac{\cosh 2X' - \cos 2\delta}{\delta \sin \delta} \quad . \qquad (3-15)$$

For $\beta>\beta_c$ and $y'=L$ the stagnation point, x' is given by

$$x' = \frac{L}{\pi} \log_e \left[\cos 2\delta - \beta\delta \sin 2\delta + \sqrt{\left[(\cos 2\delta - \beta\delta \sin^2\delta)^2 - 1 \right]} \right] \quad . \qquad (3-16)$$

Figure 3–3 shows three cases: a) the ambient discharge to or from a stream, q_a, is due only to lateral throughflow, with $\Phi_2 > \Phi_1$ and $N=0$; b) q_a is due only to local vertical recharge, with $\Phi_2 = \Phi_1$; and c) q_a is due to both vertical and lateral recharge with $\Phi_2 > \Phi_1$. When there is no local recharge and the streams are different in elevation, the well will always capture flow from the upper stream as it moves toward the lower stream, as shown in Figure 3–3a. When local vertical recharge is present, a groundwater divide can form within the flow domain parallel to the stream boundaries, as in Figure 3–3b, with characteristic cusping action of the capture zone along the divide (Lee, 1986; also compare to the stream–barrier case, $q_a=NL$). The divide's location is dependent on the relative magnitudes of vertical and lateral recharge.

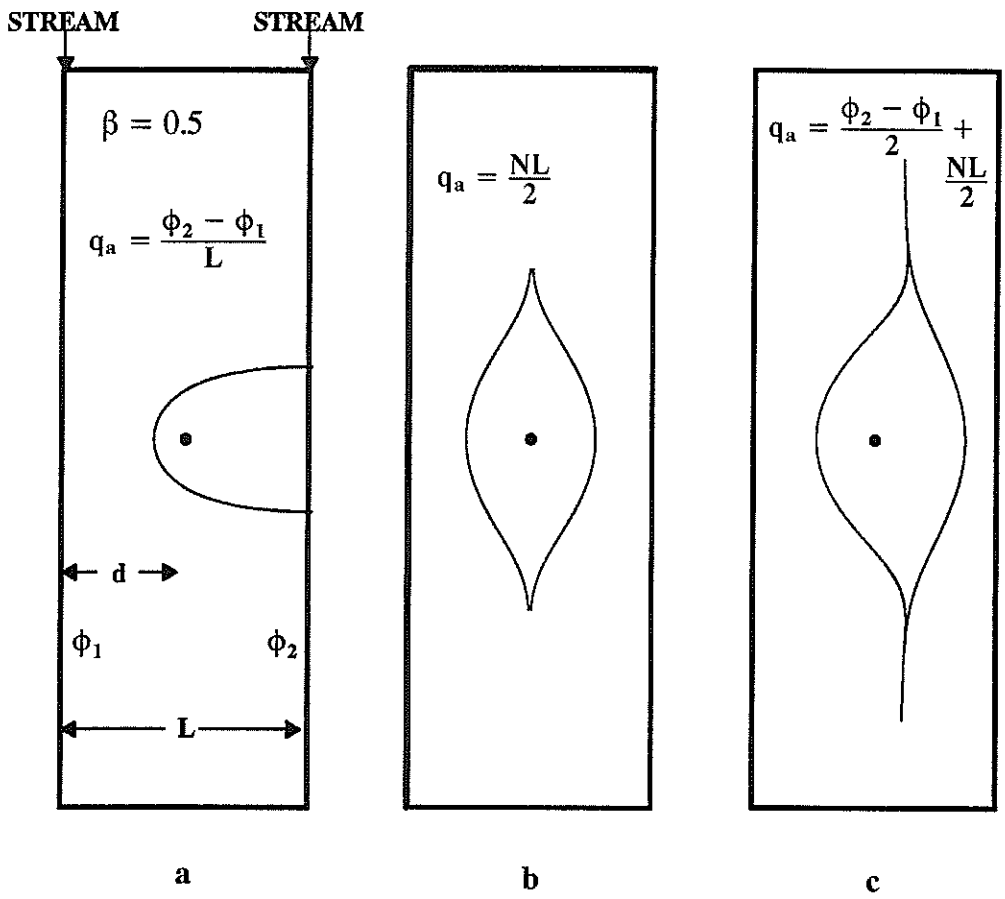

Figure 3–3. Capture zones for a well in a stream-stream bounded aquifer for a) lateral recharge, b) vertical recharge, c) 50% lateral and 50% vertical recharge.

In Figure 3–3c, the divide is located to the right of the pumping well since lateral recharge is from right to left.

We can compare the stream–stream and stream–barrier scenarios for the case where all recharge is due to lateral recharge and is equal for the two systems. In the stream–barrier case, the flux crossing the barrier on the right is specified and equally distributed along the barrier. In the stream–stream case, head is initially specified along the right boundary such that the lateral recharge, $q_L=(\Phi_2-\Phi_1)/L$, is the same as the specified flux across the barrier in the stream–barrier case. However, as pumping commences, the head within the aquifer is lowered resulting in variable flux across the boundary. This disturbs the shape and size of the capture zone, as shown in Figure 3–4. The capture zone for the stream–barrier case is larger than for the stream–stream case because it lacks the additional stream as a source of recharge.

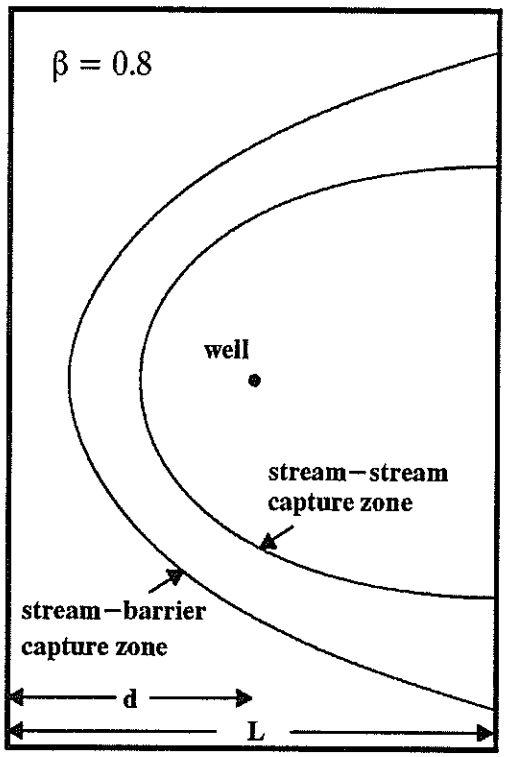

Figure 3−4. Capture zones for stream-barrier and stream-stream bounded aquifers superposed, using equivalent other conditions.

AMBIENT FLOW AT AN ANGLE TO STREAM BOUNDARY

The simple cases presented so far consider lateral recharge perpendicular to the stream boundary only. Because of this, the streams are assumed to be constant head boundaries with essentially no slope. If we impose a gradient in the direction parallel to the prescribed head stream boundary, the stream gains slope. In our case we impose this gradient from the top, so that the stream is flowing from the top of our domain to the bottom, as depicted in Figure 3−5. Our lateral recharge or ambient flux term is now a function of the angle of flow and q_a in the second term on the right hand side of (3−4) is defined as $q_a=q_L(y \cos \alpha+x \sin \alpha)$ where q_L is the magnitude of the ambient flow and α is its orientation, counter-clockwise from the y-direction (perpendicular to the stream). For implementation we can define the ambient x−direction flux as $q_x=q_L \sin\alpha$ and the y−direction flux as $q_y=q_L \cos\alpha$. Newsom and Wilson

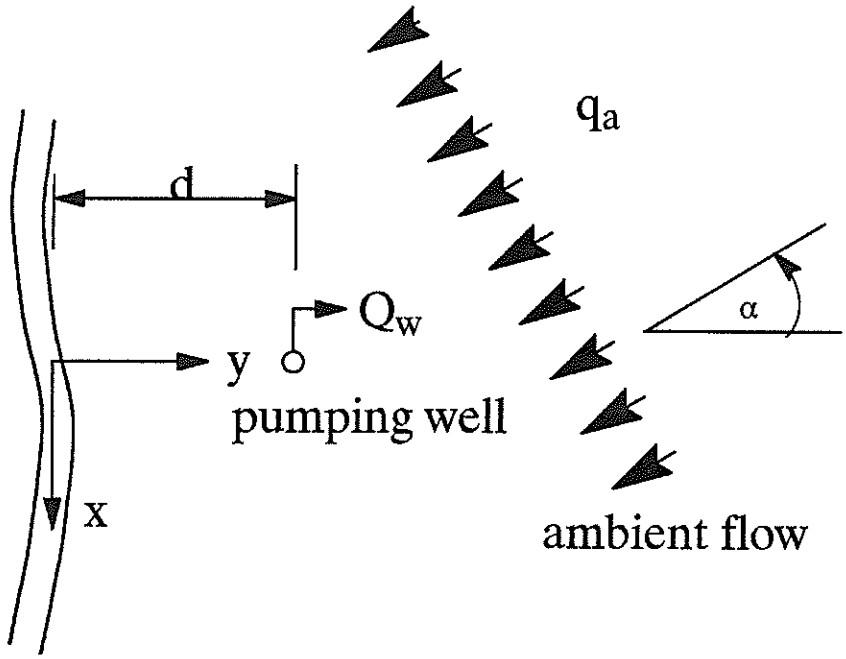

Figure 3−5. Schematic of ambient flow approaching the stream at an angle.

(1988b) have developed the analytical solution for flow at an angle in the semi−infinite case. In the case of the stream−barrier and stream−stream case, a finite difference flow code was used to solve for heads using respective boundary conditions for the two systems. Edge block velocities were calculated from the head field (Appendix A) and were used in locating stagnation points, as well as in particle tracking. What follows are some representative cases of the three flow systems.

Semi−Infinite System

When the ambient flow is perpendicular to the stream, $q_y=0$, the capture zone grows symmetrically as the pumping rate, β, increases (see Figure 3−1). This symmetry is lost when there is a component of ambient flow parallel to the stream. Consider a well located far from the stream, but pumping at a low rate. As shown in Figure 3−6 the capture zone does not 'feel' the effects of the stream, and simply 'swings' into the direction of the ambient flow. When pumping at a higher rate the capture zone is influenced by the stream and, depending on the angle of ambient flow, becomes distorted (see Figure 3−7). At high pumping rates and high ambient flow angles (strong stream gradients) the capture zone intercepts the stream, as in Figure 3−7c, causing induced infiltration. Newsom and Wilson (1988b) derived curves for induced infiltration as a function of variation in pumping rate and ambient flow angle.

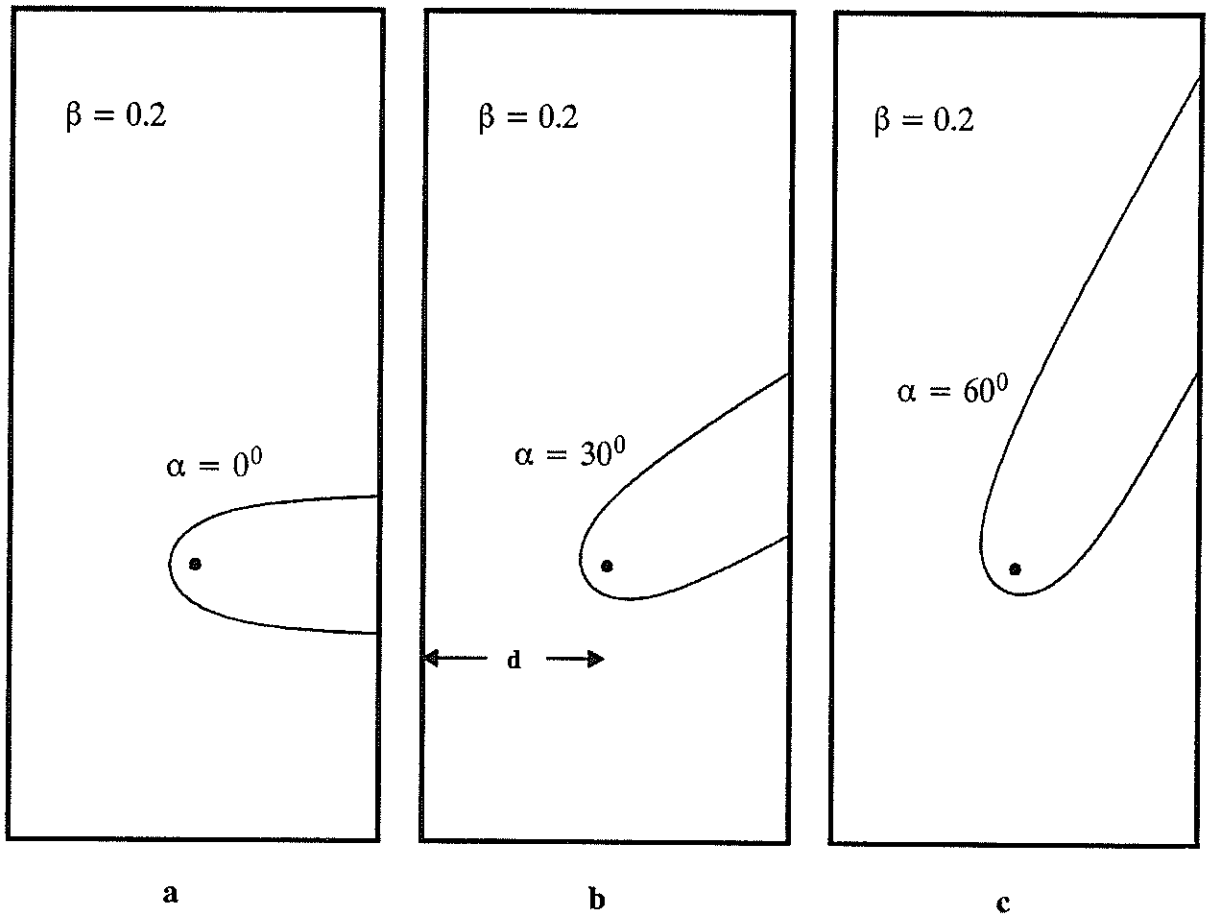

Figure 3–6. Capture zones for three different ambient flow directions with a well pumping at a low rate in a semi-infinite aquifer.

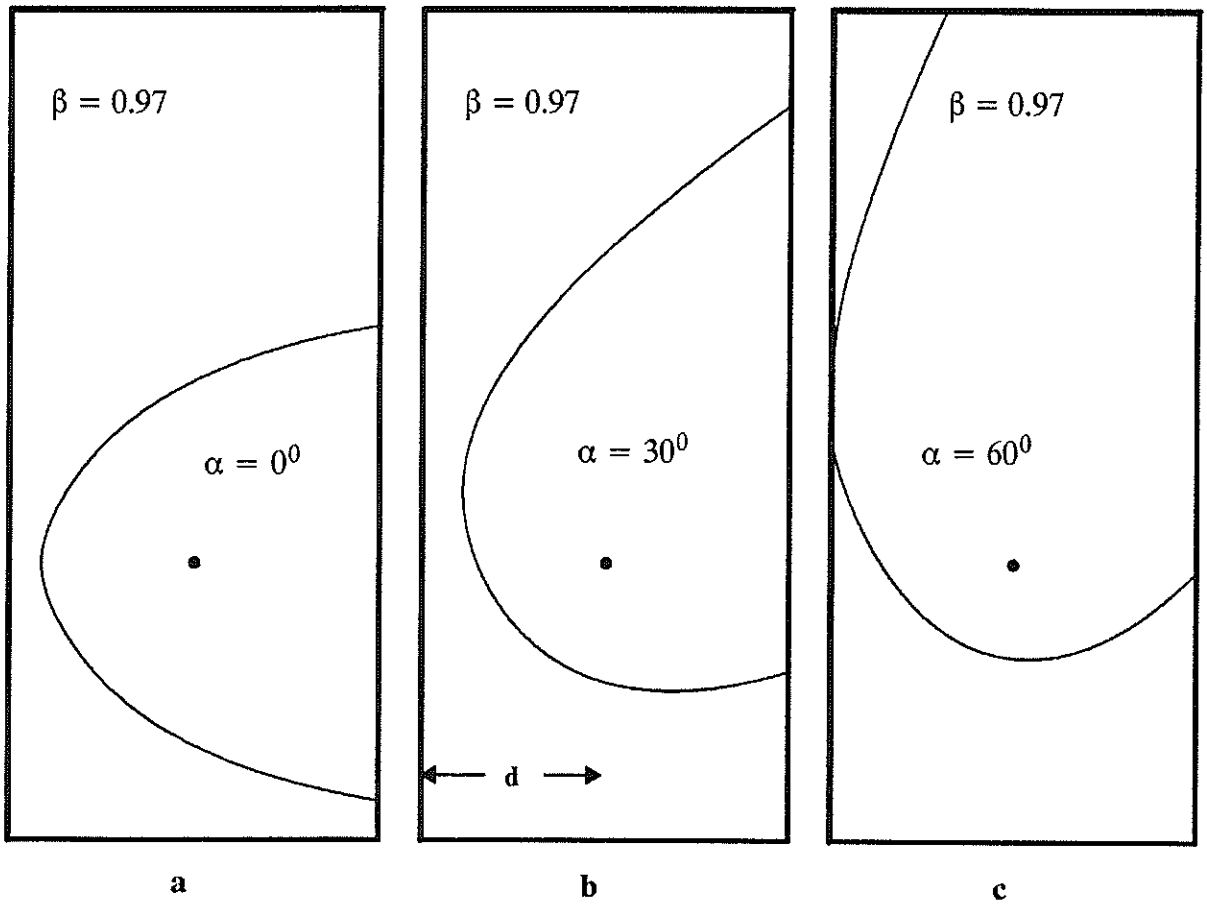

Figure 3–7. Capture zones for three different ambient flow directions with a well pumping at critical rate in a semi-infinite aquifer.

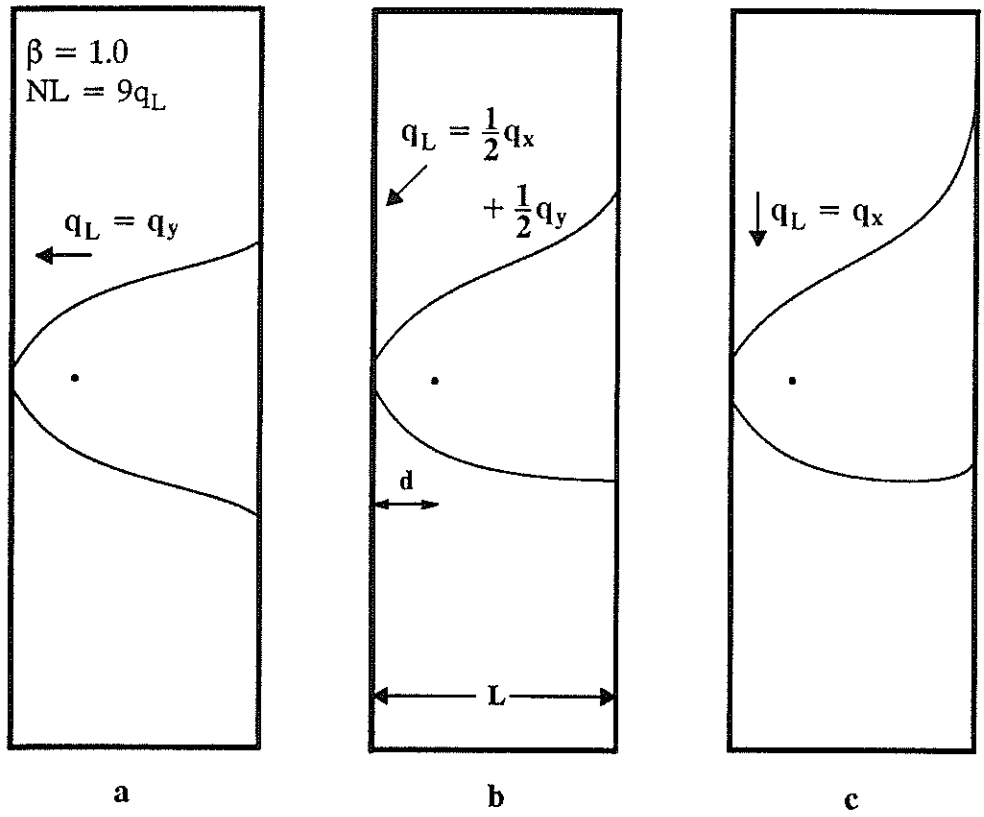

Figure 3–8. Capture zones for three different ambient flow directions for a well in a stream-barrier bounded aquifer (d=L/4).

Stream–Barrier System

In Figure 3–2 we presented three capture zones for a well centrally located between a stream on the left and a barrier on the right, all with the same β value but which vary in shape due to varying sources of recharge. Figure 3–8 shows three capture zones with varying components of ambient flow in the x and y directions, allowing for ambient discharge to the stream at angles $\alpha=0^0$, 30^0, and 60^0. We set 10% of the total recharge rate, q_a, due to lateral inflow, q_L, and 90% due to local vertical recharge, N. As the component of flow crossing the barrier boundary on the right is reduced and the angle and stream gradient increase, the capture zone begins to extend up along the barrier in the direction of the incoming ambient flow. As shown in Figure 3–8c, when all lateral inflow is parallel to the stream, $q_y=0$, the cusping action of the capture zone is entirely unidirectional, extending upgradient along the barrier toward the incoming ambient flow from the top of the domain. The amount of induced infiltration has also increased in Figure 3–8c as compared to Figures 3–8a and b.

Figure 3–9 shows an aquifer with no lateral inflow across the barrier boundary on the right, although there is an ambient downstream component of inflow. In Figure 3–9a we have equal amounts of both local vertical recharge and inflow, while in Figure 3–9b there is no local

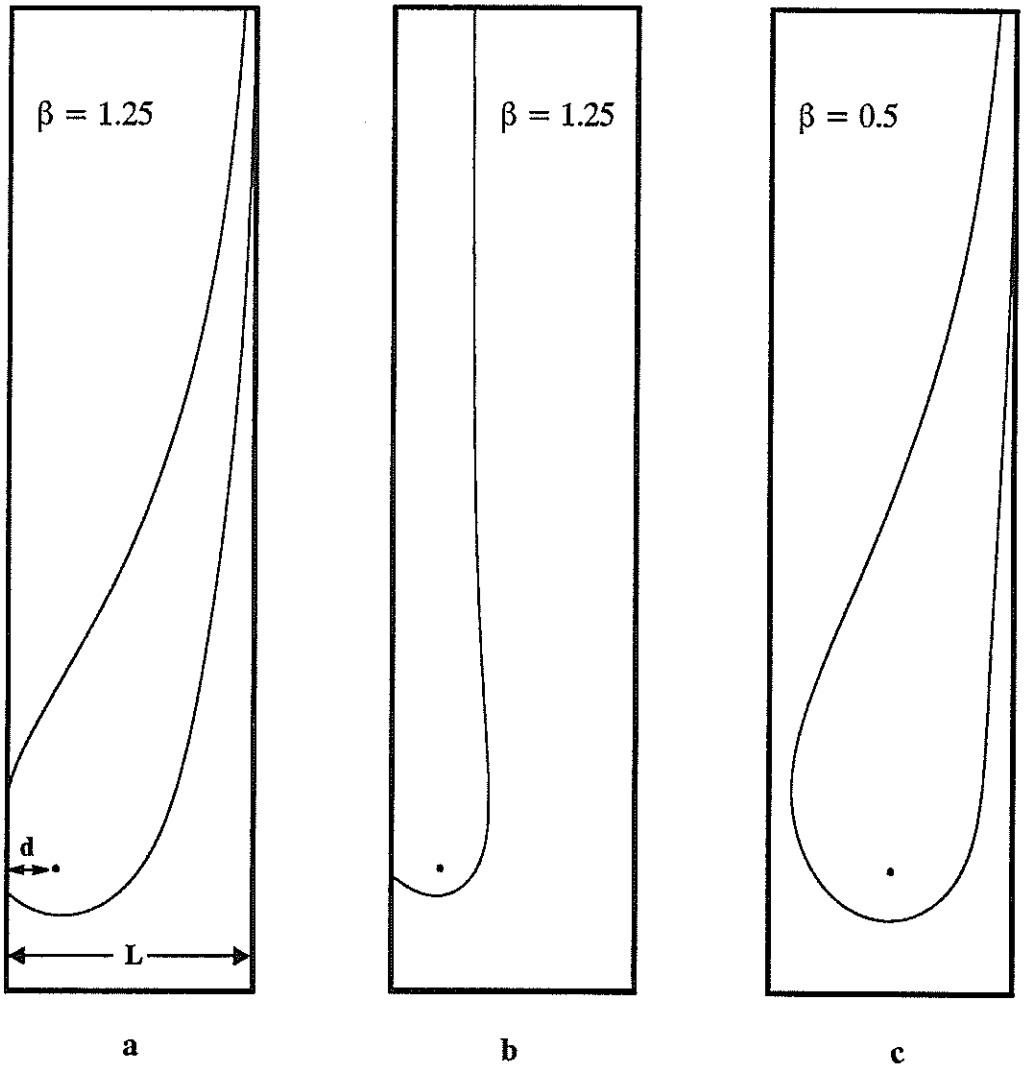

Figure 3−9. Capture zones for wells in a stream-barrier bounded aquifer with various combinations of lateral and vertical recharge: a) $q_y=0$ $q_L=NL/2$ $d=L/4$, b) $q_a=q_x$ $N=0$ $d=L/4$, c) $q_y=0$ $q_L=NL/2$ $d=L/2$

recharge. The effect of local vertical recharge is to cause the capture zone to move away from the stream, by effectively changing the angle of ambient flow to the stream. When near the well, two capture zones withdraw water from the same portion of aquifer; while further from the well, the capture zones are quite disparate.

As the well in Figure 3−9a is positioned further from the stream (or pumping rate is decreased or ambient flow rate is increased) the well ceases to interact with the stream (Figure 3−9c), even though the two capture zones in Figures 3−9a and c are similar in shape. Either scenario may be favorable depending on the prevailing conditions. For instance, if a spill were to occur within the capture zone, it may be desirable to use stream water to dilute the concentration of the well water below some minimum safe limit and the Figure 3−9a scenario would

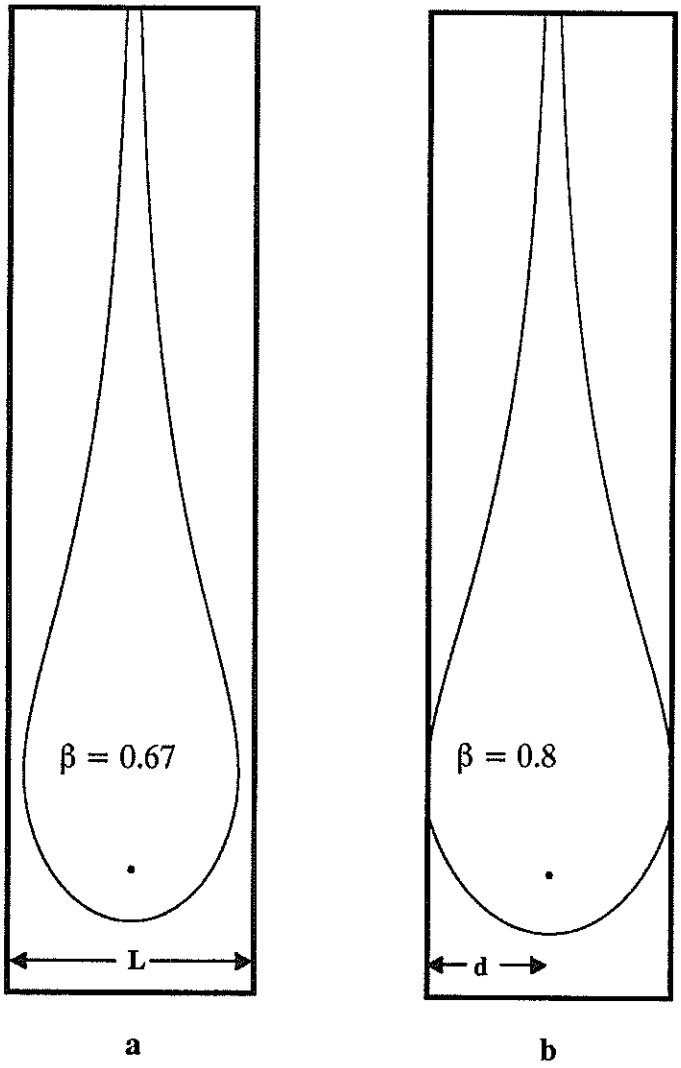

Figure 3–10. Capture zones for wells in a stream-stream bounded aquifer with $q_x=0$.

be desirable. On the other hand, it may be that the stream water is contaminated. In this case, interception of the stream by the capture zone would be undesirable and the scenario shown in Figure 3–9c would be preferred where all of the recharge water to the well is derived from vertical recharge.

Stream–Stream System

The scenario depicted in Figure 3–10 is for a pumping well centrally located between two streams of equal elevation. The two streams have the same slope. In this case, half the total recharge is due to vertical recharge and half is due to recharge moving from the upper to the lower portion of the flow domain, i.e., $q_a=q_x+NL$. As can be seen, this flow system produces a long teardrop shaped capture zone which extends far upstream along the groundwater divide.

Figure 3−10a and b are identical except for pumping rates. The smaller capture zone has β=0.66 and the larger one has β=0.8, representing a 21% increase in pumping rate. If a contaminant spill occurred upgradient of the well between the capture zone and the stream in either scenario, it would first migrate to the water table and then migrate toward the stream at an angle, eventually reaching the stream and exiting the groundwater flow system. However, with the increased pumping rate of Figure 3−10b, the capture zone intercepts both streams and induces infiltration. In this case, a simple approach to protecting the well from contamination would be to monitor stream water chemistry just upstream of the stream−capture zone contact for increases in contaminant concentrations. As the spill moves downstream the pump could be shut down allowing the potential threat to pass. If the spill occurred along the groundwater divide far upstream of the well, then theoretically some of it would eventually find its way to the well, albeit at extremely long travel times.

TIME-DEPENDENT CAPTURE ZONES: FRONTS

We have presented capture zones which can be viewed as representing the ultimate capture zone. These capture zones represent the dividing streamline of the flow system such that a particle of water placed just inside this line will ultimately be pumped by the well given unlimited time and assuming continuous pumping. Time-dependent capture zones account for the travel time of water particles to the well. Aquifers have a capacity to attenuate pollutants by some form of degradation or dilution. The time required for the concentration of a particular contaminant species to drop to a predetermined safe level can then be used to determine the relevant time-dependent capture zone.

Time-dependent capture zones are defined by particle fronts, or equal travel time contours. The value of time t associated with a front represents the time it will take for the particles located on that contour to reach the well under the given conditions. All water on the well side of the contour will be extracted from the aquifer within this period of time whereas all water between this contour and the dividing streamline will be pumped later. Thus the dividing streamline can also be viewed as representing the front obtained as $t \rightarrow \infty$.

The approach to front delineation is in all aspects similar to that for delineating the dividing streamline except one: the location of where the particles are initially placed into the velocity field for tracking. In the case of the dividing streamline, the stagnation point (or some other critical point) was first located, then two particles were offset from this point and tracked backward. In the case of fronts, we place several particles very close to and equidistant from the well and then backtrack these particles in the negative velocity field. The number of particles must be large enough to accurately define the front, but too many particles will be computationally cumbersome. This dilemma is handled by allowing for the adaptive addition (and subtraction) of particles along a front through a dynamic front tracking scheme (Schafer−Perini, 1990; Schafer−Perini and Wilson, 1991b; see Appendix A). Dimensionless time for fronts is given as

$$\tau = \frac{tQ_w}{nbd^2} = \frac{tq_a\pi\beta}{nbd}. \qquad (3-17)$$

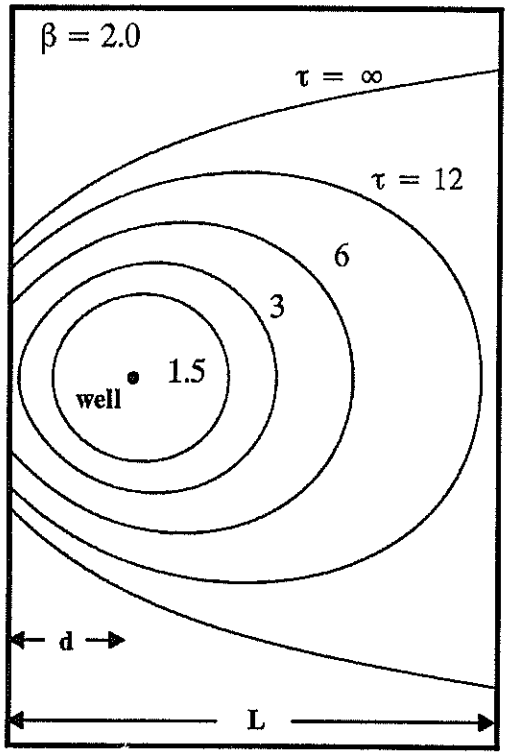

Figure 3−11. Time-dependent capture zones for a well in a stream-barrier bounded aquifer with lateral inflow.

Fronts for several times, and the dividing streamline, are shown in Figure 3−11 for a stream−barrier system. As τ becomes large the front approaches the dividing streamline. For fronts intersecting the stream, an instantaneous induced infiltration can be specified, which is the amount of stream water induced to flow into the well at a given (front) time.

From equation (3−17) it is apparent that τ is a function of the porosity, n, and the aquifer thickness, b. In addition, we have assumed that the aquifer thickness is a constant, as could be the case in a confined aquifer or a linearized Dupuit model. This approach can also be modified to account for a spatially variable saturated thickness throughout the flow domain, which in turn allows variation of hydraulic conductivity, K, and the stream stage or reference head, h_o. The parameters, n, b, h_o, and K act to vary the magnitude of the velocity field but do not individually affect the location of the stagnation streamline or the rate of induced infiltration. With this in mind, we examine these parameters with respect to time-dependent capture zones or fronts.

Porosity Effects

The porosity, n, is used to calculate the average linear velocity, V_x and V_y, given by (3−5),

$$V_x = \frac{q_x}{nb} \quad , \qquad V_y = \frac{q_y}{nb}, \tag{3−18}$$

which are the velocities used in the particle tracking scheme. As can be seen, the porosity acts only as a scalar multiplier of the Darcy velocity and has no effect on the solution of Darcy velocities spatially. It follows from this that the location of the stagnation streamline is not spatially effected by porosities, although the velocity magnitudes and the location of equal time contours are affected. For a fixed time and a constant saturated thickness, b, the dimensionless time τ will increase for decreasing porosity as shown in Figure 3−12a for n=0.1, 0.2, and 0.3. As porosity increases, the velocities decrease and the distance traveled for a given real time becomes shorter and τ becomes smaller. Time dependent capture zones are smaller in aquifers with larger effective porosities.

Constant Saturated Thickness Effects

Using equation (3−18), we can now hold porosity and ambient flow constant and examine the effects of saturated thickness on front location. In this representation, the saturated thickness is assumed to be spatially constant and we wish to examine front development with respect to different thicknesses. As in the case of porosity, thickness does not change the ultimate capture zone. It only effects the location of equal time front contours. In this analysis, assume that the thickness $b=h_o$. As shown in Figure 3−12b, the time-dependent capture zone shrinks as saturated thickness increases. For very small saturated thicknesses, velocities become large and the time-dependent capture zone quickly approaches the ultimate capture zone ($\tau = \infty$).

Variable Saturated Thickness Effects

One of the assumptions made in the application of the velocity solution is that the saturated thickness of the aquifer can be represented by a constant value, b or h_o. This can be expressed for the x component using the Dupuit model and a first type linearization as follows:

$$\frac{\partial^2\Phi}{\partial x^2} = \frac{K}{2}\frac{\partial^2 h^2}{\partial x^2} = Kh\frac{\partial^2 h}{\partial x^2} \approx Kb\frac{\partial^2 h}{\partial x^2} = \frac{\partial^2\Phi}{\partial x^2}, \tag{3−19}$$

where b is a constant, the right side of the approximation is the solution linearized in h ($\Phi=Kbh=Th$), and the left side is linear in h^2 ($\Phi=Kh^2/2$). Velocity for the x direction based on (3−19) is given by

$$V_x = \frac{q_x}{(nb)} = \frac{-Kb}{(nb)}\frac{\partial h}{\partial x}, \tag{3−20}$$

where the last term of (3−20) has been obtained from the right-hand side of the approximation in (3−19).

To account for the spatially variable saturated thickness of the aquifer, h, which is expressed in a non−linear fashion on the left-hand side of (3−19), we first solve for h using the Dupuit formulation which is linear in h^2, and then divide the Darcy velocity per unit depth by (nh) instead of (nb), giving

Figure 3−12a..

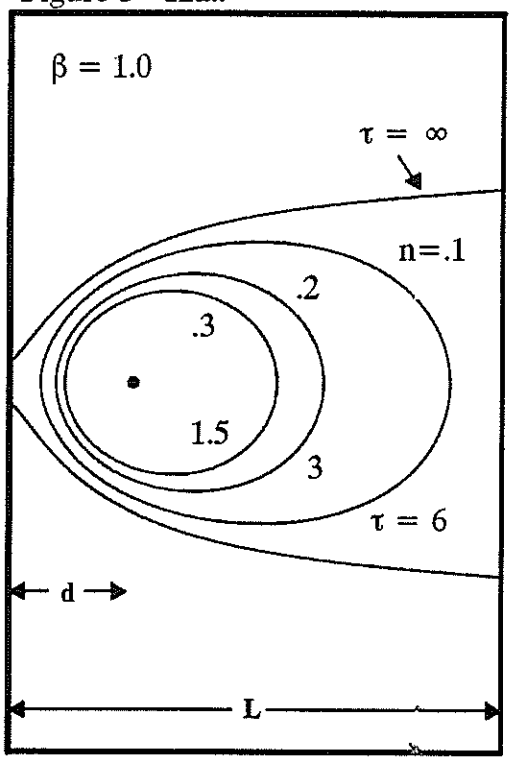

Figure 3−12b.

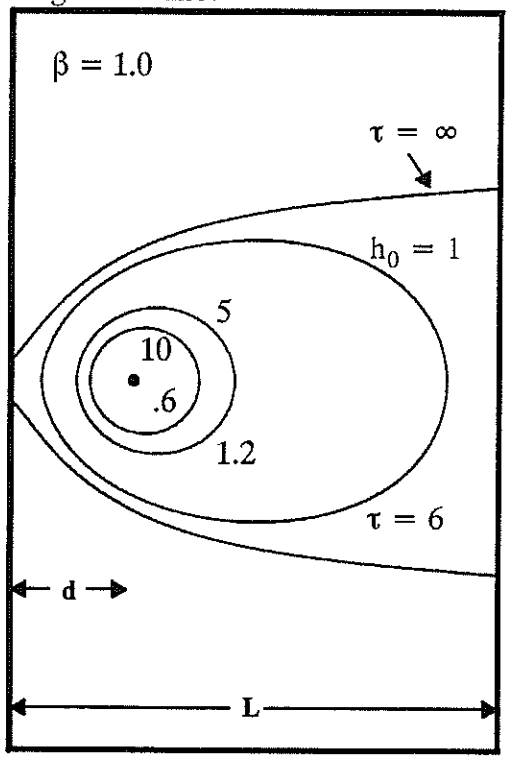

Figure 3−12c.

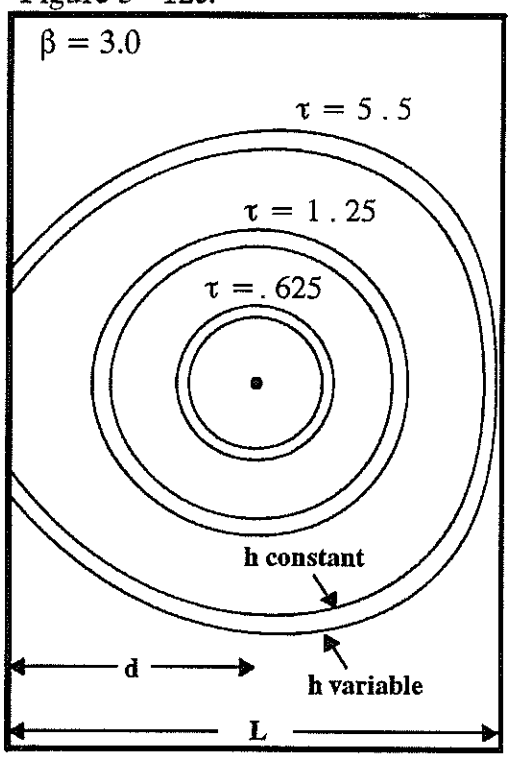

Figure 3−12d.

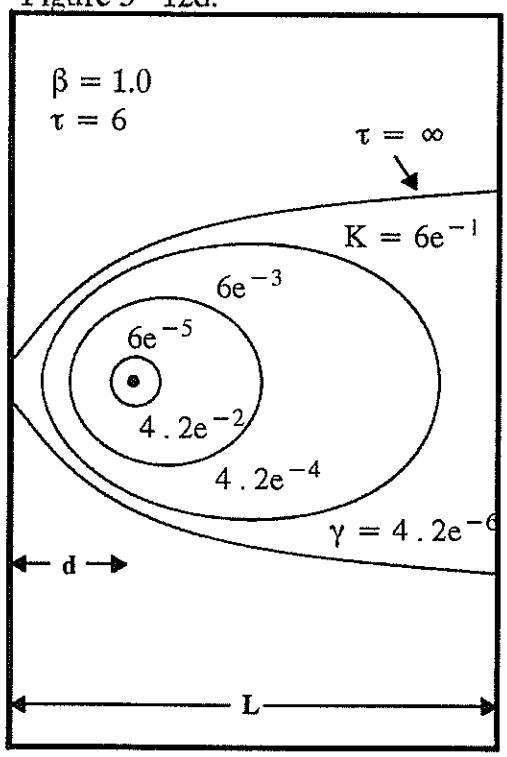

Figure 3−12. Capture zone time fronts in a stream-barrier bounded aquifer influenced by a) porosity changes, b) variable saturated thickness, c) nonlinear conception of h (variable), d) conductivity changes.

$$V_x = \frac{q_x}{nh}. \qquad (3-21)$$

In contrast to effects of n and b, however, h varies spatially whereas n and b were assumed constant.

This approach introduces two additional effects on front development. Both the reference head, h_o, and the hydraulic conductivity, K, are now included in the representation of head. We modify the dimensionless value τ to accommodate h_o by replacing the constant aquifer thickness b by the boundary condition h_o, giving

$$\tau = \frac{tQ_w}{nh_o d^2} \qquad . \qquad (3-22)$$

Note that this normalization depends on the value of h_o, and makes no sense if $h_o=0$ (i.e., if the stream elevation equals the aquifer bottom elevation; but then there would be no possibility for induced infiltration in this case anyway). The explicit presence of hydraulic conductivity requires a new dimensionless parameter, which we define as γ,

$$\gamma = \frac{Q_w}{d^2K} \qquad . \qquad (3-23)$$

There is very little difference between the linearized and non-linearized models when h_o is large relative to the variation of h across the aquifer. An example of this can be seen in Figure 3-12b, where if the variable saturated thickness capture zones were plotted they would be indistinguishable from the results shown. Increasing the pumping rate or the ambient flow rate, increases the variation of h and expands the time dependent capture zones, as shown in Figure 3-12c. Capture zone fronts for the two different model representations are shown. Evident from this figure is that much of the difference between the two fronts for a given time occurs early, near the well, where the differences in saturated thickness are largest.

The effect of hydraulic conductivity on front location is shown in Figure 3-12d. By varying γ, the distance traveled for a given τ and β is seen to increase with increasing K. As $K \rightarrow \infty$, $\gamma \rightarrow 0$, which is the limiting case of the maximum distance a particle can be positioned from the well and still reach the well for the given front time and pumping constraints.

MULTIPLE PUMPING WELLS

In many cases water is pumped from a cluster of wells, often referred to as a well field. Here we look at the simplest case of a well field, involving only two wells, both of which are pumping at equal rates and are located midway between a stream (on the left) and a barrier boundary (on the right), as illustrated in Figure 3-13. The appropriate equation of state is expressed by

$$\frac{\partial^2\Phi}{\partial x^2} + \frac{\partial^2\Phi}{\partial y^2} + N + Q_w[\delta(x - x_{w1})\delta(y - y_{w)}] + Q[\delta(x - x_{w2)}\delta(y - y_{w2})] = 0, \qquad (3-24)$$

where the two wells are located at (x_{w1}, y_{w1}) and (x_{w2}, y_{w2}), subject to the boundary conditions

$$\begin{aligned} y &= 0, \Phi = \Phi_0 \\ y &= L, q_L = q_y \end{aligned} \qquad . \qquad (3-25)$$

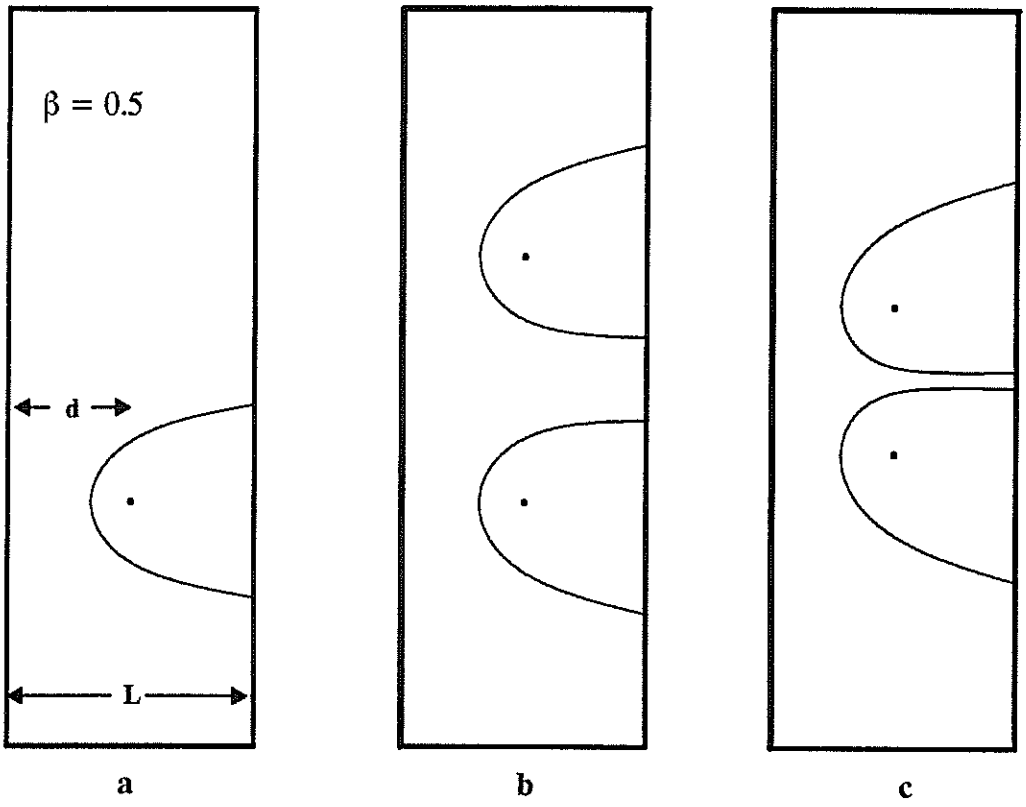

Figure 3–13.
Capture zones in a stream-barrier bounded aquifer for combinations of two wells: a) single well base case, b)–d) influence of well separation distance, e) influence of low transmissivity zone at stream bank (width=0.016L).

In these examples the total recharge is due entirely to lateral recharge across the barrier boundary on the right. We present results derived from a two-dimensional finite difference code. It should be noted that multiple well analytical solutions can easily be obtained in a straight forward manner from application of superposition, as described in Section 2. Javendel and Tsang (1984) describe analytical solutions for multiple well capture zones in the absence of a stream boundary.

Figure 3−13a illustrates the capture zone for a single well. Notice y−axis symmetry of the capture zone as it intercepts the barrier boundary on the right. Figures 3−13b to d show the influence of the well separation distance on the shape of the capture zones produced by the two wells, each with a pumping rate of β=0.5. In Figure 3−13b the wells are fairly far apart and with little interference between them. The capture zones are only slightly distorted (compare to Figure 3−13a), and appear to spread away from each other, attempting to intercept enough recharge to supply the wells. Moving the wells closer together in Figure 3−13c, increases the repulsion of the capture zones from each other. With only a slight additional movement (or a slight increase in pumping), the capture zones merge (Figure 3−13d). The merged capture zone has the appearance of the capture zone for a single well pumping at the same rate as the well field. This similarity improves as the wells get even closer. As the capture zones merge, they expand downstream, in this case leading to induced infiltration. The closely spaced wells are not able to gather the lateral inflow as efficiently, and thus seek out the stream for the necessary recharge.

Suppose a zone of lower transmissivity exists along the stream. We would expect this to reduce the propensity for induced infiltration. In Figure 3−13e this zone has a width of 16/(1000L), and half the transmissivity of the remainder of the aquifer. This scenario can be thought to represent the lower conductivity material deposited by a stream along its course. Comparing to the same situation in the homogeneous aquifer shown in Figure 3−13d, we see that the capture zone no longer intercepts the stream for the heterogeneous system. Thus even a small difference between the two transmissivity zones can lead to important effects on capture zone patterns.

AQUIFER HETEROGENEITY

In the previous work, we briefly introduced the effect of aquifer heterogeneity on capture zone delineation. By introducing a thin strip of lower conductivity material along the river or stream, the well no longer induced infiltration from the stream into the aquifer. In the following cases, we consider variations in hydraulic conductivity along strips that are parallel to the stream and barrier boundaries. The conductivities are assumed isotropic. This type of heterogeneity loosely corresponds to that found in fluvial deposits.

In a heterogeneous system the equation of state is given by

$$\frac{\partial}{\partial x}\left(T(x)\frac{\partial h}{\partial x}\right) + \frac{\partial}{\partial y}\left(T(y)\frac{\partial h}{\partial y}\right) + N + Q_w[\delta(x - x_w), \delta(y - y_w)] = 0 \qquad (3-26)$$

where T(x) and T(y) are the transmissivities in the x and y directions, respectively. The results that follow were derived using a finite difference flow code.

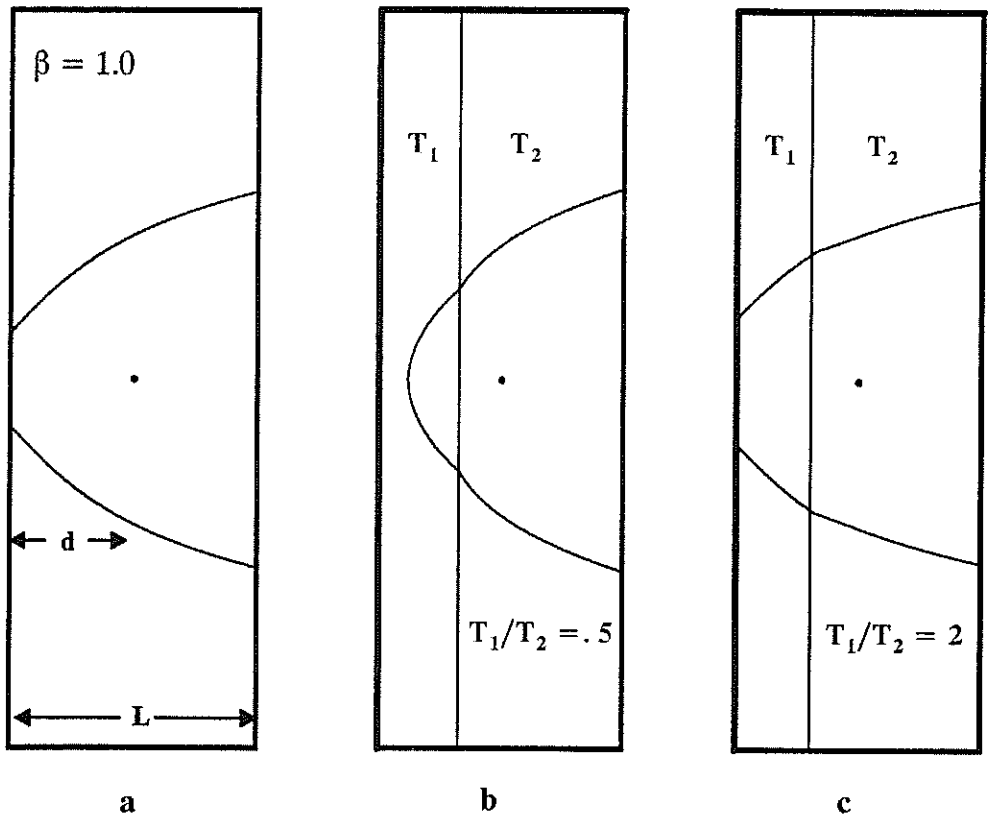

Figure 3−14. Capture zones in a stream-barrier bounded aquifer influenced by simple transmissivity contrasts.

Figure 3−14a shows a capture zone for a well located midway between a stream boundary (left) and a barrier boundary (right) in a homogeneous strip aquifer. Recharge is due entirely to lateral recharge across the barrier boundary and the well is pumping at the critical rate, $\beta=1.0$. In Figures 3−14b and 3−14c the transmissivity is heterogeneous and has been divided into two zones. The first zone, T_1, extends from y/L=0 to y/L=0.3 and the second zone extends from y/L=0.3 to y/L=1.0 (zones are separated by dashed lines in the figures), with both zones running the length of the flow domain in the x direction. In Figure 3−14b a low transmissivity deposit surrounds the stream, in which $T_1/T_2=0.5$. There is a characteristic break in slope of the capture zone where it crosses the contact between the two zones at y/L=0.3. This is the capture zone equivalent to the 'law of streamline refraction' at the interface between different porous media (Bear, 1979). The zone of lower transmissivity reduces the propensity for induced infiltration, and encourages a wider capture zone along the barrier. The well obtains all its water from lateral inflow. In Figure 14c a high transmissivity deposit surrounds the stream, in which $T_1/T_2=2$. Induced infiltration is enhanced and less lateral inflow is captured.

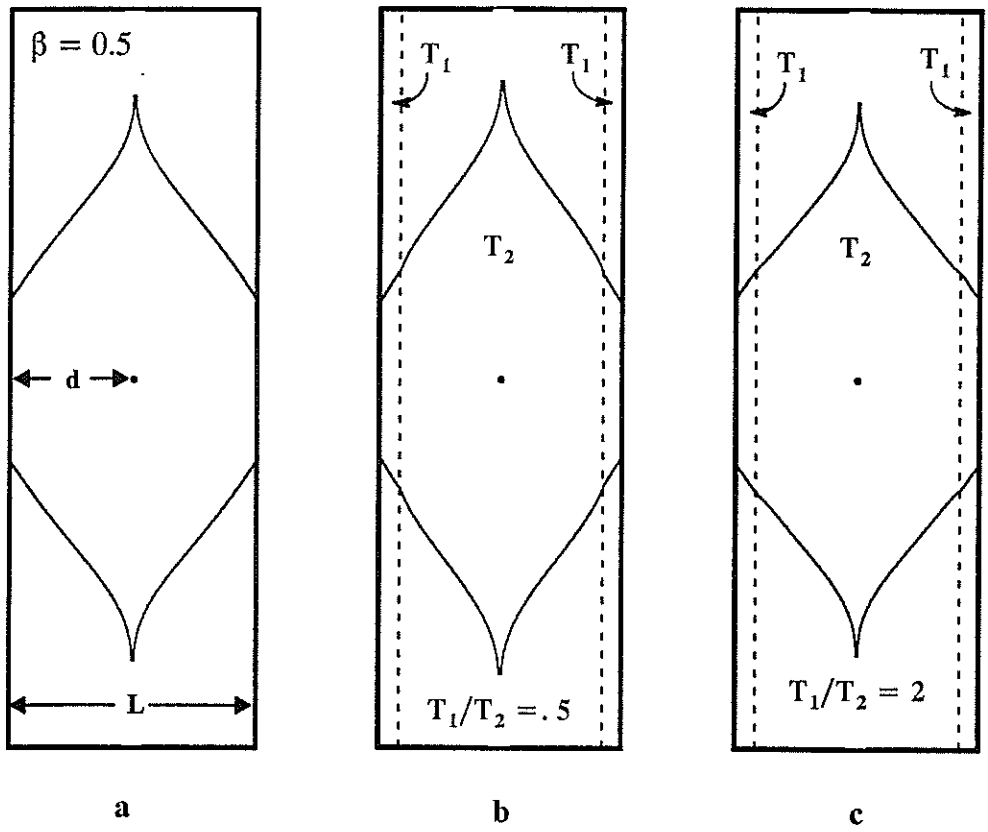

Figure 3−15. Capture zones in a stream-stream bounded aquifer influenced by transmissivity contrasts near each stream bank.

The system depicted in Figure 3−15a represents flow to a well in a completely homogeneous strip aquifer located between two streams. In Figure 3−15b there are three transmissivity zones. Two of these, T_1 and T_3, comprise narrow strips of lower conductivity material surrounding each of the two streams. They extend in the x direction from y/L=0 to y/L= 0.084 and y/L=0.916 to y/L=1.0 (zones are separated by dashed lines in the figures). The zone in the center has uniform transmissivity T_2, where $T_1/T_2=T_3/T_2=0.5$. By careful comparison with Figure 3−15a it can be seen that induced infiltration has been reduced and the proportion of pumped water obtained from local recharge has increased due to heterogeneity effects. In Figure 3−15c high conductivity strips bound the streams, with $T_1/T_2=T_3/T_2=2.0$. The size and extent of the capture zone, especially in the x direction, has been reduced while induced infiltration has increased.

The contrasts in conductivity examined here are small and could be expected to be larger in a real world setting, further encouraging the observed effects presented here. Heterogeneities play a significant role in determining the pattern of capture zones.

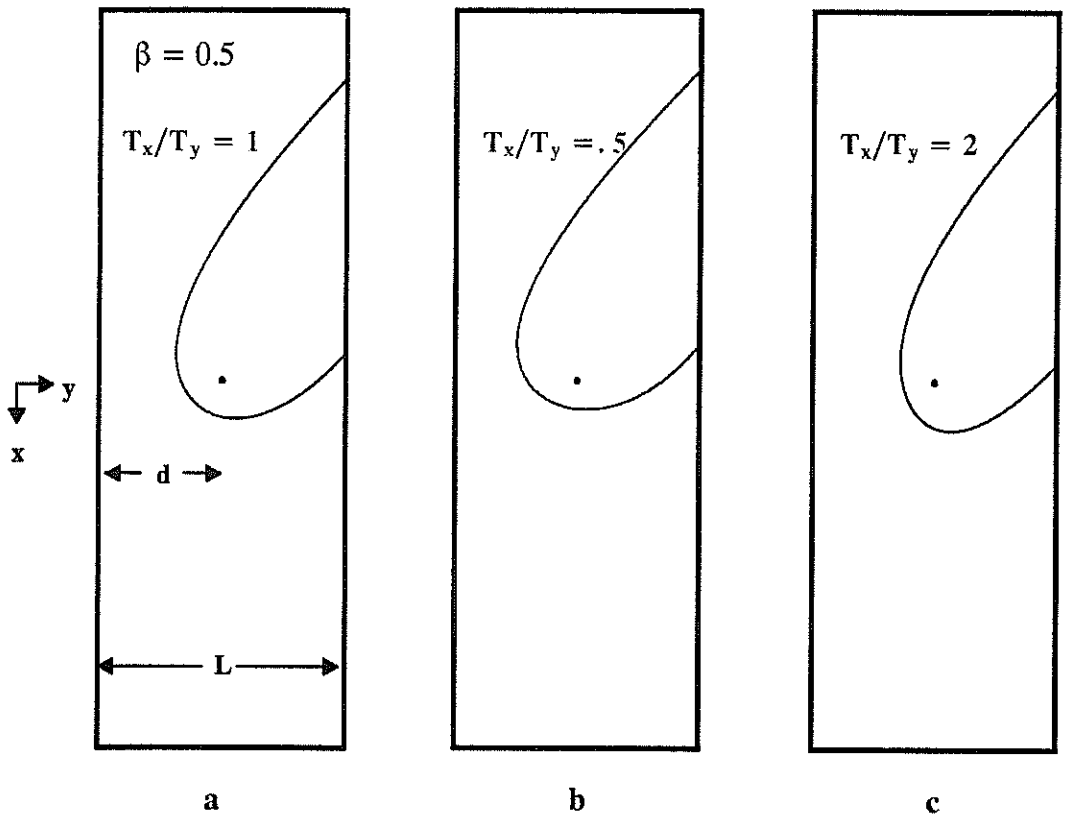

Figure 3−16. Capture zones for a low-rate pumping well in a stream−barrier bounded aquifer showing influences of anisotropic transmissivity.

AQUIFER ANISOTROPY

As in the case of aquifer heterogeneity, our previous results have only dealt with aquifers which were assumed to be isotropic. Here we examine the effect of anisotropic hydraulic conductivity on capture zones. For a homogeneous, anisotropic system, the equation of state is given by

$$T_x\frac{\partial^2 h}{\partial x^2} + T_y\frac{\partial^2 h}{\partial y^2} + N + Q_w[\delta(x - x_w), \delta(y - y_w)] = 0 \qquad (3-27)$$

where (x,y) are the principal directions of the transmissivity tensor. In a practical sense this means that the depositional pattern is aligned parallel to the stream, a reasonable assumption for fluvial systems. The solution presented here was obtained using the finite difference flow code, although it could have also been geometrically transformed from the analytical results.

We first examine the simple case of a well midway between a stream and barrier with lateral recharge in the x direction and y direction equal, $q_x=q_y$, and no local vertical recharge. An isotropic aquifer is illustrated in Figure 3−16a, in which $T_x=T_y$. Anisotropy is illustrated in Figures 3−16b and 3−16c, in which $T_x/T_y=0.5$ and $T_x/T_y=2$, respectively. The first represents

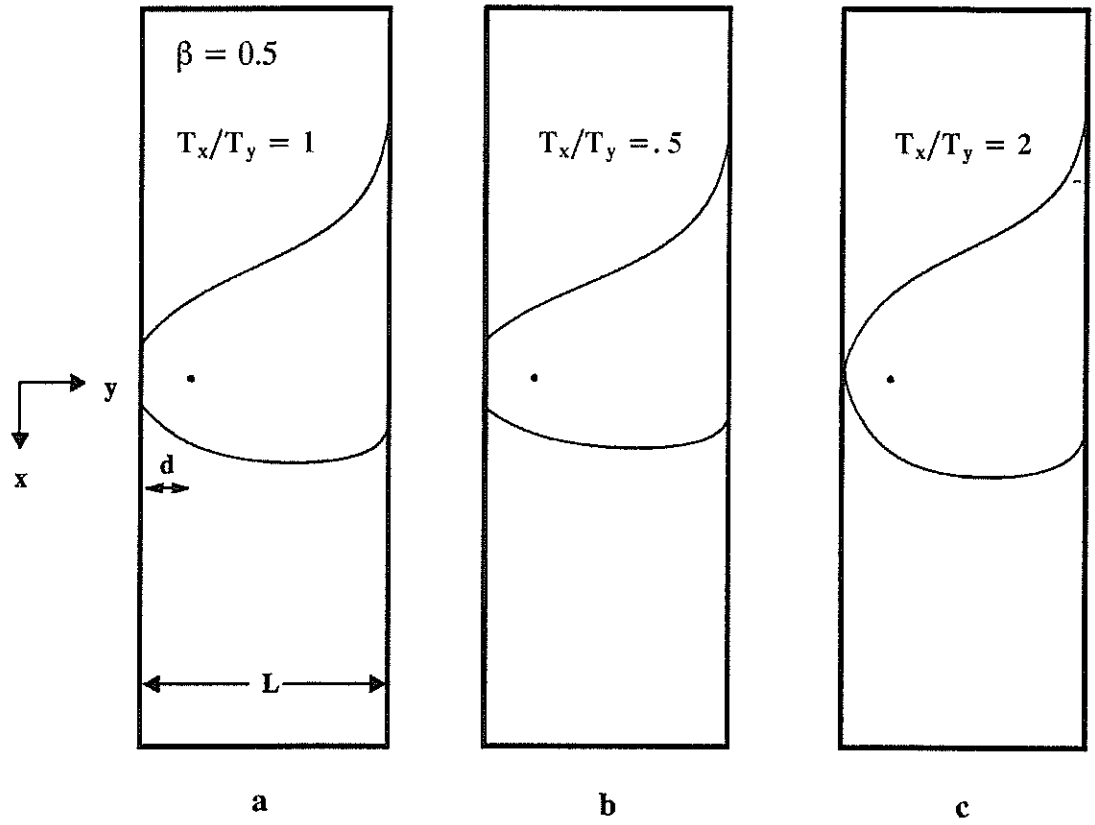

Figure 3−17. Capture zones for a critical-rate pumping well in a stream-barrier bounded aquifer where $NL=0.9q_0$, $q_x=0.1q_0$, $q_x=0$.

aquifers with a greater transmissivity normal to the channel direction, the expected condition for flow past alluvial fans and mountain fronts. The associated capture zone is stretched out in the y direction, toward the stream. The second (Figure 3−16c) represents a greater transmissivity parallel to the stream, and is the expected condition in fluvial deposits. The nose of the capture zone is flattened out in the y direction and elongated in the x direction. For all three cases, the width of the capture zone where it intercepts the right boundary is identical, since this is the only source of recharge that is intercepted.

Figures 3−17a, b and c represent a well between a stream and barrier with the following conditions: $\beta=0.5$; one−tenth of total recharge coming from flux in the x direction, giving the stream a slope; and the remaining recharge due to vertical recharge. For $T_x/T_y=0.5$, as in Figure 3−16b, the capture zone is narrowed in the x direction. Compare this to Figure 3−17c with $T_x/T_y=2$. The capture zone covers a larger aquifer area with no induced infiltration from the stream.

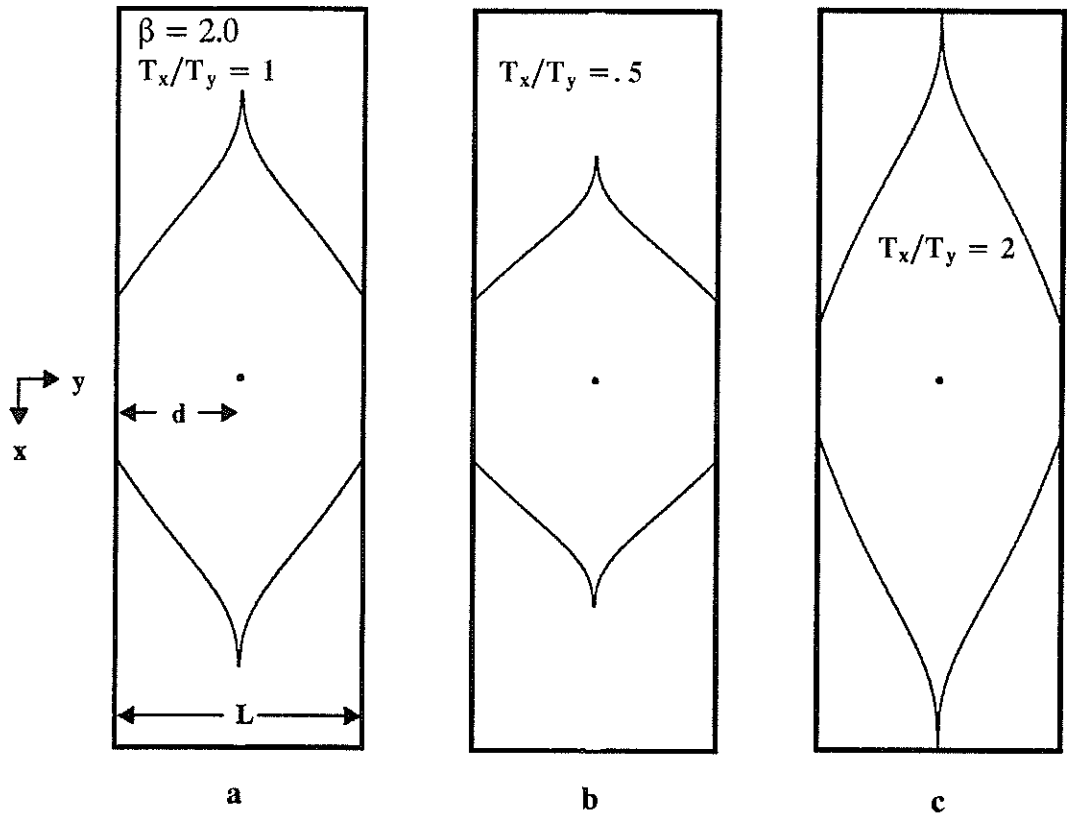

Figure 3–18. Capture zones for a well in a stream-stream bounded aquifer showing various effects of anisotropic transmissivity.

Next, we examine the effect of anisotropy on a capture zone for a well between two streams of equal gradient and with local vertical recharge between them. Figure 3–18a is for $T_x=T_y$ and Figure 3–18b shows the case for $T_x/T_y=.5$. The capture zone in Figure 3–18b is smaller and the stream–capture zone contact length has actually decreased, because with T_y larger, the rate of induced infiltration has actually increased. In Figure 3–18c, for $T_x/T_y=2$, induced infiltration has decreased and the capture zone covers a much larger area.

We can also look at a well between two streams with the lateral inflow parallel to the streams, that is, in the y direction (Figure 3–10). Figure 3–19a, with $T_x=T_y$ is included here for comparison purposes. Figure 3–19b shows the capture zone for $T_x/T_y=0.5$. The capture zone spreads laterally and is now closer to the stream, but is not yet inducing infiltration. In Figure 3–19c, T_y is larger still, such that $T_x/T_y=0.3$. The capture zone now intercepts both streams and shrinks in size since the pumping demand is no longer only supplied by vertical recharge.

These results indicate two important effects of the anisotropy ratio (T_x/T_y). The first is the noticeable variation in the shape of the capture zones with different anisotropies. The capture zone tends to expand in the direction of greater transmissivity and contract in the direction of

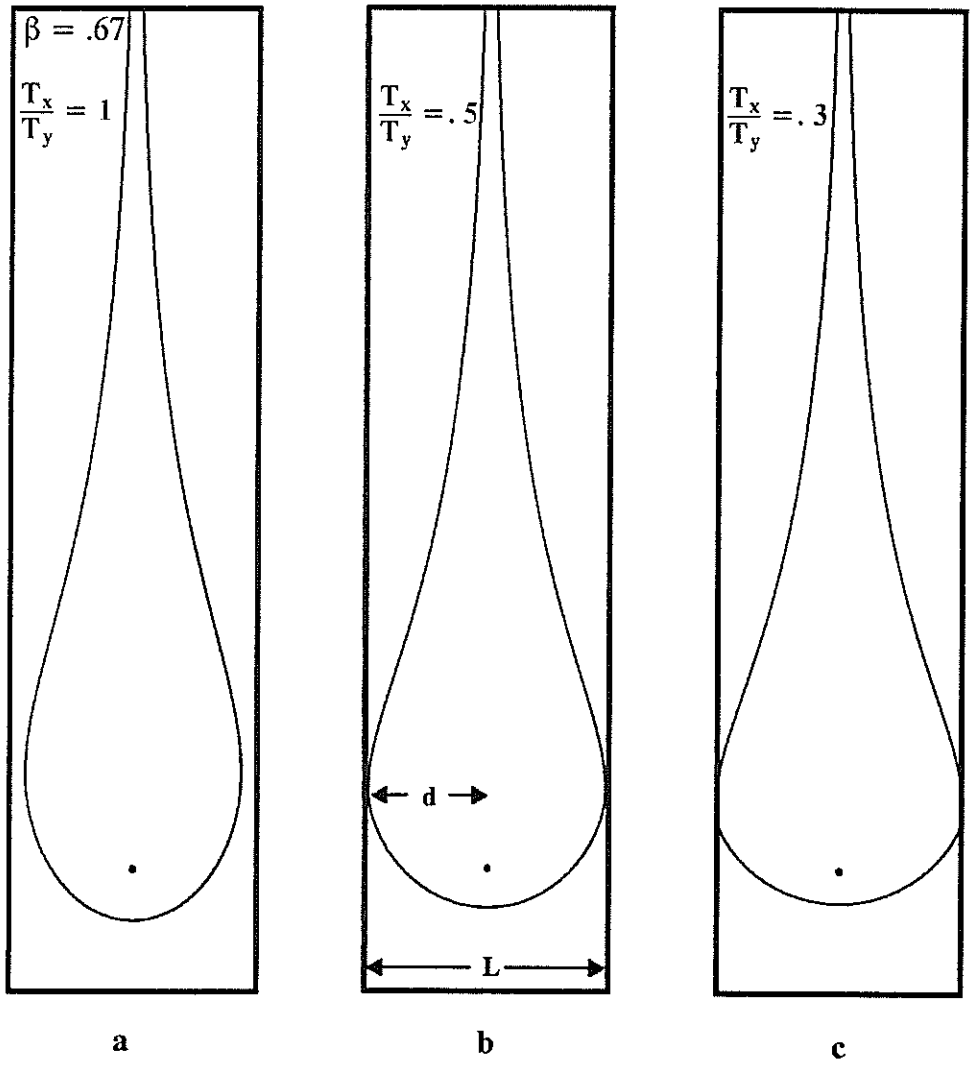

Figure 3–19. Capture zones for a well in a stream-stream bounded aquifer where $q_L=q_y$ and $q_x=0$.

lesser transmissivity. The second is that the propensity for induced infiltration is enhanced if the greater transmissivity is normal to the stream and is reduced if the greater transmissivity is parallel to the stream.

CONCLUSIONS

This section's first goal was to present the three basic capture zone models for wells located near streams, following the conceptualizations given in Section 2. We then extended these conceptualizations by including conditions of ambient flow at an angle to the stream boundary, time-dependent capture zones or fronts, multiple wells and aquifer heterogeneity

and anisotropy. Although we could have derived the flow fields using only analytical techniques, we chose to employ numerical methods as a foundation for more complex modeling in the future. Ultimate and time-dependent capture zones were computed numerically, using particle tracking. In general, our results have produced capture zones varying widely in shape and size depending on the model and parameters used to delineate the capture zone. These results are summarized below:

1. The source of recharge strongly influences the shape of the capture zone in the aquifer and the propensity for induced infiltration. Strong local vertical recharge leads to larger capture zones, and 'cusping' of the capture zone along barrier boundaries and groundwater divides. Strong lateral inflows lead to capture zones that orient on the direction of the inflow.

2. Boundaries have a significant effect on capture zone patterns. Barrier boundaries lead to wider capture zones, because there is no aquifer upgradient from which to capture water. Stream boundaries lead to smaller capture zones, because they have an 'inexhaustible' supply of recharge water.

3. When the stream has a significant gradient, and the lateral inflow approaches it at an angle, the capture zone becomes non−symmetric. Propensity for induced infiltration is increased.

4. Time-dependent capture zones, or fronts, provide information regarding equal travel time contours. Front delineation is dependent on magnitudes as well as direction of velocities. Parameters effecting velocities include porosity, saturated thickness of the aquifer and hydraulic conductivity. Ultimate capture zones are not effected by these parameters. Time-dependent capture zones can be scaled by porosity and saturated thickness. If the saturated thickness varies significantly, then capture zone estimates based on uniform thickness are in error, mostly around the well and near the stream.

5. Multiple wells pumping at low rates behave independently. When they pump at higher rates, or are closer, they begin to interfere with each other. Their capture zones repel each other. At still higher pumping rates the capture zones merge, and the wells begin to act as one. As capture zones merge, the propensity for induced infiltration increases.

6. Small variations in transmissivity bordering the stream control intersection of the stream by the capture zone and the propensity for induced infiltration. Differences in transmissivity in a real-world scenario may be greater than those simulated here, producing an even more pronounced effect.

7. Small differences in x and y transmissivities produce relatively large differences in the capture zone. Both stream interaction and areal extent within the aquifer are noticeably modified. The capture zone expands laterally and the propensity for induced infiltration increases when the transmissivity is greater in the direction normal to the stream. The capture zone expands longitudinally (up and

down the 'valley'), and the propensity for induced infiltration decreases when the transmissivity is greater in the direction parallel to the stream.

From these analyses, we can make some general statements regarding capture zone delineation. Using simple two-dimensional flow models, we have derived numerous capture zone representations by looking at variation of individual parameters. The combined effects of some parameters may act to further vary capture zone representation. As the number of possible perturbations increases, the modeling effort becomes more demanding and complex and the amount of data needed, to provide an accurate model also increases. In a real world setting it would not be possible to include all possible processes occurring, or to perhaps accurately portray all of these processes in the model. As a result, we are attempting to represent complex hydrologic phenomena using a deterministic model with a given number of assumptions. The number of simplifying assumptions made for a model usually increases with decreasing data availability. Correspondingly, less data and more assumptions contribute to the inaccuracy of the model. We can conceptually categorize this inaccuracy as model uncertainty and it should be of concern for any party doing capture zone delineation. This uncertainty issue is the subject of the next section.

SECTION 4

CAPTURE ZONE UNCERTAINTY IN AN INFINITE FLOW DOMAIN

INTRODUCTION

The role of modeling in capture zone analysis is to further our understanding of the nature of capture zones and to provide us with a tool with which to make management decisions. An important component of decision making is evaluating the risk involved with various capture zone solutions. Deterministic solutions resulting in single representations of the capture zone may not always provide adequate information on which to base a risk analysis. In previous sections, we developed simple two-dimensional mathematical models to delineate capture zones using a deterministic approach. The effects of uncertainty can be incorporated into these models providing us with probabilistic or 'fuzzy' capture zones (Linderfelt et al., 1989; Leppert, 1990).

The uncertainty of an ultimate capture zone is most easily represented by defining a suite of capture zone boundaries, each with a different probability of capture. Along a contour line labeled P=0.40, a particle would have a 40% chance of being captured, and a 60% chance of bypassing the well. These fuzzy capture zones have two interpretations. The first, referred to above, is the probability that a particle released at that point will enter the well. The second probability represents the proportion of a chronic release (e.g., long-term contaminant source) that reaches the well. This last interpretation is only valid for some of the uncertainty issues we examine.

Capture zone uncertainty may originate from a variety of causes. For example, the conceptual model itself may be uncertain. In some sense the sensitivity analyses presented in Section 3 address this issue but, we assumed that the conceptualization and its associated mathematical model was appropriate. Treatment of aquifer spatial parameters as a stochastic random field can also lead to capture zone uncertainty. For the purposes of this study, we assume a spatially deterministic model. Instead, we focus on two sources of capture zone uncertainty, parameter uncertainty and dispersion. Parameter uncertainty is that due to uncertainty in the flow equation parameters, such as pumping rate, ambient flow rate and direction, and aquifer thickness, all of which are considered constant but uncertain parameters. That is, we assume that the magnitude of the ambient flow rate has a certain value but that we are unable to measure it precisely. Dispersion-induced uncertainty as examined here is that due to mechanical and macro-dispersion (Bear, 1979), which allows particles to cross streamlines. In this way contamination initially located outside of the capture zone can enter it.

METHODOLOGY

In order to focus on the uncertainty issue, we will address uncertainty issues for a hypothetical flow system consisting of a single pumping well in an infinite flow domain with a component of uniform ambient flow, schematically shown in Figure 4-1. The solution to the flow field can be represented in its entirety by the complex function Ω given by

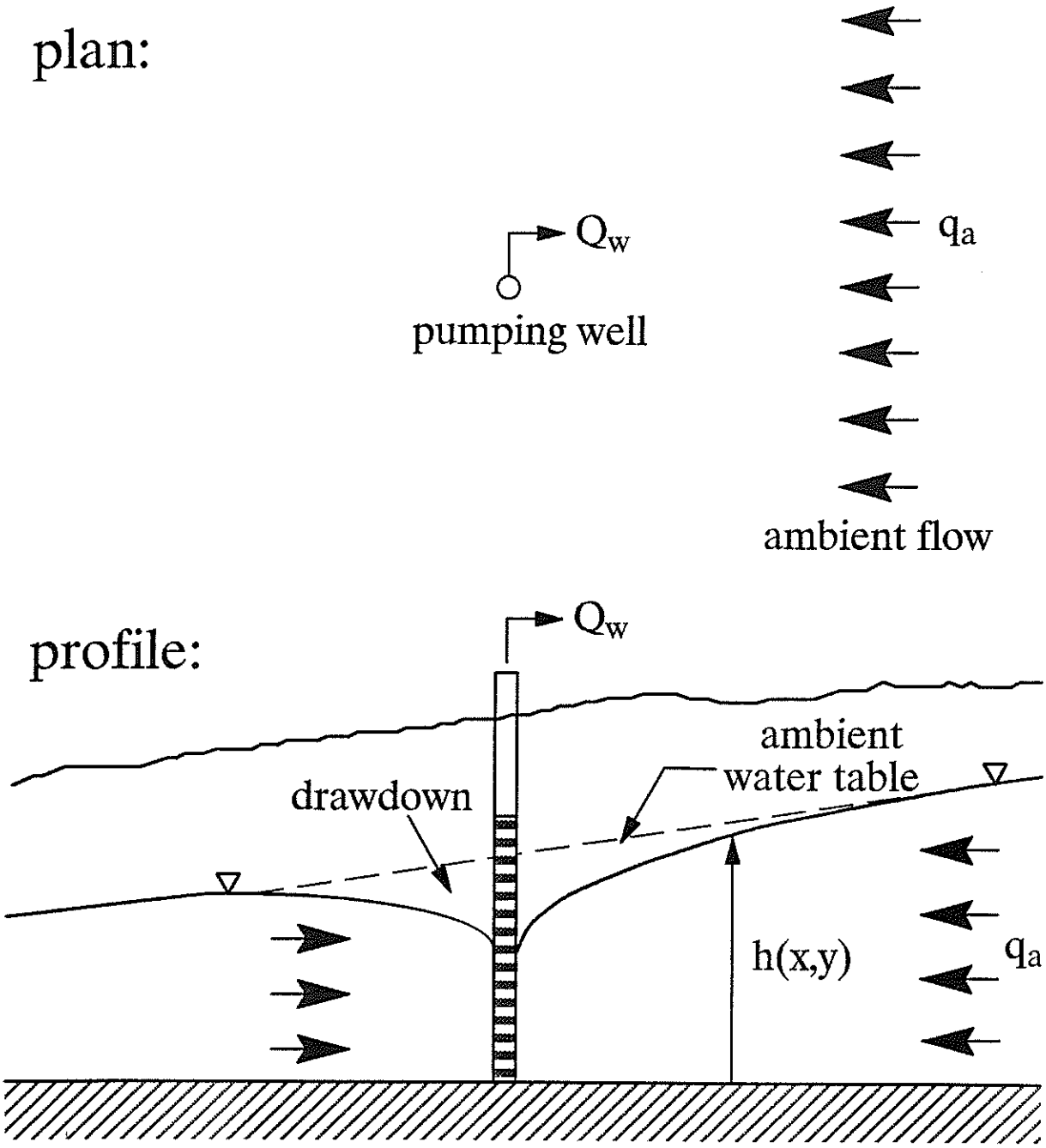

Figure 4-1 Schematic of a pumping well in the vicinity of a stream in the presence of ambient flow in an infinite aquifer.

$$\Omega = \Phi + i\Psi \tag{4-1}$$

where Φ is the complex potential function, Ψ is the complex stream function, and under steady-state conditions Φ satisfies the LaPlace equation, $\nabla^2\Phi = 0$. The state variable Φ [L^3/T] takes on different definitions in confined and phreatic aquifers,

$$\Phi = \begin{cases} Th & , \text{ confined or linearized phreatic aquifer,} \\ \frac{Kh^2}{2} & , \text{ Dupuit type phreatic aquifer,} \end{cases} \tag{4-2}$$

where h [L] is depth averaged head (also water table elevation in the phreatic aquifer case), K [L/T] is horizontal hydraulic conductivity, and T= [L^2/T] is transmissivity. Using superposition, Φ can be shown to be

$$\Phi = \Phi_0 + q_a y + \frac{Q_w}{4\pi}\ln(x^2 + y^2) \tag{4-3}$$

where Φ_o is the reference potential taken to be zero here, q_a [L^2/T] is the ambient flow rate per unit aquifer depth, and Q_w [L^3/T] is the pumping rate. If all parameters are known exactly, that is, if there is no uncertainty in any of the input parameters of (4-3), then a deterministic solution to the capture zone can be derived. To accomplish this, we first find the velocity field by taking the derivative of (4-3) with respect to x and y space coordinates to obtain Darcy velocities, then divide these by the porosity, n, and the aquifer thickness, b, to obtain average linear velocities (note: for a more detailed explanation of this general procedure of capture zone delineation, see Section 2):

$$-\frac{\partial\Phi}{\partial x} = q_x \; ; \qquad -\frac{\partial\Phi}{\partial y} = q_y \tag{4-4}$$

$$V_x = \frac{q_x}{nb} \; ; \qquad V_y = \frac{q_y}{nb} \tag{4-5}$$

We then set the two equations in (4-5) equal to zero and solve for the x and y locations of the stagnation point. Two particles are then 'placed' into the flow system, being slightly offset from the stagnation point, and tracked backwards using a numerical distance-increment tracking scheme such as Euler's method or, for higher accuracy but higher computational effort, a fourth-order scheme can be used such as the Runge-Kutta method. For the simple flow system considered here, an adaptive Euler's method proved adequate provided the length constant is kept small where needed. An example of a capture zone derived in this way is shown in Figure 4-2.

The capture zone can also be derived from a stream function solution (Milne-Thomson, 1968; Bear, 1979): $\Psi = -q_a x + (Q_w/2\pi)\tan^{-1}(-x/y)$. The dividing streamline that defines the capture zone is given by $x/y = \pm \tan(2\pi q_a x/Q_w)$, in which the capture zone is characterized by the dimensionless pumping rate β

$$\beta = \frac{Q_w}{\pi b q_a}. \tag{4-6}$$

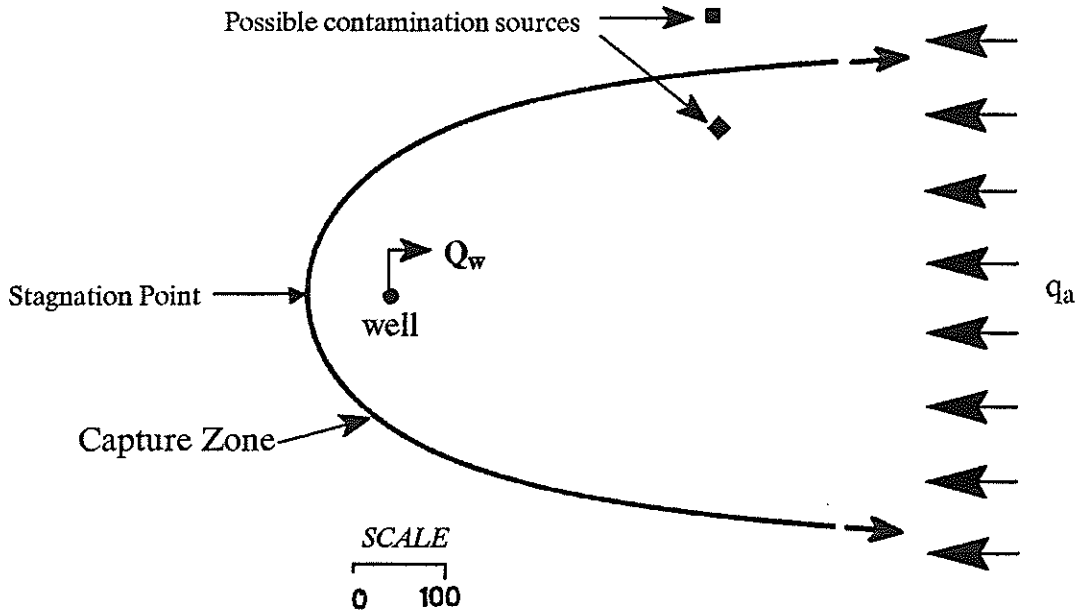

Figure 4–2. Capture zone in infinite flow field showing ambient flow, q_a, the well with flow rate, Q_w, and contamination sources inside (◆) and outside (■) the capture zone.

Q_w is the pumping rate, π is a constant, b is the aquifer thickness, and q_a is the ambient flow rate (note that this is a different definition for β than found in the other chapters). Thus $x/y = \pm \tan(2\beta\ x/b)$. The stagnation point is located a distance $y_s = -Q_w/2\pi q_a = b\beta/2$ downstream of the well and the capture width approaches $w = Q_w/q_a = \pi b\beta$. Suppose that β were to take on different values, then the capture zone would take on a size proportional to β, although it would retain the same shape.

The capture zone obtained using these methods is, again, derived using a deterministic approach. The capture zone is composed of an area delineated by a single, sharp boundary where it is assumed that all the water on the well–side of the capture zone boundary is eventually pumped by the well (assuming continuous pumping rate) and the water on the opposite side of the capture zone boundary continues in the direction of ambient flow, eventually passing out of the well's influence altogether. A contaminant source located outside the capture zone would therefore not be a threat to the water quality in the well, while contamination from a source located inside the capture zone would be pumped by the well. The capture zone depicted in this scenario does not allow for any uncertainty or variation in the input parameters, and as a result the location of the capture zone is assumed to be perfectly known. The drawback

to this type of model lies in the uncertainty in some or all of the input parameters used to delineate the capture zone, but nowhere has this uncertainty been incorporated into the model. Our next step is to incorporate uncertainty into the model.

PARAMETER UNCERTAINTY

Here we assume that the model parameters are constant but uncertain. Let us further assume that this uncertainty can be characterized by a mean and a variance (first and second moment), or better yet, by a probability density function such as a Gaussian probability density function (PDF). In the first case the uncertainty can be modeled using a first order, first and second moment analysis (Dettinger and Wilson, 1981). While the full distributional approach requires the method of derived distributions (Benjamin and Cornell, 1970), the Monte Carlo approach (Carter and Cashwell, 1975), or even, as in a special case which follows, a numerical integration approach. The first order, first and second moment method has the disadvantage of not modeling a complete probability distribution, assuming its availability. However, for simple cases and where parameters show a sufficiently small variance, this approach may be adequate. It has the advantage of minimal computation cost. The Monte Carlo approach has the disadvantage of being expensive computationally, yet can provide good results for mathematically intractable problems. EPA (1990) has proposed it for capture zone analysis. The method of derived distributions provides an analytical solution, but derivation of the mathematical equations may be cumbersome and subsequent integrations may have to be handled numerically. For many of the simple models of this report, the derived distribution method is tractable.

In the derived distribution method, an 'uncertain' input parameter with a known distribution is used to analytically derive a solution for the output parameter which then exhibits the required distribution. For example, let the model be given by (4−6), where β is output and Q_w and q_a are the inputs. If we can obtain the distribution of β, then we have characterized our uncertain or fuzzy capture zone. Mathematically this is stated as

$$g(\beta) = f(w_1(\beta))|J| \qquad (4-7)$$

where g() is the desired distribution of the output, f(w) is the distribution of an input, and J is the Jacobian. For example, if the pumping rate exhibited a certain distribution, represented by $f(Q_w)$, then we have

$$Q_w = w_1(\beta) = \pi b q_a \beta \quad . \qquad (4-8)$$

The Jacobian would be given by

$$|J| = |w'_1(\beta)| = \pi b q_a \qquad (4-9)$$

and the resulting distribution for β in terms of the distribution of Q_w is given by

$$g_1(\beta) = f(w_1(\beta))\pi b q_a \quad . \qquad (4-10)$$

For this simple linear case it is seen that the distribution of β is the distribution of Q_w translated by the constant $\pi b q_a$. Once density functions are obtained in this way, probabilities are obtained by integrating $g_1(\beta)$ between an arbitrary lower limit, β_0, and the maximum value, β_{max}.

$$P(\beta_0 \leq B \leq \beta_{max}) = \int_{\beta_0}^{\beta_{max}} g_1(\beta)d\beta \quad . \tag{4-11}$$

For uncertain ambient flow rate, the density function of β is given by the non-linear functional

$$g_2(\beta) = f(w_2(\beta))\frac{Q_w}{\pi b}\frac{1}{\beta^2} \quad . \tag{4-12}$$

Probabilities are found from

$$P(\beta_0 \leq B \leq \beta_{max}) = \int_{\beta_0}^{\beta_{max}} g_2(\beta)d\beta \quad . \tag{4-13}$$

The first example considered here is that of an uncertain pumping rate, Q_w, distributed in a skewed fashion, as shown in Figure 4-3, using a beta distribution designated by

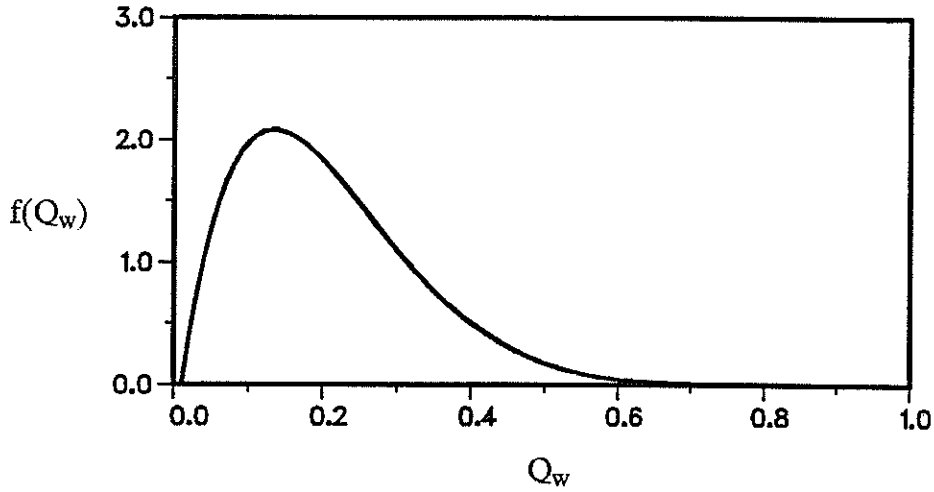

Figure 4-3. Probability density function of pumping rate.

$$f(Q_w) = \frac{1}{D_w}(Q_w - Q_{min})^{p_w-1}(Q_{max} - Q_w)^{r_w-1} \quad , \tag{4-14}$$

where Q_{max} and Q_{min} are maximum and minimum pumping rates equal to 1.0 and 0.01 m^3/min, respectively, and p_w and r_w are distribution parameters. D_w is the beta function given by (note: we reserve the use of the term 'β' for our dimensionless pumping rate defined by (4-6)):

$$D_w = \int_{Q_{min}}^{Q_{max}} (Q_w - Q_{min})^{p_w - 1}(Q_{max} - Q_w)^{r_w - 1} dQ_w \quad . \qquad (4-15)$$

For p_w and r_w equal to 2 and 6, respectively, $1/D_w = 42.0$ with a mean of $\mu_{Qw} = 0.24$ m^3/min and a variance of $\sigma^2_{Qw} = 0.020$ m^3/min. The ambient flow rate is $q_a = 0.0002$ m^2/min and the aquifer

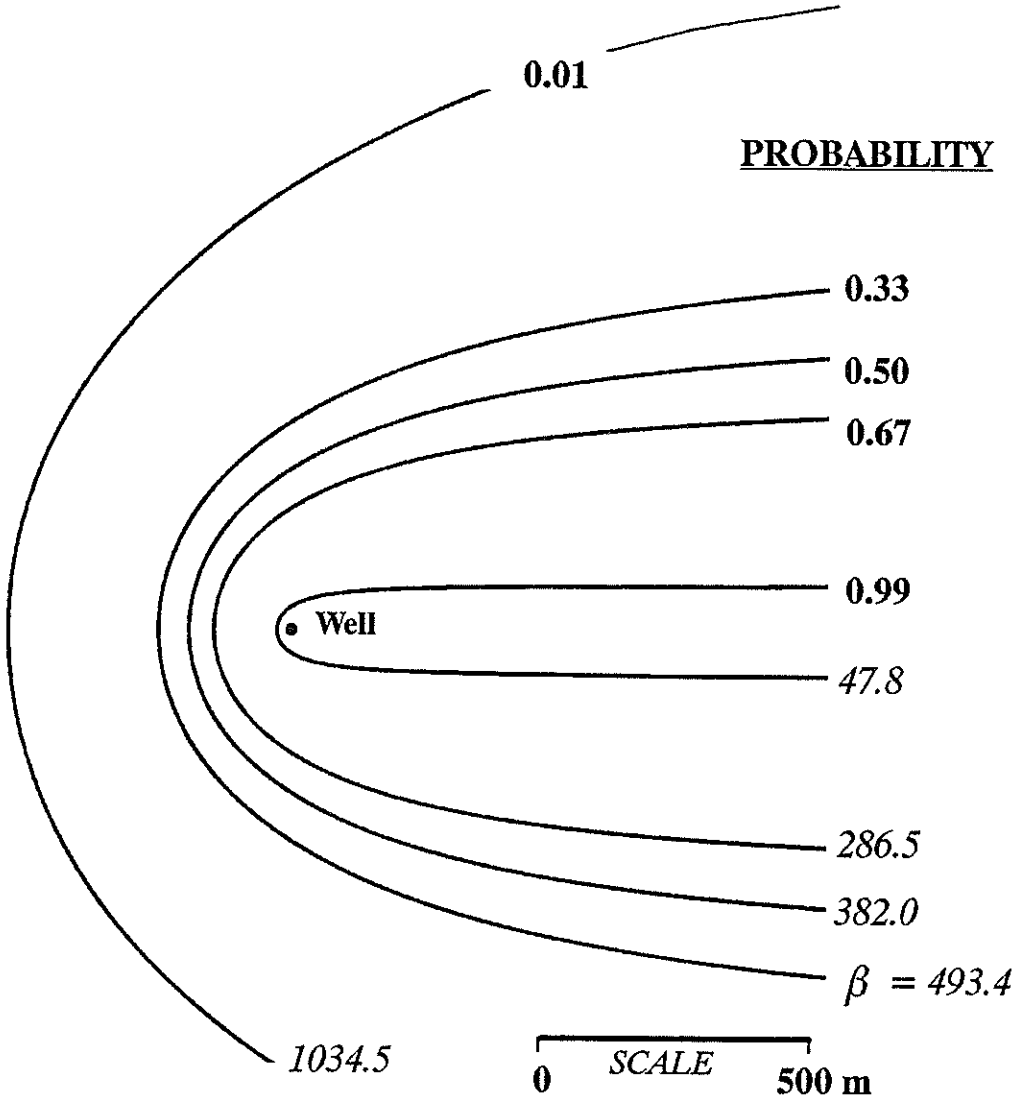

Figure 4–4. Fuzzy capture zone for pumping well located in infinite flow field with ambient flow. Probabilities correspond to associated dimensionless capture zone parameter β derived from uncertain pumping rate Q_w.

thickness is b=1.0. The beta distribution is used here since it allows for larger coefficients of variations without truncated distributions and also provides for a large variety of distributions

using a straight forward, easy to integrate functional. The minimum pumping rate is set at 0.01 since we are not interested in non−pumping solutions.

The capture zone shown in Figure 4−4 is fuzzy. There is no longer a single, deterministic, capture zone but rather a distribution of capture zones, each represented by probabilities which can be regarded in two different ways. Probability values can be thought to represent the probability of a capture zone being greater than or equal to the associated β value, or alternatively, a particle or contaminant source located on any given contour line will have the associated probability of eventually reaching the well. The type of contaminant referred to in this scenario is an acute contaminant release such as a spill.

Uncertainty in the magnitude and direction of ambient flow can also be incorporated into the model. The magnitude of ambient flow would be treated as outlined above and will not be presented here. The case of ambient flow at some angle θ to the positive x−axis is shown schematically in Figure 4−5. Our analysis starts again by assuming a beta distribution for the

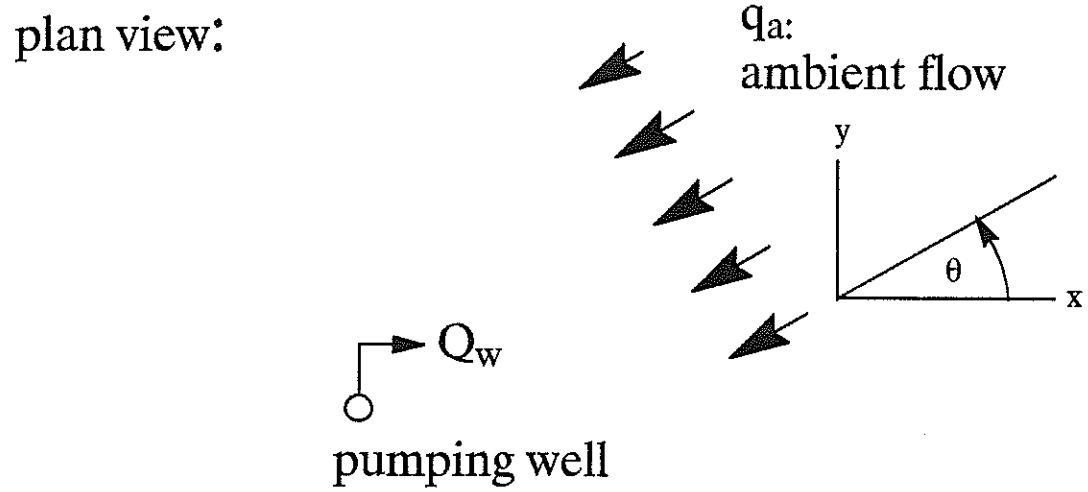

Figure 4−5. Schematic of pumping well in infinite flow field with ambient flow at angle θ.

angle of ambient flow with the direction varying between 0^0 and 90^0. The beta−function can be expressed in trigonometric form as (Boas, 1983)

$$D_\theta = 2\int_0^{\frac{\pi}{2}} (\sin\theta)^{2p_\theta - 1}(\cos\theta)^{2r_\theta - 1}d\theta \quad . \tag{4−16}$$

The parameters p_θ and q_θ are again 2 and 6, respectively, and $1/D_w$ is again equal to 42.0. The mean angle of flow is 22.5^0 and the PDF for ambient flow direction is shown in Figure 4−6.

Probabilities were derived for the uncertain angle problem using a numerical integration approach where each respective capture zone is overlayed onto a grid and internal grid points

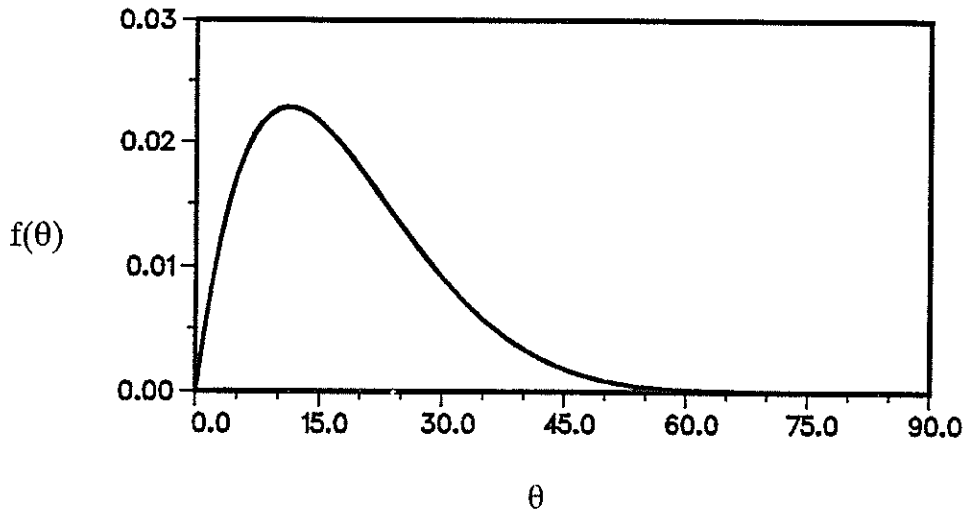

Figure 4−6. Probability density function of direction of flow in terms of angle, θ.

assigned to an appropriate density value. Density values were derived by dividing the distribution range into 90 separate angles, essentially discretizing the region between 0 and 90 degrees. Grid points overlapped by successive capture zones were assigned superposed density values, which were then normalized by the sum of total densities, thus providing the required probabilities.

The 90 curves used, representing the 90 angles, is shown in Figure 4−7. An important feature to note is that the 0^0 and 90^0 curves enclose an obvious tear drop shape and the densities of all 90 curves are represented within this area. This means there is, effectively, a probability of 1.0 that the water within this zone will be pumped by the well regardless of the distribution, given the same minimum and maximum θ values. If θ were normally distributed, the axis of this tear drop zone would coincide with the mean θ, $\mu_\theta = 45^0$. In our example the mean is 22.5^0, leading to the skewed fuzzy capture zones of Figure 4−8. In addition, all of the contours are closed like the high probability capture zone contour labeled 0.99. Closed contour lines indicate that there is an upgradient limit to the reliable prediction of capture zones.

Multiple uncertain input parameters are demonstrated in the example shown in Figure 4−9. The ambient flow direction and pumping rate are both uncertain, essentially combining the results shown in Figures 4−4 and 4−8. A two−parameter derived distribution is not used in this case because the angle problem is solved using the numerical approach. The pumping rate distribution problem is solved using derived distributions and the probabilities of these curves, normalized to the densities of the respective angles, are then superposed for successive angles as before. The resulting fuzzy capture zone is derived using the same distributions as above.

As seen in Figure 4−9, the influence of uncertain pumping rate superposed on uncertain flow angle is to make the capture zone fuzzier by spreading out the probabilistic curves over a larger area. Also, the higher probability curves have been reduced in size so that the overall effect is to increase the uncertainty in the capture zone.

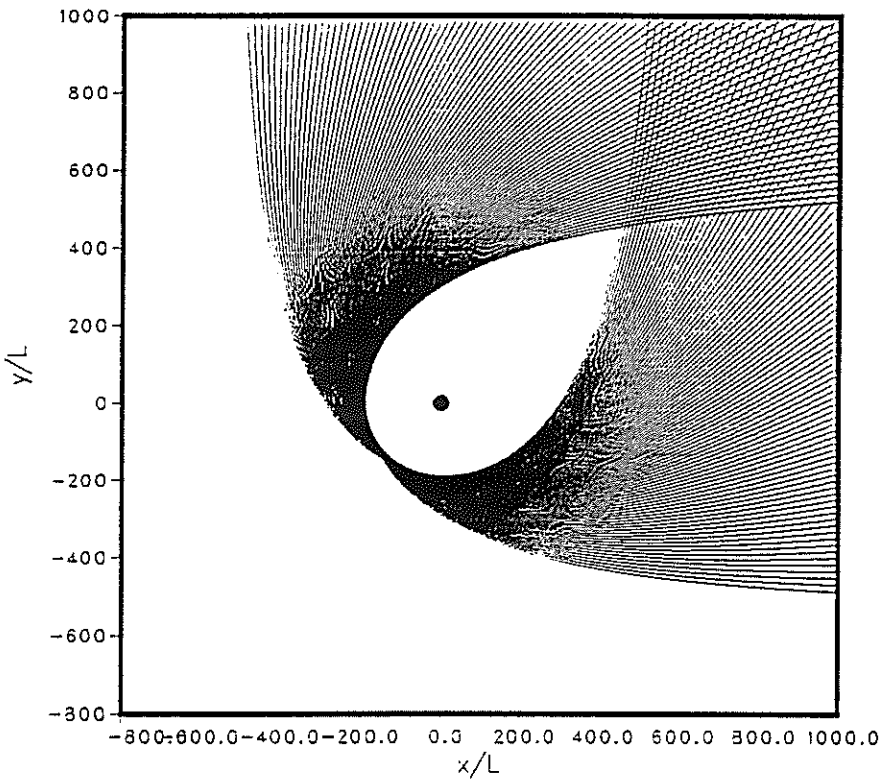

Figure 4−7. Plot of 90 angles used in numerical integration to calculate probabilities for uncertain ambient flow direction problem.

HYDRODYNAMIC AND MACRO DISPERSION INDUCED UNCERTAINTIES

Dispersion effects on capture zone uncertainty is evaluated using two different approaches. Given a deterministic capture zone based on potential flow theory, such as described earlier in this paper, the flux of water across the capture zone boundary, a streamline, is defined to be zero. Thus, for a given contamination source outside the capture zone as shown in Figure 4−2, and assuming a chronic contamination source such as a long−term leak, our deterministic capture zone model indicates that none of the contaminant will be pumped by the well. However, due to hydrodynamic or macro−dispersion, there is a chance some contamination will cross the capture zone boundary and enter the well. This can easily be shown by implementing the random walk method of advection−dispersion modeling for a contaminant source outside but near the capture zone boundary.

By considering point sources at every point within the flow domain, points exhibiting equal proportion of contamination crossing the capture zone could be identified and specific 'equal−proportion' capture zones could be derived simply by connecting or contouring these points. We refer to the associated contour values as a type of partition coefficient. Point sources generally closer to the capture zone boundary would exhibit a larger partition coeffi-

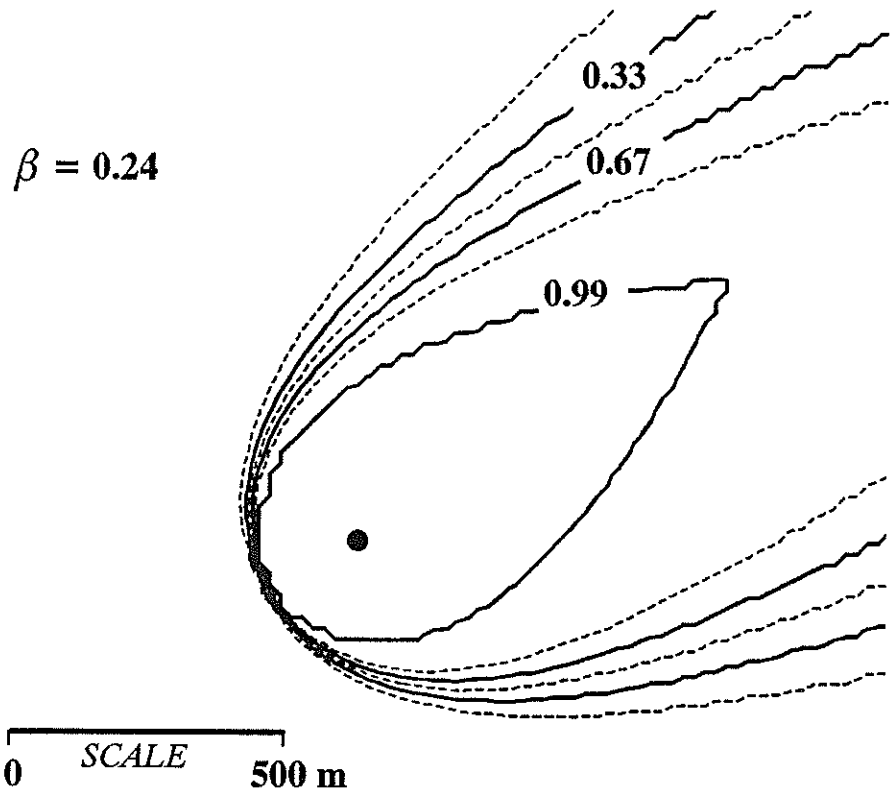

Figure 4–8. Fuzzy capture zone for ambient flow direction uncertian and constrained between 0^0 and 90^0. Pumping rate and ambient flow rate are constant.

cient and would have a higher proportion of contamination going to the well. Sources on the deterministic flow–parameter capture zone would have a 50% chance of being pumped by the well. The uncertainty or fuzziness in the capture zone is now not due to a probability of locating the capture zone as before, but instead is due to the dispersion process spreading the contaminant into a plume. The term 'uncertainty' in this case is not purely correct since we are saying that for different locations in the aquifer (and assuming we know the aquifer's dispersive properties) we can predict exactly the amount of contamination crossing the capture zone boundary and entering the well. A more proper use of the term uncertainty in this scheme is that of model uncertainty where the decision to (or not to) incorporate dispersion into the model affects the results.

Conceptually the above approach of contouring equal partitioned sources is easy to envision. Computationally, however, defining the partition coefficient for each point within the flow domain would be prohibitive. A more direct, analytic approach to obtaining these capture zone partitioning curves is to solve what we call the 'backward' dispersion model where the advection–dispersion equation is solved using the negative velocity field (Linderfelt et al., 1989). Two different source locations can be used depending on the desired outcome. For ti-

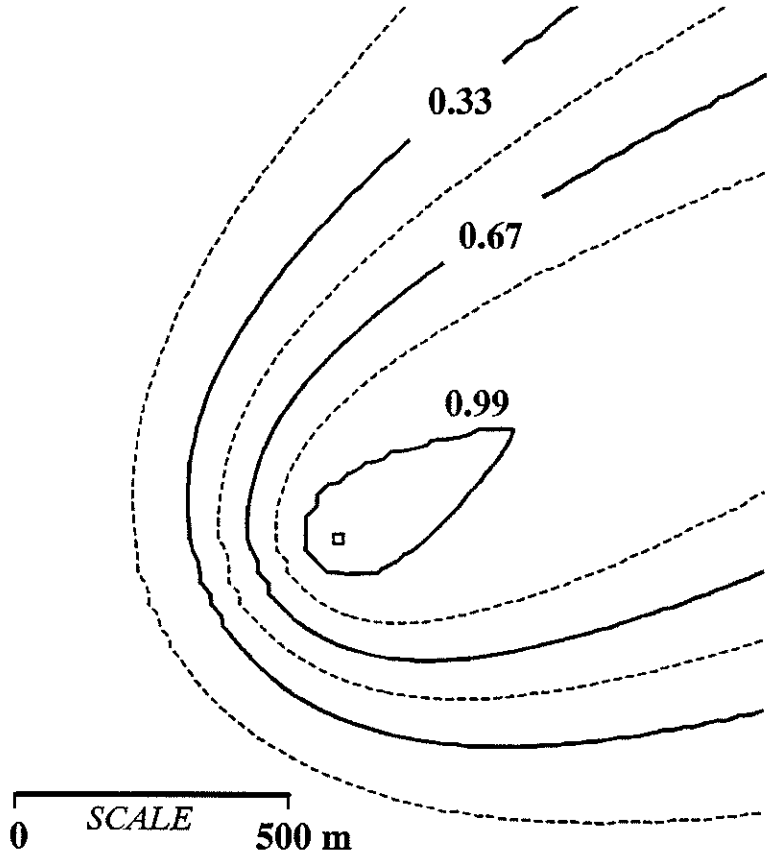

Figure 4–9. Fuzzy capture zone for ambient flow direction and pumping rate uncertain as shown in Figures 4–4 and 4–8.

me–dependent capture zones, such as fronts, the contaminant 'source' is placed at the well with concentration $C/C_0=1.0$ and the flow field solution is reversed by reversing, in sign, the flux boundaries. Pumping wells become injection wells and flux–in boundaries become flux–out boundaries, and so on. Dispersed fronts would move out from the original pumping well with the $C/C_0=0.5$ front representing the deterministic time–dependent capture zone front and the C_i/C_0 values representing the partition coefficients. If only the capture zone boundary (i.e., the capture zone for $t=\infty$) is of interest, the stagnation point is used as the source and the negative or reverse of the original flow field is used. The example we present is for the capture zone boundary, which we solve with an approximate analytical solution. We have verified this solution with the random walk method (Linderfelt et al., 1989) and, in cooperation with E. Sudicky, with a LaPlace Transform Galerkin numerical solution to the backward advection–dispersion problem (Sudicky, 1989). The latter has been applied to a variety of capture zone problems that we'll present at a latter time.

To derive the analytical backward advection–dispersion solution, we start with the advection dispersion equation given by (e.g., Bear, 1979)

$$\frac{\partial c}{\partial t} = \frac{\partial}{\partial x_i}\left(D_{ik}\frac{\partial c}{\partial x_k} - v_i c \right) \tag{4–17}$$

where c is the concentration, x_i $(i = 1,2)$ are Cartesian coordinates, D_{ik} are components of the factor of dispersion D which is a second–order symmetric tensor, and v_i are average velocity components. The equation is then transformed into an orthogonal curvilinear coordinate system. For the system being analyzed here, it is most convenient to transform (4–17) into the coordinate system of streamlines and equipotential lines. The resulting equation for two–dimensional plane flow is given by

$$\frac{\partial c}{\partial t} = v\left[\alpha_I \frac{\partial^2 c}{\partial s_\phi^{\,2}} + \alpha_{II}\frac{\partial^2 c}{\partial s_\psi^{\,2}} - \cos(v, 1s_\phi)\ \frac{\partial c}{\partial s_\phi} \right] \tag{4–18}$$

where α_I and α_{II} are longitudinal and transverse dispersivities, respectively, s_ϕ and s_ψ are length along the respective coordinate axes, and $cos(v, 1s_\phi)$ is the cosine of the angle between the base vector in the positive direction along the s_ϕ coordinate and the direction of v. It has value ± 1 and is positive in this instance. For the case of steady flow, (4–18) simplifies to

$$\alpha_I \frac{\partial^2 c}{\partial s_\phi^{\,2}} + \alpha_{II}\frac{\partial^2 c}{\partial s_\psi^{\,2}} = \frac{\partial c}{\partial s_\phi} \quad . \tag{4–19}$$

A further simplifying assumption comes from realizing that for a steady state solution and given the specific flow domain geometry for this problem, only transverse dispsersion will affect the ultimate capture zone. This allows us to further simplify the problem to the straight forward parabolic equation

$$\alpha_{II}\frac{\partial^2 c}{\partial s_\psi^{\,2}} = \frac{\partial c}{\partial s_\phi} \tag{4–20}$$

with the initial conditions of a step change in concentration at the origin

$$\begin{aligned} &c = c_0 && s_\psi < s_{\psi 0} \\ &c = 0 && s_\psi > s_{\psi 0} \quad \text{at} \quad s_\phi = 0 \end{aligned} \tag{4–21}$$

with

$$\begin{aligned} &c \to c_0 \quad \text{as} \quad s_\psi \to -\infty \\ &c \to 0 \quad \text{as} \quad s_\psi \to \infty \quad \text{for} \quad s_\phi > 0 \quad . \end{aligned}$$

The solution of (4–20) subject to these boundary conditions is well known:

$$C(s_\psi, s_\phi) = \frac{1}{2} C_0 \; erfc\left[(s - s_\phi)/(4as_\phi)^{\frac{1}{2}}\right] \quad . \tag{4-22}$$

This solution is plotted in Figure 4-11 for four different dispersivity values (Linderfelt et al., 1989). For dispersivities of 2 to 5 meters and more this approximate solution may not be quanti-

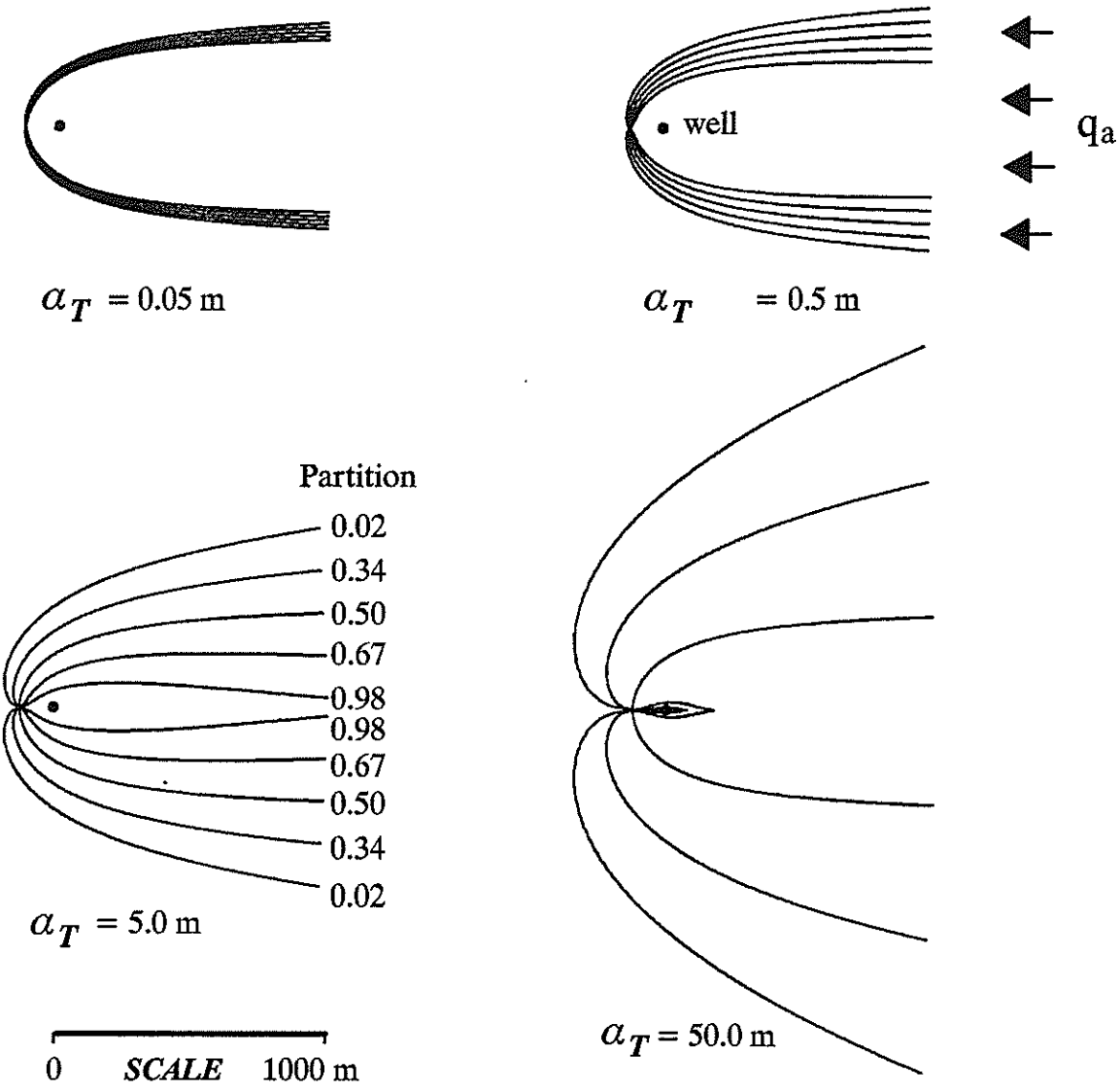

Figure 4-10. Fuzzy capture zones derived from dispersion affects for a single β value. Dispersivities vary from α_T = 0.05 to 50.0 m.

tatively accurate. Among other things it ignores interference of dispersion along one bounding streamline with the other.

As stated before, for a chronic source located on a particular contour, the associated partition coefficient represents the proportion of that source crossing the flow–parameter capture zone (i.e., the 50% capture zone delineated using the original deterministic flow model). As the dispersivity increases, for individual sources we would see the contaminant plume grow larger with an increase in the fuzziness of the capture zone. As the dispersivity becomes very small, dispersion becomes less significant and the fuzziness in the capture zone is reduced.

With our proposed model, we are saying there is some chance that any source within the flow domain will contribute to the well. In reality we realize there are limitations to how far away a source can be located from the well and still contaminate it, based on the magnitude of the velocities in the flow field. In a practical sense, we can interpret our results with respect to well head protection areas and zoning. In areas underlain by aquifers exhibiting very small dispersivities, the deterministic capture zone may act as an adequate predictive model. For aquifers with larger dispersivities, simple deterministic capture zone modeling based solely on potential flow theory may be inadequate in defining capture zones for use in the decision making process. Zoning regulations based on a deterministically derived capture zone may in fact not be protecting the water pumped from the well head, especially for contaminants toxic at trace concentrations.

CONCLUSIONS

We have developed capture zone models which are no longer deterministic in nature but provide insight into the uncertainty of capture zone behaviour. Capture zone uncertainties have two interpretations. The first, referred to in the case of parameter uncertainty, is the probability that a particle released at a given point will enter the well. The second is that the probability represents the proportion of a chronic release, such as a long term contaminant source, reaching the well. This last interpretation is valid for the effects of dispersion, but not for parameter uncertainty.

A deterministic solution to a capture zone reflects the use of single, representative values for the various model input parameters. These values usually reflect limited knowledge of the individual parameters and usually are assumed to represent a mean or average value of the system, sometimes with a margin of safety included. The method of parameter uncertainty presented here assumes that enough data exists with which to infer a PDF. In some instances, the form of the PDF may be assumed. For instance, uncertainty in the pumping rate may be due to random errors of measurement which are generally assumed to take on a Gaussian distribution. In this case, a reduction of the uncertainty may not be possible given certain conditions of measurement.

In other cases, additional data may provide for a reduction in the output uncertainty. For instance, additional head measurements, both spatially and in time, could better define the direction or rate of ambient flow. However, even if a very large amount of data is collected, random fluctuations in measurements will always exist such that a single, representative parameter value may not be obtainable.

The incorporation of dispersion into the capture zone model is shown here to play a potentially important role in capture zone delineation. Capture zone uncertainty due solely to dis-

persion may be as large as uncertainty due to constant but uncertain flow parameters. The decision to include dispersion into the model is important since it requires previous knowledge of the effects of dispersion on capture zone delineation, and involves both an additional commitment to data collection and analysis, and more sophisticated models.

SECTION 5

THREE–DIMENSIONAL ANALYSIS OF CAPTURE ZONES WITH AMBIENT FLOW

INTRODUCTION

Most of our previous work on delineation of capture zones has concentrated on two–dimensional vertically integrated solutions to flow. The major assumptions inherent in this type of analysis include a fully penetrating pumping well and, if it exists, a fully penetrating stream boundary. Rarely are both conditions met. When either the stream or the well does not fully penetrate the aquifer,there is vertical flow. This vertical flow influences the size and shape of the capture zone and the propensity for induced infiltration. As the depth of penetration becomes smaller, vertical flow becomes more pronounced and must be included in the model if an accurate representation of the capture zone and induced infiltration is to be obtained.

In two dimensions we represented the capture zone boundary using imaginary particles tracked backward within the velocity field (see Section 3 and Appendix A). Ultimate capture zones were obtained by starting one or two particles near a stagnation point and recording their paths as they moved away. Time-dependent capture zone fronts were started with a group of particles placed around the well. After the particles had moved away from the well for a prescribed travel time,their positions were connected together to produce the predicted capture zone front. In these two–dimensional models the capture boundaries are composed of curved lines, and the capture zone itself is represented by the area within these lines. In three–dimensions the capture zone is defined by a volume and the capture zone boundary is represented by a surface. The basic concept of tracking particles backward in the velocity field is still applicable, but now the capture zone surface must be divided into smaller partitioned surfaces in the form of polygons. The simplest polygon that defines a surface is a triangle defined by three vertices or particles.

Induced infiltration from a partially penetrating stream has been previously studied by Chow and Wilson (1988) and Larson et al. (1987). Chow and Wilson (1988) used a superposition of analytical solutions for partially penetrating streams near wells (Boulton, 1942), ambient flow to a line sink (Milne–Thomson, 1968) and flow to a partially penetrating well (Muskat, 1937) to study induced infiltration. Larson et al. (1987) used a finite difference code to examine capture zones and induced infiltration in site study. They were unable to discretize the domain in any great detail.

To study capture zones in three dimensions we use a three–dimensional block centered finite difference flow code along with a particle tracker utilizing triangular elements (Schafer–Perini, 1990; Schafer–Perini and Wilson, 1991b,c). We investigate various well and stream penetrations, and the distance between the well and stream. Comparisons are made to the fully penetrating, vertically integrated flow models (i.e., flow in two–dimensions) where appropriate, in order to determine when the assumption of essentially horizontal flow holds. Three general flow scenarios are studied, 1) a fully penetrating stream and a partially penetrating well with no induced infiltration (subcritical pumping), 2) a fully penetrating stream and

a partially penetrating well with induced infiltration (pumping above the critical value), and 3) a partially penetrating stream and a partially penetrating well.

METHODS, MODELS AND PARAMETERS

Solution to the head field is first obtained using a three–dimensional block centered finite difference flow code with a pre–conditioned conjugate gradient solver (Schafer–Perini, 1990). Once the head field is determined, side–of–grid–block velocities are calculated using Darcy's law with harmonic averaging of block conductivities, and linearly interpolated into the block (Schafer–Perini and Wilson, 1991b; Goode, 1987). Particles are then placed equidistant around the well and at uniform intervals over the length of the well. Right triangles are constructed from the particles over the length of the well. For a partially penetrating well a particle is positioned at the bottom or top of the well, depending on whether the well is partially penetrating at the bottom or top, respectively. Triangles are then formed from the last ring of particles around the well in a 'pie' pattern. Once all triangles have been constructed, the particles are tracked backwards through the velocity field using trilinear velocity interpolation. Triangle sizes are limited based on side length criteria. A more detailed review of the methods used here is given in Schafer–Perini (1990) and Schafer–Perini and Wilson (1991a,b; Appendix A; and Pollock, 1988).

Non–uniform finite difference grids were used for all simulations in order to reduce the size of the coefficient matrix. Maximum dimensions for any of the problems studied were 48x81x31 in the case of the partially penetrating stream and partially penetrating well problem for a total of 120,528 blocks. Blocks had 10, 15 or 20 meter block faces with shapes ranging from cubic to non–cubic rectangles. Blocks 10 meters on each side were used where more accurate results were required, such as around the well and where the capture zone intersects the stream. Block sizes were graded up to 20 meters on each side as distance from sensitive areas increased. Half block boundaries were specified at $x=x_{min}$ and x_{max}, $y=y_{min}$ and y_{max}, while full block boundaries were specified at $z=z_{min}$ and z_{max}. As an example, Figure 5–1 shows the grid used in the partially penetrating stream and partially penetrating well problem. The well is located at x=410 m, y=600 m, and z=300 to 400 m (above the bottom). The stream is located at x=330 m, y=0 to 1200 m and z=390 to 400. The top boundary of the aquifer represents a no-flow aquiclude in the case of a confined aquifer, and a no-recharge water table in the case of a phreatic aquifer. In the latter case, since we do not consider downward movement of this boundary under pumping, we are assuming small drawdowns. The porosity is 0.2. The hydraulic conductivity of 1 m/day is treated as homogeneous and isotropic. Note that the results also apply to a shallow anisotropic aquifer, where the modeled domain is the distorted isotropic equivalent. Bear (1979) gives the necessary scaling ratios and we have used them for a variety of three–dimensional front tracking problems (Schafer–Perini and Wilson, 1991b,c).

FULLY PENETRATING STREAM, PARTIALLY PENETRATING WELL

The first flow scenario examined is a fully penetrating stream and a partially penetrating well, with the well sufficiently far from the stream that no induced infiltration from the stream to the well occurs. This flow system is shown schematically in Figure 5–2. This analysis is

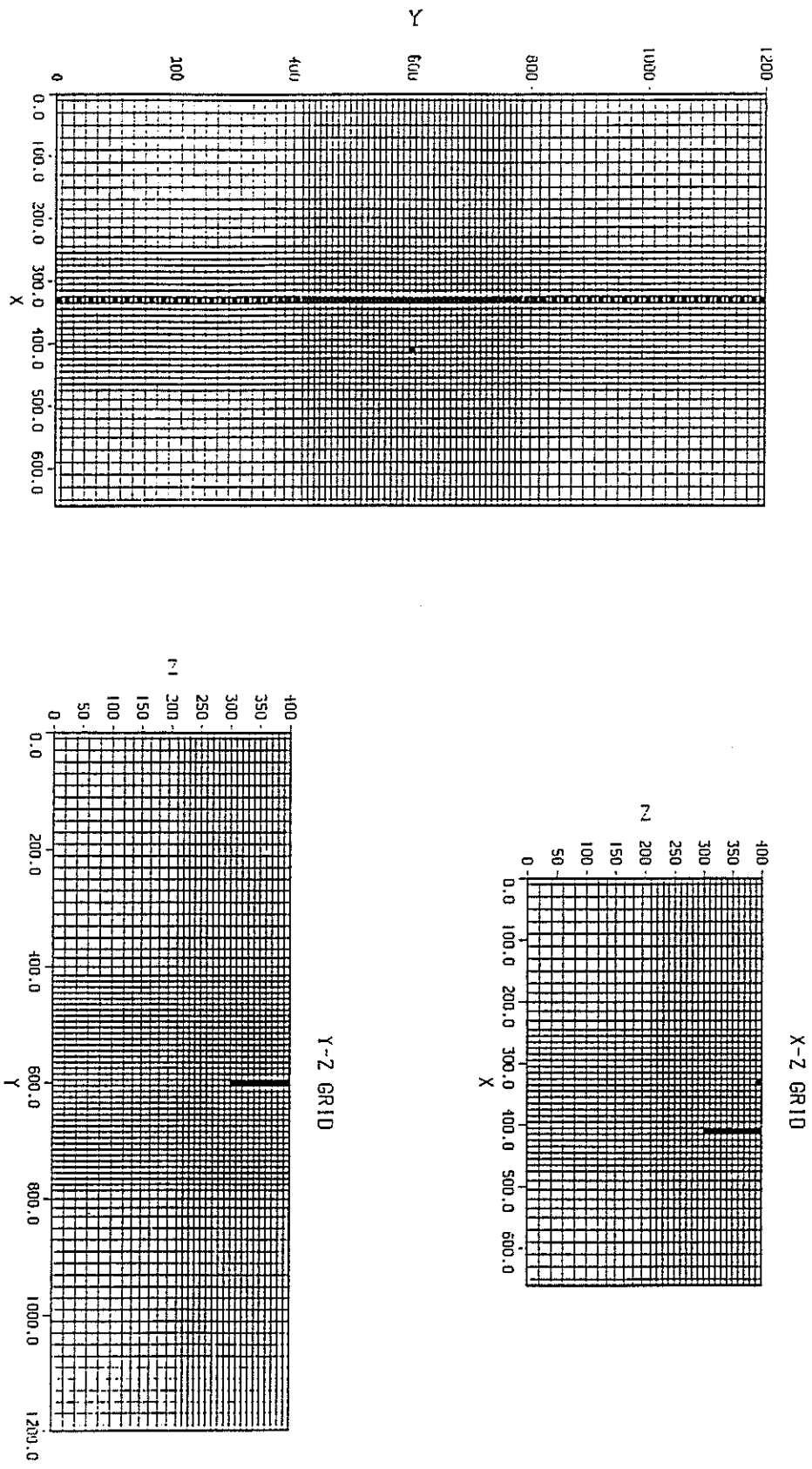

Figure 5−1. Finite difference grids for x−y, x−z, and y−z planes.

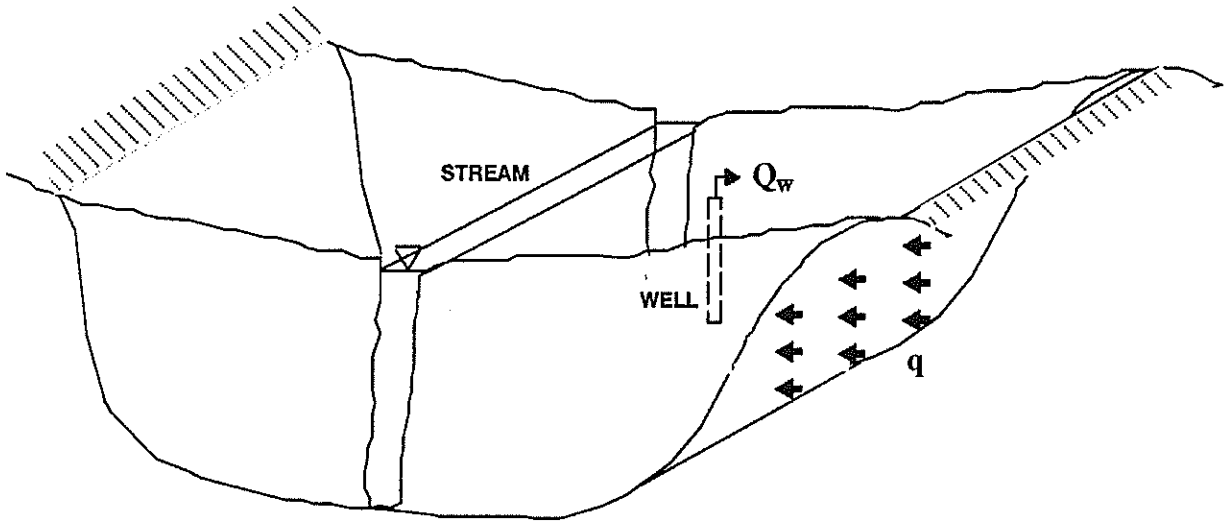

Figure 5–2. Schematic of stream–aquifer system with fully penetrating stream; partially penetrating well pumping at rate Q_w m^3/day; lateral recharge at rate q m/day.

useful in providing 'generic' results less affected by the stream boundary. Using these generic results, capture zone shapes for various well penetrations can be compared.

As in previous sections of this report, we refer to the constant head boundary as a stream boundary. In the simplest case examined here, this boundary has no slope to it such that the stream we refer to does not actually flow. It is actually more like a lake. However we use the term 'stream' for any type of constant head boundary for purposes of generality.

The stream boundary is on the left at x=0, there is a barrier boundary on the right at x=600 m, and there are no flow boundaries at y=0 and 600 m and z=0 and 400 m. Prescribed lateral incoming Darcy flux at the barrier boundary is 0.003 m/d, for a total volume flux of 720.0 m^3/day,which constitutes the ambient discharge to the stream. A single well is positioned at {x,y}={350,300} meters providing for symmetry around y=300 m. The pumping rate is a constant 541.0 m^3/day, a substantial portion of the lateral inflow. At this large pumping rate,the nearby no−flow boundaries influence the solution. The results cannot be directly compared to the generic semi−infinite aquifer results of Section 3. Larger domains, involving many more grid blocks, would be required to reduce the boundary influence. This is beyond the resources available for this effort. Four cases of well penetration are examined: P_w=0.10, 0.25, 0.50, and 1.0, where the dimensionless well penetration parameter is defined as

$$P_w = \frac{D_w}{b} \qquad (5-1)$$

D_w is the depth of well penetration, b is the aquifer thickness, and P_w=1 for full penetration. In order to examine the ultimate capture zone surface, as $t \rightarrow \infty$, the particle tracking routine would have to be run for a long time, due to low velocities and large travel times considered here. Instead, we modeled time-dependent capture zones at t=100, 1000, and 2500 days and then stopped the simulation.

In addition, other critical information exists which can help to delineate the shape of the ultimate capture zone. In the x−y plane, the surface expression of the capture zone (i.e. the expression of the capture zone at the top surface of the aquifer, the water table) can be delineated by finding the stagnation point determined by x and y velocities for the upper tier of nodes, then placing a particle into the flow field at this x position, at z=400 m, and at y slightly offset from 300 m, for instance y=300.1 m. At the upper surface of the capture zone, V_z=0 if there is no vertical recharge, and our particle tracked backward in the velocity field will define the surface expression of the capture zone. The extent of the capture zone in the y−z plane at the inflow barrier boundary can be determined similarly. In this case the stagnation point in the x−y plane for each tier of cells in the z direction is located and a particle placed at this x and z location, again being slightly offset from the plane of symmetry in the y direction. Particles tracked from these locations will move along the outer surface of the capture zone and eventually arrive at the barrier boundary upstream from the well. Finally, the shape of the capture zone in the x−z plane at y=300 m can be defined using these same x−y plane stagnation points.

The initial particle locations and corresponding triangles are shown in Figure 5−3 for P_w=0.1, 0.25 and 0.5. Figure 5−3d shows the triangle configuration looking down the inside of the initial triangle configuration for P_w=0.1. All triangles are right triangles along the sides

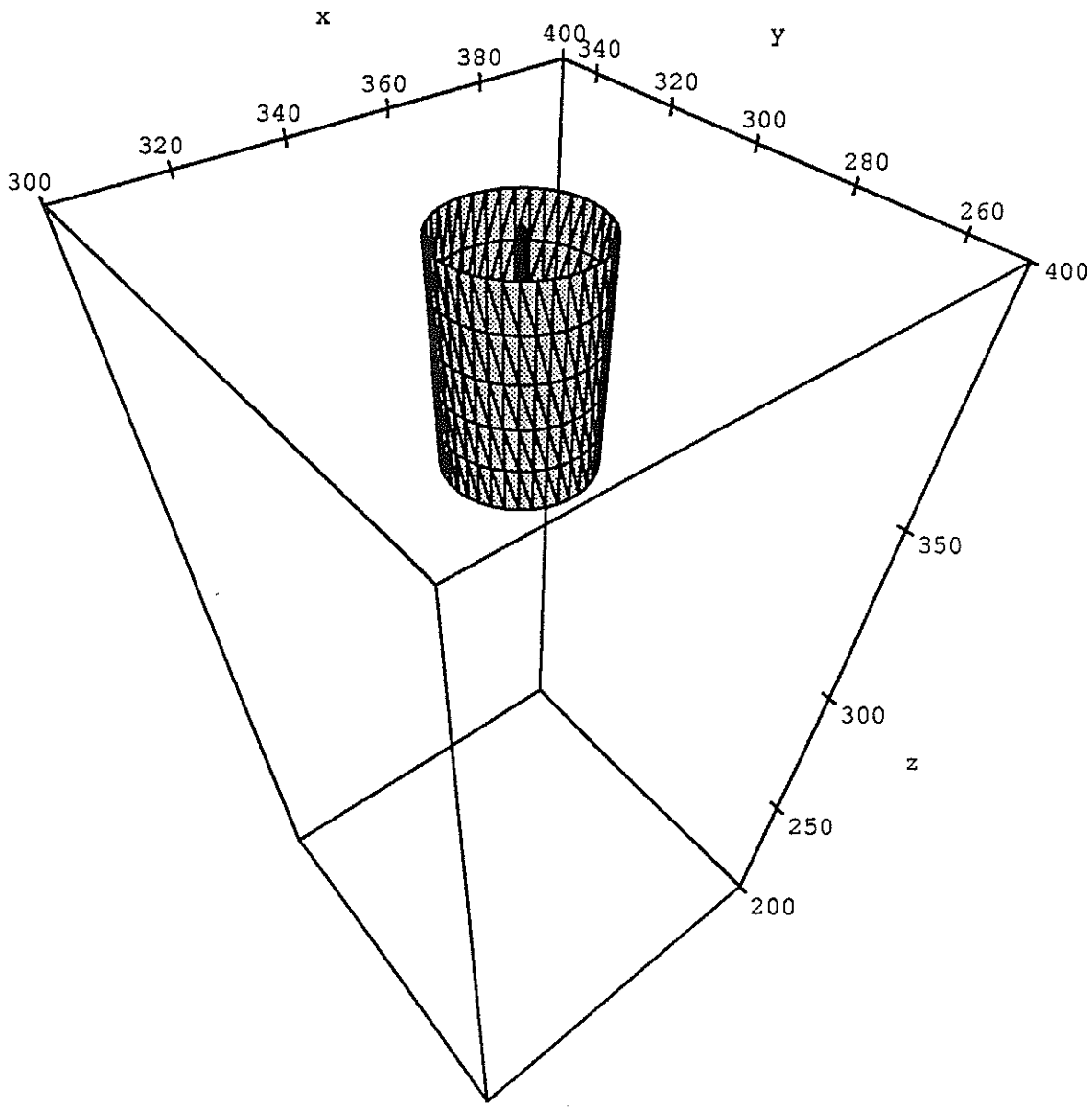

Figure 5−3a. Initital particle and triangle positions around well for P_w=0.1.

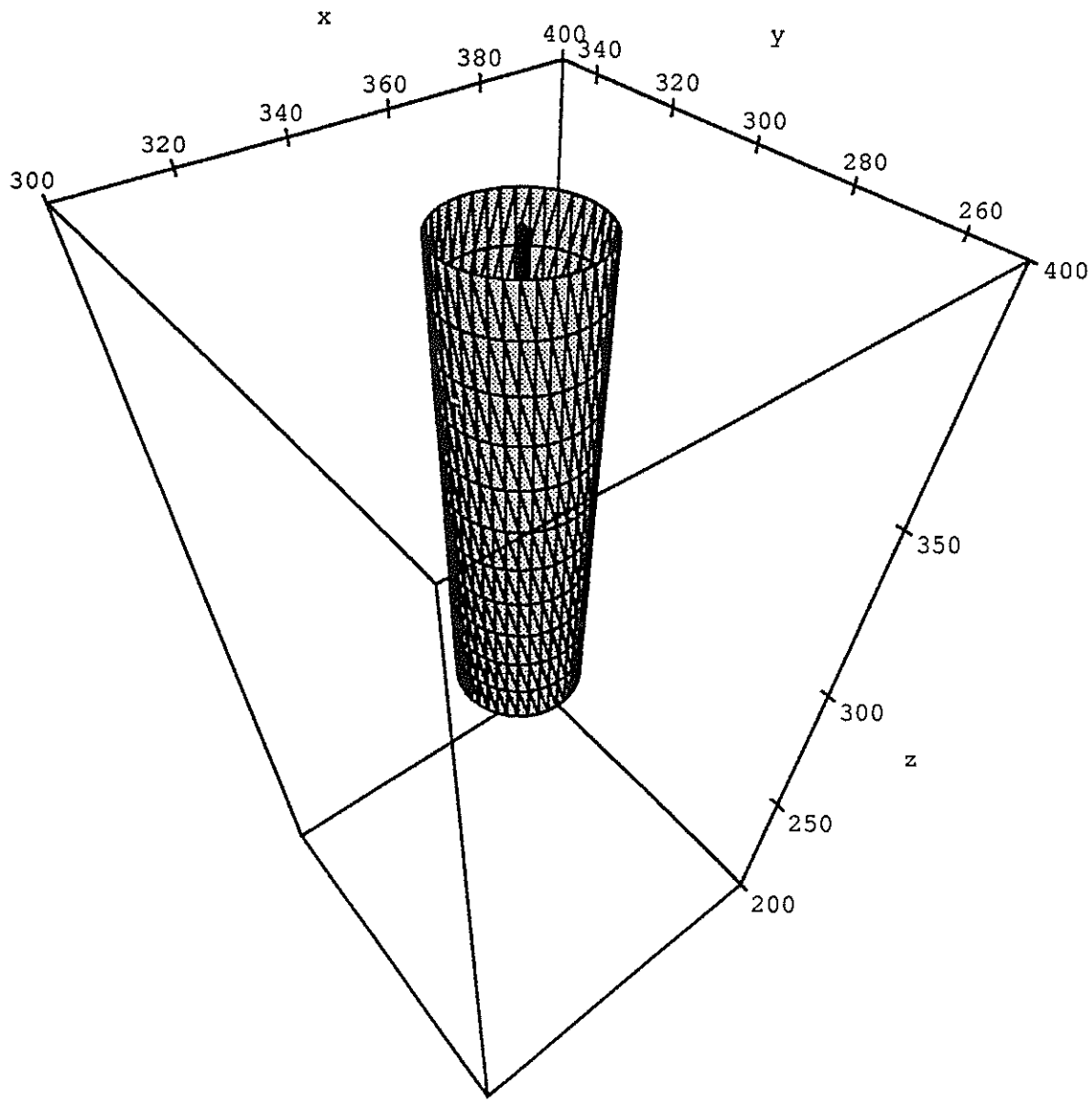

Figure 5−3b. Initital particle and triangle positions around well for P_w=0.25.

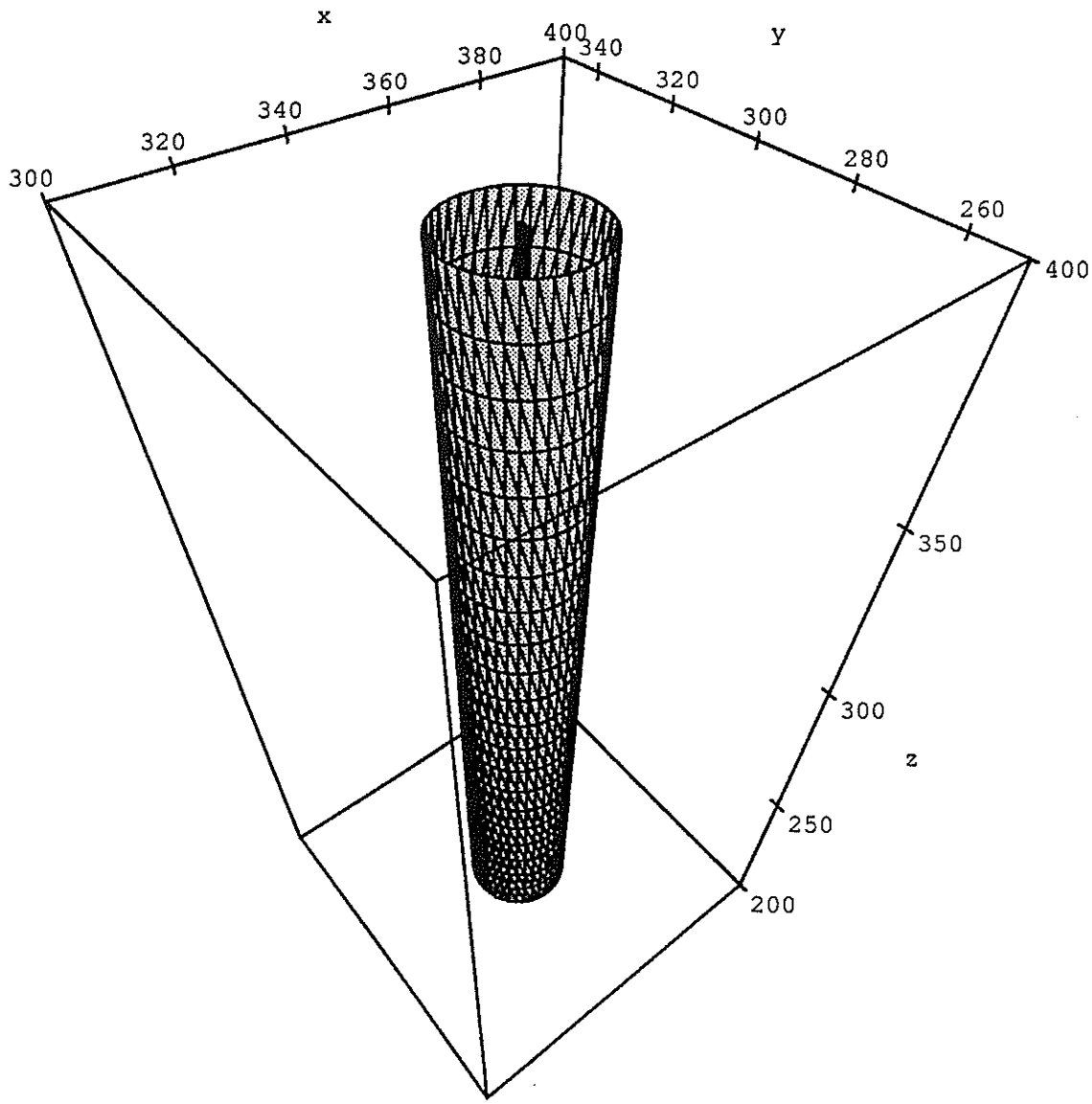

Figure 5−3c. Initital particle and triangle positions around well for P_w=0.5.

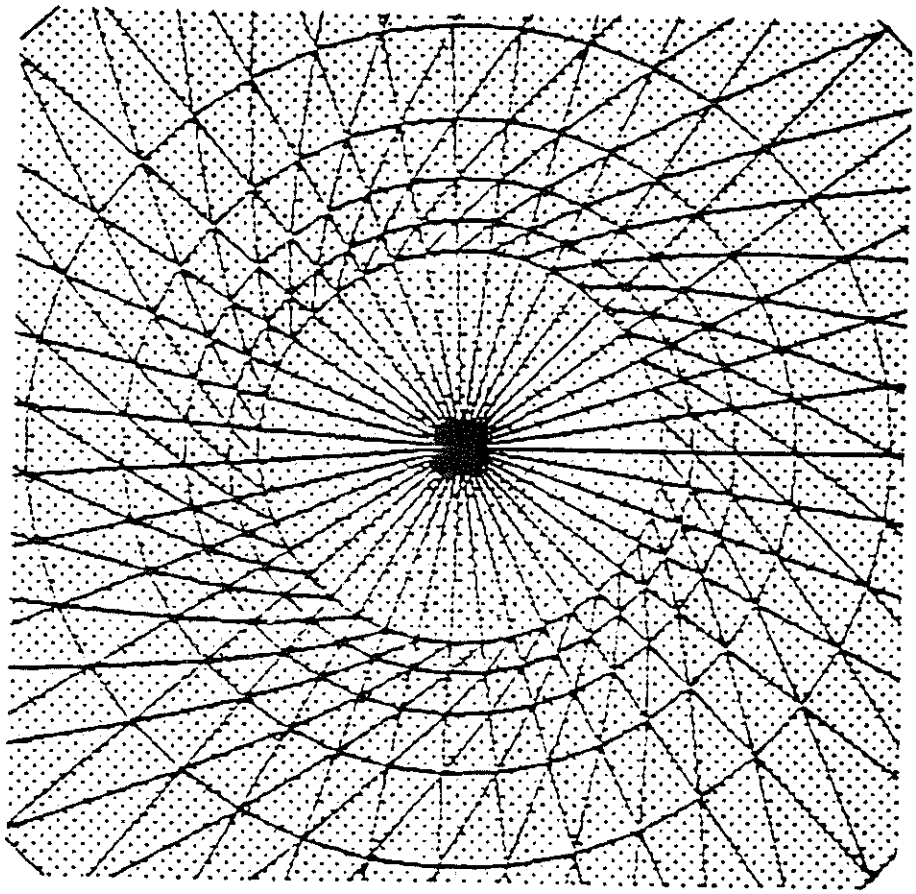

Figure 5−3d. Top view of well for P_w=0.1 showing initial particle and triangle positions. Side trianlges are all right triangles, bottom triangles are arranged in a 'pie' format. Note: The perspective is looking down the tube formed by the initial particle posititions and their respective triangles. The dark spot in the center is the well; the top of the tube has been clipped to form a rectangular two−dimensional image.

while the triangles at the bottom are arranged in a pie pattern. The top of the well is visible in these plots as a portion of a thick line within the center of the capture zone and is represented similarly in all other three–dimensional plots. Gray scale rendering using Mathematica™ is used for the remainder of the three–dimensional capture zone plots, since resolution of individual triangles is generally not possible at this scale. Figures 5–4a thru c show the position of the capture zones for t=100 days, Figures 5–5a thru c show capture zones for t=1000 days, and Figures 5–6a thru c are for t=2500 days. Figure 5–6d is identical to 5–6c except that triangle edge locations have been included. Eventually the fronts reach the ultimate capture zone. The surface expression for this is shown in Figure 5–7 for all four well penetrations. Figure 5–8a, b and c show the surface expressions of the time capture zones for all well penetrations and times considered, and the ultimate capture zone. Because of the nearby boundaries, the capture zones are artificially constrained, particularly at y=0 and y=600 m. If the boundaries were further from the well,these capture zone shapes would be somewhat wider, as will be shown later.

As well penetration P_w increases, the areal extent of the time dependent and ultimate capture zones becomes smaller, and its depth increases. Well penetrations of less than 0.25 lead to very similar ultimate capture zones, which perhaps could be represented by a point sink. None of the partial penetrating wells lead to a capture zone nearly as small in areal extent as the fully penetrating case. In studies of drawdown issues it has been suggested that beyond a radius of r=1.5b, a partially penetrating well leads to the same drawdowns predicted by a fully penetrating well (e.g., Bear, 1979). For capture zones we can argue that the equivalent effective radius must be larger. Nevertheless, assuming the same criteria applies, the capture zone would have to have moved 600 m from the well. Figure 5–8 shows only 100 m movement, so this case does not provide an opportunity to investigate this criteria.

Figure 5–9 makes other comparisons between the three-dimensional simulations, and a variety of approximately equivalent two–dimensional models. Suppose we examine P_w=0.1, which represents a well drilled to a depth of 40 meters. The surface expression of the three–dimensional capture zone is represented by curve a in Figure 5–9a. There are two possible choices in applying a two–dimensional model. The first is to assume the well is fully penetrating to a depth of 40 m and pumping at a rate of 541 m^3/day, producing a capture zone that encompasses the entire aquifer domain and thus is not represented in the figure. This scenario is equivalent to pumping a fully penetrating well in the real aquifer at 5410 m^3/day. The second simple option is to assume the aquifer is 400 meters thick, the well is fully penetrating over the entire 400 m thickness, and total Q_w is 541 m^3/day. This result is represented by curve d for the fully penetrating case. This curve grossly underestimates the size of the capture zone. Alternatively, an aquifer thickness of only 40 m grossly overestimated the size of the capture zone. This points out the lack of correspondence between two–dimensional and three–dimensional model applications.

As a further comparison, we have matched two–dimensional capture zone curves at critical points on the original three–dimensional capture zone surface representation. Matching at the original stagnation point, or at the location where the capture zone boundary intersects

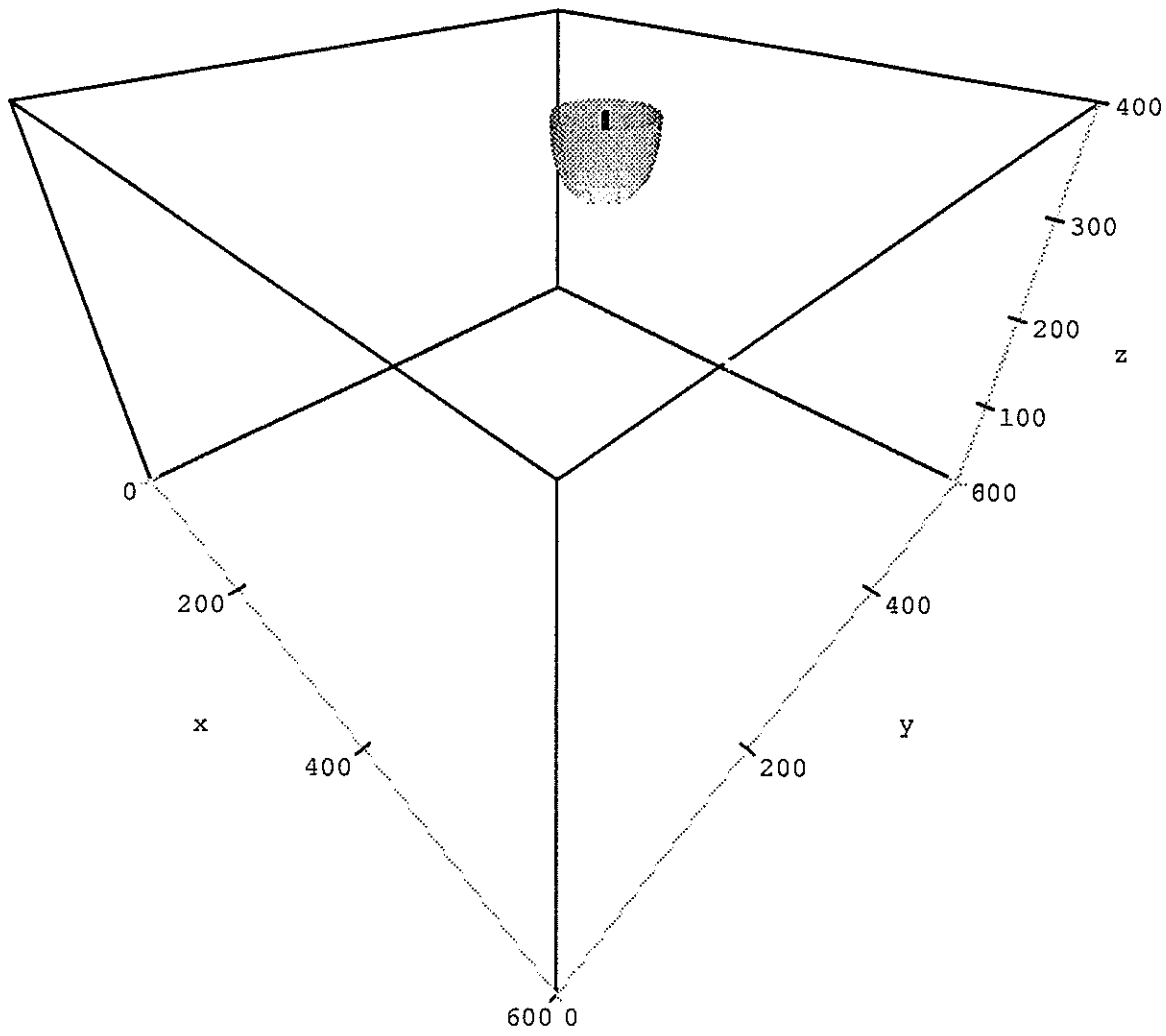

Figure 5−4a. Capture zone for P_w=0.1, t=100 days.

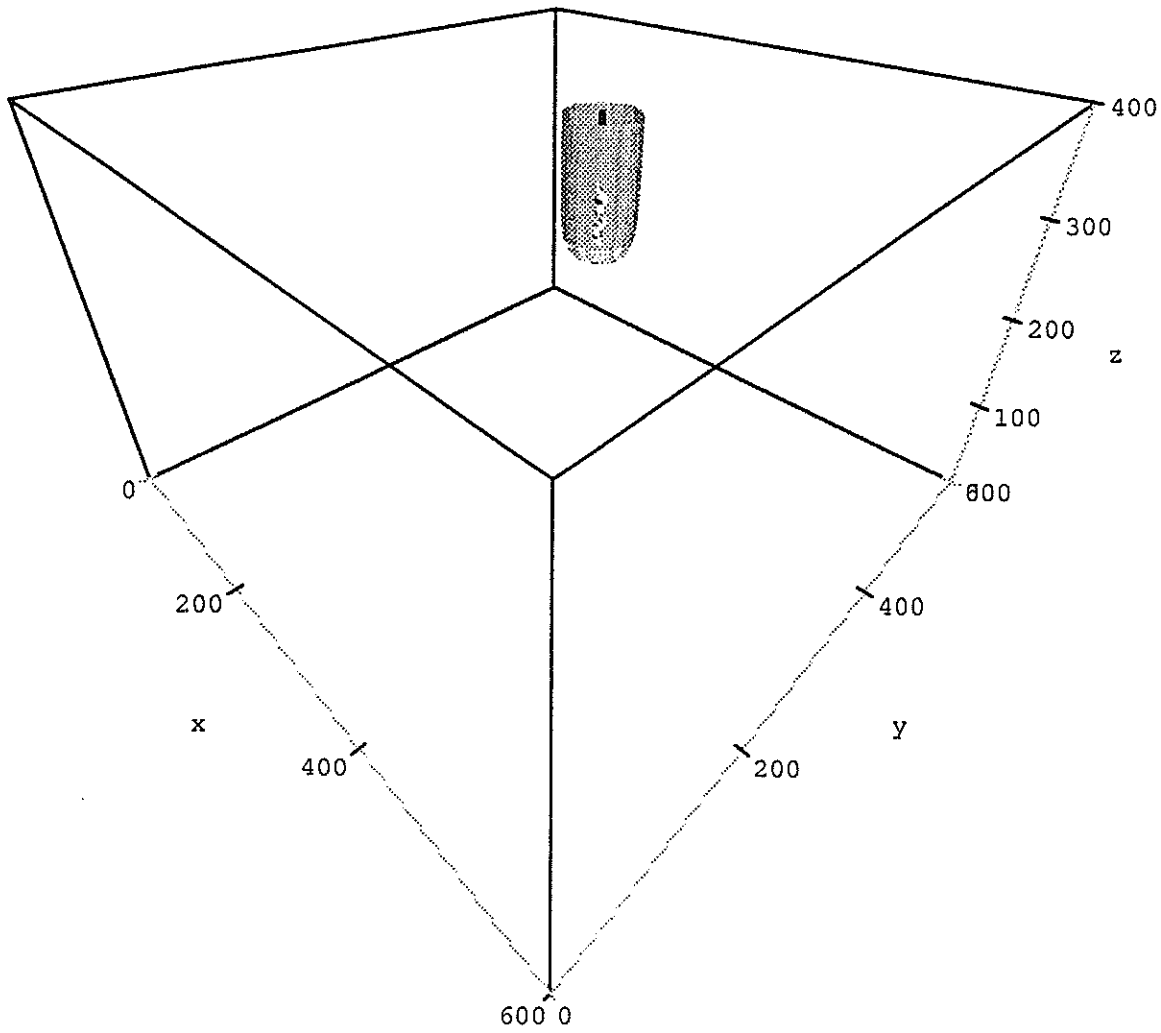

Figure 5−4b. Capture zone for P_w=0.25, t=100 days.

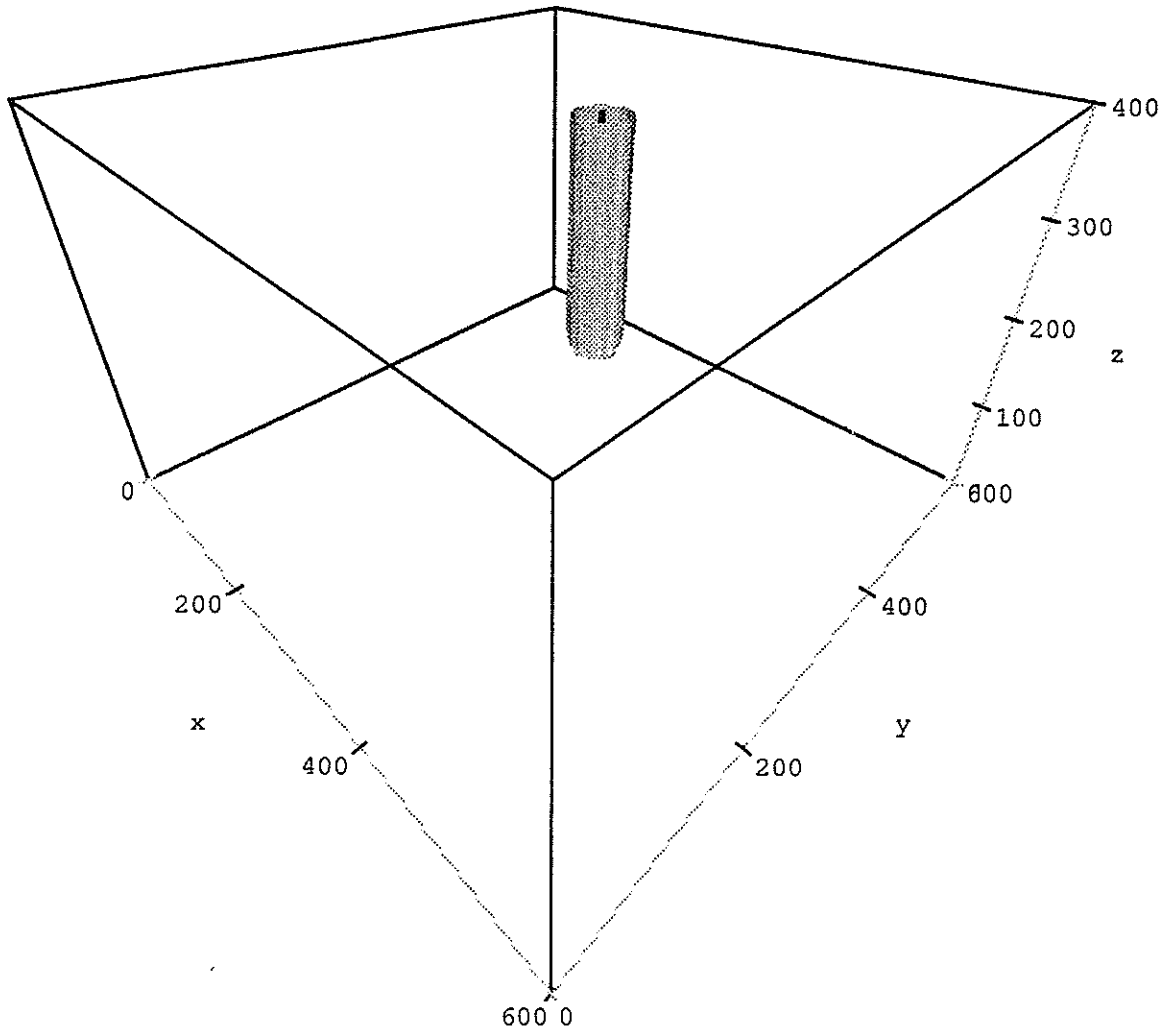

Figure 5−4c. Capture zone for P_w=0.5, t=100 days.

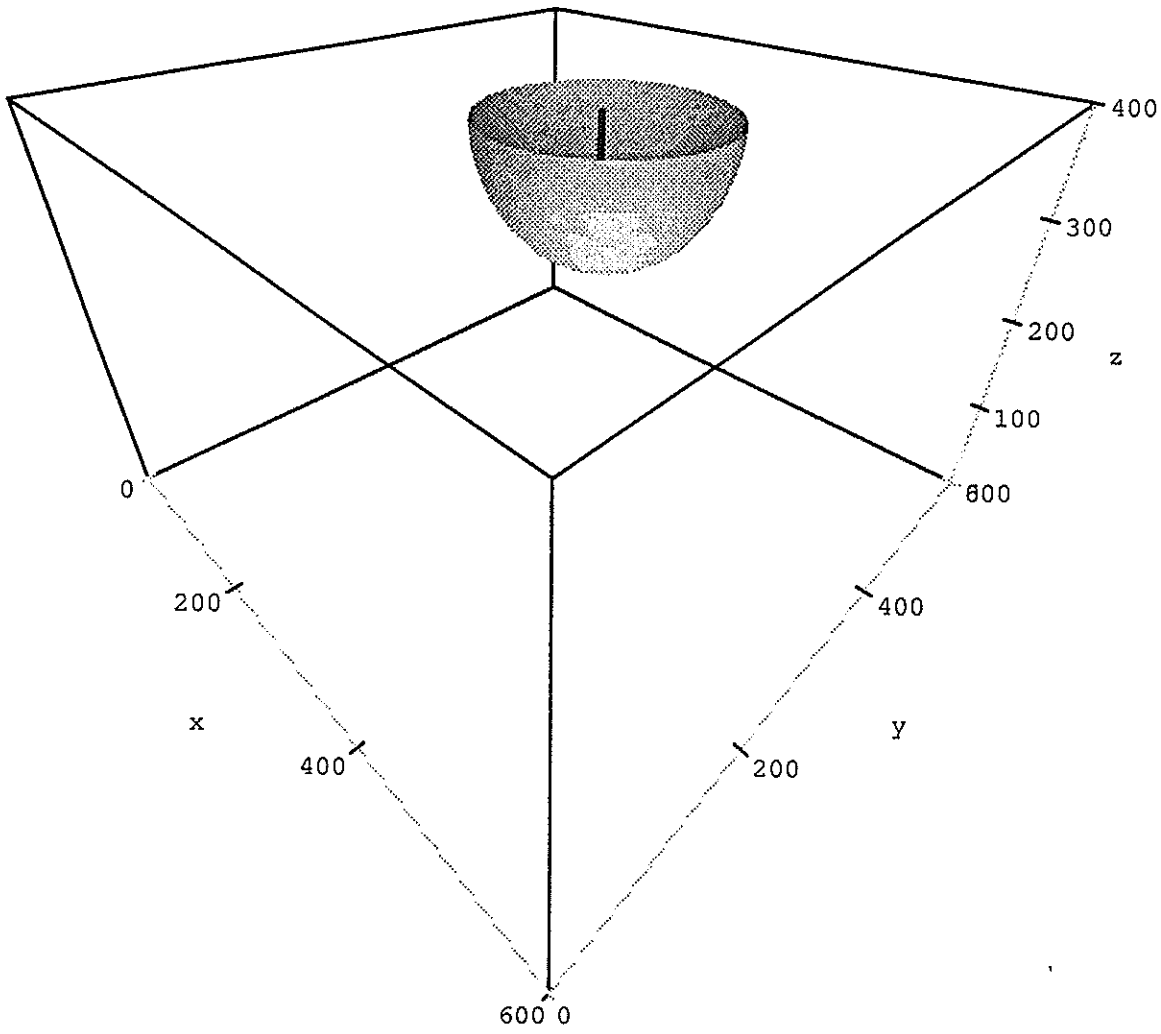

Figure 5−5a. Capture zone for P_w=0.1, t=1000 days.

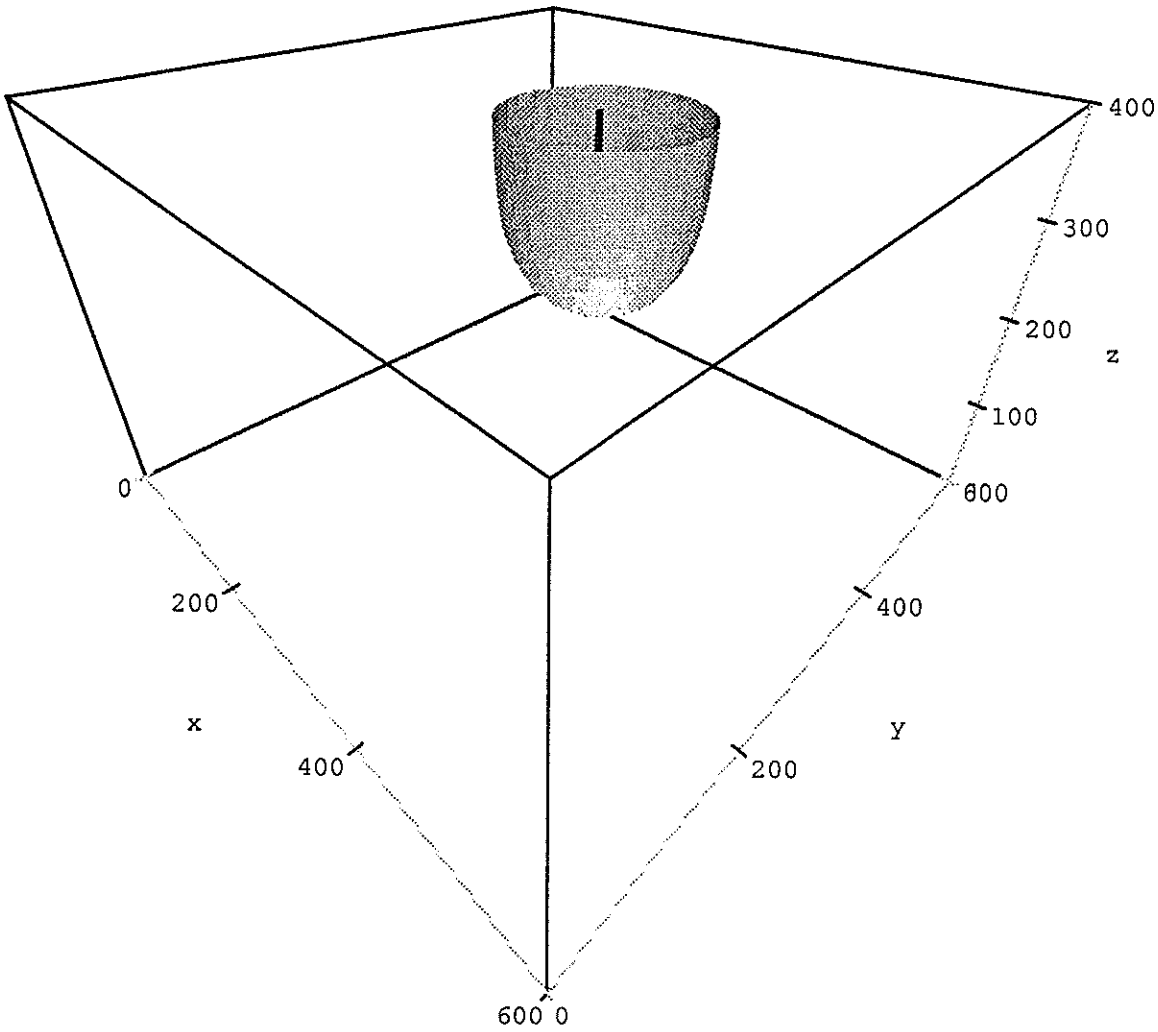

Figure 5−5b. Capture zone for P_w=0.25, t=1000 days.

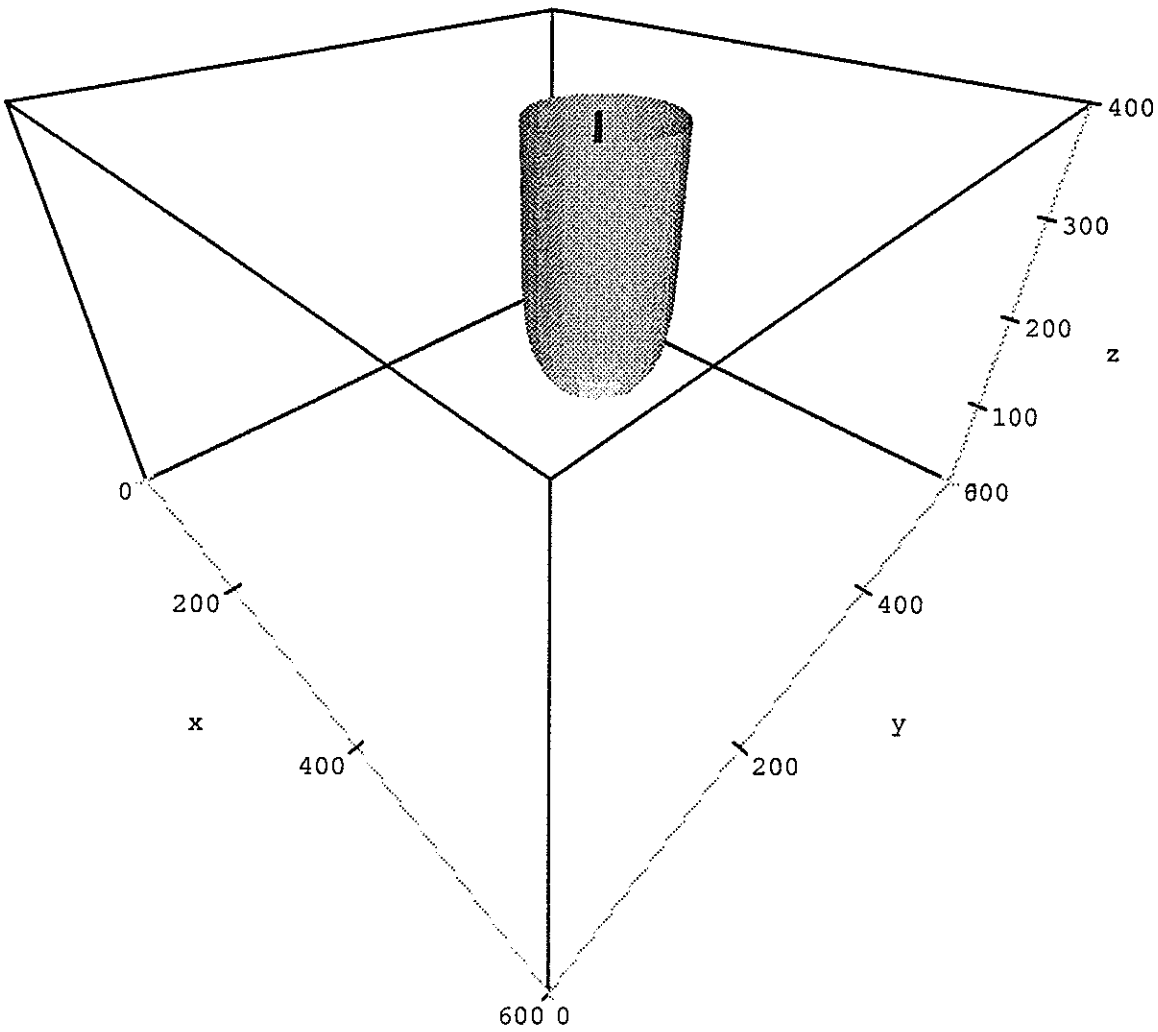

Figure 5−5c. Capture zone for P_w=0.5, t=1000 days.

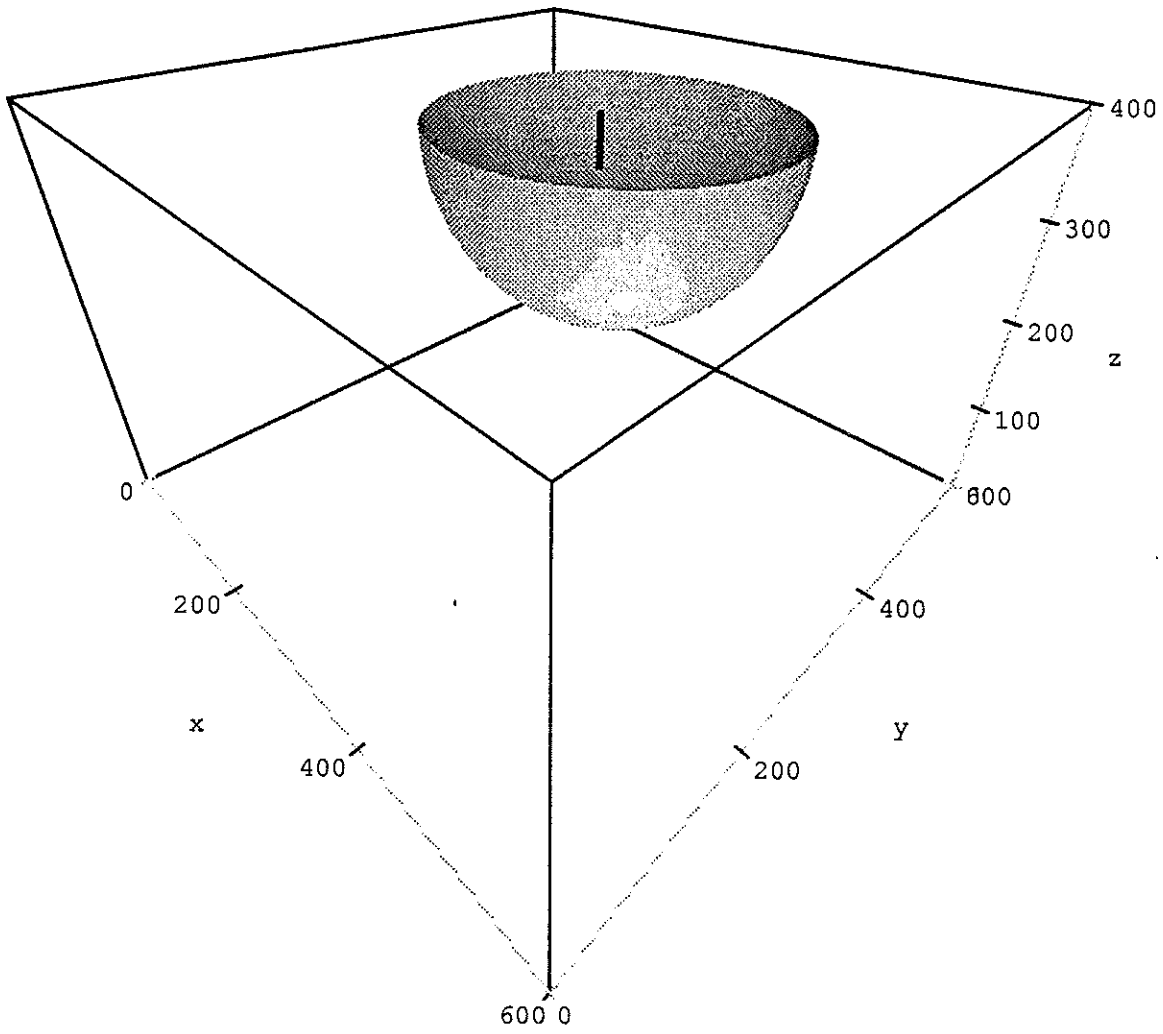

Figure 5−6a. Capture zone for P_w=0.1, t=2500 days.

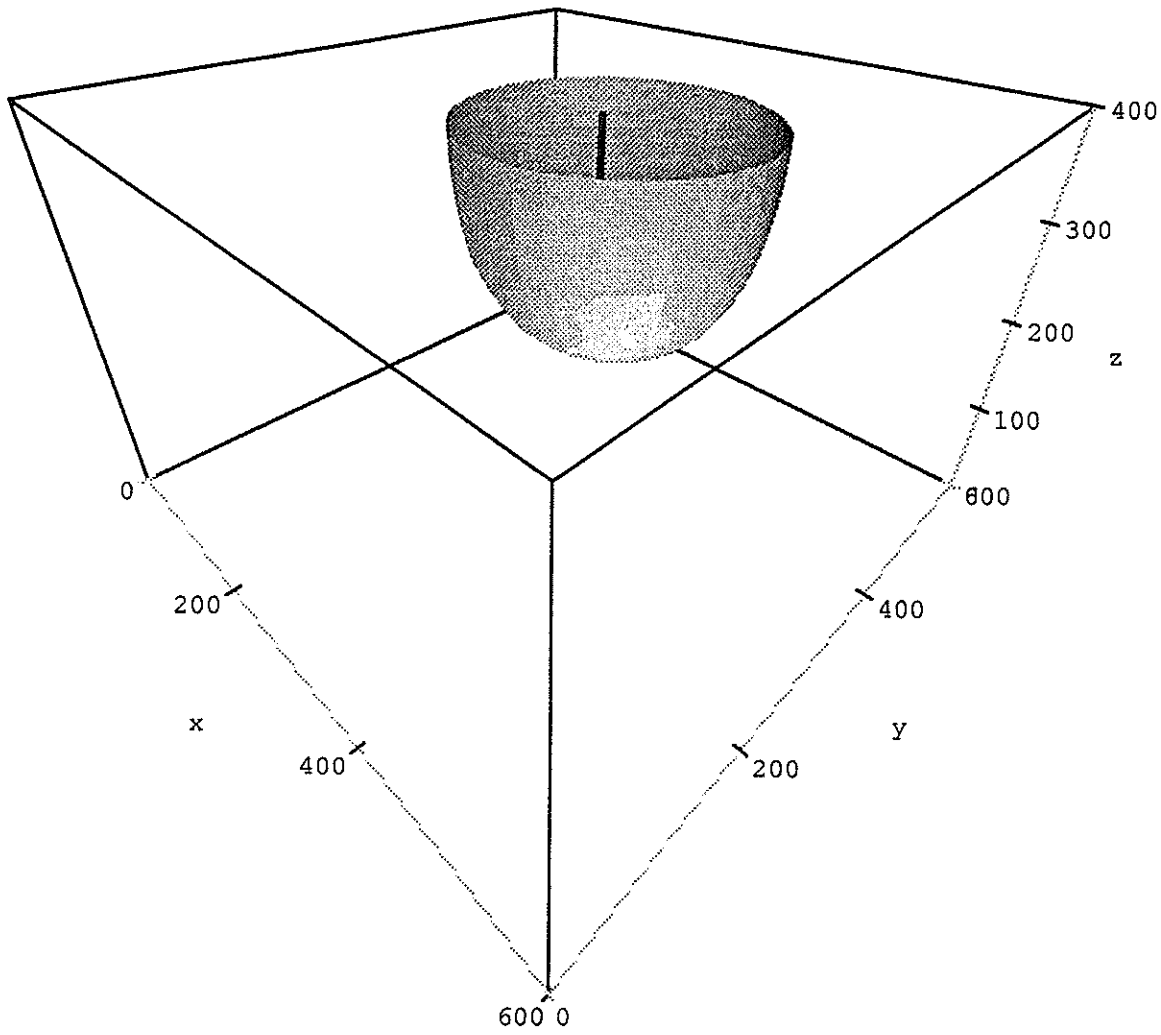

Figure 5−6b. Capture zone for P_w=0.25, t=2500 days.

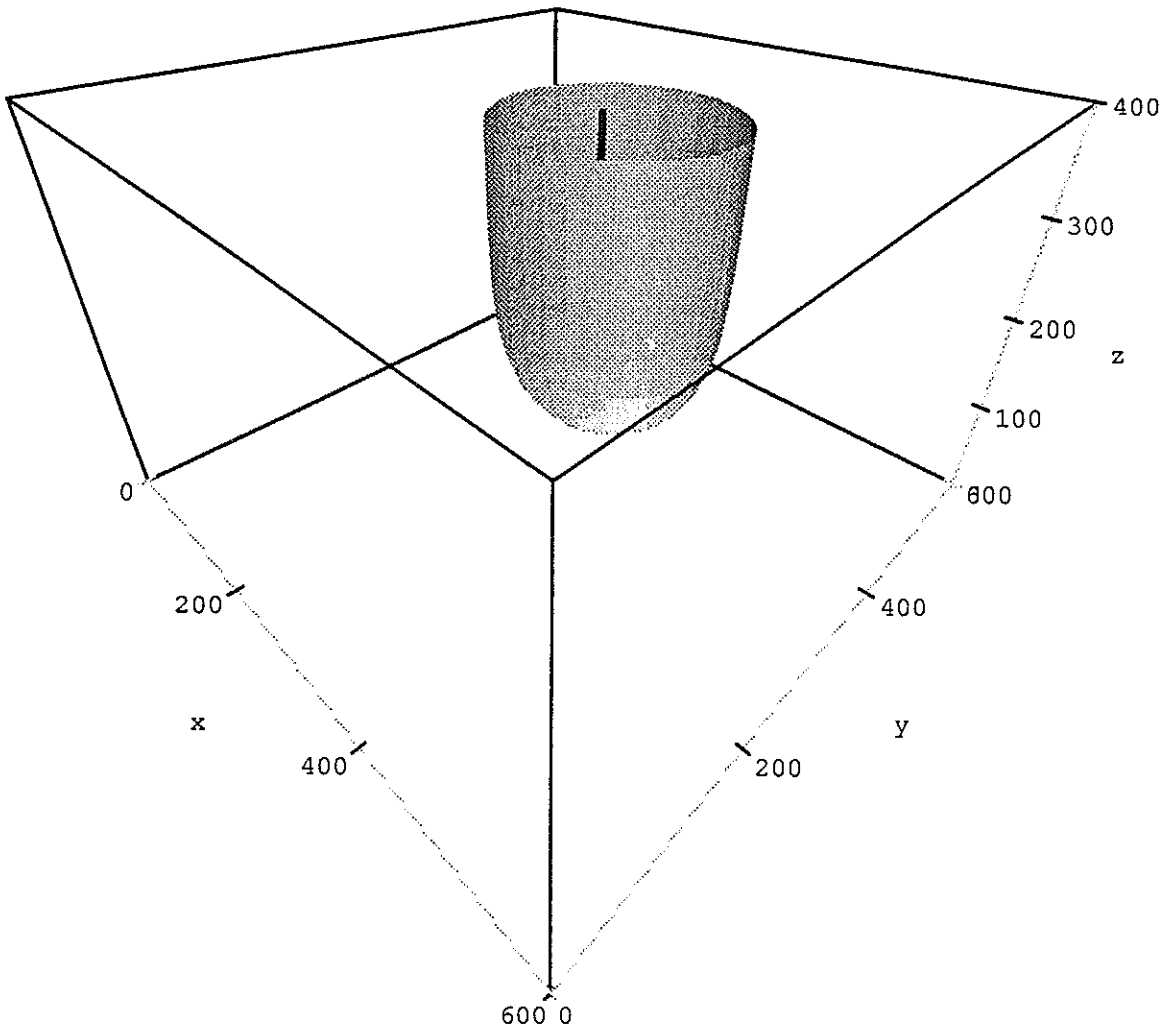

Figure 5−6c. Capture zone for P_w=0.5, t=2500 days.

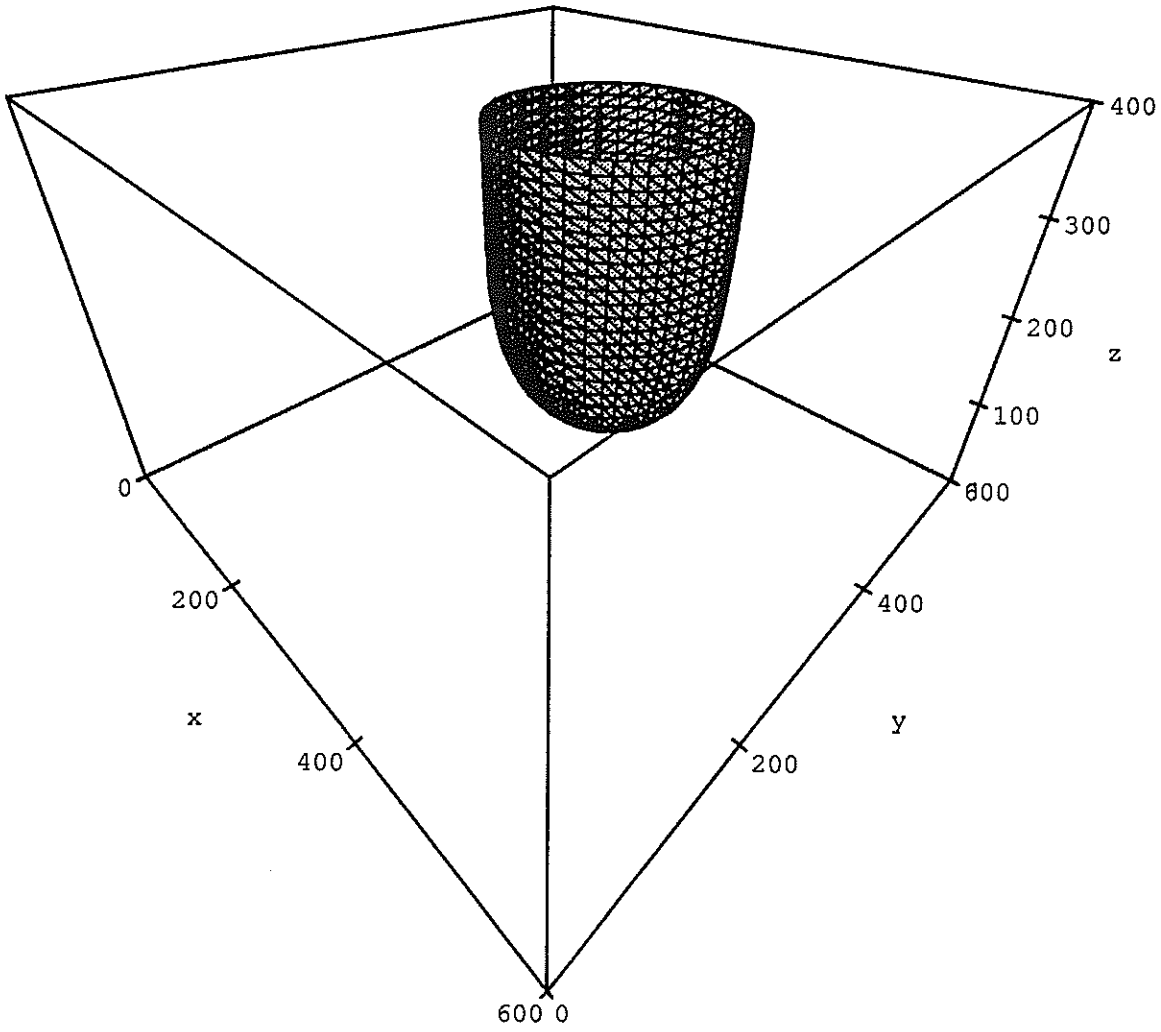

Figure 5−6d. Capture zone for P_w=0.5 at t=2500 days showing position of triangles.

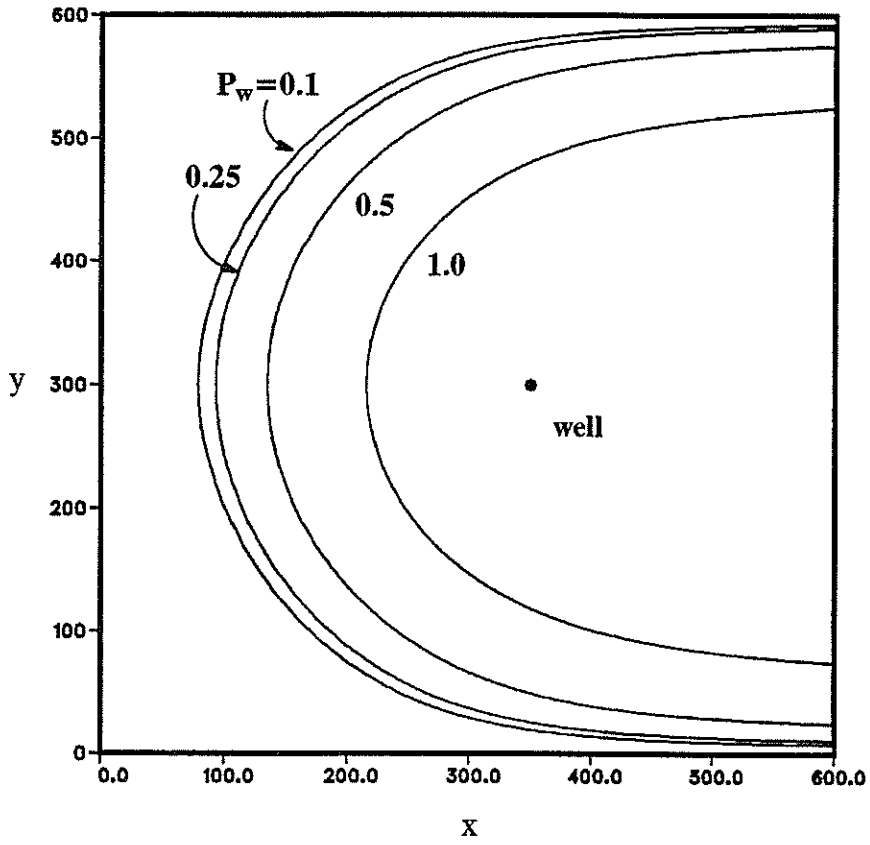

Figure 5–7. Water table expression of three-dimensional capture zones at t= ∞, for well penetrations of P_w=0.1, 0.25, 0.5, and 1.0. Pumping rate is 541.0 m^3/day.

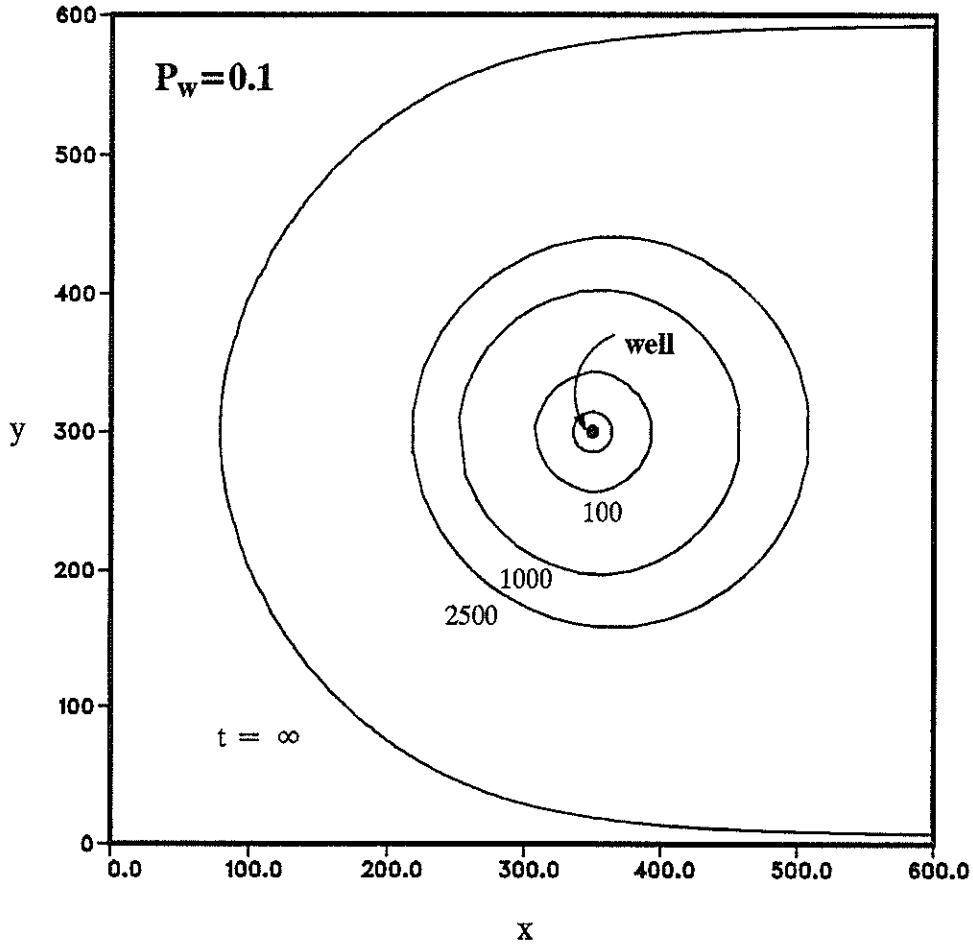

Figure 5–8a. Water table expression of three-dimensional capture zones for a well penetration of P_w=0.1 at front times of t=100, 1000 and 2500 days and for the ultimate capture zone at t=∞. Small circle surrounding well represents initial particle positions. A fully penetrating stream boundary is at x=0.0 m, a flux boundary is at x=600.0 m with flux toward the stream, and top and bottom boundaries are no–flow boundaries.

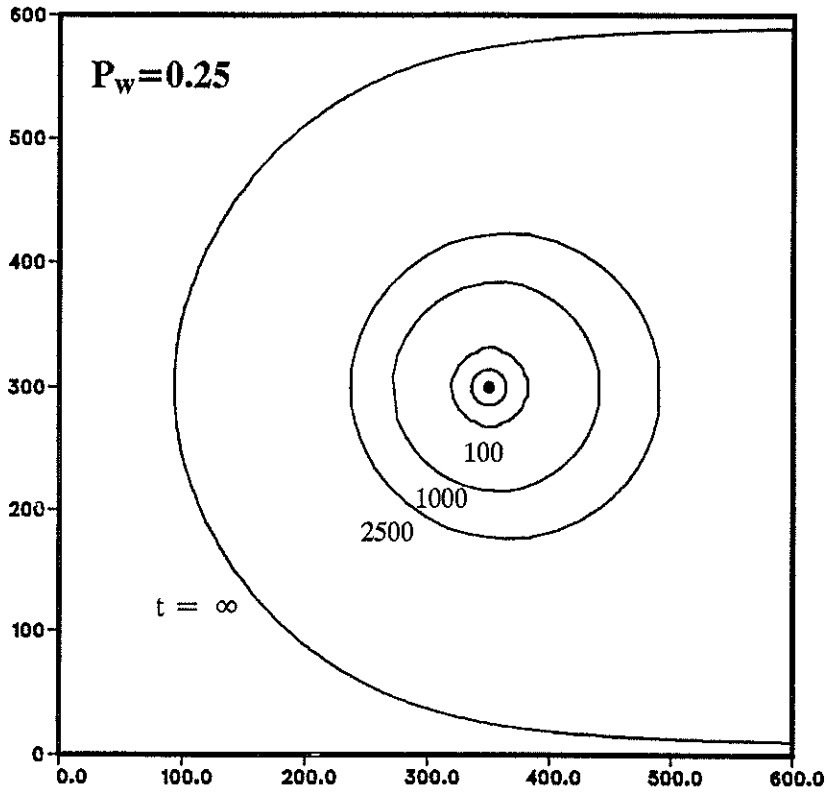

Figure 5−8b. Water table expression of three-dimensional capture zones for a well penetration of P_w=0.25 at front times of t=100, 1000 and 2500 days and for the ultimate capture zone at t= ∞. Small circle surrounding well represents initial particle positions. Boundaries are as before.

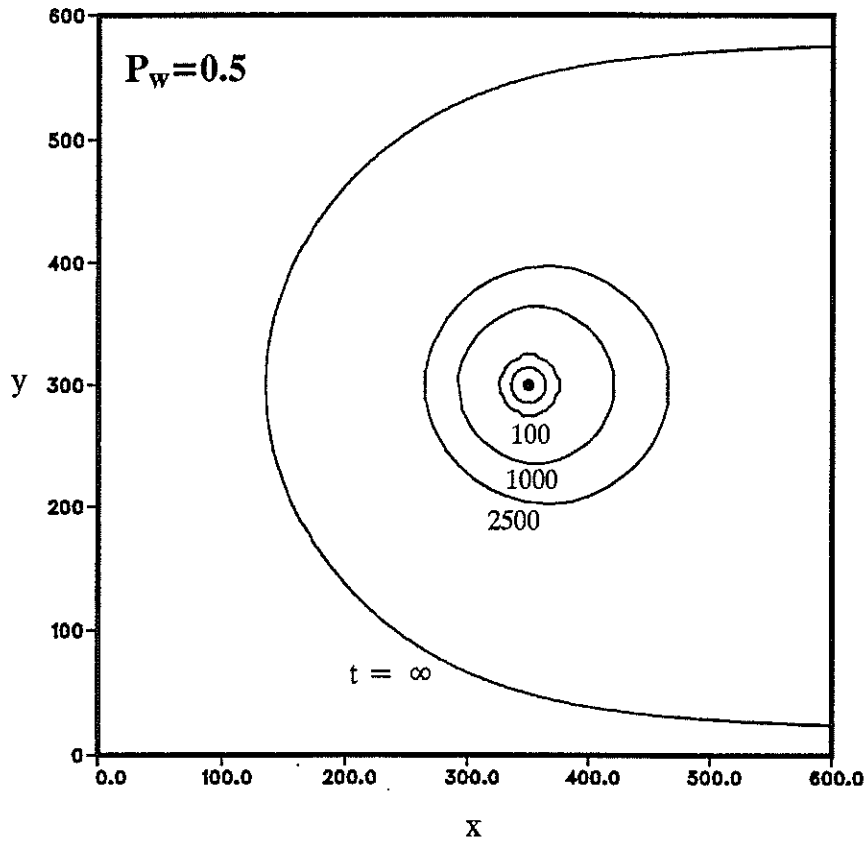

Figure 5−8c. Water table expression of three dimensional capture zones for a well penetration of P_w=0.5 at front times of t=100, 1000 and 2500 days and for the ultimate capture zone at t= ∞. Small circle about well represents initial particle positions. Boundaries are as before.

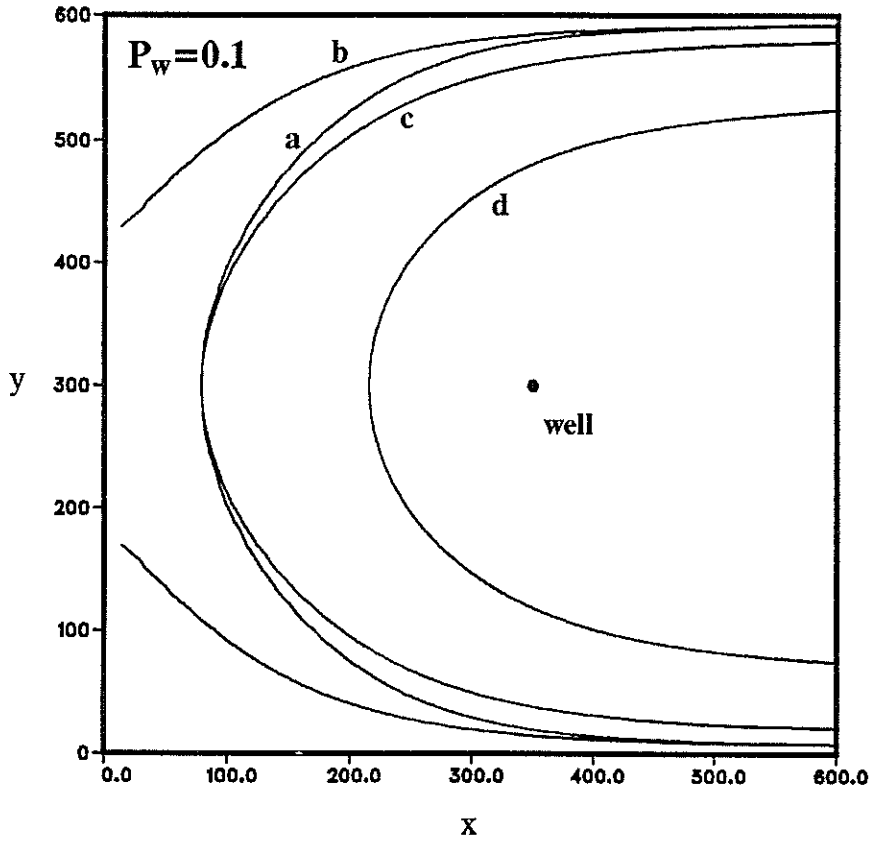

Figure 5−9a. Water table expression of three−dimensional capture zone for well penetration of P_w=0.1 along with two−dimensional counterparts assuming full well penetration for aquifer depth of 400 m: Curve a is the original 3D curve, Q_{3D}=541.0; Curve b is 2D matching at x=600.0, Q_{2D}=711.2; Curve c is 2D matching at 3D stagnation point, Q_{2D}=670.0; Curve d is for Q_{3D} distributed over the entire aquifer depth, Q_{2D}=541.0. Pumping rates are in m^3/day. Y-axis is a fully penetrating stream boundary, x=600.0 m is a flux boundary with flux toward the stream, and top and boundaries are no−flow boundaries.

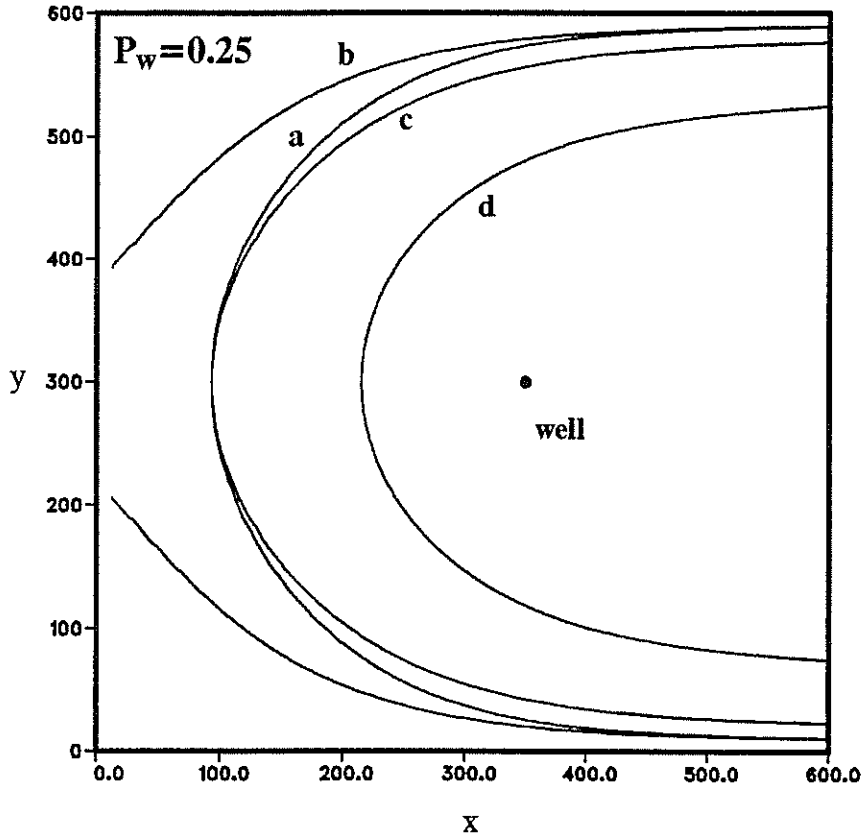

Figure 5−9b. Water table expression of three dimensional capture zone for well penetration of P_w=0.25 along with two−dimensional counterparts assuming full well penetration. Curve a is the orginal 3D curve, Q_{3D}=541.0; Curve b is 2D matching at x=600.0 m, Q_{2D}=696.4; Curve c is a 2D matching at 3D stagnation point, Q_{2D}=664.4; Curve d is for Q_{3D} distributed over the entire aquifer depth, Q_{2D}=541.0. Pumping rates are in m^3/day. Boundaries are as before.

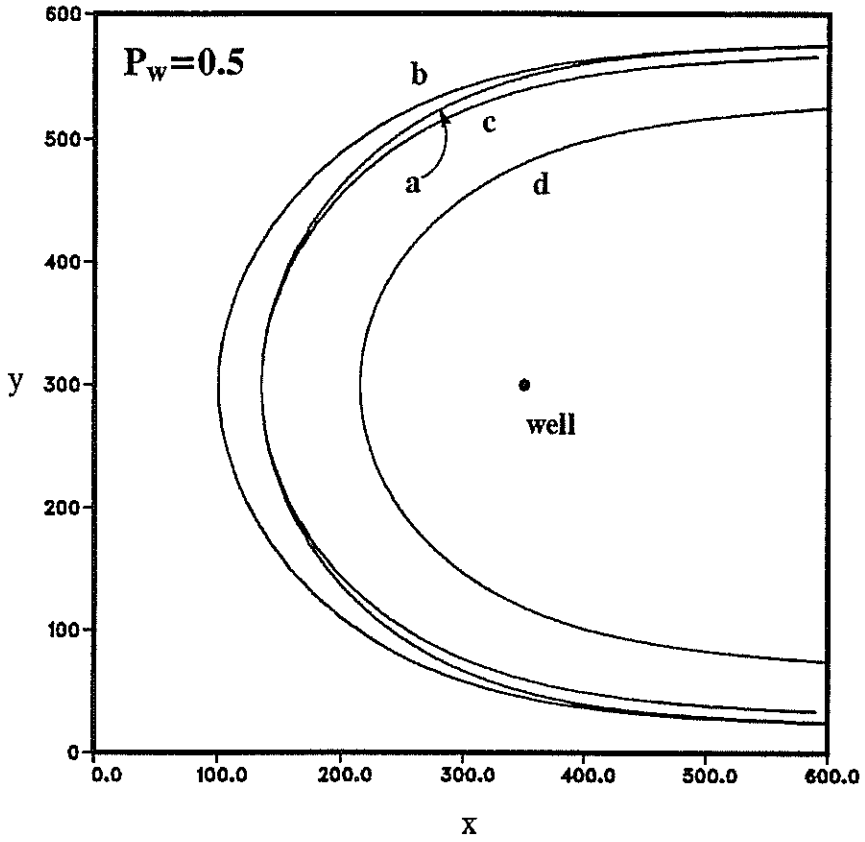

Figure 5−9c. Water table expression of three dimensional capture zone for well penetration of P_w=0.5 along with two−dimensional counterparts assuming full well penetration. Curve a is the original 3D curve, Q_{3D}=541.0; Curve b is 2D matching at x=600.0, Q_{2D}=660.8; Curve c is 2D matching at 3D stagnation point, Q_{2D}=639.2; Curve d is for Q_{3D} distributed over the entire aquifer depth, Q_{2D}=541.0. Pumping rates are in units of m^3/day.

the flux boundary at $x=x_{max}$, leads to curves c and b, respectively, in Figure 5−9a. Curve c again underestimates the capture zone's size, but its not a bad approximation. The two−dimensional 'equivalent' pumping rate for curve c is $Q_w=670.0$ m^3/day. Curve b overestimates the size of the capture zone, especially near the stagnation point, and incorrectly predicts induced infiltration. The pumping rate for curve b is $Q_w=711.2$ m^3/day. For purposes of well head protection regulation, an overestimation would be desired, yet the capture zone of curve b has the potentially undesirable quality of intersecting the stream boundary at x=0. If this model were to be used for predictive uses, for instance to determine source contributions, significant error would result.

The results for $P_w=0.25$ and 0.5 are similar and shown in Figures 5−9b and c, respectively. As the well penetration approaches 1.0, curves b and c become better approximations to the actual three−dimensional capture zone surface representation. However, the two simple approximations based on lack of knowledge of the flow system are still inadequate predictors of the actual capture zone at the aquifer's surface. Our major emphasis has been on the surface expression of the three−dimensional capture zone. We have done this because the most likely sources of pollutants originate at the ground surface and are introduced at the aquifer's surface after they migrate vertically downward through the unsaturated zone. Should a source of pollutant originate somewhere within the aquifer, then an areal two-dimensional analysis would not be appropriate.

As described earlier we can also find the shape of the capture zone as it crosses the barrier boundary at $x=x_{max}$. These curves are plotted in Figure 5−10 for the three partially penetrating well cases along with the fully penetrating case. The general form of these curves is similar to an ellipse where the power, n, is allowed to vary between 0 and ∞,

$$\frac{|y_{sym} - y|^n}{a^n} + \frac{(z_{max} - z)^n}{b^n} = 1 \quad . \tag{5−2}$$

The term y_{sym} is the y value for the x−z plane of symmetry and z_{max} represents the maximum value of z at the top of the aquifer. The parameter n is found by first using only half of the data determined by the plane of symmetry defined by y=300 m. The data is then transformed such that the origin of both the z data and y data is at (0,0) and the vertex for the y' axis is (1,0) and for the z' axis is (0,1). The value of n is then determined by fitting curves for various values of n to the data in the transformed space for an equation of the form

$$y'^n + z'^n = 1 \quad . \tag{5−3}$$

Once the value of n is determined, values of a and b are determined by alternatively setting z and y to z_{max} and y_{sym} in (5−2) and solving for a and b for known y and z values, respectively. The values of a and b can also be found by noting that they are the vertices of the semi−major and semi−minor axes of the original curve. Following this method, values of n, a and b were derived for each well penetration and are listed in Table 5−1:

Table 5−1. Characteristic fitted parameters for three−dimensional capture zone cross−sections in a system with no induced infiltration.

P_w	n	a	b
0.10	2.8	292.38	352.24
0.25	2.8	289.27	357.87
0.50	2.8	275.37	376.95

The value of n for all three depths of well penetration is the same. There is a small amount of spread to the data not presented here. However, the deviation from the curve was small and the value for n is within ±0.05 units. Identical values for n are also suggested in Figure 5−10 where it is seen that all the curves, including the capture zone curve for P_w=1.0, have the same cross−over intersection point. The similarity of n for all three curves suggests that the shape of the curve is predictable for a given set of boundary conditions, recharge rates, and source and sink terms. Should this be the case, it may be possible to derive a set of characteristic curves for various well penetrations, pumping rates, ambient flow rates and well locations.

We next examine the same situation, but with less distance between the well and the stream, so that there is some induced infiltration. The distance between the well and the right flux boundary has been kept the same while the stream−well distance has been reduced to 80 meters. Only one well penetration, P_w=0.25, is presented. Figures 5−11a thru d show the three−dimensional representation of the capture fronts for the initial particle positions and for t=100, 1000 and 2500 days. The stream is on the left. Between t=100 and t=1000 days our backward moving front intercepts the stream boundary indicating induced infiltration from the stream will take from 100 to 1000 days to reach the well. For front times larger than this stream intersection time, overall front size will be relatively smaller than those in Figures 4, 5, and 6 due to the recharge effect of the stream.

To determine the affect of the no−flow boundaries at y=0 and y=600 meters, an additional simulation was performed with these boundaries extended an additional 300 meters in each direction from the well giving the dimensions y_{min}=0, y_{max}=1200 and y_{well}=600 meters. These plots are shown in Figures 5−12a thru d. The effect of enlarging the range in the y direction is not readily apparent in the three−dimensional plots. The surface expression plots, shown in Figures 5−13a and b, are more revealing. The main difference between Figure 5−13a and b is evident in the ultimate capture zone. In the larger domain the capture zone is narrower near the stream and wider near the right flux boundary. The stagnation point is only approximately located, because of discretization error. A sensitivity analysis was performed to determine the dependence of the capture zone curve mapping with respect to the initial particle position near the stagnation point along the stream. A 10 meter (one block size) difference in the initial position changes the location of the capture zone at the right boundary by less than 0.2 meters. However, this only minimizes the error once the stagnation point is located. It does not reduce the error involved in locating the stagnation point. Improved stagnation point calculation can be accomplished only by decreasing the grid spacing along the

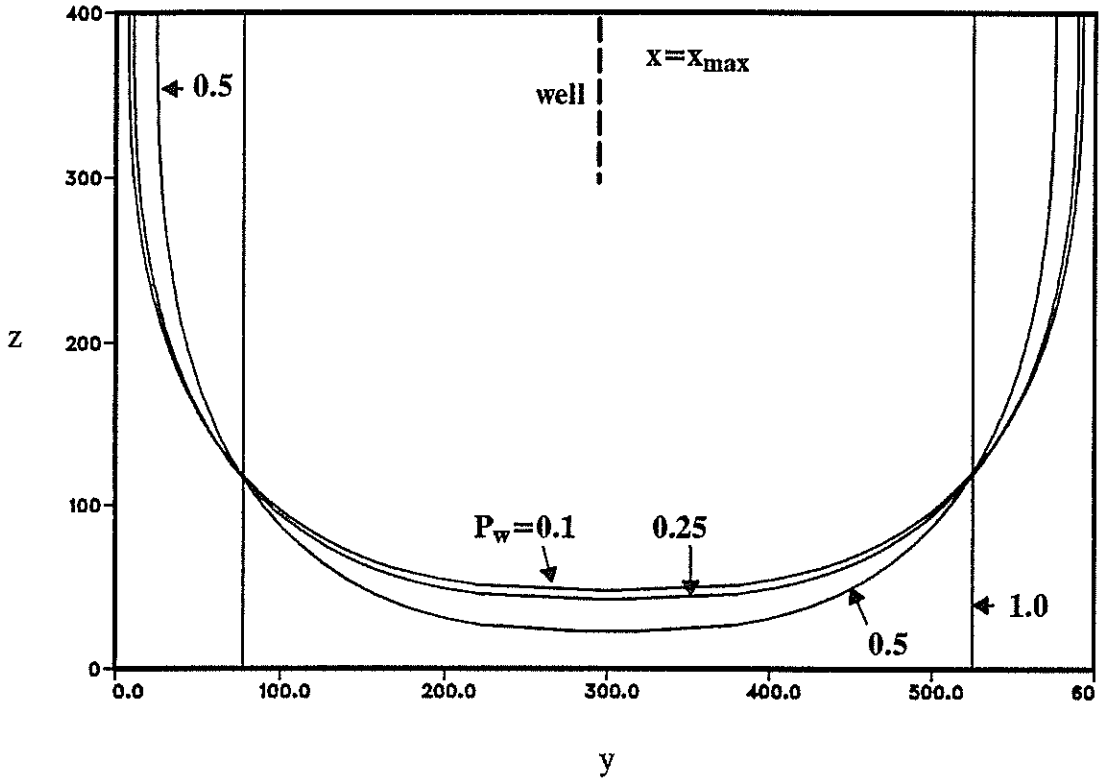

Figure 5−10. Capture zone expressions in z−y plane for well penetrations of P_w=0.1, 0.25, 0.5 and 1.0 at the barrier boundary, (x=600.0). The respective curves for values of partial penetration were derived from fitting an equation to particle tracking data of the form $y^n/a^n + z^n/b^n = 1$. The location of the well for P_w=0.25 has been projected onto the $x=x_{max}$ (x=600 m) plane for visualization purposes.

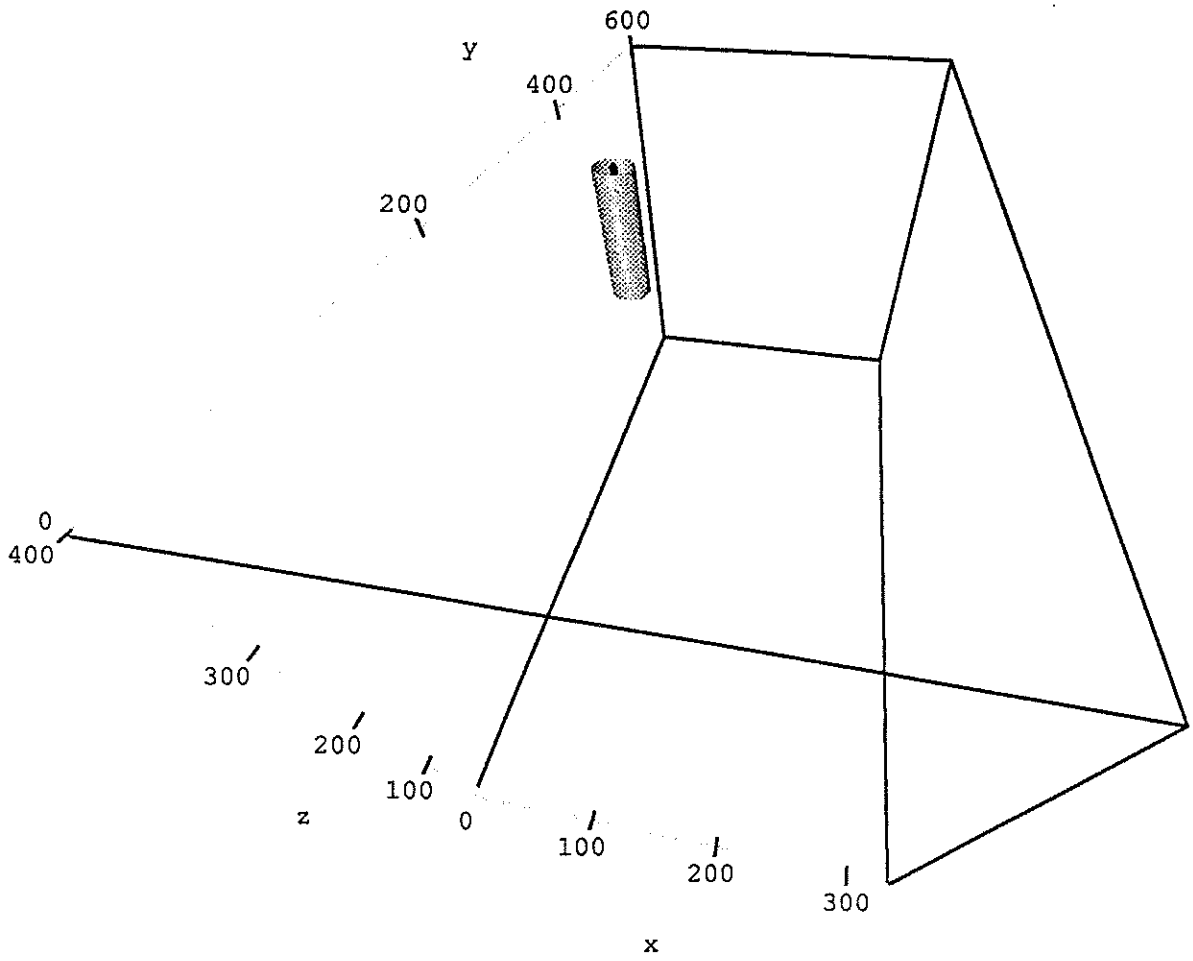

Figure 5−11a. Initial particle positions for P_w=0.25, y_{max}=600 m, distance from stream to well is 80 m.

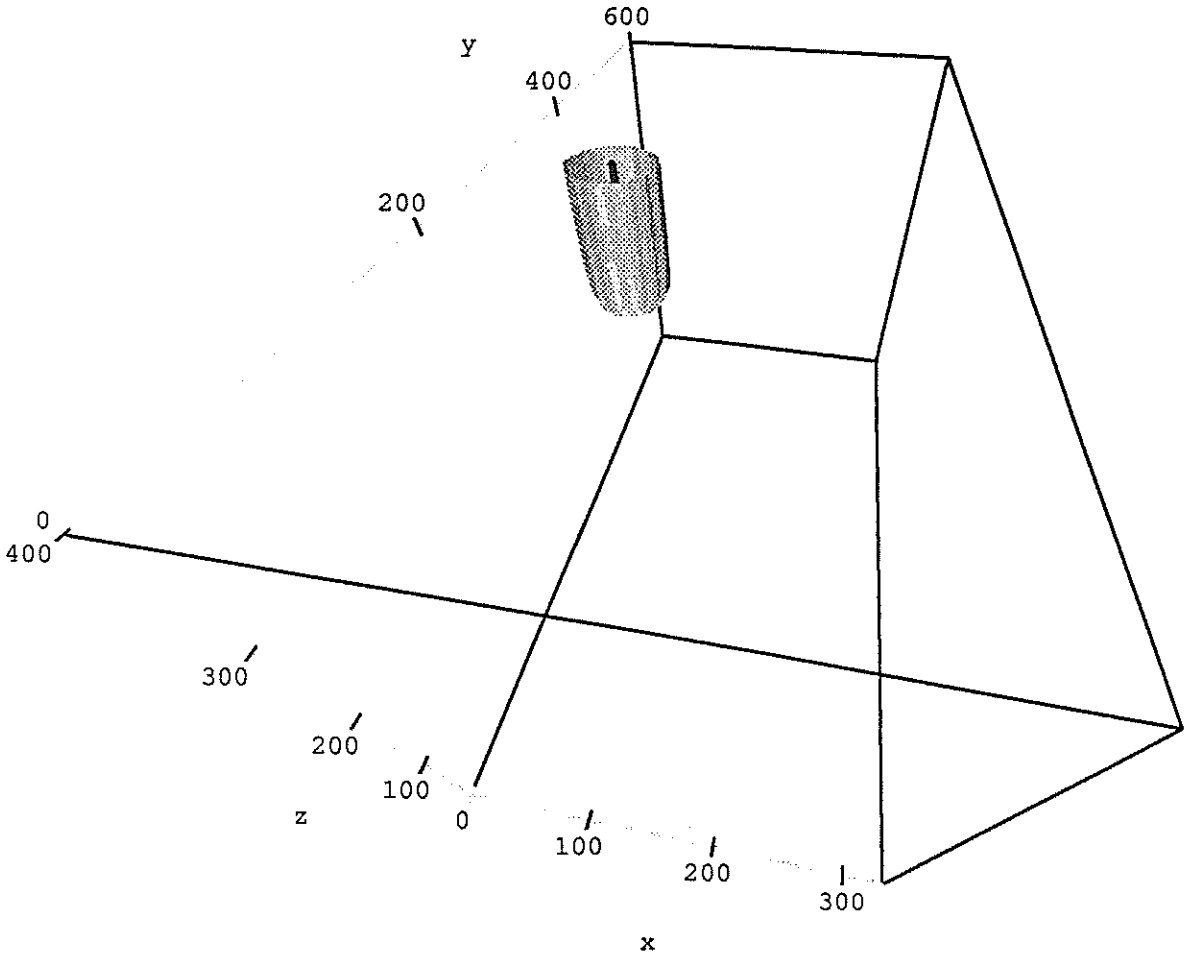

Figure 5−11b. Capture zone for P_w=0.25, t=100 days, y_{max}=600 m.

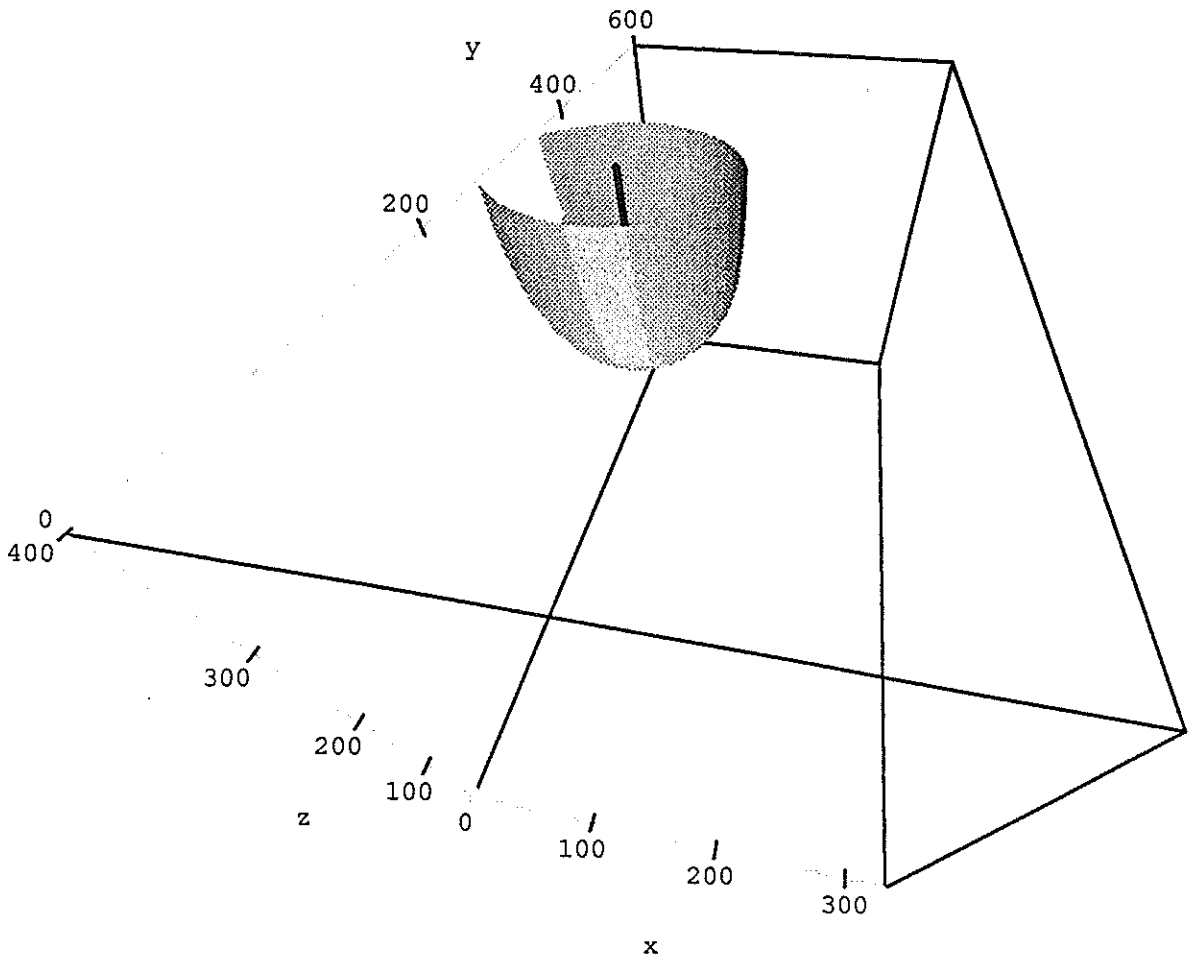

Figure 5−11c. Capture zone for P_w=0.25, t=1000 days, y_{max}=600 m.

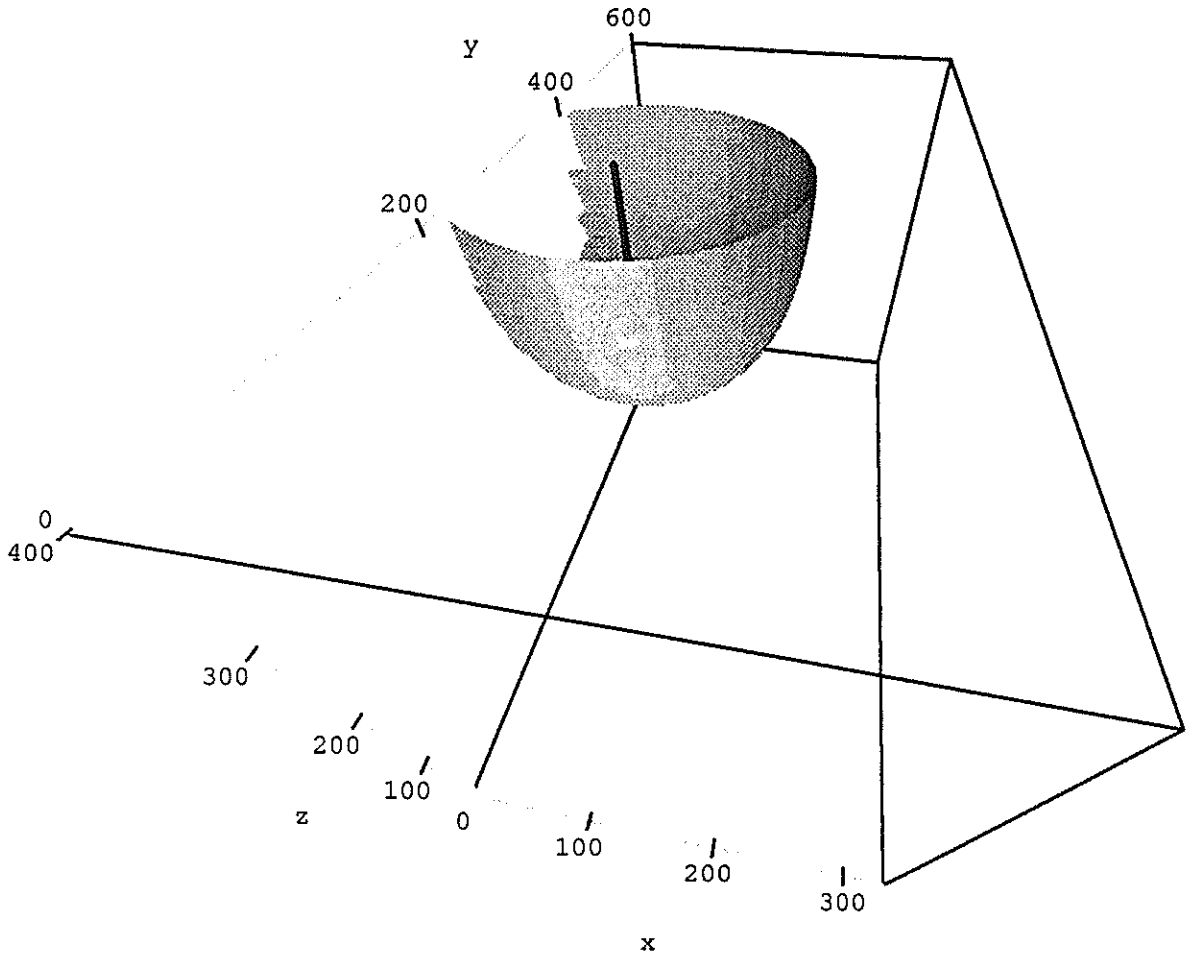

Figure 5−11d. Capture zone for P_w=0.25, t=2500 days, y_{max}=600 m.

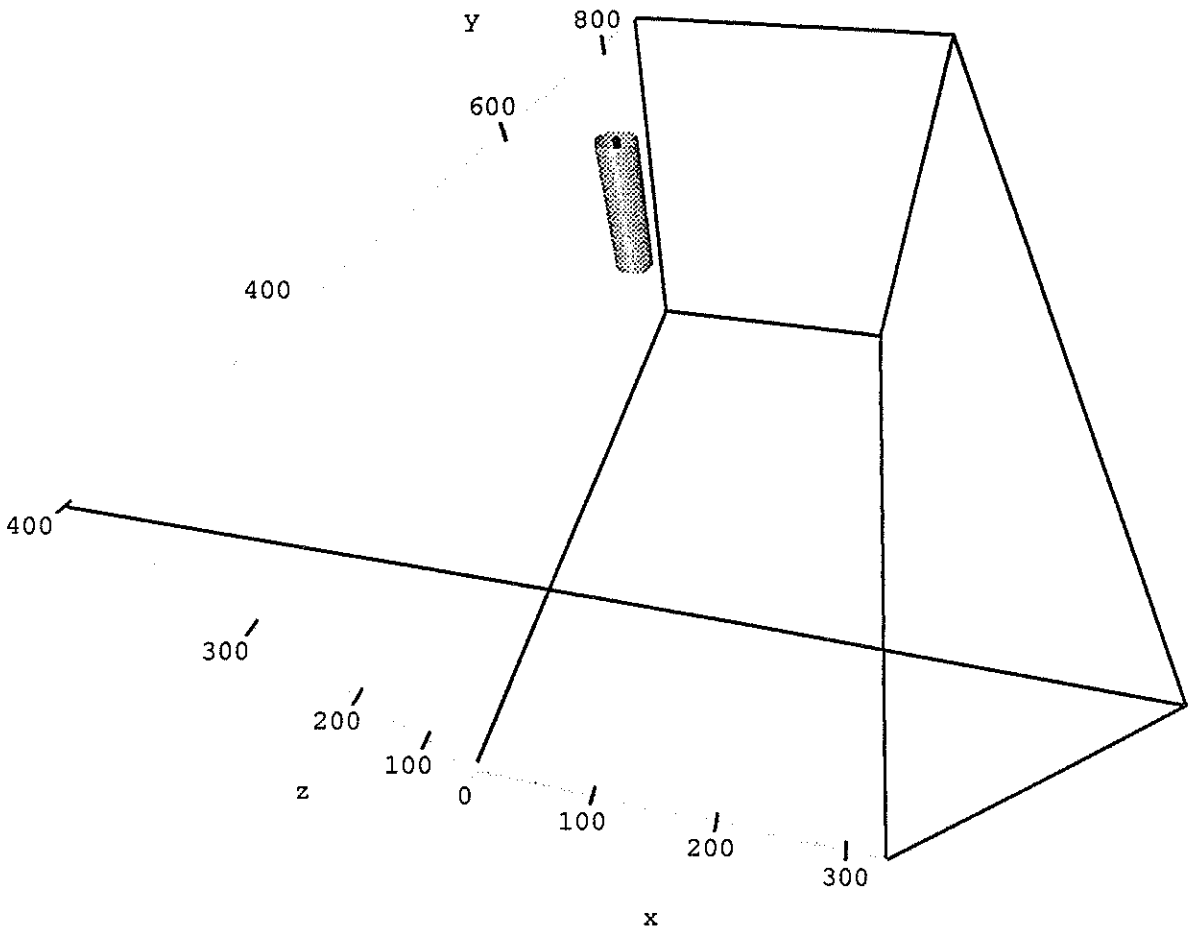

Figure 5−12a. Initial particle positions for P_w=0.25, y_{max}=1200 m, distance from stream to well is 80 m.

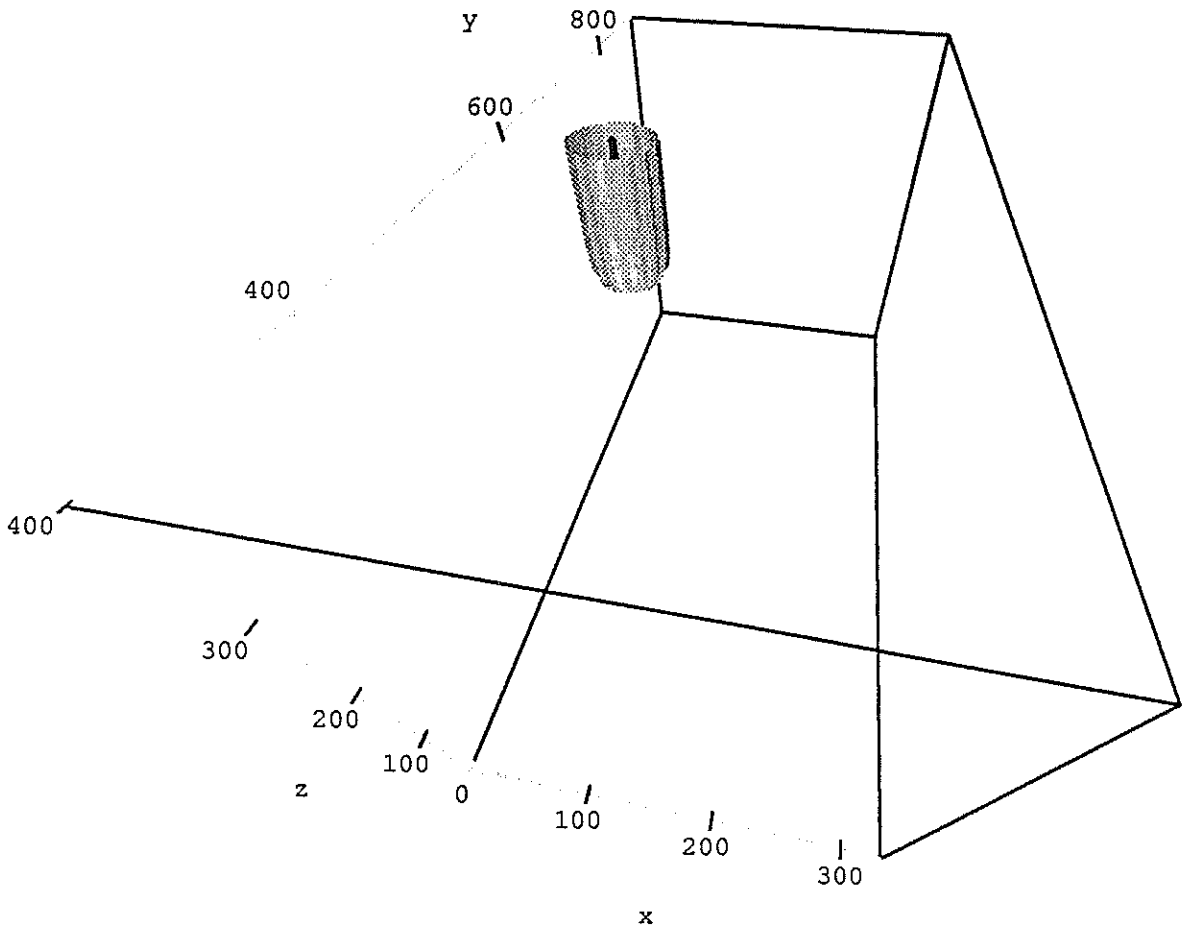

Figure 5−12b. Capture zone for P_w=0.25, t=100 days, y_{max}=1200 m.

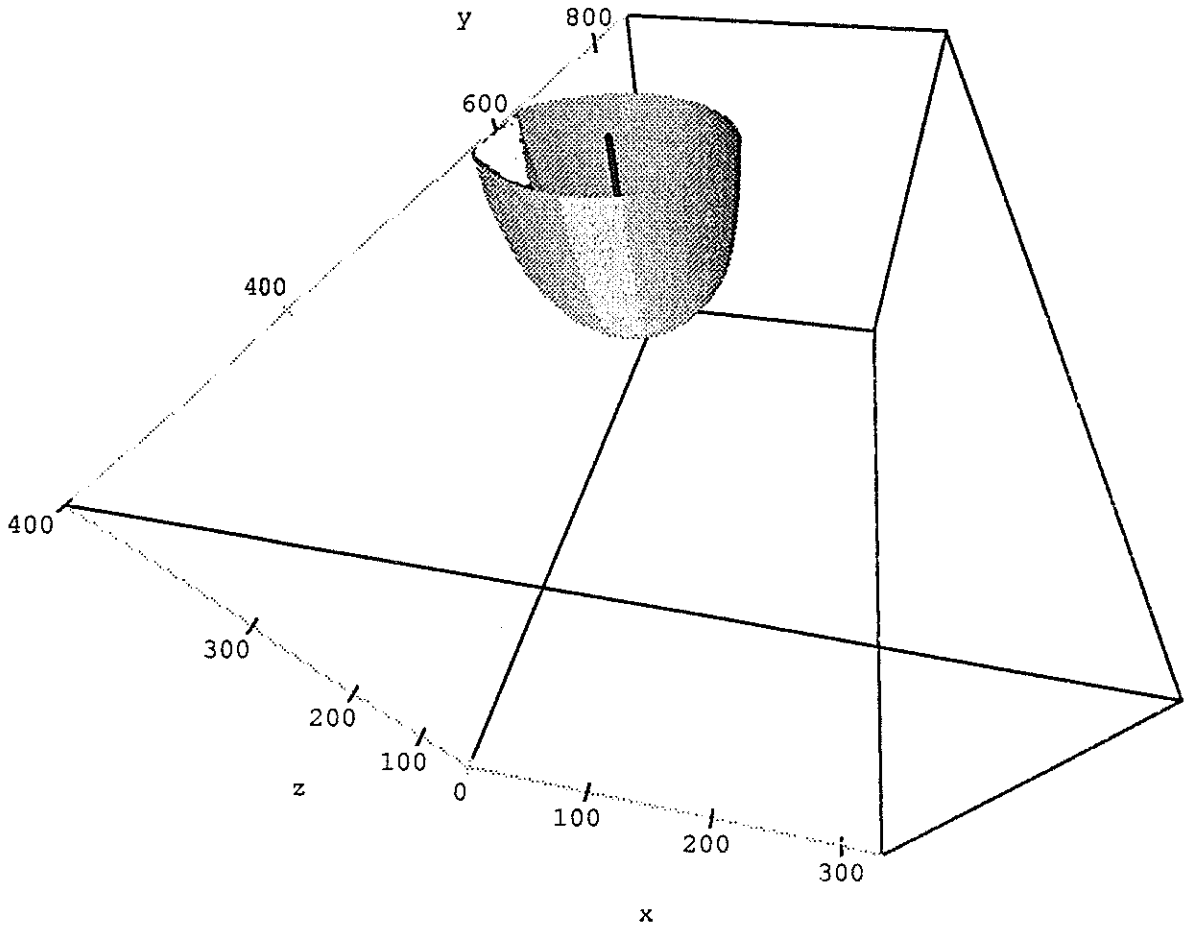

Figure 5−12c. Capture zone for P_w=0.25, t=1000 days, y_{max}=1200 m.

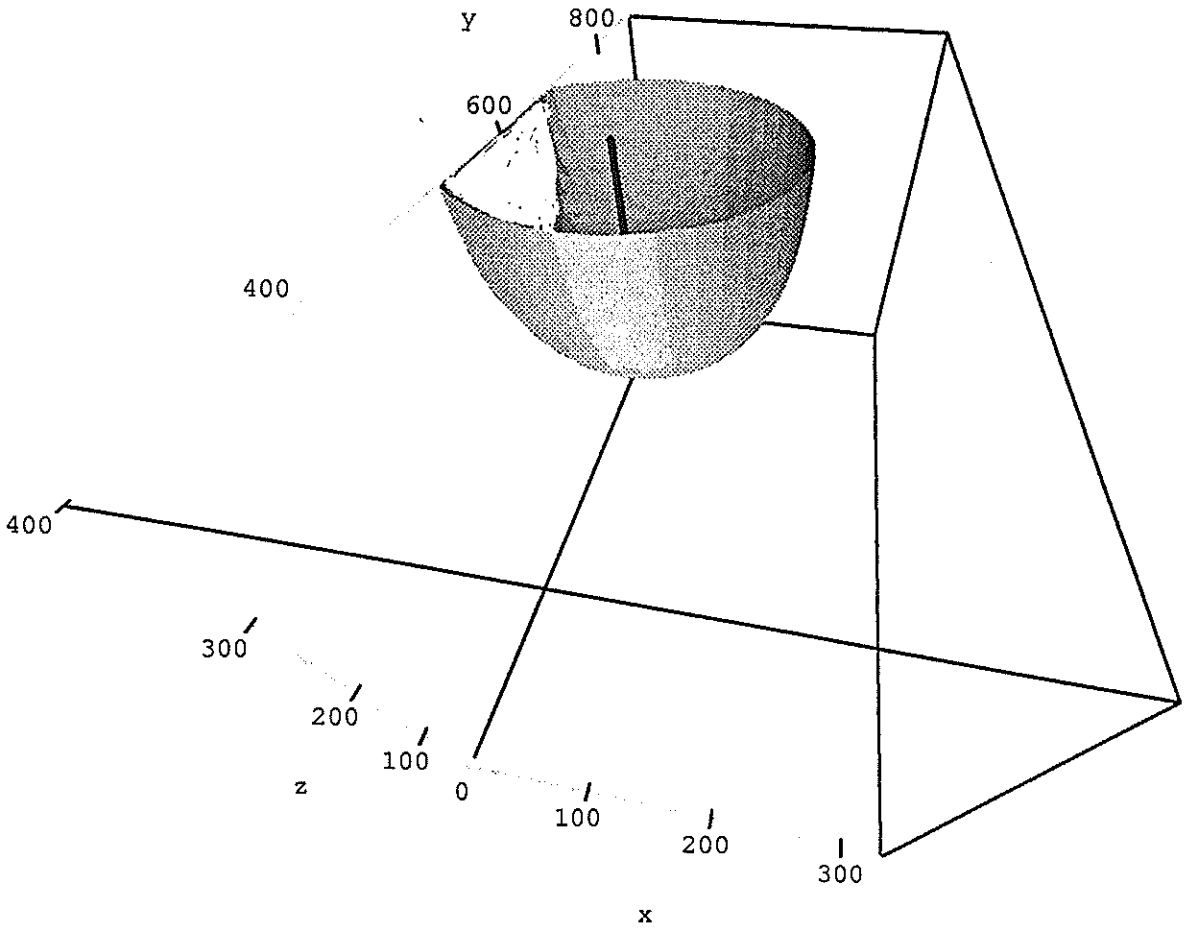

Figure 5−12d. Capture zone for P_w=0.25, t=2500 days, y_{max}=1200 m.

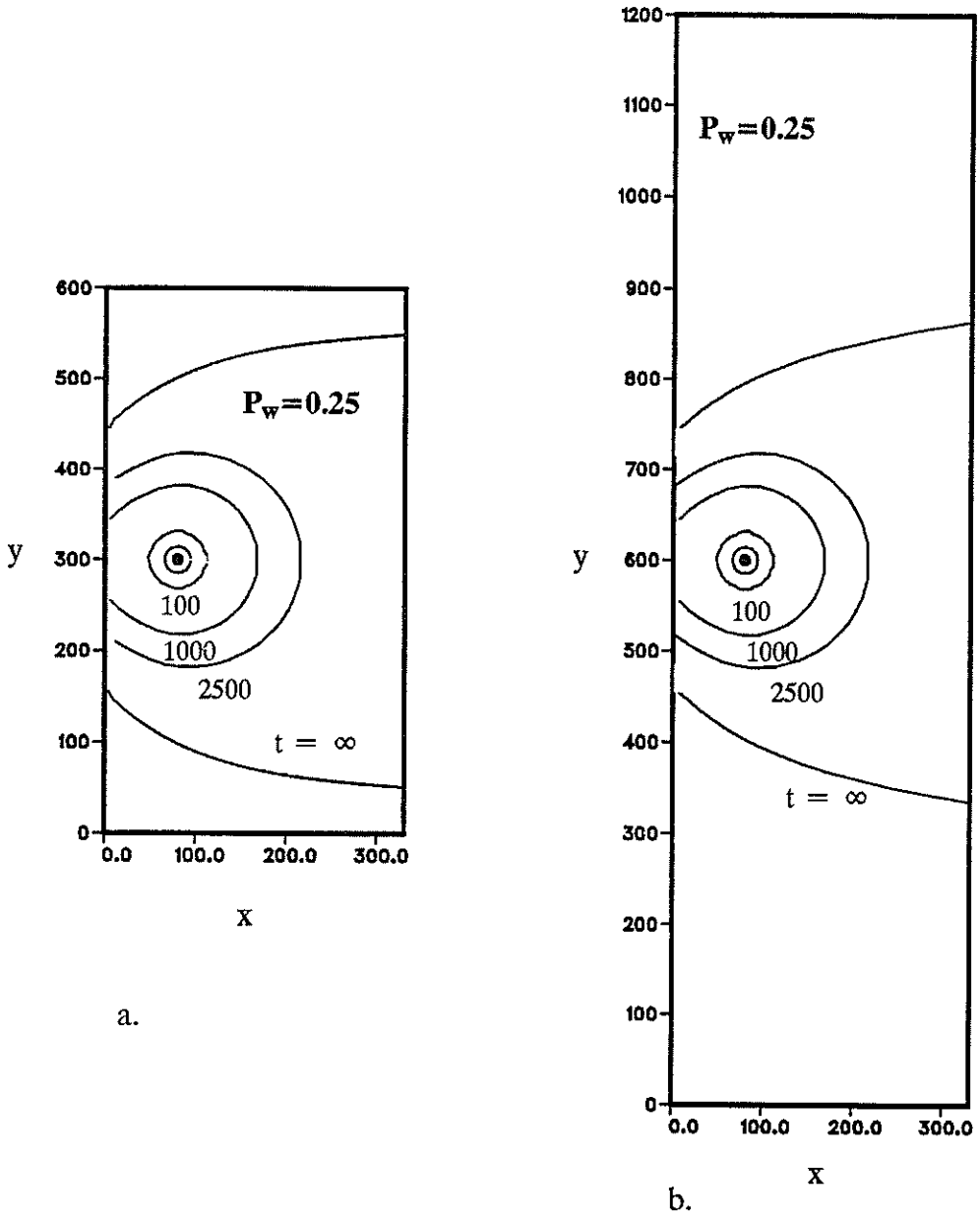

Figure 5−13. Water table expressions of three dimensional capture zones for a well penetration of P_w=0.25 at front times of t=100, 1000 and 2500 days and for the ultimate capture zone at t= ∞. Size of y direction domain is 600m in (a), 1200m in (b). Left boundary is a fully penetrating stream boundary, right boundary is a barrier boundary with flux across it. Boundaries at y=0.0 and y_{max} are no−flow boundaries. Small circle surrounding well represents initial particle positions.

boundary, using higher order numerical methods, or other techniques such as boundary integral element methods.

Figure 5–14a and b presents a comparison of the surface capture zone to various two–dimensional curves for the ultimate capture zone, following the procedure documented in Figure 5–9. For the smaller domain, represented in Figure 5–13a, the match of capture zones using both the stagnation point and the intersection at the right boundary criteria are essentially identical. This is not the case in the larger domain, as seen in Figure 5–14b, where there is more separation of curves a,b and c. An interesting point concerns the location of curves b and c with respect to curve a. In Figure 5–9a, b, and c, curve b was larger and outside (i.e. with respect to the well location) of curve a. Curve c was smaller and inside curve a. These relative positions are reversed in Figures 5–14a and b, probably because of the induced infiltration. Also note in the figure caption the relatively large pumping rates needed to derive the two–dimensional 'equivalent' capture zones of curves b and c. These pumping rates are roughly twice as high as the initial three–dimensional pumping rate. Finally, on Figure 5–14b we have plotted a fifth curve, curve e, which is the equivalent two–dimensional capture zone curve obtained if it was assumed that the well was fully penetrating and the aquifer was only 100 meters thick, all else being identical. This would translate to an effective two–dimensional pumping rate of 2164.0 m^3/day in our 400 m deep aquifer. Haitjema (1987) reported similar findings indicating if recharge area and aquifer thickness were on the same order of magnitude, two–dimensional modeling gives inaccurate areal representations of three–dimensional modeling results.

Our final analysis of this scenario examines the cross–sectional shapes of the capture zone as it intersects the right flux boundary and the stream boundary. Figure 5–15 shows the intersection of the capture zone with the stream boundary, for both the standard and enlarged domains. The area inside of the curves represents that portion of the stream boundary over which there is induced infiltration. The curves have been plotted on the same y axis by normalizing the data to the y value of symmetry, y_{sym}=300.0 m and y_{sym}=600.0 m, respectively, for comparison purposes. Also, only part of the y range is shown here for the extended domain case. The location of these curves are again subject to discretization errors. Each curve is defined by the set of points separating positive and negative x–velocities. Within the capture zone, V_x is positive along the stream boundary as water is flowing from the stream to the aquifer. Outside the capture zone, V_x is negative as water is flowing from the aquifer to the stream. Since block centered velocities for a given direction represent the velocity over the entire block, our capture zone boundary has a stair–step appearance. The curves in Figure 5–15 were fitted,to the data, as before, assuming a power function relationship. The two curves shown in Figure 5–15 have the same shape and the same values of power n.The only difference is with respect to the values for a and b. It is suspected that in reality the curves do not resemble each other as closely as shown here,but have a slightly different appearance. This is substantiated by examining the intersection of the capture zone with the flux boundary at $x=x_{max}$, shown in Figure 5–16. These two curves were produced by backtracking from the initial points where the capture zone intersects the stream boundary (i.e., the same points used to produce the curves in Figure 5–15). As described above for the first case,these curves are believed to be fairly accurate, due

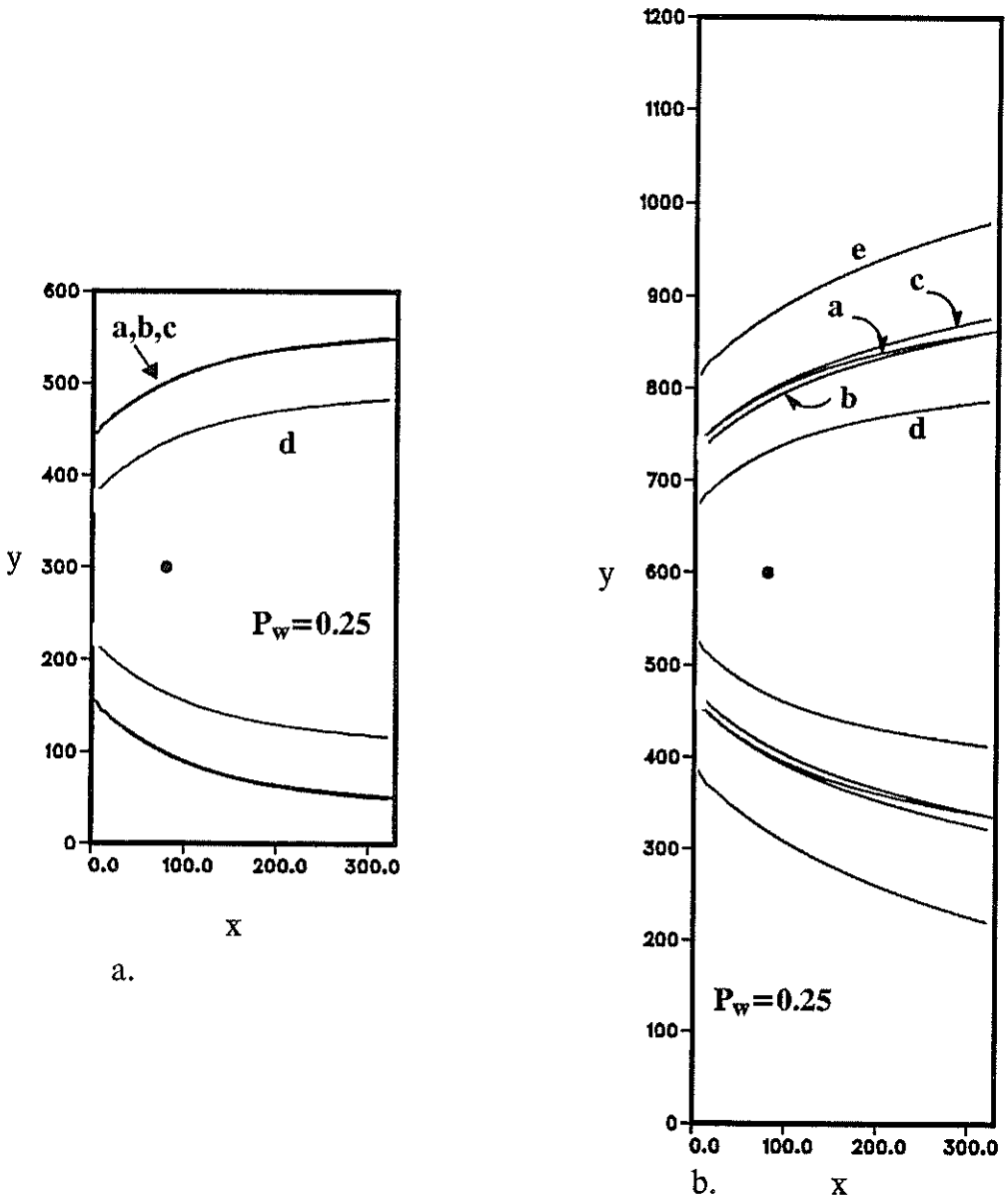

Figure 5–14. Water table expressions of three–dimensional capture zone for well penetration of P_w=0.25 along with two–dimensional counterparts assuming full well penetration for two aquifers differing in size in y dimension only. Curve a is the original 3D curve, Q_{3D}=541.0; Curve b is 2D matching at x=600.0, Q_{2D}=996.00; Curve c is 2D matching at 3D stagnation point, Q_{2D}=1108.0; Curve d is for Q_{3D} distributed over the entire aquifer depth, Q_{2D}=541.0; Curve e represents the capture zone assuming the aquifer is 100 meters thick and Q=541.0. Pumping rates are in m^3/day.

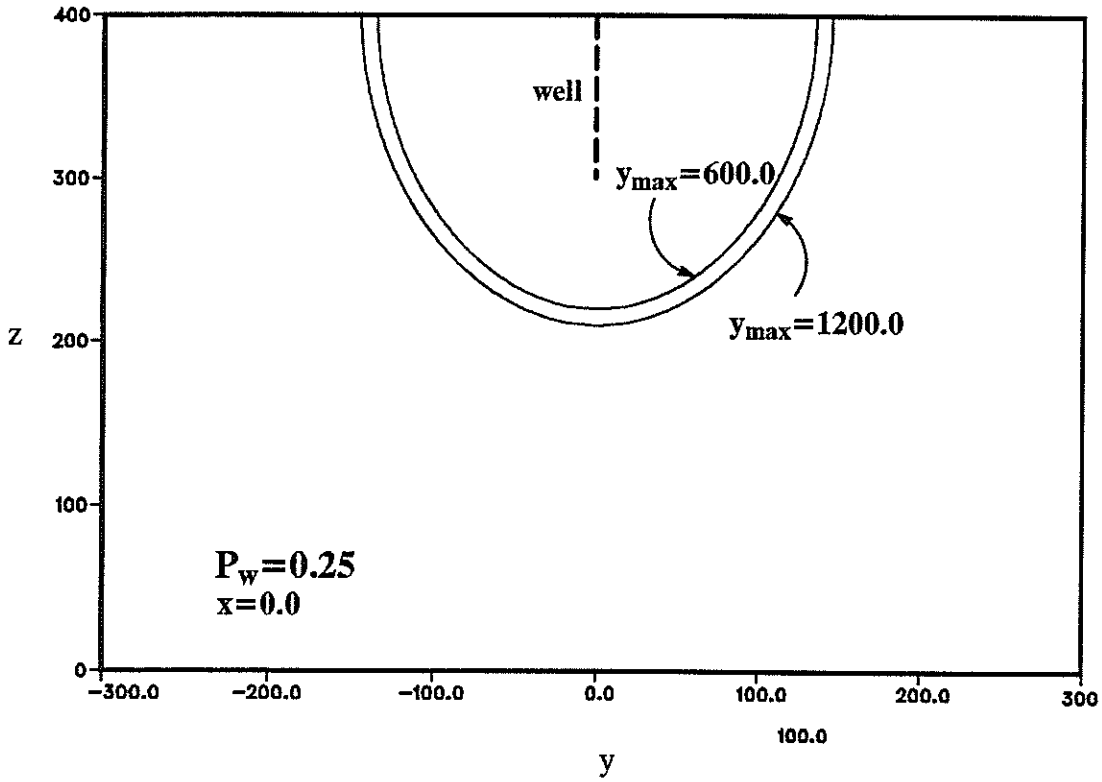

Figure 5−15. Capture zone expressions in z−y plane for well penetration of P_w=0.25 at the stream boundary, i.e. x=0.0, for two different y dimensions; y=1200.0 and y=600.0 m. The location of the well has been projected onto the x=0.0 plane for visualization purposes. In addition, scale in y dimension is now in reference to well location for comparison purposes. The curves were derived from fitting an equation to particle tracking data of the form: $y^n/a^n + z^n/b^n = 1$.

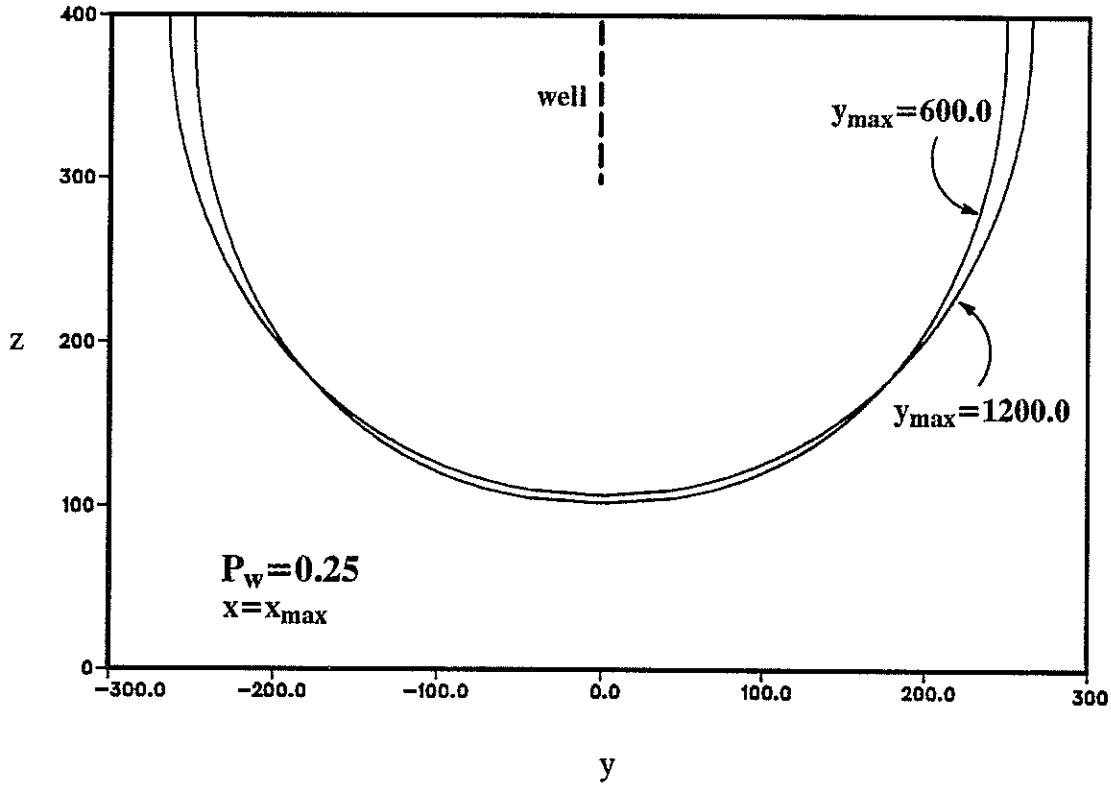

Figure 5−16. Capture zone expressions in z−y plane for well penetration of P_w=0.25 at the barrier boundary, i.e. x=600.0, for two different y dimensions; y=1200.0 and y=600.0 m. The location of the well has been projected onto the x=600.0 plane for visualization purposes. In addition, scale in y dimension is now in reference to well location for comparison purposes. The curves were derived from fitting an equation to particle tracking data of the form: $y^n/a^n + z^n/b^n = 1$.

Table 5−2. Characteristic fitted parameters for three−dimensional capture zone cross−sections in a system with induced infiltration.

y−z plane	y_{sym}	n	a	b
x=0	300.0	1.95	145.10	190.10
x=0	600.0	1.95	135.10	180.10
$x=x_{max}$	300.0	2.20	249.19	297.61
$x=x_{max}$	600.0	2.08	264.61	292.88

to the low sensitivity of the final particle locations to starting location. Although the data is not shown with these curves, the fits were excellent. The values for a, b and n are presented in Table 5−2.

Clearly evident from the curves presented in Figure 5−16 is the effect of the finite size aquifer boundaries on the shape of the capture zone. The effect of a smaller domain is to 'squash' the capture zone together decreasing the overall y−dimension width and increasing the overall z−dimension depth. These effects are also represented in the equation used to describe the shape of the curves given by (5−2). The fit of the curve to the data was very good for both curves at $x=x_{max}$. As the influence of the lateral no−flow boundaries in the y direction decreased, the value of n slightly decreased. This is reasonable since we would expect the value of n to approach 2.00 as the boundary influences at $x=x_{max}$ are moved further from the well.

At a very small pumping rate, the boundaries have very little influence and the shape of the capture zone at $x=x_{max}$ is unconstrained and takes on the natural shape of a semi−ellipse. As the pumping rate increases, the capture zone becomes constrained by the boundaries. When this happens, the capture zone takes on more and more of the aquifer's shape and $n \rightarrow \infty$. Based on the results presented for the first three cases, the depth of well penetration appears to have little affect on the value of n. This is plausible as long as the pumping rate does not become excessive and the well penetration remains sufficiently small.

PARTIALLY PENETRATING STREAM, PARTIALLY PENETRATING WELL

Our final three−dimensional capture zone analysis examines an alluvial basin bordered on each side by mountain fronts with a partially penetrating stream flowing along the center of the valley, as illustrated in Figure 5−17. On one side of the valley near the stream is a partially penetrating well pumping at rate Q_w. Ambient aquifer flow parallel to the stream is assumed to be zero, flux across both mountain fronts is into the aquifer at rate q. There is no local vertical recharge.This flow domain is an extension of the previous one studied. The stream penetrates only the upper layer of grid blocks and is one grid block wide. It is represented by a constant head in these blocks. The aquifer extends to 330 meters to both sides of the stream. The stream−aquifer system is symmetric with respect to the stream in the y direction. The

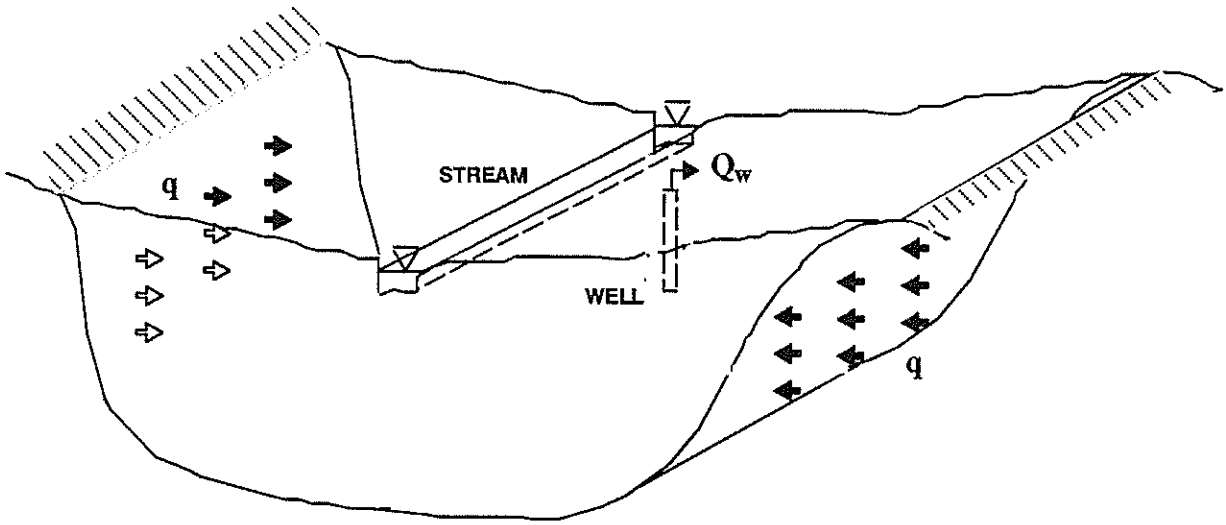

Figure 5–17. Schematic of stream–aquifer system with a partially penetrating stream, a partially penetrating well pumping at rate Q_w m^3/day and lateral recharge at rate q m/day.

location and penetration of the well with respect to the stream and right boundary is the same as in the previous case: the distance between the stream and the well is 80 m; the distance from the well to the right boundary is 250 m; the well penetration ratio is P_w=0.25.

Figures 5−18a thru f show initial particle positions and the three−dimensional capture zones for t=100, 1000, 2500, 4000 and 7000 days. For early times there is very little variation in the shape of the capture zone. For t=1000 days we begin to see the influence of the stream and other boundaries. The top portion of the capture zone is opening toward the right flux boundary while its lower portion is bulging out toward the stream and left boundary. Figure 5−19 shows the shape of the capture zones at the aquifer's surface. The stagnation point in this two−dimensional plane is between the well and the stream,and the capture zone never intersects the stream at the surface. The right side of the capture zone at the surface migrates towards the right flux boundary eventually intersecting it and drawing water from it. As time passes, the lower portion of the capture zone continues to migrate toward the left boundary. Eventually the bottom of the capture zone protrudes under the stream. It appears to be moving toward the left boundary, rather than the stream.

Will the capture zone miss the stream, as indicated by Figure 5−18e? To answer this question,a particle was placed into the velocity field near the stagnation point at the aquifer's surface and tracked backwards. Figure 5−20 is a cross section in the x−z plane through the well, showing relative magnitudes of velocity vectors with relative scales indicated by the length of shaft of the arrow. The resulting particle tracking curve is shown as the dividing streamline. From this view it is apparent that the capture zone does not intersect the stream. Figure 5−20 also shows the various sources of water and the respective termini for them in this plane. The stream obtains water from the left boundary only (in this cross−section). The well induces underflow beneath the stream, drawing water from both the left and right boundaries. The line extending from the lower portion of the well to the base of the aquifer separates the two sources of water flowing toward the well. It is interesting to note that along this x−z plane, all of the water over the entire depth of the aquifer between this line and the right boundary flows to the well. This is compared to previous capture zones (e.g., see Figures 5−6, −10, and −16) where it can be seen that the capture zone does not intersect the bottom of the aquifer for any of the partially penetrating well cases previously presented. It is hypothesized that the effect of drawing water from the lower portion of the left boundary to the well has modified the flow system to where water over the entire aquifer depth at the right boundary now also flows to the well. There is no induced infiltration.

Comparing Figures 5−19 and 5−20, a discrepancy exists with respect to the sources defined in Figure 5−20. In Figure 5−19, water reaching the well at the surface of the aquifer seems to originate entirely from the right boundary. This includes water flowing between the stagnation point and the well. Figure 5−20 indicates that the water in this vicinity actually originates at the left boundary. Water flowing beneath the surface stagnation point to the well from the right boundary actually originates at the bottom of that aquifer boundary. The rest of the water flowing from the stagnation point area originates in the bottom 100 meters of the left boundary. The plot in Figure 5−19 is the surface expression of the capture zone. It does not recognize the subsurface movement at the aquifer's bottom.

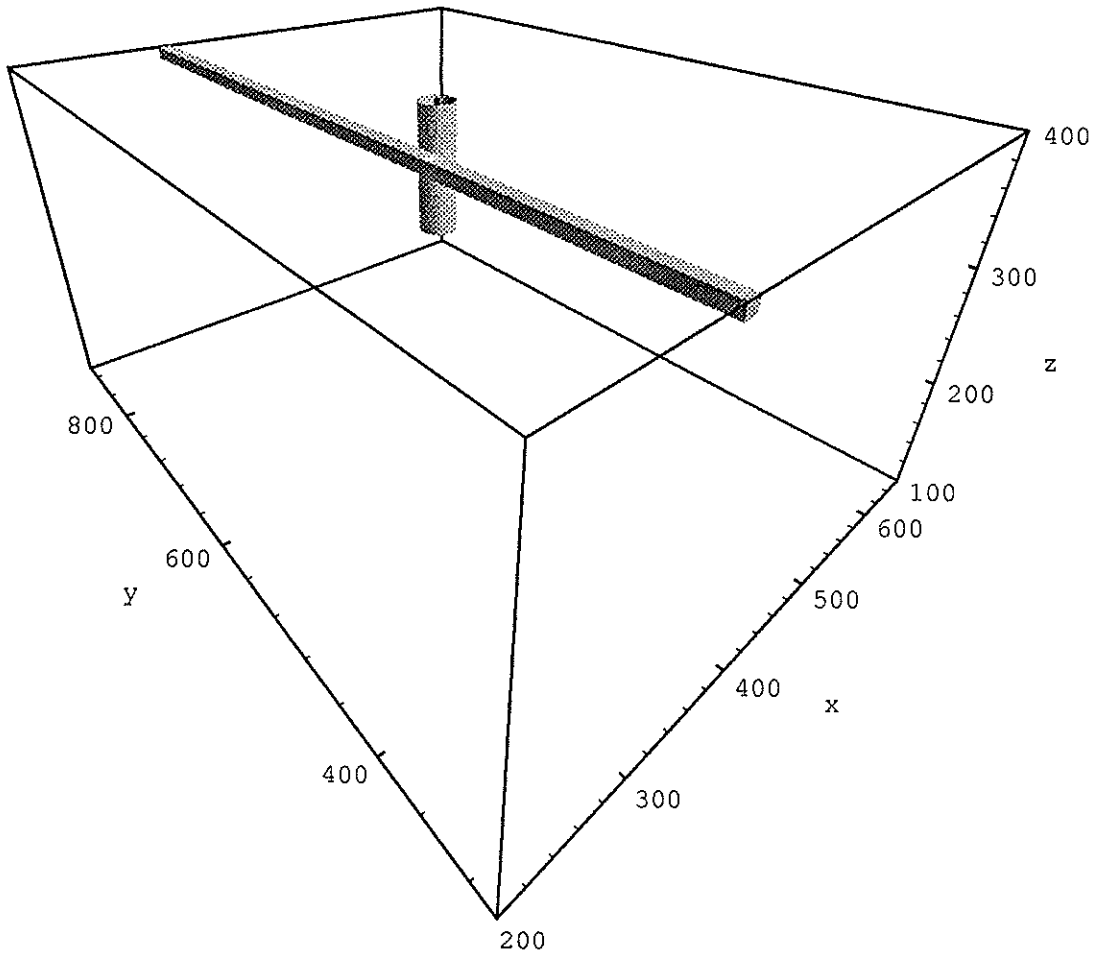

Figure 5−18a. Initial particle positions for well penetration P_w=0.25, near a partially penetrating stream which is shown as a long rectangular structure at top of aquifer.

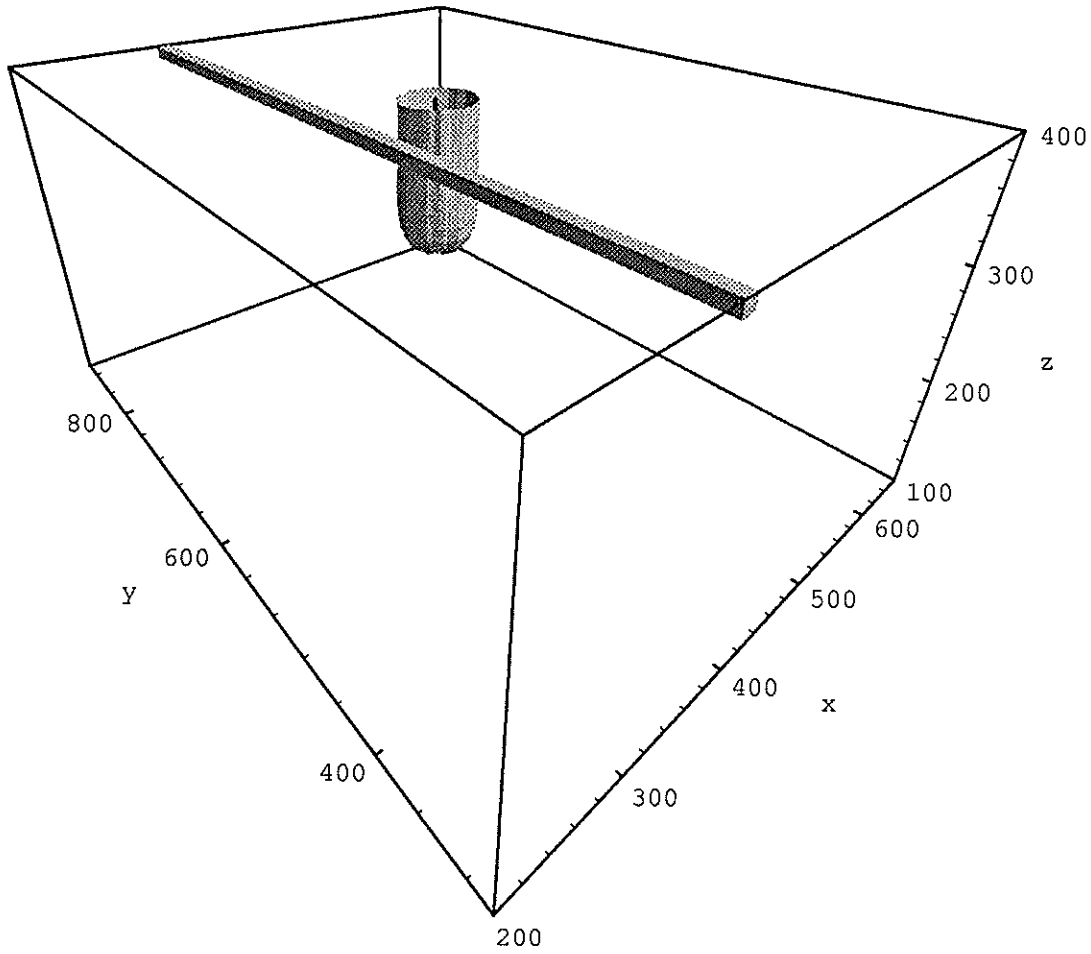

Figure 5−18b. Capture zone for t=100 days.

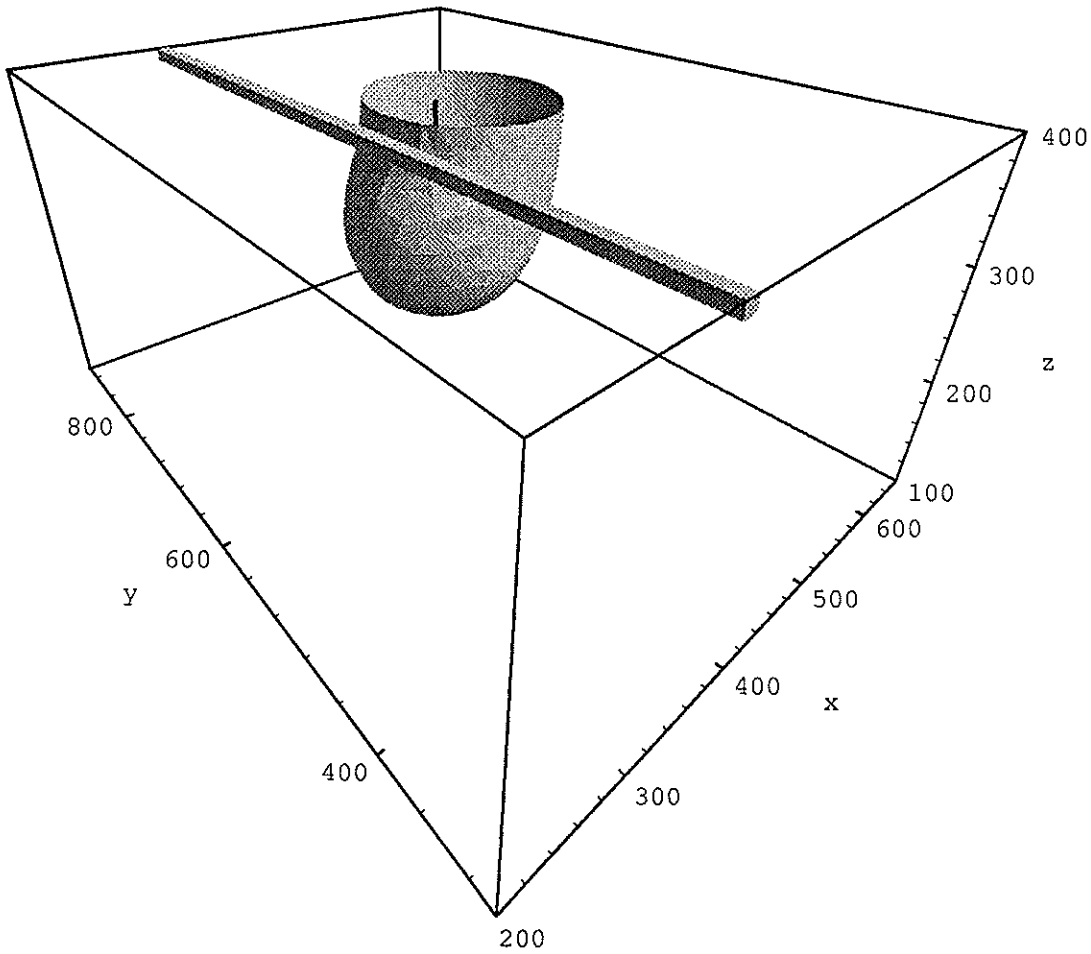

Figure 5−18c. Capture zone for t=1000 days.

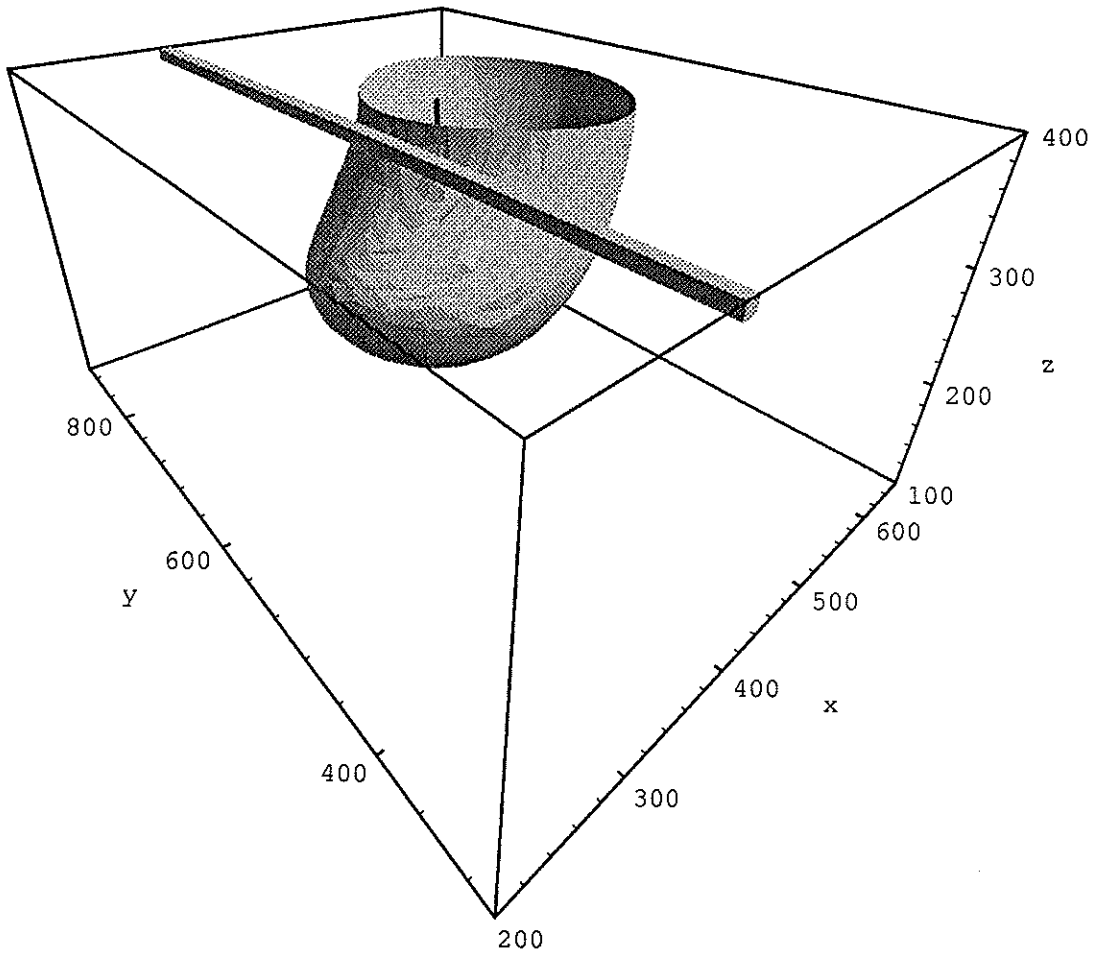

Figure 5−18d. Capture zone for t=2500 days.

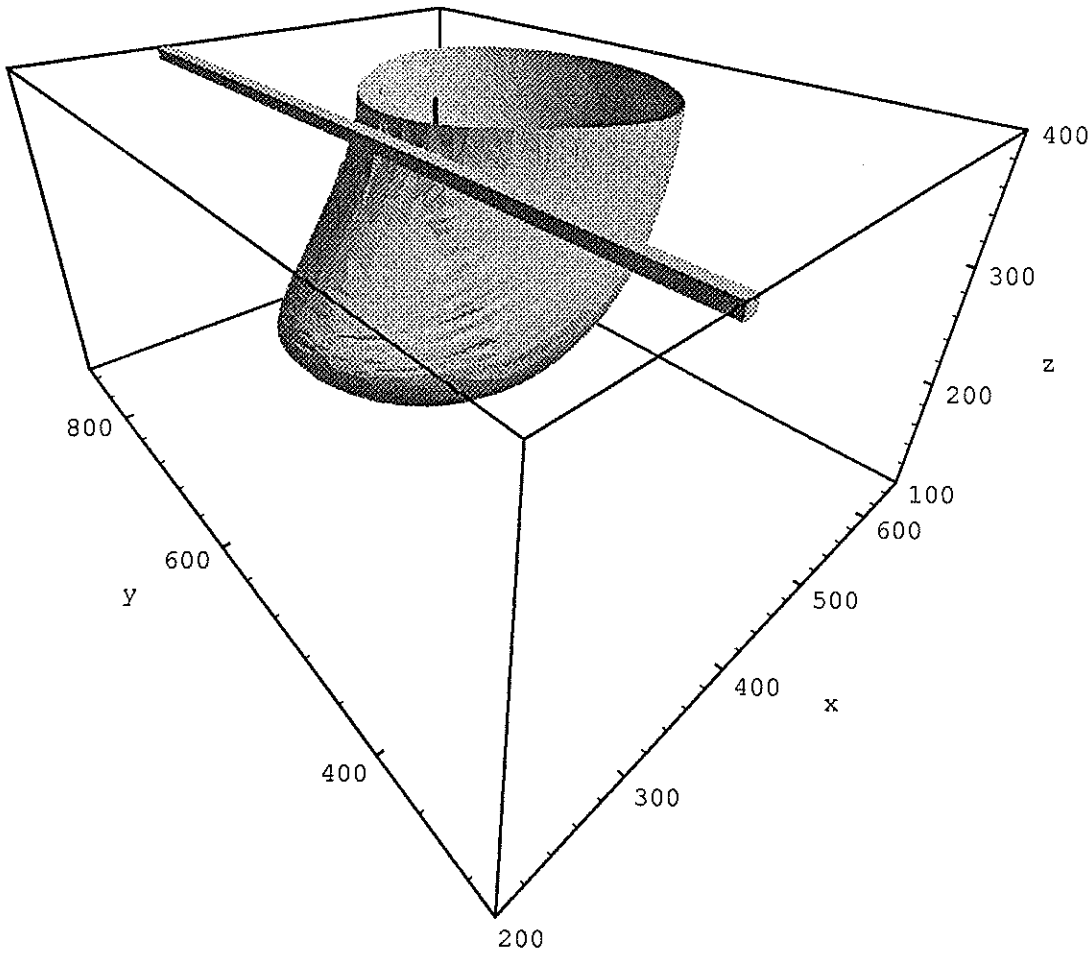

Figure 5−18e. Capture zone for t=4000 days.

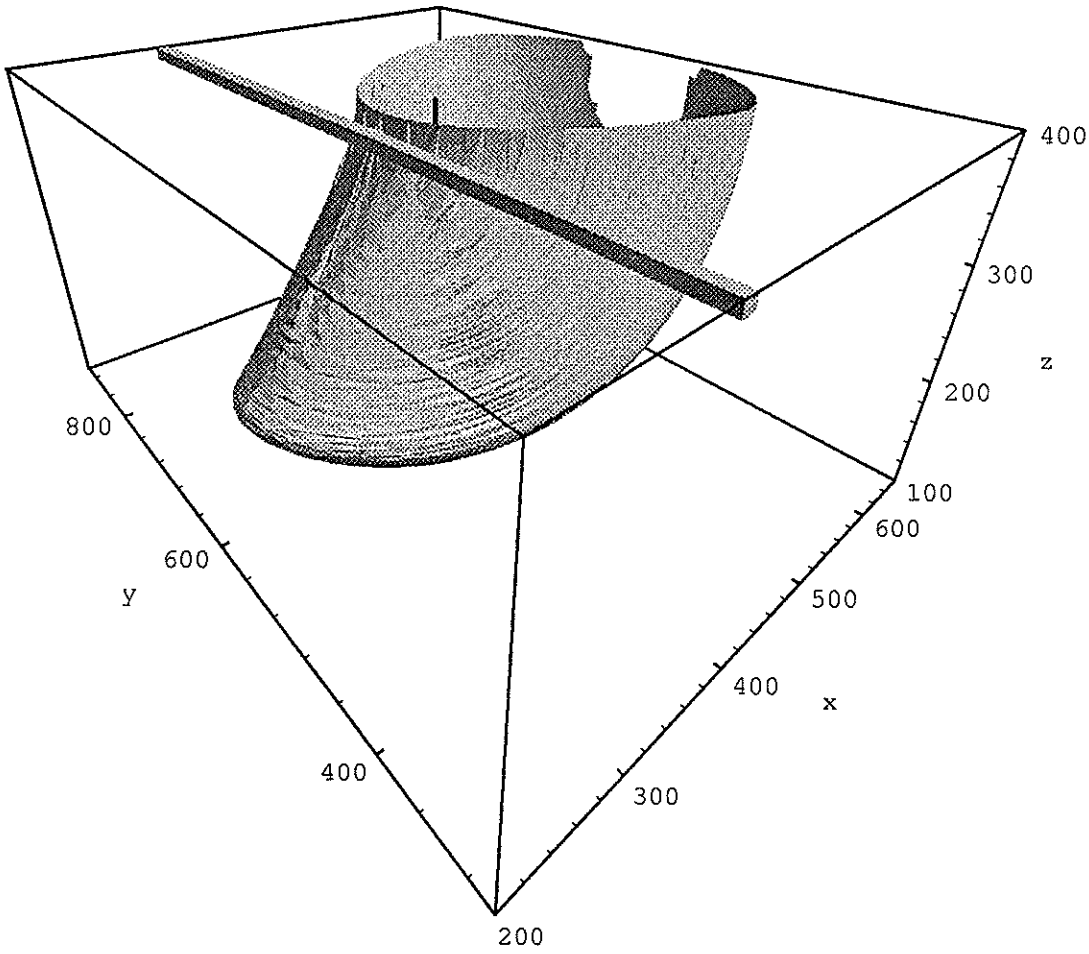

Figure 5−18f. Capture zone for t=7000 days.

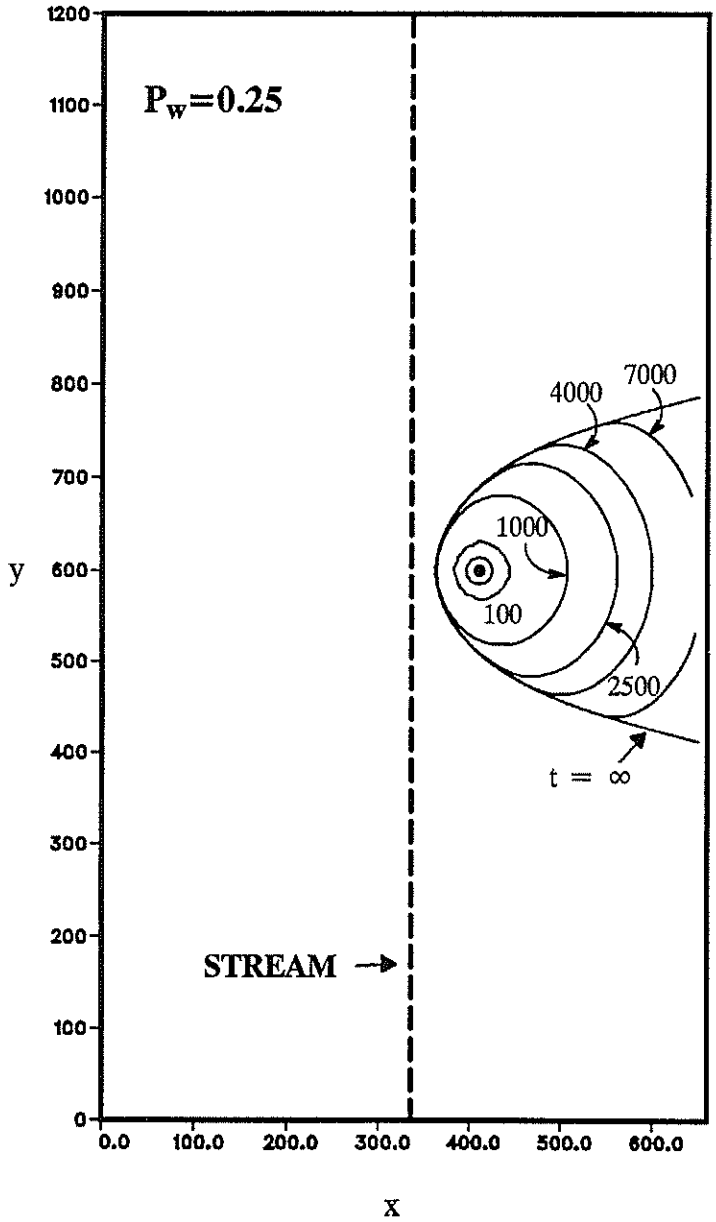

Figure 5−19. Water table expression of three−dimensional capture zones for a well penetration of P_w=0.25 at front times of t=100, 1000, 2500, 4000 and 7000 days and for the ultimate capture zone at t = ∞ . The stream penetrates 10 meters into the aquifer. Left and right boundaries are flux boudaries, both with flux towards the stream; the upper and lower boundaries are no−flow boundaries. Small circle surrounding well represents initial partical positions.

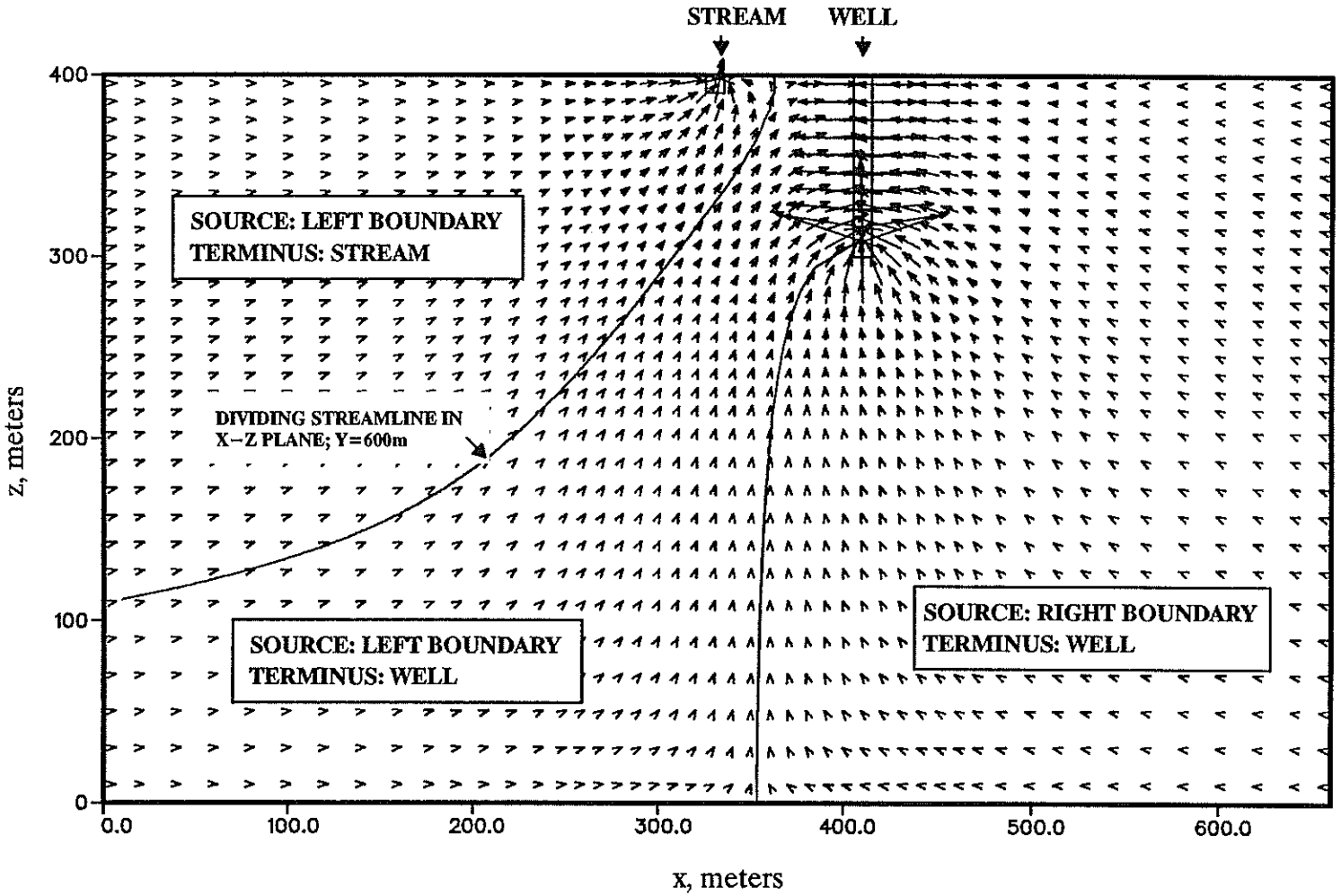

Figure 5–20. Block center velocity vectors in x–z plane through well at y=600 m. The dividing streamline separates water flowing to well from water flowing to stream. The other line extending downward from well indicates boundary between water derived from left and right boundaries flowing to well.

We can also compare the surface expression of the three–dimensional capture zone with various two–dimensional representations as before. These results are shown in Figure 5–21, where curves a thru e are derived in an analogous manner to the previous plots. The relative positions of curve b and c with respect to curve a are the same as in Figure 5–9. The equivalent pumping rates for curves b and c are much lower than for the same curves in Figures 5–9 and 5–13. This is caused by the size reduction of the surface expression of the three–dimensional capture zone in the presence of a new recharge source,the left boundary.

CONCLUSIONS

In our analysis of three–dimensional capture zones we have examined several aspects of capture zone delineation:

- Analysis of 'generic' capture zones to see the effects of well penetration;
- Effect of induced infiltration on shape of the capture zone;
- Comparison of two–dimensional approaches to capture zone modeling to three–dimensional modeling results;
- Modeling of the shape of the capture zone at intersection with boundaries: the stream, the barrier, and the (water table) surface of the aquifer.
- Effects of no–flow boundaries on all aspects of capture zone delineation;
- Analysis of partially penetrating stream and partially penetrating well system.

Our 'generic' capture zone analysis revealed several interesting results. Most notable of these was the varying overall shape of the capture zones for varying well penetration. For P_w=0.1, the capture zone was shallow and wide with the aquifer surface expression encompassing the largest area of all three cases considered. As the capture zone expanded it became spherical in shape, as long is it was not influenced by boundaries. As well penetration P_w increased with pumping Q_w held constant, the capture zone elongated vertically and became more cylindrical and the surface expression area decreased.

The change in cross–sectional shape of the capture zone was evaluated where it crossed the flux boundary. All three partial well penetration curves and the full well penetration curve intersected at the same crossover intersection point and all three partial penetration curves exhibited the same value for the curve fitting parameter n. This indicates that the shape of the capture zone at the flux boundary may be fixed and predictable for a given flow system, although further simulations are required to substantiate this for larger penetration, P_w. This behavior is substantiated somewhat by similar curves produced when the well is moved closer to the stream. In this case, the value of n decreases slightly, essentially enlarging the flow domain in the direction parallel to the stream. This effect is in agreement with the hypothesis that the value of n approaches 2.0 as boundary effects are reduced. The value of n=1.95 obtained where the capture zone intersected the stream boundary is thought to reflect the non-

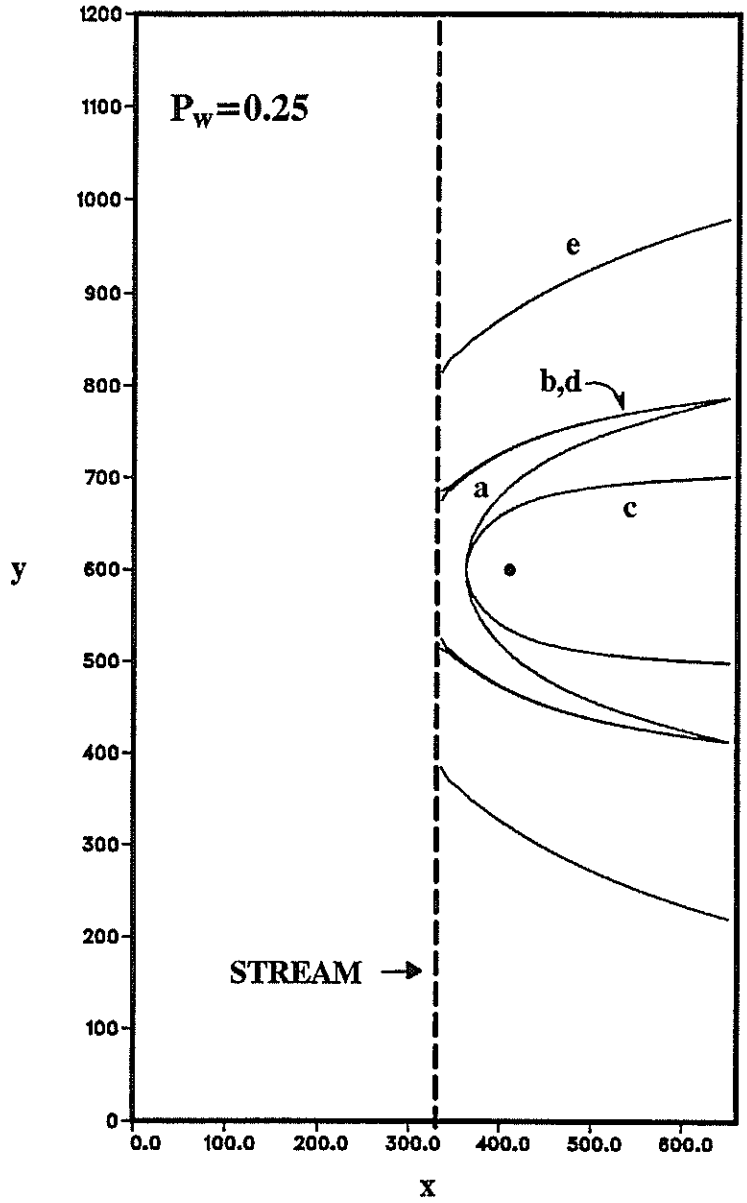

Figure 5−21. Water table expression of three dimensional capture zone for well penetration of P_w=0.25 along with two dimensional counterparts assuming full well penetration: Curve a is the orginal 3D curve, Q_{3D}=541.0; Curve b is 2D matching at x=660.0, Q_{2D}=536.0; Curve c is 2D matching at 3D stagnation point, Q_{2D}=244.4; Curve d is for Q_{3D} distributed over the entire aquifer depth, Q_{2D}=541.0; Curve e represents the capture zone assuming the aquifer is 100 meters thick and Q=541.0. Pumping rates are in m^3/day.

uniform flux to the aquifer across the plane of induced infiltration, which is consistent with a constant head boundary.

Attempts to derive equivalent two–dimensional capture zones at the surface of the aquifer indicates two–dimensional capture zone modeling in a three–dimensional flow field could produce some very significant errors in capture zone prediction. The simple approaches of assuming full well penetration either grossly over–predict or under–predict the size of the true capture zone. This effect is reduced as well penetration approaches P_w=1.0. Attempts at matching two–dimensional capture zones at critical points also indicated that deriving an equivalent two–dimensional capture zone, which is useful in prediction of the true three–dimensional capture zone, is less successful as the well penetration decreases. An interesting side point is that the relative positions of the two critical point curves with respect to the original three–dimensional curve are reversed depending on whether the capture zone interacts directly with the stream and induces infiltration.

Finally, our analysis of a partially penetrating well near a partially penetrating stream produced some interesting results. For the depth of stream penetration considered, the capture zone did not intersect the stream but instead extended under the stream and intersected the ambient groundwater flow on the opposite bank, taking this flow from the aquifer's bottom. Another result which varied from the previous simulations is that the capture zone penetrated to the bottom of the aquifer. This is most likely related to the effect of the stream and lack of induced infiltration. Since water from the left boundary flows to the stream at the top of the aquifer, the water available to the well from the left boundary comes from the bottom of this boundary. This in turn affects the hydraulics between the well and the right boundary such that the well now pumps water from the bottom part of the right boundary also. Interaction of the capture zone with the stream, by increasing stream penetration, increasing pumping or decreasing the stream–well separation, will most likely strongly affect the shape of the capture zone and the location of source waters flowing to the well.

SECTION 6

SUMMARY AND CONCLUSIONS

Well-water quality depends on the relative amounts of water drawn from different hydrologic units (aquifers, streams, etc.), and the particular capture zones within those units. A contaminant spilled within an aquifer capture zone will eventually enter the well. A spill outside the capture zone may eventually discharge elsewhere, perhaps to a nearby stream. If the stream is normally gaining, pumping can locally reverse gradients, causing it to become losing. Stream water can then enter the well by induced infiltration.

Most of this report invokes a two–dimensional conceptualization of aquifer flow, induced infiltration, and capture zones. Flow to a well is intrinsically areal in nature because the flow approaches the well bore radially. Areal, or vertically integrated, models assume that the flow is essentially horizontal and that hydraulic equipotentials are essentially vertical. This conceptualization is commonly employed in hydrology, and is the origin of such concepts as transmissivity and aquifer storativity, and of many models including the Theis drawdown equation. Using this essentially horizontal flow conceptualization, the issue of induced infiltration is introduced for fully penetrating streams and wells. Several different aquifer geometries are examined, and induced infiltration is calculated as a function of well location and pumping rate, aquifer size and geometry, and the various sources of recharge. We extend these results to look at spatial capture zones, with special emphasis on the influence of the source of aquifer recharge, the effects of large stream gradients, variable aquifer thickness, and spatially variable properties. The effects of parameter uncertainty on capture zones is then discussed, and the concept of fuzzy capture zones is introduced. Finally, three–dimensional groundwater flow systems and capture zones are introduced, which examine the effects of partially penetrating streams and wells on capture zones.

The models addressed several questions. Below are the questions and a summary of our findings. More detailed summaries and conclusions are provided at the end of each section. Explanations for the findings can be found there and in the text.

- Under what conditions does induced infiltration take place?
- What are the contributions of the stream and other sources to the well? How much water is drawn from each source?

  The propensity for and rate of induced infiltration increases as well pumping rates go up, the well is located closer to the stream, well penetration decreases, stream penetration increases, ambient flow decreases, the number of alternative sources of water decreases, the aquifer pinches out nearby, aquifer conductivity increases near the streambed, aquifer conductivity perpendicular to the stream is greater than conductivity parallel to the stream, or multiple wells interfere with each other. Induced infiltration from one stream decreases if there is another stream nearby. Induced infiltration is not as strongly influenced by the nature of the recharge (lateral inflow versus local vertical recharge) as by the amount, by the presence of a moving water table so long as the requirements for the Dupuit assumption are met, or by the angle of ambient flow as much as the magnitude.

- What are the capture zones and related travel times? Where is the water coming from and how long does it take to reach the well?

  There are two types of capture zones defined in our studies. Ultimate capture zones define that portion of an aquifer that will eventually contribute water to a well, whereas time-dependent capture zones define that portion of the aquifer that will contribute water within a prescribed time. Capture zone shape and size is strongly influenced by the recharge source. Strong local recharge leads to larger capture zones, and 'cusping' of the capture zone along groundwater divides and barrier boundaries. Strong lateral inflows lead to capture zones that orient in the direction from which the flow comes. Boundaries have a significant effect on capture zones; barriers lead to wider capture zones, while other nearby streams lead to smaller capture zones. When there is a strong gradient parallel to the stream, capture zones become non−symmetric. Small levels of hydraulic conductivity or transmissivity heterogeneity or anisotropy can have a significant impact on the capture zone. Capture zones for multiple wells merge as the wells become closer or their pumping rate increases. Time-dependent capture zones are much more sensitive to certain parameters than are ultimate capture zones. Such parameters include porosity, aquifer thickness, the accuracy of the Dupuit approximation, and well penetration. Capture zones are very sensitive to three-dimensional flow issues such as stream and well penetration. Partially penetrating streams allow the capture zone to move below the stream to intercept ambient aquifer flow from the opposite bank of the stream, even though there is no induced infiltration from the stream. It is not always reasonable to define a two−dimensional capture zone model that is equivalent to a three−dimensional capture zone situation.

- How do the answers to these questions depend on the assumed stream−aquifer conceptual model and related parameters? For example, what are the effects of well location and pumping rate, aquifer properties, hydrodynamic dispersion or macrodispersion, time varying pumping rate, parameter uncertainty, etc?

  Parameter uncertainty leads to fuzzy capture zones. For example, ultimate capture zones are defined in terms of probability levels of capture. Thus there is a certain probability that a particle released at a certain location will eventually reach the pumping well. For time-dependent capture zones, this becomes the probability that the particle will reach the well within a prescribed time. This concept was illustrated for a well in an infinite flow field with uncertain pumping rate and uncertain ambient flow rate and direction. The resulting capture zone probability contour lines closed upgradient of the well, indicating that there is an upgradient limit to the reliable prediction of the capture zone. The contour lines sometimes extended downstream of the mean stagnation point, indicating that the down−gradient mean estimate of the capture zone is not conservative. Hydrodynamic dispersion and macrodispersion are another source of uncertainty. Dispersion allows particles to cross streamlines. Thus a particle originating outside of the capture zone has a random chance of wandering into the capture zone. In this case two interpretations apply, the one above and another: the probabilities also represent the proportion

of a chronic (continuing) contamination source at a certain location that enters a continuously pumping well. Two different modeling techniques were used to illustrate these concepts for the well in an infinite flow field.

The models' primary purpose is to provide engineers, scientists, and other water resources professionals with a better understanding of the mechanics of stream–aquifer interaction and related capture zones, when well-water quality is of concern. The models' secondary purpose is assist the preliminary screening of policy decisions, or for a 'first cut' evaluation of site-specific design or operation decisions. It may also be tempting to use them in the liability assessment for past contamination activities, but that is not the intent since the models are generic and somewhat idealized. Finally,the models can also be used for numerical model validation, as in EPA (1990). Although the principle application of these models is to well–head protection, they can also be employed in a variety of other roles as outlined in the first section, including aquifer remediation.

REFERENCES

Aziz, K. and A. Settari, 1979, Petroleum Reservoir Simulation, Elsevier, New York.

Bair, E.S., A.E. Springer and G.S. Roadcap, 1991, Delineation of Traveltime-Related Capture Areas of Wells Using Analytic Flow Models and Particle Tracking Analysis, Ground Water, 29(3), 387–397.

Bear, J., 1979, Groundwater Hydraulics, McGraw–Hill, New York.

Bear, J. and M. Jacobs, 1965, On the Movement of Water Bodies Injected into Aquifers, J. of Hydrol., 3: 37–57.

Benjamin, Jack R., and C. Allin Cornell, 1970, Probability, Statistics and Decision for Civil Engineers, McGraw–Hill, New York.

Boas, Mary L., 1983, Mathematical Methods in the Physical Sciences, John Wiley & Sons, New York.

Boulton, N.S., 1942, The Steady Flow of Groundwater to a Pumped Well in the Vicinity of a River, Philosophical Magazine, 7(33), 34–50.

Carter, L.L. and E.D. Cashwell, 1975, Particle–Transport Simulation withthe Monte Carlo Method, Technical Information Center, Energy Research and Development Administration.

Chow, J. and J.L. Wilson, 1988, Induced Infiltration from a Partially Penetrating Stream in an Aquifer with Ambient Flow, presented at the Spring Mtg., Amer. Geophy. Union, Baltimore.

DaCosta, J.A. and R.R. Bennett, 1960, The Pattern of Flow in the Vicinity of a Recharging and Discharging Pair of Wells in an Aquifer Having a Real Parallel Flow, Proceedings IUGG General Assembly of Helsinki, Intl. Assoc. Sci. Hydrology, Publ. No. 52, 524–536.

Edelman, J.H., 1972, Groundwater Hydraulics of Extensive Aquifers, Bulletin 13, Inter. Inst. for Land Reclamation and Improvement, Wageninjen, the Netherlands.

Dettinger, M. and J.L.Wilson, 1981, First Order Analysis of Uncertainty in Numerical Models of Groundwater Flow, Water Resources Research, 17(1), 149–161.

Environmental Protection Agency, 1987, Guidelines for the Delineation of Wellhead Protection Areas, Rpt. EPA 440/6–87–010, Office of Ground–water Protection, Washington, D.C.

Environmental Protection Agency, 1990, WHPA, An Integrated Semi–Analytical Model for the Delineation of Wellhead Protection Areas, Office of Ground–Water Protection, Washington, D.C.

Farmer, C.L., 1987, Moving Point Techniques, in Advances in Transport Phenomena in Porous Media, Bear, J. and M.Y. Corapcioglu (Eds.), NATO ASI Series #128, Nijhoff, Boston.

Ferris, J.G., D.B. Knowles, R.H. Brown, and R.W. Stallman, 1962, Theory of Aquifer Tests, Water Supply Paper 1536–E, U.S. Geological Survey.

Glover, R.E. and G.G. Balmer, 1954, River Depletion Resulting from Pumping a Well Near a River, Trans. Amer. Geophys. Union, 35(3), 468–470.

Goode, D., 1987, Velocity Interpolation Schemes for Average Transport in Heterogeneous Aquifers, presented at Fall Mtg., Amer. Geophy. Union, San Francisco.

Gradshteyn, I.S. and I.M. Ryshik, 1980, Table of Integrals, Series, and Products, Academic Press, Inc., New York.

Haitjema, Henk M., 1987, Comparing a Three–Dimensional and a Dupuit–Forchheimer Solution for a Circular Recharge Area in a Confined Aquifer, J. Hydrol., 91: 83–101.

Hantush, M.S., 1959, Analysis of Data From Pumping Wells Near a River, Jour. Geophys. Res., 64(11), 1921–1932.

Hantush, M.S., 1965, Wells Near Streams With Semipervious Beds, Jour. Geophys. Res., 70(12), 2829–2838.

Jacob, C.E., 1950, Flow of Groundwater, Chap. 5 of Engineering Hydraulics, John Wiley & Sons, New York.

Javendel, I., C. Doughty and C–F Tsang, 1984, Groundwater Transport, Water Res. Mono. Series 10, Amer. Geophy. Union, Washington, DC.

Javendel, I. and C–F Tsang, 1984, Capture–Zone Type Curves: A Tool for Aquifer Cleanup, Ground Water, 24(5), 616–625.

Kazman, R.B., 1946, Notes on Determining the Effective Distance to a Line of Recharge, Trans. Amer. Geophys. Union, 27(6), 854–859.

Kazman, R.B., 1948, Induced Infiltration of River Water of Wells, Trans. Amer. Geophys. Union, 29(1), 85–92.

Keeley, J.F. and C–F. Tsang, 1983, Velocity Plots and Capture Zones of Pumping Centers for Ground–Water Investigations, in Proceedings of the Third National Symposium on Aquifer Restoration and Ground–Water Monitoring, Natl. Water Well Assoc.

Larson, S.P., C.B. Andrews, M.D. Howland, and D.T. Feinstein, 1987, Three–dimensional Modeling Analysis of Groundwater Pumping Schemes for Containment of Shallow Groundwater Contamination, in Solving Ground–Water Problems with Models, NWWA.

Lee, K., 1986, Pollution Capture Zones for Pumping Wells In Aquifers with Ambient Flow, M.S. Thesis, Hydrology Program, New Mexico Institute of Mining and Technology, Socorro, New Mexico.

Lee, K. and J.L. Wilson, 1986, Pollution Capture Zones for Pumping Wells in Aquifers with Ambient Flow, presented at Fall Mtg., Amer. Geophy. Union, San Francisco.

Leppert, S.C., 1990, Capture Zones in Transient Flow Fields: Simulations and Analysis, M.S. Independent Study, available as Open File Report 90–7, Hydrology Program, New Mexico Institute of Mining and Technology, Socorro, New Mexico.

Linderfelt, W.R., S.C. Leppert and J.L. Wilson, 1989, Capture Zones for Wellhead Protection: Effect of Time Dependent Pumping, Saturated Thickness , and Uncertain Parameters, , presented at Fall Mtg., Amer. Geophy. Union, San Francisco.

Milne–Thomson, L.M., 1949, Theoretical Hydrodynamics, 2nd ed., St. Martin's, New York.

Milne–Thomson, L.M., 1968, Theoretical Hydrodynamics, 5th ed., MacMillian, New York.

McCormick, S., 1987, Multigrid Methods, 3, Frontiers Series, SIAM, Philadelphia.

Morrisey, D.J., 1987, Estimation of the Recharge Area Contributing to a Pumped Well in a Glacial Drift River Valley Aquifer, USGS Open File Rpt. 86–543.

Muskat, M., 1937, The Flow of Homogeneous Fluids Through Porous Media, McGraw–Hill Book Co., New York.

Newsom, J.M. and J.L. Wilson, 1988a, The Effect of Ambient Flow Direction on Pumping Near a Stream, presented at Spring Mtg., Amer. Geophys. Union, Baltimore.

Newsom, J.M. and J.L. Wilson, 1988b, Flow of Groundwater to a Well Near a Stream: Effect of Ambient Groundwater Flow Direction, Ground Water, 26(6), 703–711.

Pollock, D.W., 1988, Semi–Analytical Computation of Path Lines for Finite–Difference Models, Ground Water, 26(6), 743–750.

Rorabaugh, M.I., 1956, Groundwater in Northeastern Louisville, Kentucky with Reference to Induced Infiltration, Water Supply Paper 1360–B, U.S. Geological Survey.

Russel, T.F. and M.F. Wheeler, 1983, Finite Element and Finite Difference Methods for Continuous Flows in Porous Media, Chapter 2 of The Mathematics of Reservoir Simulation, 1, Frontier Series, SIAM, Philadelphia.

Schafer–Perini, A., 1990, Numerical Study of the Influence of Permeability Heterogeneity in Non–Uniform Steady–State Flow Systems, Ph.D. Thesis, New Mexico Institute of Mining and Technology, Socorro, New Mexico.

Schafer–Perini, A., M. Perini and J.L. Wilson, 1991a, Efficient and Accurate Front Tracking for Two–Dimensional Groundwater Flow Models, in press, Water Resour. Res..

Schafer–Perini, A. and J.L. Wilson, 1991b, Efficient and Accurate Front Tracking for Three–Dimensional Groundwater Flow Models, submitted, Water Resour. Res..

Schafer–Perini, A. and J.L. Wilson, 1991c, Three-Dimensional Stochastic Flow and Displacement in a Five–Spot Pattern, SPE paper 21243, Proceedings 11th SPE Sym. of Reservoir Simulation, Soc. of Petro. Engr., Anaheim, Calif.

Shafer, J.M., 1987a, Reverse Pathline Calculation of Time Related Capture Zones in Non–Uniform Flow, Ground Water, 25(3), 283–289.

Shafer, J.M., 1987b, GWPATH: Interactive Ground–Water Flow Path Analysis, Bulletin 69, Illinois Department of Energy and Natural Resources.

Sudicky, E.A., 1989, The Laplace Transform Galerkin Techinique: A Time–Continuous Finite Element Theory and Application to Mass Transport in Groundwater, in Contaminant Transport in Groundwater, Kobus and Kinzelbach (eds), Balkema, Rotterdam.

Theis, C.V., 1941, The Effect of a Well on the Flow of a Nearby Stream, Trans. Amer. Geophys. Union, 734–738

Walton, W.C., 1970, Groundwater Resource Evaluation, McGraw–Hill NewYork.

Wilson, J.L., 1981, Analytical Methods in Groundwater Hydrology, in Groundwater Hydrology, Boston Society of Civil Engineers, GeoTechnical Lecture Series, Boston.

Wilson, J .L., 1986, Induced Infiltration in Aquifers with Ambient Flow, presented at Fall Mtg., Amer. Geophy. Union, San Francisco.

Wilson, J.L. and W.L. Linderfelt, 1989, The Influence of Streams, Barriers, Groundwater Divides, and other Hydrogeologic Features on Well Capture Zones, 28th Intl. Geological Congress, Symposium on Wellhead Protection, Washington, D.C.

Zheng, C., 1988, New Solution and Model for Evaluation of Groundwater Pollution Control, Ph.D. Thesis, University of Wisconsin, Madison, Wisconsin.

APPENDIX A

WATER RESOURCES RESEARCH, VOL. 27, NO. 7, PAGES 1471–1485, JULY 1991

Efficient and Accurate Front Tracking for Two-Dimensional Groundwater Flow Models

ANNETTE L. SCHAFER-PERINI AND JOHN L. WILSON

Department of Geoscience, New Mexico Institute of Mining and Technology, Socorro

Four new algorithms are presented to cost-effectively delineate displacement fronts and capture zones via particle tracking in complex flow fields. These algorithms include methods of (1) defining path lines using "mixed distance and time particle tracking"; (2) computing displacement fronts and capture zones using "dynamic particle allocation front tracking," allowing insertion/deletion of particles to optimize front definition; (3) obtaining accurate breakthrough curves by using simultaneous "mass redistribution," reallocating particle mass among particles defining the displacement front; and (4) determining production well breakthrough curves using "optimized sorting algorithms" when backward tracking to map capture zones. Examples are shown for capture zones and aquifer remediation applications. Comparisons are made to conventional algorithms. Results show that the number of particles required to define displacement fronts and breakthrough curve is a function of time, position, and flow field complexity. Dynamic front tracking results in significant savings of storage and computational expense, even for relatively simple velocity fields. A corresponding increase in the accuracy of breakthrough curves is obtained.

INTRODUCTION

Particle and front tracking techniques are a popular approach to modeling groundwater pollutant transport and aquifer remediation. This popularity has grown as these techniques are used to help delineate wellhead protection areas as defined by capture zones [e.g., *Shafer*, 1987; *Newsom and Wilson*, 1988]. For example, an "ultimate capture zone" is the region of the aquifer from which a pumping well ultimately draws its fluid. Only part of this fluid enters the well within a fixed time, defining a "time-dependent capture zone" that can be used to designate a protected area around the well. Although we focus on capture zones in our examples and explanations, the techniques we describe are also appropriate for pollutant transport prediction and aquifer remediation design [e.g., *Bear*, 1979, sections 7–10; *Bear and Jacobs*, 1965; *Nelson*, 1979; *Javendal and Tsang*, 1984; *Javendal et al.*, 1984; *Wilson et al.*, 1986; *Wilson*, 1984].

Using particles to track a pollutant displacement front or capture zone neglects the effects of small-scale local dispersion. This approximation is often adequate when tracking fronts through flow fields containing dominant sources (injection wells) and sinks (production wells), or physically heterogeneous aquifer properties. The neglected local dispersion accounts for processes occurring at a smaller scale (for example, lower level heterogeneity, mechanical dispersion, and molecular diffusion). Assuming that sources, sinks, and heterogeneity in aquifer properties are sufficiently characterized, the front tracking approach is valid. This is not always an appropriate assumption, in which case an advection dispersion model should be used.

Analytic solutions for the ultimate capture zone can be obtained for simple steady state systems by determining the dividing path line as defined by the stream function [e.g., *Newsom and Wilson*, 1988]. All fluid inside the dividing streamline eventually flows into the well, and outside it flows elsewhere. To obtain the time-dependent capture zone, we must determine the travel time moving outward from the well by integrating backward in time along each of the path lines terminating at the well [e.g., *Lee and Wilson*, 1987; *Shafer*, 1987]. This is often difficult to do analytically, and we employ numerical integration via particle tracking instead. Numerical delineation of the path lines naturally lends itself to defining time-dependent displacement fronts and capture zones in steady flow fields and to defining displacement fronts in transient flow fields.

Particle tracking can be used for path line generation in both steady and transient flows, regardless of the heterogeneity, and with any distribution of sources and sinks. Particles are placed in the system at initial vector positions, $\mathbf{x}_0$, at an initial time t_0. The position of the particles at any later time, t, is computed by solving the system of equations defined by the seepage velocity $\mathbf{v}_s = \mathbf{v}/\phi = d\mathbf{x}/dt$, where ϕ is the effective porosity and $\mathbf{v}$ is Darcy velocity. For example, the time-dependent capture zone can be obtained by starting several particles around a fluid sink, such as a pumping well, moving the particles backward in time, and connecting the particle positions at any given time with line segments (transients require special handling when backward tracking). Displacement fronts, or the position of fluid moving outward from an injection well or other source, can be obtained in a similar manner by moving the particles forward in time. Thus the capture zones and displacement fronts for a multiple well aquifer pump and treat system can be obtained. In addition to knowing the spatial location of the displacement front it is often desired to determine the arrival time distribution of the injected fluid at a pumping well. Such breakthrough curves (BTCs) can be computed at the same time as capture zones or displacement fronts.

As the complexity of the velocity field increases, numerical delineation of the path lines, fronts, capture zones, and breakthrough curves becomes more difficult. Historically, the velocity equations have been solved using a first-order Euler method with very small time steps [e.g., *Bear*, 1979; *Nelson*, 1979; *Javendal et al.*, 1984] or fourth-order Runge-Kutta methods [e.g., *Shafer*, 1987]. In a complex velocity

Paper number 91WR00720.
0043/1397/91/91WR-00720$05.00

field these methods can lead to either prohibitively expensive solutions, or excessive error. In a divergent velocity field, as in the case of flow diverging from an injection well, the number of particles needed to adequately resolve both the front and breakthrough curves increases with time. Uniform initial particle spacing in convergent and divergent flow fields also results in very irregular particle spacing at large times, with a resulting loss of resolution.

This paper presents a method for dynamic particle allocation front tracking that allows an optimal number of particles to be assigned for both front delineation and breakthrough curve computation. Spacing between particles on the front is bounded above and below and can be adjusted according to the particular application. As particles are allocated or removed in order to preserve correct and accurate BTCs, particle mass is adjusted via a mass redistribution algorithm. These front tracking rules can be easily implemented for transient flows and for velocity fields obtained from either analytic solutions or numerical discretizations (finite difference, finite element) of the flow field. The rules are illustrated for steady flow fields using a new and efficient mixed method for the exact path line integration of the velocity field consistent with a five-point finite difference solution of the steady state continuity equation.

PATH LINE GENERATION

During steady flow path lines concide with streamlines. They define the path along which a particle of fluid will travel toward a final destination. In simple steady state homogeneous systems the path lines can be solved for directly [e.g., *Bear*, 1979; *Newsom and Wilson*, 1988] by simply computing the stream function. As the flow domain becomes more complex, or the flow unsteady, the path lines are determined numerically. Numerical computation of path lines consists of two main steps. The first step is the determination of the velocity components at the current particle position. The velocity is a vector quantity relating an incremental distance along each coordinate direction to an incremental distance in time. Step two consists of moving the particle. Knowing the velocity and current particle location, the next position is determined by solving the velocity equations along the appropriate path line.

Path line generation is accurate when the exact velocity is known. Velocities can be obtained analytically for relatively complex steady state problems by considering the head distribution and applying the vector form of Darcy's law. If the flow domain becomes too complex for analytic evaluation of the velocities, they can be determined numerically. For the five-point finite difference discretization of the two-dimensional, steady state mass balance equation velocities can be determined exactly. Following our development of these velocity equations, we present a convenient method of computing path lines using analytic or numerical velocities.

Numerical Velocity Computation

The quantity of most importance in the prediction of fluid displacement is the velocity. Arbitrarily obtaining the velocity field without consideration of the head formulation will generally result in mass balance errors leading to inconsistent velocity interpolation functions. A consistent interpolator will preserve mass locally within a grid cell while providing a continuous field across the cell. This section will review an exact method of determining the interblock velocity interpolator derived from a consistent velocity and head relationship defined on a block-centered finite difference grid. Because the mathematical details of obtaining consistent velocity and head have been reviewed in the context of finite differences and mixed finite elements by *Shubin and Bell* [1984], *Russel and Wheeler* [1983], and *Farmer* [1987], only the most general results will be given here.

A bilinear velocity interpolator is consistent with a five-point finite discretization of the two-dimensional steady state groundwater flow equations. This result can be obtained by assuming that the normal components of the Darcy velocity, $v_x(i \pm 1/2, j)$ and $v_y(i, j \pm 1/2)$, are constant along their respective grid block cell faces. Integration of the normal components over all faces results in an expression of mass balance in a steady state system. The following is an expression of mass balance defined on a variable size nonstaggered block-centered finite difference grid:

$$[v_x\Delta y](i + 1/2, j) - [v_x\Delta y](i - 1/2, j) + [v_y\Delta x](i, j + 1/2) - [v_y\Delta x](i, j - 1/2) = \frac{Q(i, j)}{B} \quad (1)$$

where Δx and Δy, are the i, jth block width and length respectively, B is the aquifer thickness, and $Q(i, j)$ is the net flux out of the i, jth grid block. Applying Darcy's law across the grid block face, the velocity in the normal direction can be related to the head and hydraulic conductivities of any two adjacent cells.

$$v_x(i + 1/2, j) = -2K(i + 1/2, j)\frac{h(i + 1, j) - h(i, j)}{\Delta x(i, j) + \Delta x(i + 1, j)} \quad (2)$$

In the above expression for the x direction velocity, $K(i+1/2, j)$ is the harmonic average of the hydraulic conductivity between the (i, j) and $(i + 1, j)$ cells. The choice of using a harmonic average is not arbitrary but is necessary for consistency with the discretized form of the equation governing the flow and giving rise to the head solution h. The equivalent y direction velocity is given by

$$v_y(i, j + 1/2,) = -2K(i, j + 1/2)\frac{h(i, j + 1) - h(i, j)}{\Delta y(i, j) + \Delta y(i, j + 1)} \quad (3)$$

After applying appropriate boundary conditions and substituting (2) and (3) into (1) the resulting system of linear equations is solved for the head using any of the methods available as outlined by *Golub and Van Loan* [1983]. Consistent edge of block x and y direction velocities are obtained by back substitution of the heads into (2) and (3), respectively.

Path line generation algorithms require the velocity within each grid cell. Given the edge of block velocities, the velocity within a cell is computed at any point using interpolation. The interpolation used between velocities at the cell edges to obtain inner cell values must be consistent with the zero divergence condition of (1). A bilinear interpolator

is both continuous across the cell and solenoidal, leading to an expression of the x and y direction velocities within any cell of the form:

$$v_x = a + b(x - x_0); \qquad v_y = c + d(y - y_0) \tag{4}$$

where the constants a, b, c, and d are determined from the edge of block velocities and grid block dimensions. For example, the slope, b, of the linear interpolator in the x direction is computed using

$$b = \frac{v_x(i + 1/2, j) - v_x(i - 1/2, j)}{\Delta x(i, j)} \tag{5}$$

with the intercept given by

$$a = v_x(i - 1/2, j) \tag{6}$$

In (4) it is assumed that the x coordinate has its origin at the leftmost side of the first grid cell and that x_0 is the coordinate of the leftmost face of the current grid cell. $x_0 = x(i, j) - \Delta x(i, j)/2$. The expression for the slope and intercept for the y direction velocity can be obtained by analogy from (5) and (6). Local coordinates within a given cell are used instead of global coordinates, simplifying the expression. In subsequent expressions the distance into the cell relative to the left face, $x - x_0$, will be replaced by a local coordinate, x. In the literature a variety of interpolators for five-point finite differences are employed (note, for example, the incorrect interpolator by *Konikow and Bredehoft* [1978]). *Pollock* [1988] suggests three. The choice is not arbitrary. Only one preserves mass and is correct, the bilinear interpolator of (4).

Solving for the Path Lines

Given consistent interpolation functions for the numerical velocities, or continuous analytic velocities, a path line is computed uniquely. The path line is obtained by expressing the velocities as the time derivatives of distance and solving the resulting differential equations simultaneously. In the following derivation, taken from *Schafer-Perini et al.* [1988], it will be assumed that a velocity field obtained from the analytic solution has been discretized in a manner consistent with Figure 1. If the discretization interval is small enough, approximation of an analytically continuous velocity by piecewise bilinear functions should be adequate.

Assuming constant porosity ϕ within a grid block, the piecewise linear velocity interpolation functions given by (4) are used to express the Darcy velocity as time derivatives of fluid displacement:

$$v_x = a + bx = \phi \frac{dx}{dt}; \qquad v_y = c + dy = \phi \frac{dy}{dt} \tag{7}$$

The functions given by (7) are analytically integrable, allowing the relationship of travel distance with time to be determined [see *Pollock*, 1988]. Conceptually, this is very simple. In practice, care must be taken to make sure the form of the velocity interpolator is known; it can be of the form $v_x = a + bx$ or of the form $v = a$, where the slope is zero [*Schafer-Perini et al.*, 1988]. For the first form, $v_x = a + bx$, (7) can be integrated to yield an expression relating the log of the position to the time

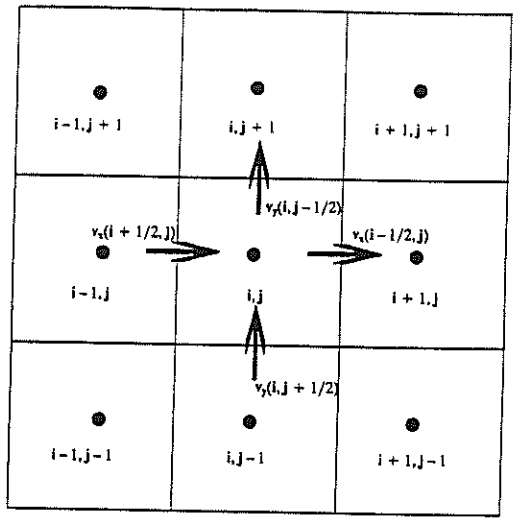

Fig. 1. Schematic of the edge of cell velocities for a five-point block centered grid..

$$\Delta t = \frac{\phi}{b} \ln\left(\frac{a + bx}{a + bx_1}\right) \tag{8a}$$

for each of the component directions, where x_1 is the initial position of the particle within a cell and Δt is the time required to move from x_1 to x. In the second case a zero slope component results in a linear relationship:

$$\Delta t = (\phi/a)(x - x_1) \tag{8b}$$

These equations can also be expressed in terms of the "initial" particle velocity, v_{x1}, or the particle velocity evaluated at location x_1:

$$\Delta t = \frac{\phi}{b} \ln\left(\frac{a + bx}{v_{x1}}\right) \tag{9a}$$

$$\Delta t = \phi[(x - x_1)/v_{x1}] \tag{9b}$$

It should be noted that (8) and (9) are only appropriate for a nonzero initial velocity. Similar forms for the y coordinate direction velocity are obtained with the same nonzero initial constraint.

$$\Delta t = \frac{\phi}{d} \ln\left(\frac{c + dy}{c + dy_1}\right) \tag{10}$$

$$\Delta t = (\phi/c)(y - y_1) \tag{11}$$

At this point, either an elapsed time Δt can be assigned, allowing evaluation of new particle x and y positions, or a distance along one of the coordinate directions is used to determine the elapsed travel time and remaining coordinate. Both of these options will be discussed below in the context of path line generation within a grid cell, and we will introduce a new mixed method that combines some of the best features of each.

Moving by time increment. When an elapsed time Δt is used to evaluate the new local coordinate position (x, y), (8) or (9) and the equivalent expressions for the y direction velocity given by (10) or (11) are used to solve directly for the new vector position x and y. We present only the most

general form of the position vector given by (8a) and (10) for the examples here and below. Solving for x and y yields

$$x = \{[(a + bx_t) \exp(b\Delta t/\phi)] - a\}/b \quad (12)$$

$$y = \{[(c + dy_t) \exp(d\Delta t/\phi)] - c\}/d \quad (13)$$

If the particle crosses the block boundary, the current or local set of interpolation constants a, b, c, and d are no longer valid. Thus the major disadvantage of moving the particle by a fixed time is the inability to guarantee that the particle stays within the current grid block. An iterative procedure may be used to determine the exact time and location that the particle crossed the boundary, but this becomes computationally prohibitive. The iterative procedure would attempt to locate the exit position of a particle at a cell face such that the time necessary for the particle to move there from the initial position in both coordinate directions was the same, thus defining the exact path line. Despite this difficulty there are two major advantages to using a fixed time for advancing particles. The first advantage is gained by realizing that, given a fixed time, the computed x and y positions guarantee that the particle is on the correct path line as long as it remains within the grid block. Secondly, in reference to the ultimate goal the algorithm lends itself to determining the position of all of the particles at a fixed time interval, naturally defining the front position.

Moving by distance increment. An alternative to moving the particles by a time increment is moving them a given x or y distance. The distance moved along any coordinate direction is not arbitrary but must satisfy the requirement that the particle not change path lines. One possible approach is to assume that the initial particle position is known, preferably on the edge of a grid block, and move the particle to the exit cell face. The exit location is uniquely determined from the initial location by first equating the expressions for travel time in the x and y directions given in (8a) and (10) resulting in one equation with two unknowns. This equation can be solved for x assuming y is known or for y given x. The exit location is determined by evaluating the combined expression at each of the cell side lengths. For example, evaluate the expression for y using the cell width Δx and determine if the y value computed lies within the extent of the cell in that direction. This requires at most three function evaluations, although there are several combinations of x and y interpolation functions that are possible. A variation of this algorithm is given in some detail by *Pollock* [1988].

Mixed distance and time method. The compromise proposed in this paper, when implemented in the context of front tracking, is a combination of the two methods. Particles are advected from cell side to cell side, computing the elapsed time from the initial condition. When the elapsed time exceeds the time at which the front is desired, the particle position within the cell corresponding to the desired time is computed. The major advantage of a combined approach is reduced computational time over a strict time stepping advection, while allowing determination of position at a fixed time.

Other methods. The intracell analytic solution of the discrete velocity equations (7) that we employ is somewhat difficult to implement, mainly due to the different forms possible for the interpolation function. Yet it accurately defines path lines through the discretized system. A more straightforward approach to defining path lines solves the system of velocity equations numerically using a first-order or Eulerian approach. We have found that an Eulerian solution for problems of moderate complexity is inadequate for a computationally reasonable time discretization, as illustrated later. There are other numerical alternatives available for solving the system of velocity equations within the necessary accuracy constraints. One such alternative is a Runge-Kutta-Fehlberg [e.g., *Burden et al.*, 1981] solution for systems of ordinary differential equations. This method offers many advantages when tracking particles in three dimensions, among which is the simplicity of the basic algorithm, and the accuracy of solution achieved with minimal computational and coding overhead.

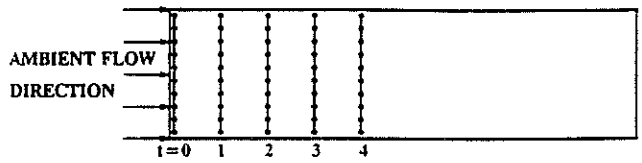

Fig. 2. Particles advected in a uniform ambient flow field, defining a uniform front with ten particles [$N(T) = 10$]. The fronts are depicted at five uniformly spaced time intervals.

FRONT TRACKING

Particle tracking has been used to account for the advective component of transport and to delineate stream function boundaries (for example, ultimate capture zones). Often, the path lines are of less interest than the travel time necessary to reach a certain location. This is especially true when predicting pollutant transport or when delineating time-dependent capture zones of a well. For simple boundary conditions in homogeneous systems the velocity field can be determined analytically, although the position of a pollutant front or time-dependent capture zone may be much more difficult to obtain. In heterogeneous or transient systems, velocities, fronts, and capture zones must be determined numerically.

Conventional Front Tracking

Front tracking is extremely simple in principle. Generally, particles are tracked through a flow field by computing the tangential component of velocity at the particle's current location and moving all of the particles forward a finite time step or alternatively by moving the particles along the path lines using the algorithms presented above. To actually define the front, adjacent particles are connected either with straight-line segments or curve fitted using splines. Generally, straight lines are used because of their inherent simplicity and to avoid the computational burden of computing splines. This concept is illustrated in Figure 2 for particles being advected in a uniform ambient flow field moving from the left to the right. The figure shows ten ($N(t) = 10$) particles moving with the advective component of velocity in a uniform flow field. Fronts are plotted by simply connecting the particles at various times with straight lines. The initial front position and the position of the front at four later times are shown. Particles are shown as black dots, and the front is defined by connecting them with straight lines. A more

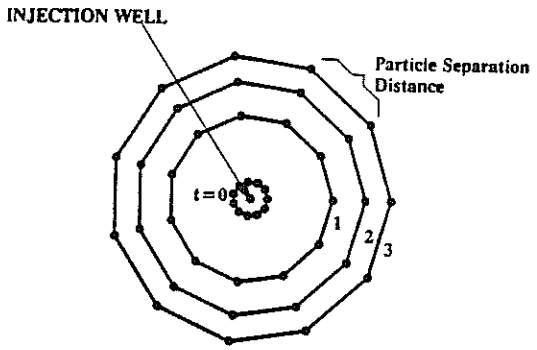

Fig. 3. Particles advected outward from a point source, defining a circular front, $N(t) = 11$.

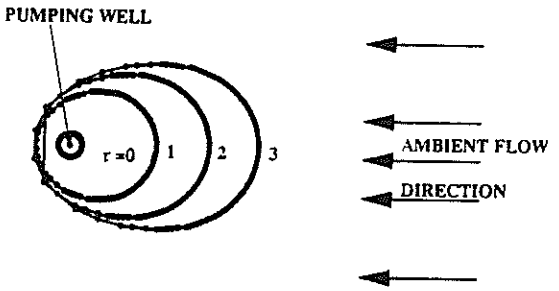

Fig. 5. Capture zone for a pumping well with an ambient flux from the right, $N(\tau) = 99$.

interesting example of particles being advected from a point source illustrates some of the problems that can occur in converging and diverging flow fields. The displacement fronts for an injection well in a large circular system are shown in Figure 3, where particles were being advected outward from a point source. Eleven particles were initially placed on a circle of radius $\gamma = 1.5$ m. The domain length was 51 m on a side, with a uniform grid block spacing, $\Delta x = \Delta y = 1$ m and thickness B of 1 m. The injection well continuously supplies fluid at rate $Q = 1/2\pi$ m^3/day in the center of the domain. The analytical radial velocity was computed exactly at grid cell sides and was bilinearly interpolated within the grid. In both of these cases, particles were initially placed into the flow field with uniform spacing between them. The particle movement shown in Figure 3 is at the end of three uniformly spaced time steps and includes the initial position. Note in Figure 2 that the distance between the particles remains constant, whereas in Figure 3 the particle separation distance has increased as the flow diverges from the well. In Figure 3 the analytic solution of the front represents a circle centered about the origin. In the numerical approximation the circular shape is lost as time progresses. The loss of circular shape is primarily due to an inadequate number of particles defining the front, leading to poor front resolution. As the flow field becomes more complex, say as with the addition of ambient flow which induces stagnation points, accurately defining the front becomes more difficult.

Figure 4 shows the time-dependent capture zones for a pumping well in an ambient flow field with a uniform flux source from the right. The capture zone is defined by tracking 11 particles backward with time, using an analytical velocity field interpolated onto a five-point grid. As particles move away from the well, the nonuniform velocity distribution forces them to separate. Particles near the downstream end (left) of the pumping well move primarily in a direction normal to the ambient flow, tending to separate. Particles near the upstream end of the front have a larger velocity component parallel to the flow field and tend to remain closer together. Capture zone fronts are shown for three dimensionless times, $\tau = t/(\phi\omega)$, where $\omega = Q/2\pi Bq_0$ with Q representing the pumping rate, q_0 the ambient Darcy velocity, B the aquifer thickness, and ϕ the effective porosity. The velocity was interpolated from a 51 × 51 grid with a dimensionless grid block size of $\Delta\xi = \Delta\eta = 0.2$ with $\Delta\xi = \Delta x/\omega$ and $\Delta\eta = \Delta y/\omega$. The particles were initially placed on a circle of dimensionless radius, $\gamma/\omega = 0.3$. Front definition can be maintained by initially allocating more particles. Figure 5 is an illustration of the same physical problem using 9 times as many particles. Even here, the ability to adequately define the front decreases at large times. As time increases, particles originating downstream of the well move outward. Connecting those particles with straight-line segments results in a capture zone that does not properly encompass the sink. This problem is typically minimized for this simple problem by placing the downstream particles on the stagnation point streamline. For more complex flow fields there may be many such streamlines and finding them requires special effort and excessive CPU time. On the upstream side of the ambient flow field the particles also spread although not nearly as rapidly. Apparently, allocating more initial particles does not offer a satisfactory solution to this problem. It leads to a final particle density that is greatest where it is least needed and unreasonably increases the computational and computer storage cost. One possible solution is to initially allocate the particles using uneven spacing, placing particles where they will eventually be needed as the front spreads. This approach requires that the necessary spacing be determined a priori. A better alternative is to allocate the particles dynamically when and where they are needed.

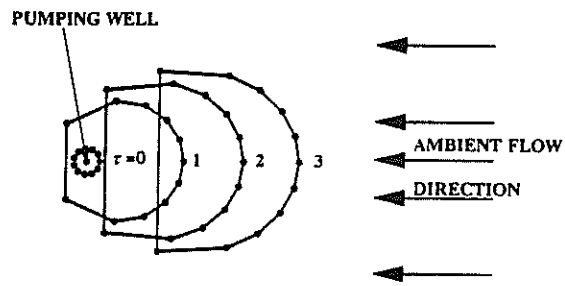

Fig. 4. Capture zone for a pumping well with an ambient flux from the right, $N(\tau) = 11$.

Dynamic Particle Allocation Front Tracking

The basic idea of dynamic front tracking is to add or allocate a particle to the system as the separation distance exceeds an allowable maximum or as the curvature at the front dictates. Because the criteria for allocation are arbitrary and somewhat problem dependent, only the criteria based upon separation distance are presented here. The magnitude of the vector separation distance between any

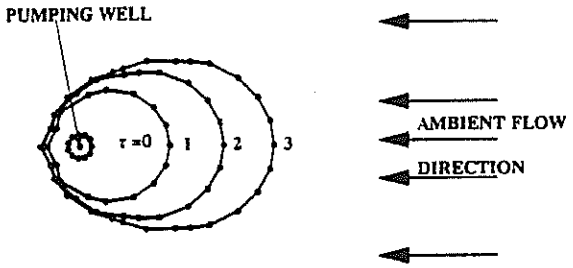

Fig. 6. Effect of dynamically allocating particles. Capture zone for a well with ambient flow from the right with an increasing number, $N(\tau)$, of particles: $N(0) = 11$, $N(1) = 16$, $N(2) = 22$, $N(3) = 28$. The time step was $\Delta\tau = 0.25$ and the infilling criteria was $r_{max}/\omega = 0.4$, with infilling after exceeding the maximum separation distance.

two particles having location (x_k, y_k) and (x_l, y_l) is determined from

$$r = \sqrt{(x_k - x_l)^2 + (y_k - y_l)^2} \tag{14}$$

Particles are added to the system if the computed separation distance r exceeds the maximum allowable distance r_{max}. Allocation of a new particle necessitates computing appropriate coordinates at which to insert it. We have found that simple linear interpolation is adequate as long as the separation distance relative to the curvature at the front is small. This insertion position can be determined from

$$x_p = (x_k + x_l)/2; \qquad y_p = (y_k + y_l)/2 \tag{15}$$

where the additional particle p is being placed between particles numbered k and l. The maximum separation distance used is arbitrary and should be chosen to minimize the error at the front. As the curvature expected at the front increases, the tolerance on the separation distance and the time elapsed between allocating more particles should be reduced, as explained below. The total time between initial particle allocation and that at which the front position is desired is broken into smaller time intervals or "time steps." Using the mixed time and space path line generation algorithm explained above, particles are advected through these smaller time steps. At the end of each time step the interparticle distance is computed, and particles are allocated. Particles can be introduced either at the end of the time step at which the separation distance is exceeded or preferably at the beginning of the time step, when the separation distance is adequate. Since there are no guarantees that the separation distances in the newly infilled portions of the front meet the separation distance criterion, multiple sweeps along the new portions of the front are necessary.

The results of inserting particles when the separation distance of is exceeded is illustrated in Figure 6, for the flow parameters used in Figure 4. In Figure 6, each of the time increments between the fronts plotted has been subdivided into four equal time intervals, $\Delta\tau = 1/4$. At the end of each of these discrete steps, particles have been added along the front where the dimensionless separation distance ($r_{max}/\omega = 0.4$) was exceeded. There is a notable improvement over Figure 4. The straight lines in the front curvature near the downstream side of the well are due to (1) linearly interpolating the new particle's position after the separation distance is exceeded; and (2) starting with only 11 particles,

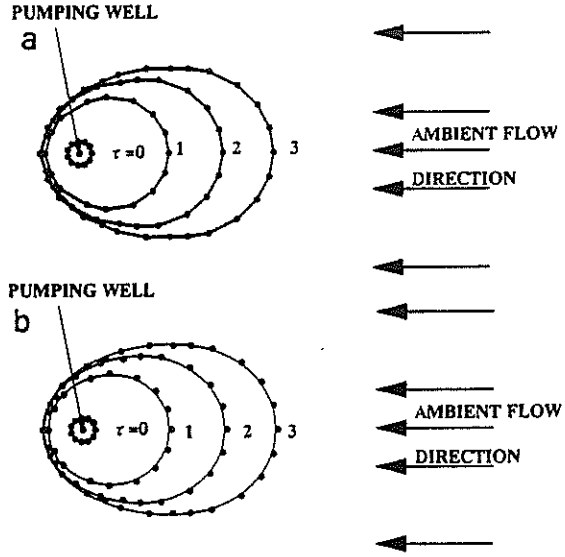

Fig. 7. Effect of dynamically allocating particles. Capture zone for a well with ambient flow from the right with an increasing number, $N(\tau)$, of particles: $N(0) = 11$, $N(1) = 16$, $N(2) = 22$, $N(3) = 26$. (*a*) Infilling prior to exceeding the maximum separation distance. (*b*) Comparison of the analytically computed capture zones (lines) to the numerical solution obtained by dynamic allocation of particles (dots) prior to exceeding the maximum separation distance. The time step was $\Delta\tau = 0.25$ and the infilling criteria was $r_{max}/\omega = 0.4$.

which appears to be inadequate for a time step of $\Delta\tau = 1/4$. This effect will decrease as $\Delta\tau$ decreases (for example, $\Delta\tau = 1/16$), as r_{max} decreases, or as the number of initially allocated particles increases. Adding particles at the beginning of the time step during which the separation distance is exceeded is illustrated in Figure 7*a*, again for the case shown in Figure 4. After allocation the particles are moved forward one time step to the current time. On the downstream side the error due to linearly interpolating the new particle position is less than that shown in Figure 6. The length of the arc being approximated by a straight line is smaller in the case where particles are allocated prior to exceeding the maximum separation distance, resulting in less error. Also note that for the same maximum separation distance, fewer particles are needed in Figure 7 than were used in Figure 6.

The analytical solution [*Bear*, 1979] for the capture zones at dimensionless times consistent with our numerical solutions have been drawn as solid lines in Figure 7*b*. Superposed on the analytic solution are the numerically computed particle positions shown in Figure 7*a*. It can be noted that the particle positions shown are consistently ahead of the analytic solution, although not at a uniform distance from it. This is a reflection of not adjusting the dimensionless times used to obtain the analytic solution to account for the initial finite release radius of the particles used in the numerical solution. The difference is small in this example, primarily because the initial release radius is small. There will be increased error as the release radius increases. It should be noted that the travel time required for each of the initial particles to reach the release radius from the well is easily acounted for using local radial flow. A higher-order correction that accounts for the local nonradial flow because of heterogeneities, boundary conditions, etc., can also be employed.

TABLE 1. Comparison of Particles Required Using Conventional Initial Uniform Spacing and Dynamic Particle Allocation for the Example Shown in Figure 7*a* Using a Maximum Dimensionless Separation Distance of $(r_{max}/\omega) = 0.4$ With an Infilling Interval of $\Delta\tau = 1/4$

Time τ	Number of Particles N_c	Number of Particles N_d
0	11	11
1	29	16
2	86	22
3	298	26
4	532	32

N_c: number of particles using initial uniform spacing. N_d: number of particles using dynamic particle allocation.

How many initially uniformly spaced particles does a conventional method require in order to preserve the same maximum particle separation distance as does dynamic tracking? Consider the same capture zone problem with a dimensionless maximum separation distance of $r_{max}/\omega = 0.4$. The results given in Table 1 show that for this simple test problem conventional methods require an order of magnitude more particles. As time increases the difference becomes even more dramatic. We have found for other more complex flow fields a several order of magnitude difference. The required storage for the dynamic particle allocation routine is $2N_d$, as compared to N_c for conventional routines. A corresponding savings in computational effort can be inferred.

Implementation of Dynamic Tracking

The dynamic particle allocation front tracking scheme is independent of the method used to derive the velocity field and fundamentally independent of the path line generation algorithm as long as the path lines are accurate. The particle allocation portion of the scheme is primarily an issue of managing one or more lists of information about the particles. In particular, the scheme must give each particle an index and maintain a list of the particles current and last location. Preserving a record of the last location permits the front to be tracked with greater fidelity, as we just demonstrated in Figure 7*b*. In *Knuth*'s [1973*a*] notation our list of particles and their locations is a singly linked linear list. Each particle has to know only one of it's two neighbors in order to construct the entire list and its relationships. Lets start at some particle which we label as particle number 1 and then move "clockwise" along the front, as seen from the point of view of an observer above and ahead of the front. We only need to know the location of the next or second particle to draw the front between them. Now located on the second particle we find its "next" neighbor, the third particle along the front, and so on until all particles are connected and the front is drawn. Particle 1 points at, or is linked to particle 2, which is linked to particle 3, etc. This linkage between particles is in one direction, in this example, the "clockwise" direction. This trivial concept is complicated in dynamic particle allocation by the insertion of new particles along the front where and when they are needed. From a programming point of view these insertions can be anywhere in the list, including between the last and first particles, if they are located next to each other along a continuously

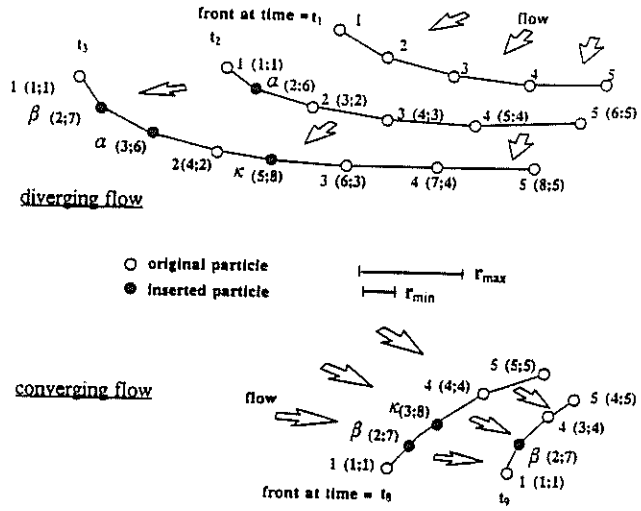

Fig. 8. Particle allocation during (top) diverging and (bottom) converging flow. Each particle is denoted by its illustrative number (1, α, β, 2, etc.) and two indices: a sequential allocation index (s) and a linked allocation index (l). These indices are contained in the parenthesis located adjacent to each particle: for example, $p(s, l)$. Thus $\kappa(5, 8)$ at t_3 indicates that inserted particle κ has sequential index 5 and linked index 8 at that time.

connected front (see, for example, Figure 7). Insertion requires that our index system adjusts to the presence of each new particle and link it with appropriate neighboring particles. If we go back to our simple example and insert a new particle, the old particle to the counterclockwise side must know that it has a new next neighbor, while our new particle must also know that its next neighbor is the old particle to the clockwise side. This issue is illustrated in the upper right-hand side of Figure 8. The front at time t_1 is constructed from five particles. It moves in a diverging flow field to the position shown at time $t_2 = t_1 + \Delta t$. During this movement, particles 1 and 2 have separated beyond the maximum distance r_{max}. A new particle, lets call it particle α, has been inserted between particles 1 and 2 at time t_1 and advected to the front at time t_2. After another Δt advection the front moves to the position marked t_3. During this additional movement the new particle, labeled α, has separated too far from particle 1. So too have particles 2 and 3. Additional new particles are inserted in each of these gaps: particle β is inserted in the first gap, while particle κ is inserted in the second one. Each is inserted back at time t_2 and advected forward to the time t_3. Managing this list of particles would be confusing if we used a mixture of numerals for original particles and letters for new ones. Instead, we use numerals for both and simply evolve the index system and list as new particles are allocated.

We have implemented two techniques for handling the dynamic lists. The first and simplest we refer to as "li bumping," and is a common technique in Fortran programming. This is the most general example of what *Knuth* [1973*a*, section 2.2.2] refers to as "sequential allocation." Whenever a new particle needs to be inserted between, say the mth and m + first particles, the list indices for all m + 1 and greater particles are increased by one. That is, their indices are "bumped" by one, as is the total number of particles, N. We avoid one of the major problems of list keeping by restricting N to be no greater than some pre-

scribed N_{max}, the maximum list dimension. Should $N = N_{max}$ we simply note in the program output that there is or can be an overflow and that the front resolution is less than desired. In the illustration shown in the upper portion of Figure 8 the sequentially allocated index for each particle at each time is given as the first number in the adjacent parenthesis. It is obvious that with this method of allocation, the particle indices simply increase by one as we move particle by particle along the front. Thus at time t_3, new particles α, β, and κ have indices 3, 2, and 5 because they are the third, second, and fifth particles along the front at this time step.

The second technique we refer to as "linked lists" and is much more flexible. *Knuth* [1973*a*, section 2.2.3] refers to it as "single connected linked allocation." It is commonly employed in the C programming language, but we implemented it in Fortran. Recall that to construct the entire front we need to have each particle linked (point) to only one of its neighbors. In our example this was the next neighbor in the progression along the front. In the linked list approach we keep track of each particle's index, location, and also its link pointing to the index of the next particle along the front. This adds one additional piece of information to monitor for each particle. We also need to keep a list of free particles that have not yet been assigned. *Knuth* [1973*a*] refers to this as the "list of available space." The total dimensionality of active particles N plus free particles M must be no greater than N_{max} and can be stored in a single integer array. If more particles are needed, we have overflow messages and the front will not be properly resolved. It is easiest to see how linked lists work by looking at an example. At time t_1 in Figure 8, particle 1 points to, or is linked to, particle 2 which is linked to particle 3 and so on. We can represent this in short hand as $1 \rightarrow 2, 2 \rightarrow 3, 3 \rightarrow 4, 4 \rightarrow 5, 5 \rightarrow$ first free index $= 6$. The list of free particles is $6 \rightarrow 7, 7 \rightarrow 8, 8 \rightarrow 9, \cdots, N_{max-1} \rightarrow N_{max}$. At time t_2 we have inserted particle α which is indexed with the first available number from the list of free particles. This is the number 6. Then particle 1 points to particle 6, which in turn points to particle 2, with the rest of the list unchanged. In short hand the linked list is $1 \rightarrow 6$, $2 \rightarrow 3, 3 \rightarrow 4, 4 \rightarrow 5, 5 \rightarrow$ first free index $= 7$, and $6 \rightarrow 2$. The list of free particles is now $7 \rightarrow 8, 8 \rightarrow 9, \cdots, N_{max-1} \rightarrow N_{max}$. The linked allocation index for each particle and time in the figure is shown by the second number in the parenthesis. At time t_3 when two more particles, β and κ are added, the linked list becomes $1 \rightarrow 7, 2 \rightarrow 8, 3 \rightarrow 4, 4 \rightarrow 5$, $5 \rightarrow$ first free index $= 9, 6 \rightarrow 2, 7 \rightarrow 6$, and $8 \rightarrow 3$. The two new indices have been taken off of the next available free values, leaving the free list as $9 \rightarrow 10, 10 \rightarrow 11, \cdots, N_{max-1} \rightarrow N_{max}$. The linked list requires slightly more storage for the links, but is inherent flexibility and much lower computational cost give it significant advantages over the sequential list approach. There are even special sorting routines for linked lists that make looking up a particular data entry extremely fast [*Knuth*, 1973*a*, *b*].

With either sequential or linked allocation, particles can also be removed as easily as they are added. Thus in a converging flow field as the particles get closer together and as we need fewer particles to resolve the front, any unnecessary particles are placed back into the list of free particles. For example, removal of particles occurs near production wells for forward tracking and near injection wells when backward tracking capture zones. Note that since particles accelerate near these features we may also be adding particles along the front at the same time as particles are being removed. A particle is removed when the separation distance between it and a neighbor is less than some prescribed minimum distance r_{min}. Particle removal requires much less CPU time with the linked list approach because of its inherent flexibility, although it requires the use of a pointer into the list of free particles. Removed particles are simply returned to the list of free particles, adjusting the list of free particles to include the removed element.

The sequential allocation of particles involves the repeated updating of the active particle list each time a new particle is inserted. This could require as few as 1 or as many as N^2 array operations, depending on the relative positions of the new particles in the sequential list. In contrast, the infilling of new particles in a linked list approach requires simply switching the particle linkage, involving on the order of N_{new} array operations. However, the linked list approach demands the allocation of additional storage space. In most applications the savings in computer time attained using the linked list approach far offsets the small additional storage cost. In addition, both methods of allocation (given the same method of infilling) result in the same end product. Therefore there are no error reducing advantages between them. The approximation error induced by linear interpolation of the new particle positions along the front is an adjustable quantity. Error is proportional to the infilling time step and the maximum allowed separation distance. We use a spatially uniform but temporally variable infilling interval Δt to contribute to a cost-effective algorithm. The maximum distance moved by any particle along the front provides a basis for estimating the next time step. The maximum distance moved r_a is compared to a standard r_b, and a new time step is constructed from a simple ratio:

$$\Delta t_{new} = \Delta t(r_b/r_a) \tag{16}$$

Evolving time steps in this way greatly enhances the run time performance of the algorithm. In the case of flow diverging from an injection well or when defining the capture zone of a pumping well it is important that the initial value of the time step be conservative. It should be chosen based upon an estimate of the maximum velocity in the vicinity of the particle release location. We note that this update in time step is not illustrated in the examples shown here to facilitate direct comparisons of the dynamic tracking algorithms.

BREAKTHROUGH CURVES

In addition to knowing the spatial location of the displacement front it is often desired to determine the breakthrough curve associated with the movement. The breakthrough curve is an expression of the temporal accumulation of mass or volume at a particular location. For example, a two-well recirculation pump and treat system involves fluid being injected at one well and extracted at another [e.g., *Wilson*, 1984]. As the injected fluid moves through the system, the position of the front defines the spatial location behind which injected fluid exists at any given time. As the front reaches the producing well, injected fluid is removed from the system. The cumulative volumetric arrival of the front at the production well is a function of time, giving rise to a volumetric breakthrough curve. This interpretation is valid for perfect advective displacement and assumes displace-

ment without local dispersion, retardation, or capillary forces. In order to define the breakthrough curve numerically a volume or mass must be assigned to each particle along the front. If a dynamically allocated front tracking algorithm is used, it is possible to also dynamically adjust the mass between the newly inserted particles. Below we outline some of the issues that arise when initially allocating mass to particles and present a method for adjusting the mass at the front for use with the dynamic front tracking method.

Breakthrough curves (BTCs) can represent the volumetric fraction of native and injected fluids being produced at a given location or the temporal distribution of solute mass arriving at a production well or another exit point from the domain. The volume fraction represents that portion of the fluid volumetric flow rate (for example, stream tube) associated with the particle. The mass fraction represents the portion of the total injected mass of a dissolved species associated with the particle. Numerical computation of BTCs involves a four step procedure: (1) assign a fraction of the source volume, or mass, to each particle for each particle source location: (2) move the particle from the initial location to its final destination: (3) sort by time and accumulate the arrived volume fractions or mass at the extraction location, for each one of the particle source locations individually, and sum the results to yield the total BTC for that sink location; and (4) sort by time and accumulate the arrived volume fractions or mass from the source location and sum the result to yield the total injection or source history curve. Step 3 allows the breakthrough curve for the destination location to be computed by particle source, which represents the mass contribution from each potential source. Step 4 allows the total breakthrough curve at the source location (well) to be determined. Below we discuss the initial assignment of volume or mass fraction to particles originating at a point source or sink of fluid (step 1 above). Assignment of particle mass for distributed sources follows this procedure but becomes more problem dependent and is not discussed explicitly in this paper. We also discuss how step 2 can be done in conjunction only with path line generation or with front tracking, too. Finally, we describe the simple sorting algorithm that accumulates volume fractions/mass at exit locations while delineating the contribution of each source. These can be added together to yield injection history curves (IHCs), representing the history of where and when the injection fluids leave the system. BTCs and IHCs are computed at the same time as the path lines and/or fronts are being generated, and are subject to the same resolution issues associated with front tracking. The algorithm can be used with either backward front tracking of capture zones or forward tracking of injection fronts.

Assigning Initial Mass or Volume Fraction

The water mass balance expressed by (1) can be generalized to any coordinate system by realizing it is an expression of the divergence theorem in Cartesian coordinates. The net flux Q, out of control volume Ω, is equal to the surface integral around η of the normal component of velocity, where volume Ω is bounded by the curve η. Mathematically, we have

$$B\int_{\eta} \mathbf{n}\cdot\mathbf{v}\, d\eta = B\iint_{\Omega} \nabla\cdot\mathbf{v}\, d\Omega = Q \qquad (17)$$

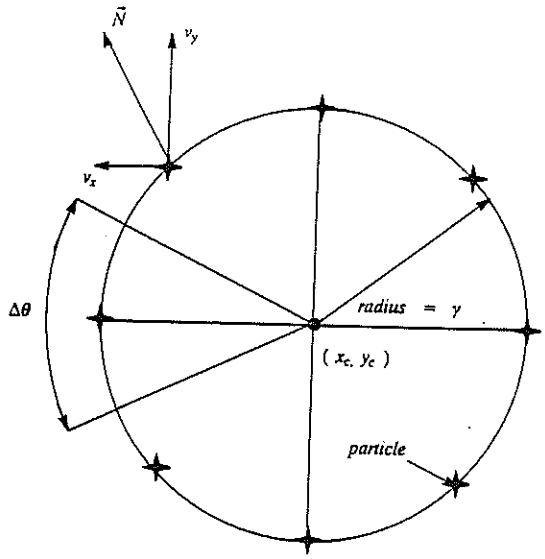

Fig. 9. Schematic of the circular control volume for determining volume fraction.

where $\mathbf{n}$ is the unit outward normal vector. Equation (1) is an approximation of (17) evaluated on a vertically integrated square control volume consisting of the grid cell (i, j). A square grid cell has normal velocity components, $\mathbf{n}\cdot\mathbf{v}$, equal to the edge of the block velocities $-v_x(i - 1/2, j)$, $v_x(i + 1/2, j)$, $-v_y(i, j - 1/2)$, and $v_y(i, j + 1/2)$, and the surface integral is approximated by assuming the normal velocity component is constant over each cell face. Under this assumption the double integral is replaced by a sum over all cell faces of the outward normal flux, which is equal to the velocity times the area perpendicular to flow. The relationship expressed in (17) is valid for any control volume. A circular control volume is appropriate for particles released at a well in a two-dimensional grid system, as illustrated in Figure 9. Volume is initially allocated to the particles by considering a pattern of release defined by a circle with radius γ centered at global coordinates (x_c, y_c). The continuity equation defined for this circular pattern of release is used to allocate volume fraction or mass to each particle. Components of the unit outward normal vector to a circle centered at (x_c, y_c) through location θ are given by $n_x = \cos(\theta)$ and $n_y = \sin(\theta)$, where θ is measured counterclockwise from the positive x axis. Within this circular control volume, assuming a constant aquifer thickness B, the divergence theorem becomes

$$\iint_{\eta} \mathbf{n}\cdot\mathbf{v}\, d\eta = B\int_{\theta=0}^{\theta=2\pi} \mathbf{n}\cdot\mathbf{v}\gamma\, d\theta = Q \qquad (18)$$

where the surface element is $B\gamma\, d\theta$, for a cylinder of uniform height B, and radius γ. The incremental rate of volume, Q, passing through any surface element bounded by $\Delta\theta = \theta_2 - \theta_2$ is

$$Q_\theta = B\int_{\theta_1}^{\theta_2} \mathbf{n}\cdot\mathbf{v}\gamma\, d\theta \qquad (19)$$

and can be approximated by

$$Q_\theta \approx B\gamma(\theta_2 - \theta_1)\mathbf{n}\cdot\mathbf{v} = B\gamma\Delta\theta\mathbf{n}\cdot\mathbf{v}$$

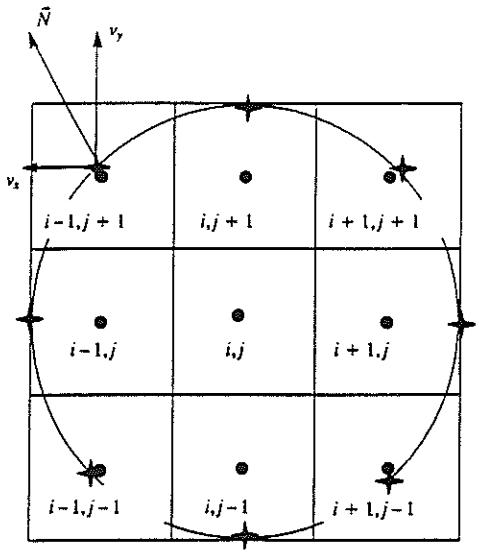

Fig. 10. Schematic of the circular control volume superposed on the five-point finite difference grid.

where v is taken at $(\theta_1 + \theta_2)/2$. A natural discretization of the circle into N equal sized surface elements, $b\gamma\Delta\theta$, is obtained by allocating N equally spaced particles along a radius γ at angles $\theta = (m - 1/2)\Delta\theta$, where $\Delta\theta = 2\pi/N$, and $m = 1, 2, \cdots, N$. Discretized in this fashion (17) is approximated by

$$Q \approx \sum_{m=1}^{N} Q_\theta(m) = \sum_{m=1}^{N} B\gamma\Delta\theta \mathbf{n}(m) \cdot \mathbf{v}(m) \qquad (20)$$

where the velocity $\mathbf{v}(m)$ and unit outward normal vector $\mathbf{n}(m)$ are evaluated at the angle $\theta(m) = (m - 1/2)\Delta\theta$, which is at the midpoint of the mth surface element. A normalization of (19) is possible by dividing through by the net flux rate Q out of the control volume. After normalization, each term in the sum represents the volume or mass fraction passing through the surface element centered between angles $\theta = (m, m - 1/2)\Delta\theta$. It is this volume or mass fraction that is assigned to the particles.

The numerical method of integration used above is the trapezoidal rule. Higher-order methods such as Simpson's rule or an adaptive quadrature could be easily applied to (17) but have not been found to be necessary. Exact integration of the outward normal component of velocity, given by a local analytic expression as a function of position, could also be used to obtain a solution to the integral in (18). Linear velocity interpolators computed using the five-point finite difference discretization also provide an analytically integrable function, although the discrete approximation given in (20) is adequate given a small enough discretization interval.

In Figure 10 we superposed the square grid shown in Figure 1 onto the circular control volume, such that the i, jth grid cell is completely contained within the circular control volume. Using the linear velocity interpolators corresponding to the grid block in which the mth particle is released yields the following expression for the associated incremental volume or mass fraction $f(m)$:

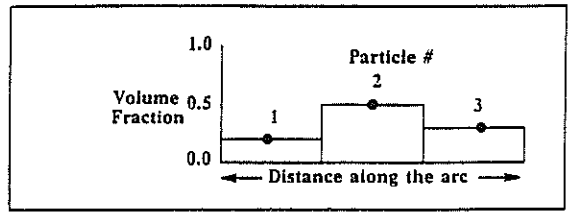

Fig. 11. Schematic of the initial volume fraction distribution between three particles.

$$f(m) = \frac{B\gamma\Delta\theta}{Q_{i,j}} [v_{xp} \cos(\theta) + v_{yp} \sin(\theta)] \qquad (21)$$

where the particle velocity components, v_{xp} and v_{yp}, have been interpolated onto the release position of the mth particle using (4). In purely radial flow the same volume or mass fraction is assigned to each particle. Most flows are not purely radial, except very near the well, because of the influence of boundary conditions, other wells, and heterogeneities. Because of this nonuniform velocity field more flow passes through some portions of the circle than others. Equation (21) allocates the initial particle volume or mass fraction f nonuniformly, weighting more those particles initially located along the major flow paths through the circle. More accurate breakthrough curves and fronts are obtained by initially allocating more particles, providing a better definition of flow conditions around the well.

Dynamic Mass Redistribution

The nonuniform or irregular velocity distributed around the particle also results in a separation of particles at the displacement front; the particles tend to group near the high-velocity and low-velocity areas, leaving the center region underpopulated. As particles are removed from the system at production wells, or other discharge locations this nonuniformity at the front is reflected in the poor resolution of the breakthrough curves. Dynamic front tracking eliminates this problem, but particle mass must be redistributed as new particles are inserted.

Equation (21) assumes that the volume or mass fraction associated with the mth particle is uniformly distributed along an arc of length $\gamma\Delta\theta$ with the particle located at the center of curvature or at radial and angular coordinates $[\gamma, (m - 1/2)\Delta\theta]$. This is illustrated in Figure 11 for three particles with an uneven volume or mass fraction distribution. As new particles are inserted between any two existing particles, only the mass between the adjacent particles should be redistributed and assigned to the new particle. For example, after new particle number 4 has been inserted between particles 1 and 2, redistribution of mass among the three particles is shown in Figure 12 for the linked allocation case. In order to reassign mass in this manner we must associate with each particle not one but two masses, one on its "clockwise" side and another on its "counterclockwise" side along the front. The initial mass assignments for each particle must be computed for each side of the particle using half of the arc length used previously. Then when a new particle is inserted, we simply remove half of the mass from the nearest sides of each adjacent particle, and assign these

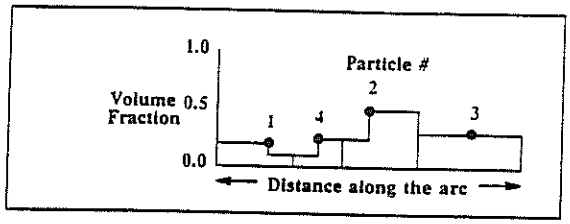

Fig. 12. Schematic of volume fraction distribution after allocating particle 4 between particles 1 and 2.

masses to the corresponding sides of the new particle. This is illustrated in Figure 12.

The mass redistribution technique requires that two values containing particle mass be stored for each particle. Implementation using the sequential allocation "bumping" algorithm for front tracking is simple and will not be outlined here. The "linked list" implementation is much less computationally expensive. In addition to the data structure used for front delineation which consisted of an array containing the particle location and an integer array pointing to the next particle in the position array, each particle must have two arrays containing the mass or volume fraction associated with each side of the particle. As a particle is inserted between any two adjacent particles, the volume fraction stored in the appropriate array locations is simply redistributed.

Test Case

Breakthrough curves computed using this redistribution technique in combination with "consistent" initial mass allocation produce accurate results. Inconsistent BTCs are obtained using an incorrect initial volume or mass fraction distribution, or when incorrectly distributing the mass. In a two-well system, consistency can be shown by comparing the two BTCs, one computed using forward tracking and the other using backward tracking. The following fronts and BTCs were computed for a quarter five-spot pattern consisting of one production and one injection well in a square domain bounded by no-flow barriers. The injection well is in the lower left corner of Figure 13, while the production well is in the upper right corner. The injection rate is equal to the pumping rate, $Q_i = Q_p = 16$ m^3/day. A 51 × 51 computational grid consisting of uniform grid blocks, $\Delta x = \Delta y = 8$ m, and uniform thickness, $B = 25$ m, was used. The heterogeneous hydraulic conductivity field used in this example was synthetically generated from a stochastically homogeneous process, with a unit variance and unit mean of the log of hydraulic conductivity, a Bessel covariance function, and a correlation parameter of 40 m. A fast Fourier transform method developed by *Gutjahr and Wilson* [1989] was used to generate the log conductivity field (field not shown here). In this example, 101 particles were initially introduced into the domain along the circumference of a quarter circle of radius 8 m located around both the injection and production wells. Figure 13 illustrates the capture zones and displacement fronts at three early times before breakthrough. The final number of particles for the capture zone shown in Figure 13*a* was 914. At the same elapsed time the final number of particles for the displacement front shown in Figure 13*b* was 815. A maximum separation distance equal to 1/2 of the grid block length was used for both forward and backward tracking.

Figure 14*a* presents forward and backward BTCs computed using dynamic front tracking with mass redistribution and initial particle volume fractions assigned using the method suggested above. Figure 14*b* contains similar BTCs computed using a uniform initial mass distribution and dynamic front tracking without mass redistribution. There are two breakthrough curves in each figure, one for forward tracking (injection) and one for backward tracking (production). The two curves should be identical in the absence of hysteretic and nonlinear effects. While the two curves in Figure 14*a* agree very well, the error shown in Figure 14*b* is excessive. Although the initial breakthrough time and ultimate recovery (90$^+$%) are insensitive to an inaccurate initial volume fraction, the intermediate values of the BTC will be in error.

Simultaneous Determination of Injection and Breakthrough Curves

In a multiple source/sink system the breakthrough history for each of the sources and sinks can be obtained by tracking the fronts either forward in time from the sources or by tracking fronts backward in time from the sinks. One does not have to do both. Here we will show that, as the capture zones and breakthrough curves for the sinks are being computed by backward tracking, the injection history curves

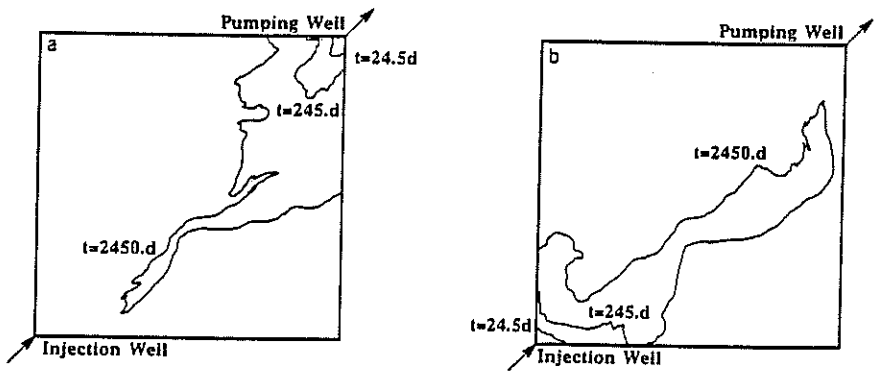

Fig. 13. A heterogeneous aquifer quarter five-spot pattern with (*a*) capture zones for the upper right-hand corner pumping well, and (*b*) displacement fronts for the injection well in lower left corner, each shown at three successive times.

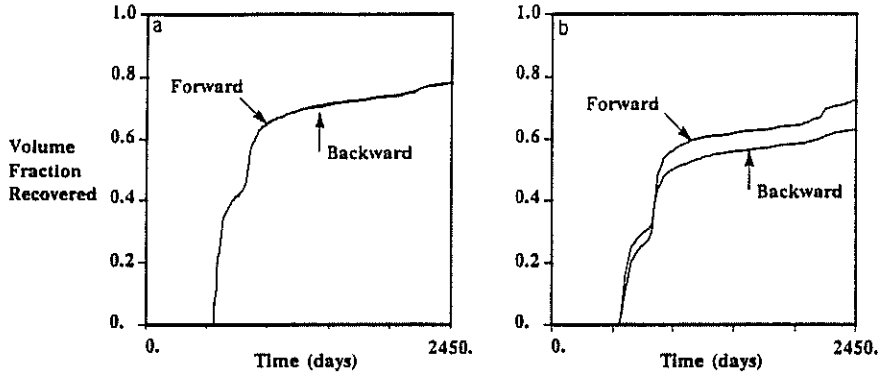

Fig. 14. Forward and backward breakthrough curves for pumping and injection wells in a heterogeneous five-spot pattern using (*a*) the initial volume fraction computed using (22) and mass redistribution as particles were added, and (*b*) assuming uniform initial mass allocation at both the injection and pumping wells, and no mass redistribution.

(IHCs) for the sources can be obtained by sorting the same files. The capture zone and breakthrough curve for a single sink, for example, a production well, are computed by assigning a volume fraction to particles originating at the sink and tracking them backward in time until they exit at source locations, for example, injection wells. If it is assumed that the displacement occurs without local dispersion, retardation, or capillary forces, the breakthrough curve for the sink is obtained by accumulating the particle volume fractions in time as particles are removed at the sources. In a multiple source/sink system, each of the particles placed around the same sink could exit the system at different sources. As the particles exit at individual sources, "source contribution data" for the sink are obtained. The source contribution data consist of marking the exit location, as well as the volumetric fraction and time when accumulating total BTCs. The source contribution data are summed by exit location to determine the contribution of each source to the total volumetric sink or production rate. If the accumulation is done as a function of time, the temporal contribution to the total breakthrough curve by each of the sources is obtained. After the capture zones, BTCs, and injection contribution data for all of the fluid sinks have been obtained, the total injection history curves (IHCs) can be computed. The IHC for a single source is obtained by accumulating the temporal distribution of particles arriving from all of the contributing sinks. Prior to accumulating the contribution from all sinks, each sink's source contribution data must be renormalized. The renormalization simply consists of multiplying each element of the source contribution data by the volumetric rate of the sink for which it was obtained and dividing by the volumetric rate of the exit location. Renormalization is necessary if the volumetric rates of the sources and sinks differ. After renormalization the source contribution data for all contributing sinks are lumped together to create the source or injection history data. The final IHCs are computed by simply sorting and accumulating the lumped injection history data by increasing time. Cocomputation of the injection and breakthrough curves can be done by using a quick sort algorithm [*Press et al.*, 1986], greatly reducing the computational burden of computing them individually.

This explanation has focused on backward tracking of the sinks. The same approach can use forward tracking from sources, and sorting will yield the BTCs from the IHCs. Both approaches provide equivalent breakthrough curves as long as numerical errors are minimized (see Figure 14). Note that the capture zones are delineated only when tracking backward and injection fronts only when tracking forward.

Breakthrough curves can be computed with very little additional effort over computing the front location. They are sensitive to the method of initial mass allocation and to errors introduced by incorrectly distributing the mass as more particles are added. Computing breakthrough curves in conjunction with a dynamic front tracking routine is very accurate and cost effective.

EXAMPLES

The dynamic front tracking algorithm coupled with the exact path line generation algorithm has been applied to a variety of groundwater flow problems. Figures 15 and 16 show the pumping well time-dependent capture zones and production history breakthrough curve for a two-well pump and treat system placed in a uniform ambient flow field. The dimensionless velocities are computed analytically on a 101×101 grid using dimensionless block sizes $\Delta\xi = \Delta x/\omega = \Delta\eta = \Delta y/\omega = 0.05$. Where the ω is defined in terms of the pumping rate Q_p. The aquifer has unit thickness, $B = 1$, and an injection to pumping rate ratio, $\beta = Q_i/Q_p = 0.8$. The wells were separated a dimensionless distance $D = 2.136$ and placed at an angle $\alpha = 20.556°$ from the ambient flow.

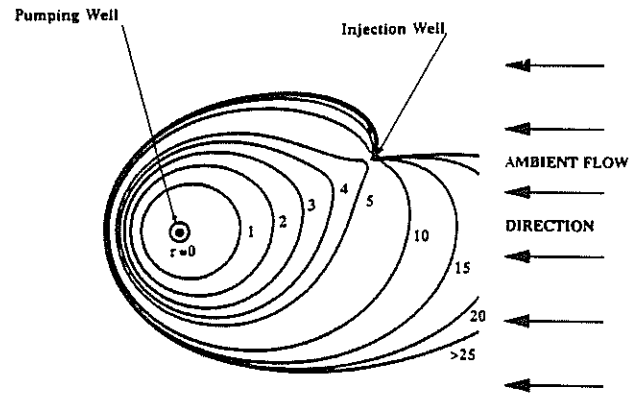

Fig. 15. Capture zones at dimensionless times for a two-well pump and treat system with an injection well and ambient flux from the right.

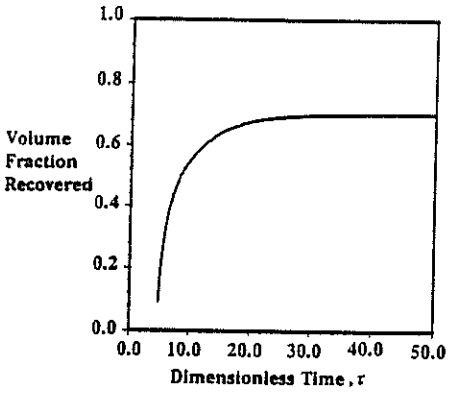

Fig. 16. Dimensionless cumulative volume fraction arriving at the pumping well from the injection well.

Note that D and α are defined as $D = [(\xi_P - \xi_I)^2 - (\eta_P - \eta_I)^2]^{1/2}$ and $\alpha = \tan^{-1}[(\eta_p - \eta_I)/(\xi_p - \xi_I)]$, respectively, in terms of the dimensionless locations of the pumping and injection wells (ξ_P, η_P) and (ξ_I, η_I). The capture zones for the pumping well are shown at 10 dimensionless times, $\tau = 4t/\phi\omega$, using an effective porosity $\phi = 1$. Adequate resolution of the capture zones is attained by initially allocating $N = 51$ particles at the injection well and bounding the particle separation distance above and below such that $(r_{min} = 0.025\omega \leq r \leq r_{max} = 0.0375\omega)$. The number of particles needed to maintain this separation distance range for each of the 10 fronts is shown in Table 2. The capture zones are computed by placing particles uniformly around the pumping well and tracking them backward in time. The breakthrough curve is normalized with respect to the pumping rate rather than to the injection rate. As particles are removed at the injection well, the volume fractions were accumulated as an increasing function of time. The breakthrough curve shows that only 71% of the pumped fluid originates from the injection well, although the injection rate is 80% of the pumping rate. The remaining 29% of the fluid pumped originates from the ambient flow, as indicated by the capture zones at $\tau > 25$. This last capture zone approximates the dividing path line and therefore the ultimate capture zone. The ultimate capture zone extends upstream, out of the domain in Figure 16. A reasonably stabilized production history curve is attained by dimensionless time $\tau = 20$.

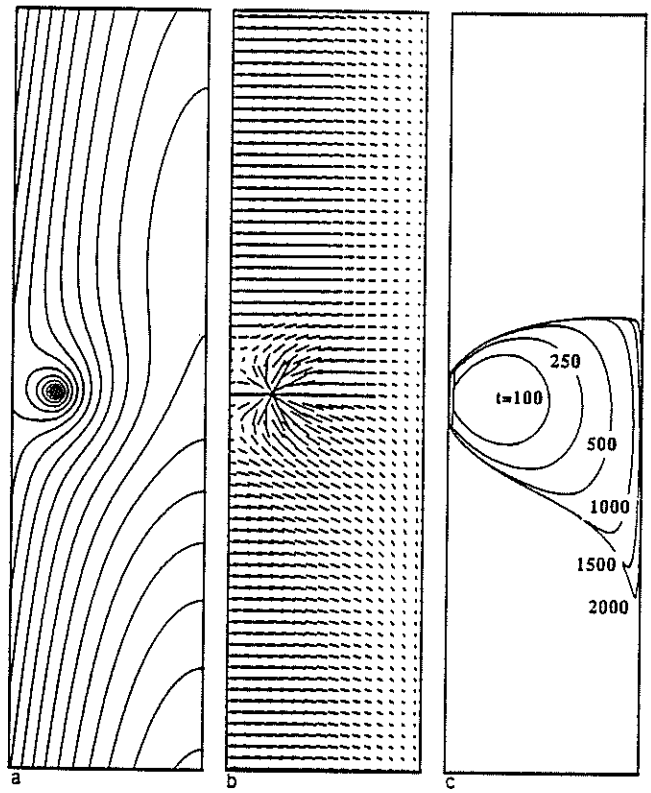

Fig. 17. (*a*) Head field, (*b*) velocity field, and (*c*) capture zones at various times for a pumping well with a sloping stream boundary, uniform recharge, and ambient flux from the bottom.

The head field, velocity field, and capture zone for a production well located near a fully penetrating stream are shown in Figure 17. The breakthrough curve for stream water arriving at the production well is shown in Figure 18. The left boundary is a sloping stream with gradient $dh/dy = -0.01$ m/m. The right side is a no flow boundary. At the bottom and top of the domain a uniform ambient flux was applied such that the flux rate is equal to the stream gradient, $q_y = -K\,\partial h/\partial y = -0.01$ m/day, with $K = 1$ m/day, and

TABLE 2. Number of Particles Active Using Dynamic Particle Allocation

τ	N
0	51
1	125
2	178
3	209
4	254
5	270
10	345
15	394
20	393
≥25	398

For the example shown in Figures 15–16 using a maximum dimensionless separation distance of $(r_{min} = 0.025\omega \leq r \leq r_{max} = 0.0375\omega)$ with an infilling interval of $\Delta\tau = 0.25$. The variable τ is dimensionless time; N is the number of particles using dynamic infilling.

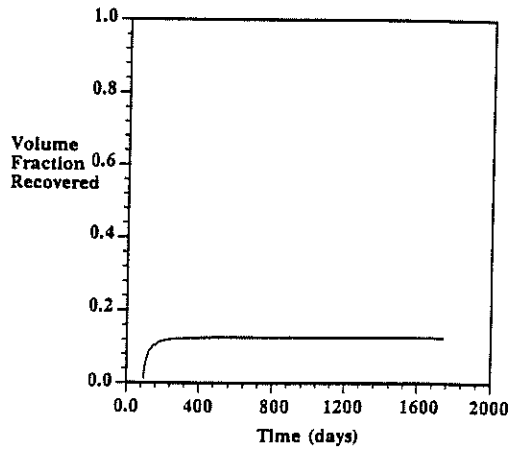

Fig. 18. Dimensionless cumulative volume fraction arriving at the pumping well from the stream.

TABLE 3. Number of Particles Active Using Dynamic Particle Allocation

t, day	N
100	136
250	201
500	262
1000	386
1500	520

For the example shown in Figures 17–18 using a maximum dimensionless separation distance of (r_{min} = 0.025 m $\leq r \leq r_{max}$ = 1.5 m) and an infilling interval of Δt = 10. The variable t is time; N is the number of particles using dynamic infilling.

B = 1 m. Within the domain a uniform recharge rate R = 0.002 m/day is applied. The domain width L = 50 m, and height H = 200 m is simulated using a 50 × 200 grid. A pumping well, Q_p = 5 m^3/day is placed at location x = 12, y = 100. The flow field is computed numerically using a five-point finite difference scheme solved by a preconditioned conjugate gradient algorithm. The head field is contoured using a uniform interval Δh = 0.25. Velocity magnitude and direction is indicated using straight-line segments; there are two stagnation points in the system. The ultimate capture zone is achieved by 2500 days, and a stabilized inflow from the stream is reached by 200 days, as indicated by the capture zones and breakthrough curve respectively. Capture zones are computed by initially allocating N = 51 particles, and bounding the dimensionless particle separation distance above and below such that (r_{min} = 0.025 m $\leq r \leq r_{max}$ = 1.5 m), using an infill time step Δt of 10 days. The number of particles needed to maintain this range of separation distances at the times of the 10 fronts is shown in Table 3. As the particles reach distributed exit locations, such as the stream boundary, it is necessary to disconnect the particle link list to avoid inappropriately infilling particles. This has not been done in this example, and the result is indicated by the portion of the ultimate capture zone that parallels the stream boundary just inside the left edge of Figure 17. An alternative to disconnecting the link list is to use a smaller time step Δt, forcing the particles to lie exactly on the stream edge. In any case the breakthrough curve is not affected.

SUMMARY AND CONCLUSIONS

A method for determining consistent velocity interpolators for a five point finite difference discretization of the steady state mass balance equation has been reviewed. The interpolating equations may also be used to approximate an exact velocity field. Using the velocity interpolators, particles can be advected through the system either by distance, by time, or by a "mixed distance and time method." Using the velocity interpolators, particle advection is independent of a time increment. The independence is made possible by the exact solution of the consistent velocity equations. Therefore the resulting pathlines are extremely accurate and easy to compute.

Using this path line generation algorithm, it is possible to delineate the temporal capture zones and displacement fronts for sources and sinks accurately and efficiently. The "dynamic particle allocation" front tracking algorithm provides a dynamic optimization of particle density along the front. Two implementation alternatives are outlined for use when either computation or storage requirements are important. The obvious advantages of dynamic particle allocation front tracking are shown by comparison to the total number of particles required using a conventional front tracking algorithm. Using dynamic particle allocation makes it possible to use several orders of magnitude fewer particles to maintain comparable front resolution. Computational and storage requirements are directly proportional to the number of particles used in defining the front. The dynamic front tracking procedures saves computer time and storage.

Breakthrough curves are also generated using particle tracking. It is important that consistent mass or volume fraction be assigned to each particle. A method of assigning initial volume fraction for each particle, by considering mass balance, is presented. Mass balance is shown for a two-well injection/production quarter five-spot system. Using incorrect initial volume fraction results in the same initial and final breakthrough times but produces incorrect intermediate curves, an important consideration for time-dependent wellhead concentrations. Using the basic volume fraction assignment equations, the method is also employed with the dynamic front tracking routine. As particles are dynamically allocated to the system as the front resolution requires, mass is redistributed among the particles. As with dynamic front tracking, "dynamic mass redistribution" results in better resolution of the breakthrough curves. The combined approach allows fronts and breakthrough curves to be computed simultaneously and efficiently.

Sorting breakthrough curve data by source as well as by destination allows computation of breakthrough curves and injection history curves simultaneously. In a multiple source/sink system it is possible to obtain an injection history curve as well as a production history curve, without tracking particles through the flow field twice. Traditionally, the injection history is obtained by tracking particles backward in time, and the production history is obtained by tracking particles forward in time, requiring considerable computational effort. In a conservative velocity field this is not necessary. However, if the particles are tracked both forward and backward in time, the sorting procedure supplies a means of checking mass balance in complex multiple-well systems. By actually tracking the particles forward and backward in time and compiling injection history curves from the production history data and vice versa it is possible to compare both sets of data. As with a two-well system, the injection history obtained by forward tracking should compare exactly to the injection history obtained by sorting the production history data.

Acknowledgments. The cooperation of A. Gutjahr and W. Soll with this work is gratefully acknowledged. This work was supported by the U.S. Department of Energy (contract DE-AC03-85BC-10850) and the U.S. Geological Survey (grant 14-08-0001-G-1632).

REFERENCES

Bear, J., *Hydraulics of Groundwater*, Mc-Graw-Hill, New York, 1979.

Bear, J., and M. Jacobs, On the movement of water bodies injected into aquifers, *J. Hydrol.*, *3*(1), 37–57, 1965.

Burden, R. L., J. D. Faires, and A. C. Reynolds, *Numerical Analysis*, 2nd ed., PWS, Boston, 1981.

Farmer, C. L., Moving point techniques, in *Advances in Transport*

Phenomena in Porous Media, *NATO ASI Ser.*, vol. 128, edited by J. Bear and M. Y. Corapcioglu, Nijhoff, Boston, Mass., 1987.

Golub, G. H., and C. F. Van Loan, *Matrix Computations*, The John Hopkins University Press, Baltimore, Md., 1983.

Gutjahr, A., and J. L. Wilson, Synthetic generation of random permeability fields for heterogeneous reservoir simulation, in *Tenth SPE Symposium on Reservoir Simulation, Proceedings*, p. 505, Society of Petroleum Engineers, 1989.

Javendal, I., and C.-F. Tsang, "Capture-zone type curves: A tool for aquifer cleanup, *Ground Water*, *24*(5), 616–625, 1984.

Javendal, I., C. Doughty, and C.-F. Tsang, *Ground Water Transport, Water Res. Monogr. Ser.*, vol. 10, AGU, Washington, D. C., 1984.

Knuth, D. E., *The Art of Computer Programming*, vol. 1, *Fundamental Algorithms*, 634 pp., Addison-Wesley, Reading, Mass., 1973*a*.

Knuth, D. E., *The Art of Computer Programming*, vol. 3, *Searching and Sorting*, 722 pp., Addison-Wesley, Reading, Mass., 1973*b*.

Konikow, L. F., and J. D. Bredehoft, *Computer Models of Two-Dimensional Solute Transport in Groundwater, Tech. of Water Resourc. Invest.*, chap. C2, Book 7, U.S. Geological Survey, Boulder, Colo., 1978.

Lee, K., and J. L. Wilson, Pollution capture zones for pumping wells in aquifers with ambient flow, paper presented at Fall Meeting, AGU, San Francisco, Calif., 1986.

Nelson, R. W., Evaluating the environmental consequences of ground water contamination, 2, Obtaining location/arrival time and location/outflow quantity distributions for steady state flow systems, *Water Resour. Res.*, *14*(3), 416–428, 1979.

Newsom, J. M., and J. L. Wilson, Flow of ground-water to a well near a stream-effect of ambient ground-water flow direction, *Ground Water*, *26*(6), 703–711, 1988.

Pollock, D. W., Semianalytical computation of path lines for finite-difference models, *Ground Water*, *26*(6), 743–750, 1988.

Press, H. W., B. P. Flannery, S. A. Teukolsky, and W. T. Vetterling, *Numerical Recipes*, chap. 8.4, pp. 235–236, Cambridge University Press, Cambridge, Mass., 1986.

Russel, T. F., and M. F. Wheeler, Finite element and finite difference methods for continuous flows in porous media, in *SIAM The Mathematics of Reservoir Simulation*, edited by Richard Ewing, chap. II, pp. 35–106, Society for Industrial and Applied Mathematics, Philadelphia, Pa., 1983.

Schafer-Perini, A. L., J. L. Wilson, and A. L. Gutjahr, "Geostatistical investigation of flow behavior in a heterogeneous well field, paper presented at Spring Meeting, AGU, San Francisco, Calif., 1988.

Shafer, J. M., Reverse pathline calculation of time-related capture zones in nonuniform flow, *Ground Water*, *25*(3), 283–289, 1987.

Shubin, G. R., and J. B. Bell, An analysis of the grid orientation effect in numerical simulation of miscible displacement, *Comput. Meth. Appl. Mech. Eng.*, *47*(1984), 47–71, 1984

Wilson, J. L., Double-cell hydraulic containment of groundwater contamination, in *Proceedings of National Conference on Aquifer Restoration and Monitoring*, pp. 65–70, National Water Well Association, Dublin, Ohio, 1984.

Wilson, J. L., B. S. RamaRao, and J. McNeish, GRASP, A computer code to perform Post-SWENT adjoint sensitivity analysis, *Tech. Rep. BMI/ONWI-625*, Off. of Nucl. Waste Isol., Battelle Mem. Inst., Columbus, Ohio, 1986.

A. L. Schafer-Perini and J. L. Wilson, Department of Geoscience, New Mexico Institute of Mining and Technology, Socorro, NM 87801.

(Received February 8, 1990;
revised March 5, 1991;
accepted March 8, 1991.)